Influence of joints on the seismic response of traditional timber frames in Turkey

Güzide Aslankaya

**UNIVERSITAT POLITECHNICA DE CATALUNYA
BARCELONATECH**

**INFLUENCE OF JOINTS ON THE SEISMIC RESPONSE OF
TRADITIONAL TIMBER FRAMES IN TURKEY**

PhD. THESIS

GÜZİDE ASLANKAYA

Department of Architectural Technology

Architectural, Building Construction and Urbanism Technology

**Directors of Thesis : PhD. Albert Albareda-Valls
PhD. Jaume Avellaneda Diaz-Grande
Tutor of Thesis : PhD. Ana Maria Lacasta Palacio**

DECEMBER 2019

**UNIVERSITAT POLITECHNICA DE CATALUNYA
BARCELONATECH**

INFLUENCIA DE LAS JUNTAS EN LA RESPUESTA SÍSMICA DE ESTRUCTURAS DE MADERA TRADICIONALES EN TURQUIA

PhD. TESIS

GÜZİDE ASLANKAYA

**Departamento de Tecnología de la Arquitectura
Technologia de la Arquitectura, de la Edificion y del Urbanismo**

**Directores de La Tesis: PhD. Albert Albareda-Valls
PhD. Jaume Avellaneda Diaz-Grande
Tutora de La Tesis: PhD. Ana Maria Lacasta Palacio**

DICIEMBRE 2019

FOREWORD

I hereby declare that all information in this thesis has been obtained and presented in accordance with academic rules and ethical conduct. Firstly, I would like to sincerely thank my thesis advisors Albert Albareda-Valls and Jaume Avellaneda Diaz-Grande for their inexhaustible patience and guidance. I am grateful to Cenk Ustundag for his great support and advices. I would particularly like to thank my family who have always encouraged me to go further. I would also like to thank workers of UPC Material Laboratory for their valuable helps during experiments.

December 2019   Güzide ASLANKAYA

CONTENTS

x

ABBREVIATIONS

BS   **:** British Standarts
cm   **:** Centimeter
GPa   **:** Gigapascal
kg/m³   **:** Kilogram per cubic metre
kN   **:** Kilonewton
LVDT   **:** Linear Variable Differential Transformer
MoE   **:** Bending Modulus of Elasticity
MOR   **:** Modulus of Rupture
MPa   **:** Megapascal
mm   **:** Millimetre
FRP   **:** Fiber reinforced polymer
CFRP   **:** Carbon fiber reinforced polymer

LIST OF TABLES

LIST OF FIGURES

INFLUENCE OF JOINTS ON THE SEISMIC RESPOND OF TRADITIONAL TIMBER FRAMES IN TURKEY

ABSTRACT

Timber frame structures which constitute an important cultural heritage of many countries, are well known as efficient seismic resistant structures worldwide and are worth to be preserved. Hımış is one common traditional Turkish timber system, which consists of a simple timber frame filled with masonry (such as bricks, adobes or stones with mortar), and a masonry ground floor, built on continuous stone foundations. These buildings are usually located in seismic areas.

This thesis aims to make a review of the structural performance of Hımış timber system under seismic loading, with specific emphasis on joints and following strengthening of joints with CFRP (Carbon fiber reinforced polymer). Due to the seismic demands these timber structures mostly depend on connections, so that the joints have to be evaluated accurately in terms of translational and rotational stiffness and moment resistance. Subsequently, a series of experimental tests on two different types of timber joints (lap joint and mortise-tenon) which are common in Turkish timber structures have been carried out under monotonic and cyclic bending loading. The numerical analysis, FEM (the finite element method) has been performed in order to the calibrate the results from experiments. Finally, a numerical analysis considering semi-rigid joints in traditional timber connections has been performed globally.

Keywords: Hımış timber frame, Traditional connections, Semi-rigid joints, Stiffness, Numerical analysis, Carbon fiber reinforced polymer.

INFLUENCIA DE LAS JUNTAS EN LA RESPUESTA SÍSMICA DE ESTRUCTURAS DE MADERA TRADICIONALES EN TURQUIA

RESUMEN

Las estructuras de madera constituyen un importante patrimonio cultural en muchos países y son conocidas como tipologías estructurales eficientes des del punto de vista sísmico por su resistencia y ductilidad. Himis es uno de los sistemas de madera tradicional más conocidos en Turquía, consistente en marcos en forma de retícula de madera simple, relleno de mampostería en su interior (ladrillos, adobe, o piedras con mortero) en plantas piso, mientras que la planta baja es totalmente de mampostería sobre de una cimentación contínua de piedra. Esta tesis tiene como principal objetivo el de realizar una evaluación de la eficiencia estructural del sistema Himis sometido a cargas sísmicas, mediante la evaluación de la respuesta de las uniones más típicas de madera y su contribución al conjunto. Esta tesis se complementa con un análisis experimental y numérico de la contribución que aporta el refuerzo de dichas uniones mediante fibras de polímeros reforzados CFRP (polímeros reforzados con fibras de carbono). La respuesta de estas estructuras frente a sismo se debe, en parte, a la rigidez y ductilidad de las uniones entre barras de madera, por lo que éstas requieren de una especial atención en términos de rigidez traslacional y rotacional. La investigación lleva a cabo una campaña experimental, cubriendo dos tipologías básicas de uniones tradicionales entre barras de madera en Turquía (junta por solape y de espiga) bajo flexión monotónica y también cíclica. Paralelamente, se evalúan dichas uniones mediante un análisis FEM debidamente calibrado con los resultados de los ensayos experimentales, que permite reproducir el comportamiento global de estas estructuras a partir del grado de rigidez de las uniones con o sin refuerzo.

Palabras Clave: Hımış Estructuras de madera, Uniones tradicionales, Uniones semirrígidas, Rigidez, Análisis numérico, Polímero reforzado con fibra de carbono.

1. INTRODUCTION

1.1 General

Timber is one of the most frequently used building materials in both traditional and modern engineering constructions. Thanks to the low weight and high load-bearing capacity, timber frame buildings can stand horizontal forces imposed during earthquakes and thus are well suited for seismic zones. Traditional timber frame structures are characterized by a timber frame filled with an infill which is mainly masonry acting as shear walls. The masonry behaves very well under compressive stresses while wood elements act as ties resisting to tensile stresses.

Timber framed constructions spread not only throughout European countries, such as Portugal (edificios pombalinos), Italy (casa baraccata), Germany (fachwerk), Greece (ksilopikti tichopiia), France (colombage), Scandinavia (bindingverk), United Kingdom (half-timber), Spain (entramados) etc., but also in India (dhaji-dewari), Turkey (hımış and bagdadi), Peru (quincha), USA (balloon frame in Chicago), Haiti (gingerbread houses) (Poletti 2014).

Since this type of construction spread through out the world, it is important to point out the similarities and differences between them in order to better understand their performance. Even the evident difference in traditional construction worldwide, there is always a common idea in all them: timber resists tension, so that timber frames show better performance under seismic loading rather than masonry and provide ductility.

Timber frame structures are particularly common in seismic regions, like Portugal. The adoption of timber as a structural material spread after the destruction of Lisbon derived from the strong earthquake in 1755. The typology of buildings that appeared after earthquake, called *Pombalino* buildings, were characterized by original external masonry walls and an adscititious internal timber structure named *gaiola* (cage), which is a three dimensional braced timber structure (Figure 1.1). The gaiola is formed by horizontal, vertical elements (sectional dimensions usually are 12x10, 12x15, 14x10, 10x10 cm), and diagonal (bracing) members (10x10, 10x8 cm). Timber framed walls are filled with rubble or alternatively with brick masonry or mud.

The framed walls of the gaiola may have different geometries in terms of infill materials and number of timber elements (Figure 1.1a). Timber elements are connected together through various traditional joints. The most common traditional joints are: Mortise-tenon, dovetail, half-

lap and mitered half-lap joints (Figure 1.1b). Besides, the posts between two floors which are not continous, are usually connected to horizontal beams through a scarf joint in order to guarantee a certain continuity. Besides, once timber elements are fitted together, in order to guarantee a proper and permanent connection, a forged iron nail is usually hammered in almost every notch or interconnection (Nunes, 2017). A serious inconvenient shown by Pombalino buildings is that under seismic actions it is inevitable that heavy masonry of the façades fell down, although the timber skeleton remains almost intact, assuring the resistance of the timber floors and keeping the building in service.

(a)   (b)
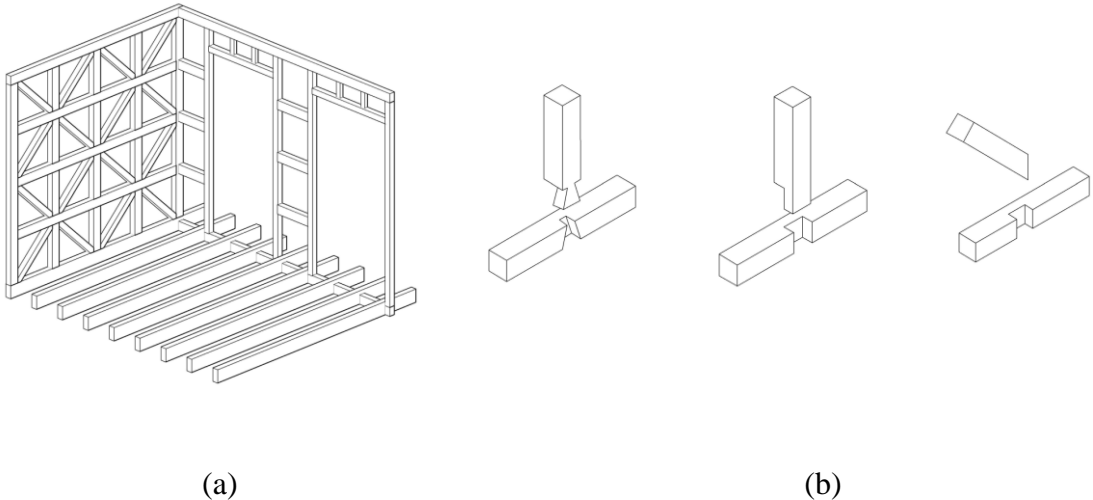
Figure 1. 1: The gaiola system (a), dovetail, half-lap, mitered half-lap joints (respectively) (b)

Timber structural buildings spread widely across Europe, not only in seismic regions but also in non-seismic regions of Northern-European countries (Germany, Scandinavia) due to the easy availability and abundance of the material.

Depending on the region in Germany, there are varied examples of timber framed structures (Figure 1.2a). Unlike in other countries, inclined posts are typical in German timber traditional houses. Furthermore, great variety of joints and roofs are used in traditional construction of Germany. For instance, mortise-tenon, overlapping, halving joints are used for column-beam connection, while cross-cut lap joint is used for beam-beam connection (Figure 1.2b). Dowel and pin are generally used as connectors.

(a)   (b)
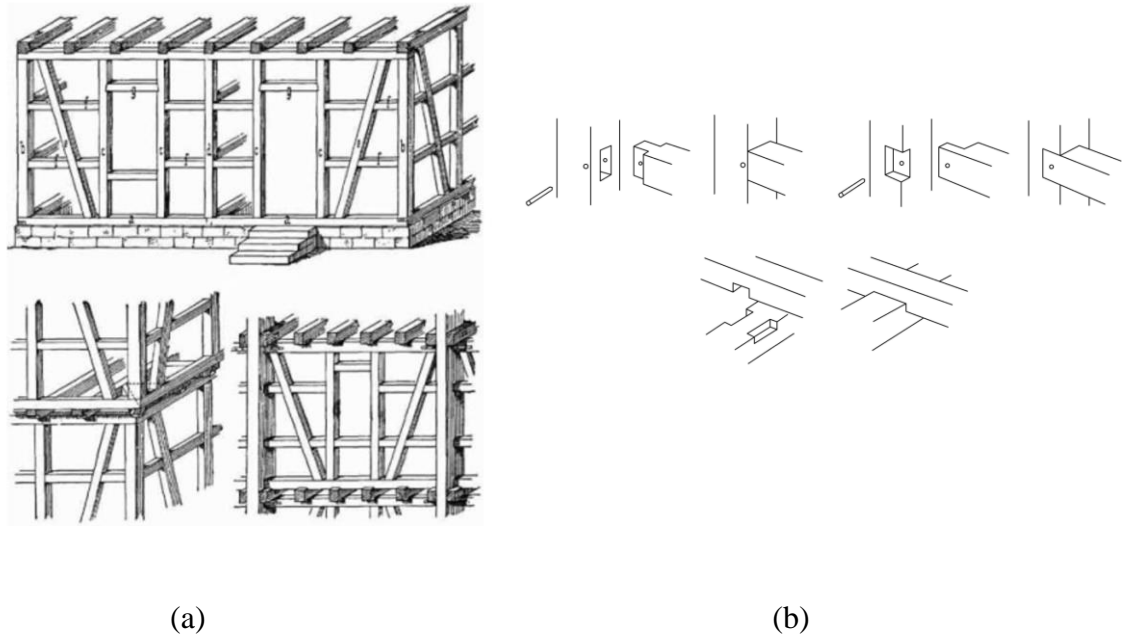
Figure 1. 2: The fachwerk system (a), mortise-tenon, halving, cross-cut lap joints (respectively) (b)

Furthermore, Asian countries have a wide tradition in timber frame buildings. Great examples of this are the tall timber temples in Japan, China and Thailand. These countries have a rooted tradition in timber construction, but traditional buildings are fully built in timber opposite to European timber frame systems. Particularly in Japan, timber framed buildings are used as a seismic efficient solution. Japanese traditional system consists only of vertical and horizontal timber members; there are no diagonal braces or rigid walls to stiffness the whole structure, what allows significant displacements. The order of the columns is a primary step of the design in the Japanese timber house: posts are set according to specific Japanese module (known as 'kens'). Each post is placed every 1 or 1.5 kens, corresponding to 1.82 or 2.73 m (Matsushita, 2004). The traditional Japanese house is divided into two main parts: the jyo-ya (secondary space) and the ge-ya (main space). Structural members are mainly posts (including jyo-ya bashira and ge-ya bashira), horizontal elements (uchinori-nuki, sashi-kamoi and ashigatame-nuki). Short posts, called ge-ya bashira, are connected to taller posts, called jyo-ya bashira, with a set of horizontal elements. Short beams, called uchinori- nuki penetrate the ge-ya bashira, which enclosed the outset part of the frame. The sashi-kamoi is a non-structural element, which holds the partition panels. Another horizontal member, ashigatame-nuki, is placed in between on foundations (Figure 1.3). The traditional Japanese house does not include any diagonal

element, despite of the severe seismic risk of the area. Structural members are attached one to each other through mortise-tenon joints without nails, nor metal fasteners.
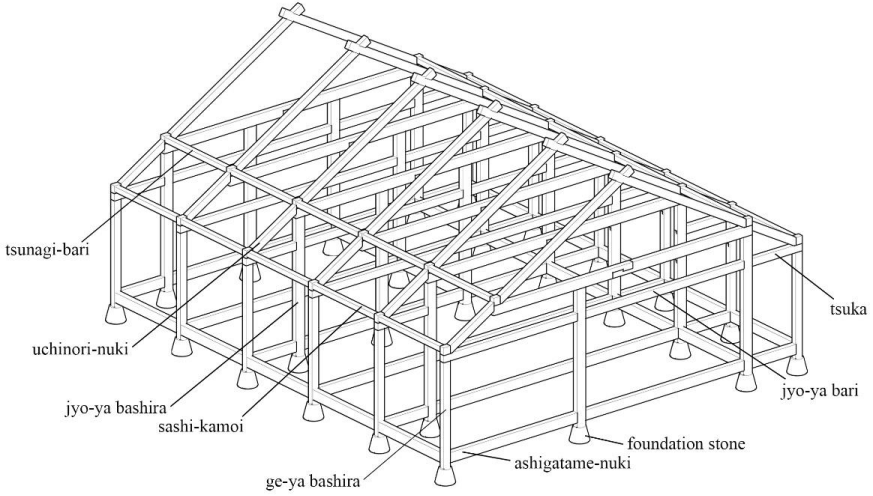
Figure 1. 3: General view of a timber structure of the Japanese house

Many types of joints can be identified in the traditional Japanese timber house. By focusing only on prevalent timber joints depending on the load-bearing system, the dovetail joint in (a), especially good under tension is used for ground plates, and the gooseneck joint (b) in Figure 1.4 (a stiffer alternative) used for the same objective. The oblique scarf joint in Figure 1.4 (c) is mostly used in beam connections: pins are inserted made of thicker wood. Mortise-tenon joint (d) and its varieties can be used for beam-post attachments (Figure 1.4). Moreover, the wedging joint (e) is used for beam-column or girder-column joints. In this system, the column is divided in half-lengthwise to reveal the internal locking system. At the same time, the tenon is manually inserted into the mortise and two wedges are attached to the tenon in order to lock it. The other typology of joints, known as double plug (f), is more suitable for central beam-column connections. Beams are spliced through the column in order to provide more tensile resistance; two keys and pin are driven in the system (Figure 1.5-c).

| (a) | (b) | (c) |
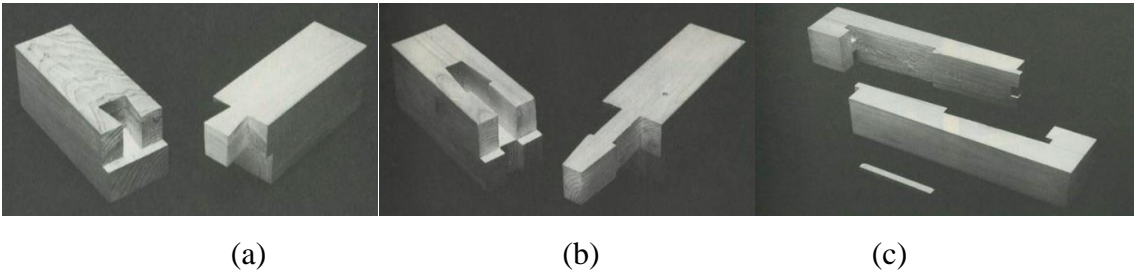
Figure 1. 4: Japanese timber joints. Respectively; dovetail, gooseneck and oblique scarf joints (Sumiyoshi et al. 1990)

4
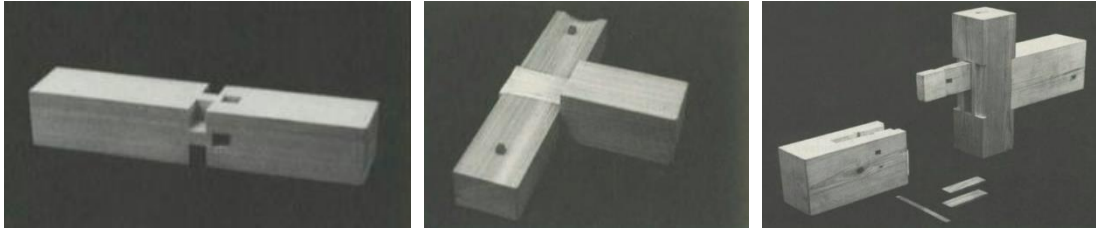
(d)   (e)   (f)

Figure 1. 5: Japanese timber joints. Respectively; mortise-tenon, wedging and double plug joints (Sumiyoshi et al. 1990)

It is known that traditional timber frame constructions show a significant ductile behaviour, which is especially interesting in seismic regions. This means that these constructive typologies become interesting even nowadays in rural areas. Historical timber structures are part of the cultural heritage and should be passed on to next generations. It is needed that these structures continue resisting future earthquakes without suffering serious damages. In order to preserve these structures, which constitute part of the most important heritage of many cities in the world it is important to better understand their response under seismic actions.

1.2 Objectives

The main goals of this research are summarized below:

- Description of the structural and seismic behavior of traditional 'hımış' timber frame structures, due to abounding existence of this system in seismic zone of Turkey,

- Evaluation of strength and ductility of timber joints under lateral loads (lap and mortise-tenon joints), which are commonly used in hımış frame structure,

- Detection of the failure mode of timber joints under seismic loads using FEM simulations,

- Research about reinforcing materials suitable for timber structures and state-of-the-art,

- Evaluation of carbon fibre reinforced polymer (CFRP) textile compared with other fibers, such as glass and basalt fibers,

- Evaluation of enhancement of the seismic performance of timber joints by means reinforcement with fiber, assessment of the influence of these strengthening

techniques on the existing timber joints through a number of bending experimental tests,

- Calibration of numerical models of reinforced timber joints by using real tests,
- Evaluation of the global seismic response of a traditional timber frame after reinforcement by using real stiffness of joints,
- Proposal of intervention on traditional timber structures for conservation.

1.3 Significance of the topic

Hımış timber structure became a well-established construction technique under seismic loading in part of the Balkans and Turkey, especially from the sixteenth century. First examples of this typology of building were found in Western Anatolia, but their general constructive features were successfully adapted within a wide geographic area extending roughly from Southern Central Anatolia to the Ottoman Balkans regardless of significant differences in local climate regime (Eldem, 1984). Hımış constructions show essential qualities that become beneficial under seismic loading. This research starts with a brief review of the current state of the art on structural performance of hımış buildings under seismic loading, with specific emphasis on joint details and discuss how these affect the overall structural behaviour under earthquakes. In Turkey since 1960s after major earthquakes, timber buildings remained intact, but suffered partial damages, such as: partial or complete collapse of infill material (stone or adobe), damages of ground floor and roof material and failure of joints. Joints bring together timber structure members. In other words, connections between timber frames are important to avoid a loss of physical integrity and to keep the box behaviour in place.

After 1944 Bolu, 1967 Mudurnu and 1970 Gediz earthquakes, it was found that timber frame structures collapsed or slipped over the foundation, since timber posts and foot plates were not sufficiently fixed to the masonry ground floor with connections (Arıoğlu, 1978). Furthermore, nailed and screwed joints over time may derive into large lateral displacements (Bayülke, 2001).

Another important feature of wood is shrinkage. This situation leads to efficiency loose connections and to seperate horizontal and vertical timber structural elements one of each other, by forming a gap around the nails or screws which connecting the wood. In this case, the rigidity of the structure severely decreases over time and the structure derives into horizontal displacements, which are usually irreversible under horizontal seismic loads.

6

Besides, due to the lightness of the timber and the use of thin sections cause problems of torsion. According to the Turkish earthquake regulations, it is essential to provide sufficient strength and rigidity in order to eliminate torsional irregularity and to prevent dangerous torsional vibrations in the load bearing system. In this case, a solution, stiffness and strength of high-load system elements need to be arranged.

This study aims to describe the capacity of timber frame structures, particulary of timber joints under seismic loading and by reinforcing the joints with CFRP in order to significantly enhance the ultimate load capacity, stiffness and flexural strength of the beam. Also, late research findings indicate that reinforcing timber with CFRP can lead to improved ductility and nonlinear behavior of timber under high stresses (Trung et al., 2015). Main objective is to contribute to the knowledge of reinforcing with fiber for recovering and increasing the mechanical properties of traditional timber elements subjected to seismic loads.

2. STATE OF THE ART

The traditional Turkish timber structural system, and therefore, timber joints against seismic loading, become the main focal point of this study. Firstly, different typologies of traditional joints and their responses within the structure have been reviewed based on a comprehensive literature research. Secondly, as a part of study and in order to understand the behavior of Turkish traditional timber structure systems under seismic loading, specific damages and modes of collapse involving timber joints depending on location (roof, beam-column connections, ground floor and foundation) have been briefly described.

2.1 Traditional Turkish Timber Structure (Hımış)

There are many different typologies of traditional timber structures in Turkey, resulting from cultural preferences determined by material availability and the climate. Traditional timber houses in Turkey can be mainly classified in: (a) log houses, (b) timber frames (*hımış, bagdadi, dizeme*) and (c) combined construction depending on the structural system. This study focuses on the most common timber typology, known as *hımış*. *Hımış* timber structure simply consists of a simple timber frame filled with masonry, bricks, adobes or stones. The basement is always

made of masonry at the ground floor (Figure 2.1). Foundations are generally made of stone, with a system which is composed of posts, studs, wall plates, joists, ledgers, braces, knee braces, windowsills and lintels (Figure 2.2). Typical typology includes diagonal bracing members to reinforce global frames.

Figure 2. 1: Turkish timber house (Turkish Timber Association, 2018)
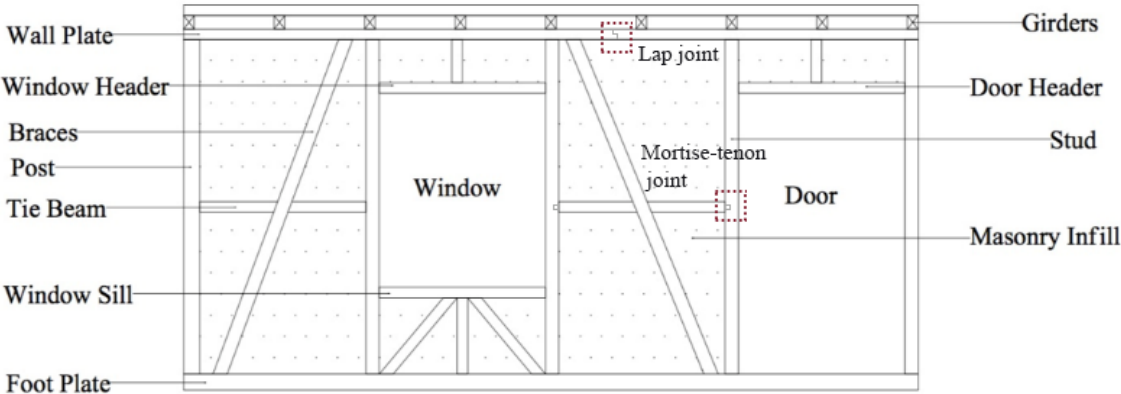
Figure 2. 2: Timber frame members

The timber frame is usually connected to the masonry basement through base wall plates by overlapping one to each other at the corners, and nailed together. Wall plates (binders) and joints appear in very different ways, such as single and double plates with one or two-way slabs (Figure 2.3). The second layer of joists is usually located perpendicular to the first layer of joists, by generating a two-way slab. The cross-section of the wall plate is usually 10x10 cm (Şahin, 2017). The studs and window studs divide the space between the main posts at constant intervals, being the cross section of the studs smaller than the posts (approximately 5x10 cm). The order of posts changes depending on the typologies of walls. For walls without windows,

the posts are placed every 100-140 cm. Studs are usually varied in intervals depending on infill materials. Horizontal members including the tie beam, windowsill, and knee braces are inserted between the studs in order to support the timber frame and to maintain the infill material in place. Cantilever is one of the peculiar features of the Turkish traditional timber house. Structural elements forming cantilevers are built together with the upper floor, as an extension of the joists. They are generally supported by bracings.

| (a) | (b) | (c) |
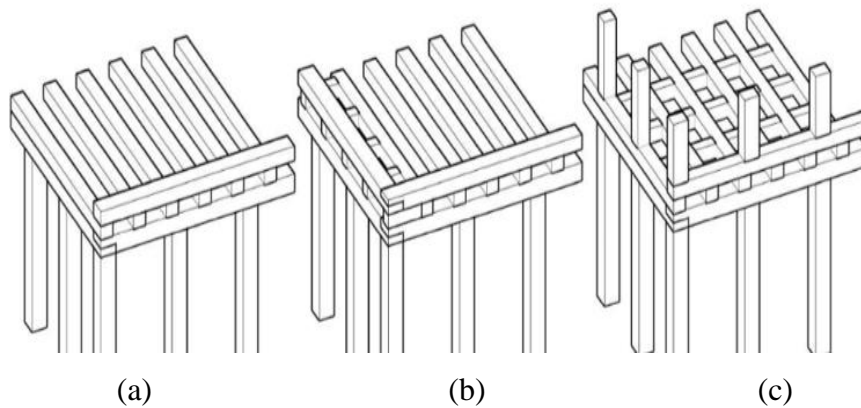
Figure 2. 3: Traditional Turkish wooden slabs. Double plates with one-way (a), single slab (b) and two-way slabs (c) using double plates

The shape of the roof system is selected after completing the whole timber frame system. Hipped roof system with 4-side slope is usually preferred. Rafters are extended 50 to 60 cm outwards, in order to form the eaves. Tiles are generally used for roofing, by overlapping one tile on another.

2.2 Traditional Turkish Timber Joints

Joints constitute usually a significant part of these structures. Many variables, such as the way of loading of timber elements, the type of fasteners, the existence of knots or even moisture content have a direct influence on timber joint design.

As summarized in Table 2.1, several sources in the existing literature classify timber joints based on different criteria (Erman, 2011). From a structural point of view, joints are classified according to the type of acting forces (shear, compression, tension and bending). However, joints can also be classified depending on the type of fastener: bolted, doweled, nailed, plate components or glued connections.

9

Another important classification comes from the geometry of the components and their location within the structure. This is reason why this classification is made under constructional criteria and carpentry production. The constructional approach emphasizes direction of the components in joints, according to their grain, such as lengthening, framing, right angle (orthogonal) and diagonal joints. With a carpentry approach, joints can be classified depending on their geometry, such as plain (butt), lap and notch joints (Graham, 1951). The two classifications are regarded to be complementary. At the same time, the relative location of the joints in the structure should be also considered: right angle (orthogonal) joints, in the horizontal and the vertical plane, and diagonal joints. The classification of timber joints is complex. To summarize, a list of basic orthogonal timber joints would be: butt, cog, comb, dovetail, finger, fork, gooseneck, half lap, housed, lap, mortise-and-tenon, notch, oblique tenon, scarf and shoulder joints. Diagonal timber joints are usually used for sloped roof planes, trusses or bracings of wall and floor framings and being mainly known as bird's mouth, bridle, butt, dovetail, lap, half lap, notch (front, back, double and tabled notch) joints, oblique tenon and step-lapped joints.

Table 2. 1: Classification of timber joints (Erman, 2011)

Sources	Structural Approach	Constructional Approach	Carpentry Approach
Binan 1990	—	a) End joints b) Corner joints c) Diagonal joints	—
Bolshakov 1967	a) Built-up joints b) Scarf joints c) Multiple joints	—	—
Götz 1989	a) Traditional joints b) Shear joints c) Dowel joints d) Nailed joints d) Glued joints	—	—
Graham 1951	—	—	a) Plain joints b) Lap joints
Güngör 1961	—	a) Lengthening joints b) Framing joints	—
Günsoy 1967	a) Direct joints,	—	—

Karlsen 1989	a) Contact surface joints, b) Connectored joints. c) Glued joints	—	—
Lloyd 1960	—	—	a) Notch joints b) Keyed joints c) Doweled joints d) Glued joints
Kliment 1989	—	a) Right angle b) End joints c) Edge joints	—
Mettem 1974	a) End joints b) Node joints c) Framing joints	—	—
Schodeck 1980	a) Butt joints b) Lap joints c) Intersecting joints	—	—
Ulrey 1970	—	—	a) Plain joints b) Lap joints
Wood Reference Handbook 1991	a) Interlocking joints b) Fastener joints	—	—

Among all these types of joints, the mortise-tenon, the preferred joint for beam-column connections (a) in Turkish traditional timber house. Another common typology is, the lap or half-lap joint (b), which is suitable for beam-beam connections (Figure 2.4-2.5). The connection between braces (diagonal) to the bottom and (angle brace of) cantilevers to the beams is achieved using tongued-grooved (c) and notch joints (d) (Figure 2.6), (Oztank, 2008). Nailed connections have been widely used in Turkish traditional timber frame structures. Nailed connections provide the ability to absorb and dissipate energy during severe earthquakes (Dogangun et al., 2015).

Figure 2. 4: Timber joints in frame (Turkish Timber Association, 2018)

<div align="center">(a)   (b)</div>
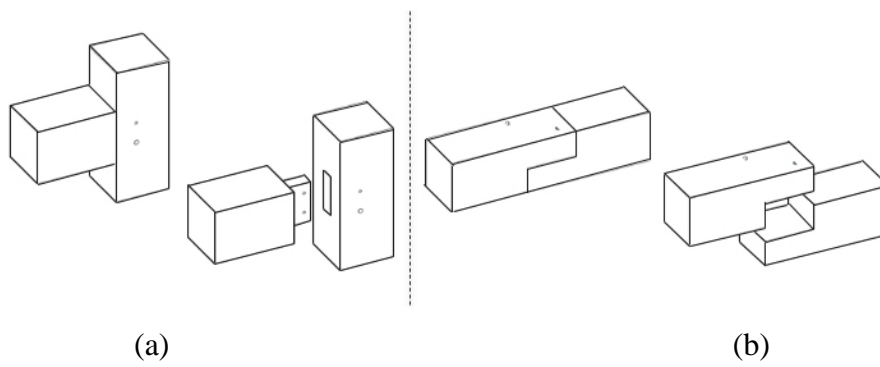
Figure 2. 5: Timber joints, mortise-tenon (a) and half-lap (b) joints
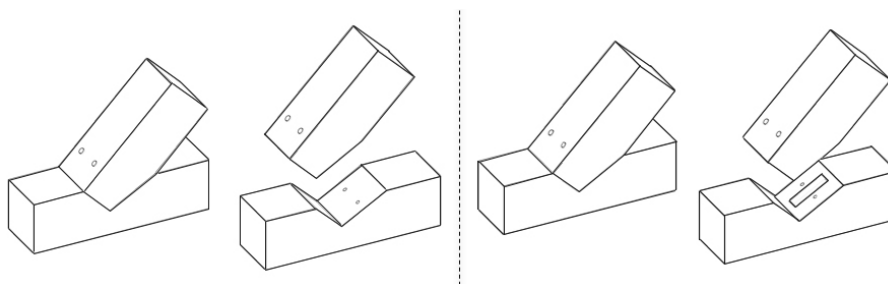
Figure 2. 6: Timber joints, tongued-grooved (c) and notch (d) joints

2.3 Seismic Behaviour of Timber Structure

Half-timbered structures (timber frame walls filled with masonry) are well known for their ductility-like behaviour. Several researches have been made on the timber frame structures. An important issue is to study these structures under cyclic and dynamic loading in order to understand their seismic behaviour. Previous studies show that the force-deformation response of a timber frame shear wall under cyclic or reverse loading behaves nonlinearly even at low loading levels (Pang et al., 2007). Furthermore, timber shear walls are capable of dissipating a large amount of energy through the behaviour of individual fasteners (Dinehart, 1998). The behaviour is also influenced by vertical load, as it increases the lateral stiffness and the energy dissipation, nail spacing and hold-down anchors (Johnston et al., 2006). It is commonly accepted that the load-deformation behaviour the absorption of energy of shear walls is mainly provided by joints. Therefore, the behaviour of connector under both monotonic and cyclic loading conditions related to shear walls has been investigated extensively by many researchers (Lam et al. 1997). Connections in timber frame construction are a key issue, as they control in-plane behavior, particularly regarding to dissipative capacity of the timber walls. As there are very different types of connections, it is expected different dissipative behaviors. This fact justifies the extense experimental research work that has been carried out in the last years with different timber frame systems (Lukic et al., 2018).

Furthermore, static cyclic tests have been performed on traditional timber framed walls, where all connections are half-lap connections, in order to study the seismic capacity in terms of strength, stiffness, ductility and energy dissipation (Poletti, 2014). It can be concluded that the predominant resisting mechanism provided by the infill is rocking, particularly in case of lower vertical pre-compression level. When the wall is excited, it may achieve large displacements without a significant loss of strength and, therefore with low damage. In case of timber frame walls with masonry infill, the fact of detaching masonry from the timber frame was evident due to the seismic excitement. During the test, masonry infill tended to move out-of-plane. Also, vertical posts and diagonals were clearly uplifting and the nail placed in the half-lap connections offered little resistance to the tearing force provided by the post (Figure 2.6a). Connections at the bottom tended to open out-of-plane, so that the post would come out, as the plastic deformation of the nail would impede the post to re-enter in its original position during unloading. Besides, notice that for masonry infill walls, most of the damage was concentrated in the lower part of the wall (Figure 2.6b), (Poletti, 2014).
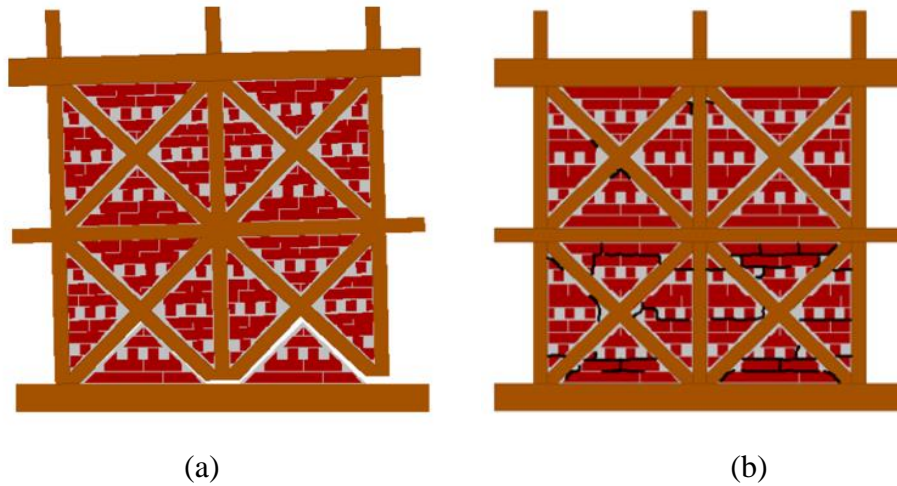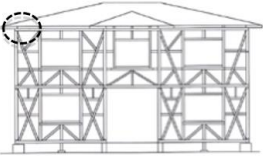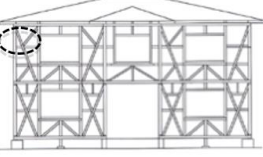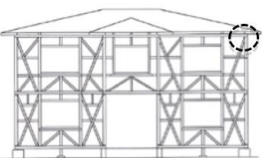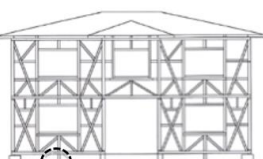
Figure 2. 7: The beaviour of timber wall during test (a) and crack pattern in masonry infill (b) (Poletti, 2014)

After a general review of the timber frame structure, especially in order to describe the seismic behavior of traditional Turkish timber houses (hımış), the different ways of damage affecting timber joints have been identified. The most relevant modes of collapse have been classified according to joints location within the structure (Table 2.2).

Damage of timber joints during an earthquake usually leads to partial collapse of the building; This is due to their crucial role in the integrity of the entire building. Also, as stated previously, timber connections in traditional Turkish structures are always complemented with nails to provide resistance against tensile or shear forces. Nails contribute to provide ductility and the ability of dissipating energy, especially if they are "semi-rigid" through nails or other metal elements, instead of being "perfectly rigid" (Palma, 2012).

Connections within the roof, floors, wall frames and bracing elements are not especially rigid in Turkish traditional timber houses, so during a seismic event, the failure of the infill usually leads to the collapse of joints by separating structural members. In case that the failure comes from a column or bracing members, large lateral displacements may lead to partial collapse.

14

Table 2. 2: Classification of joint damages in traditional Turkish house

Location	Mode of collapse	Images
	Excess of movement at top Tension splitting of nailed joints due to collapse of the heavy roof.	 (Korkmaz et al., 2010).
	Excess of tension Failure of specific joints due to pull out of nailed connections.	 (Dogangun et al., 2015).
	Failure of infill material Failure of diagonal joints due to the failure of the material infill.	 (Aksoy et al., 2005).
	Excess of global base shear Base shear is enhanced by the weight of infill.	 (Dogangun et al., 2015).

2.4 Strengthening of Timber Structures with FRP

Fiber reinforced polymer materials formed by high strength fibers and a resin matrix have a wide variety of industrial applications due to their high strength-to-weight ratio and ease of handling. FRP materials are composites comprising fibers that provide the load-bearing capacity and stiffness, embedded in a polymeric resin that transfers loads between the fibers and provides protection to the fibers. They are available in a wide variety of forms, and have properties that vary considerably depending on the fibre material, volume fraction and orientation. Typical properties of the common fibers and polymers are given in Table 2.3. For structural reinforcement, two main forms of FRP are generally used, namely, pultruded rods or plates and fabrics. For internal reinforcement, pultruded rods and plates are bonded into slots or grooves formed in the timber element. For external reinforcement, FRP plates or fabric materials are used. The reinforcement of timber with FRP is normally implemented by adhesive bonding. An important aspect of the behaviour of the composite material is the bond between wood and the fiber reinforced plastic. Besides, mechanical properties of FRP strongly depend on the fiber content in each direction and on the fiber itself. Unidirectional fiber-reinforced polymers (FRP) are highly orthotropic.

Table 2. 3: Fiber and polymer properties (Schober, 2015).

Material	Modulus of elasticity (GPa)	Tensile strength (MPa)	Failure strain (%)	Density (g/cm^3)
E-glass	70-80	2000-4800	3.5-4.5	2.5-2.6
Carbon (HM)	390-760	2400-3400	0.5-0.8	1.85-1.90
Carbon (HS)	240-280	4100-5100	1.6-1.73	1.75
Aramid	62-180	3600-3800	1.9-5.5	1.44-1.47
Basalt	82-110	860-3450	5.5	1.52-2.7
Polymer	2.7-3.6	40-82	1.4-5.2	1.10-1.25

(HM: High modulus, HS: High tensile strength)

In timber beams subjected to bending, the predominant failure occurs due to tensile stress, frequently by failure at the lower beam side. FRP have a linear elastic behavior until the yield stress, showing excellent mechanical properties, with high elasticity module and tensile strength values, in comparison to the weight and volume (Garcia, 2016). Research studies have progressively increased in order to expand the knowledge on this matter. These studies on

reinforcement of timber aiming to improve behaviour with respect to flexural capacity, stiffness, and ductility yielded results in quite a wide range.

Several research projects and applications are summarized in Table 2.4. Buell and Saadatmanesh tested the beams, reinforced by wrapping CFRP (Carbon fiber reinforced polymer) fabrics under bending. The enhancement of bending strength of these wrapped beams, based on one single control, was between 40 and 53%. The stiffness increased from 17 to 27% (Buell and Saadatmanesh, 2005).

Blass et al. investigated the influence of FRP reinforcement on bending stiffness and load bearing capability of glulam, testing different reinforcement layouts, qualities of timber and adhesives. The CFRP lamellas were bonded at the bottom of some specimens, and in another set, CFRP-lamellas were vertically slotted into the bottom part of the timber beams. They concluded that the beams with slotted in CRFP lamellas showed linear elastic behaviour nearly up to the loadbearing capacity (Blass et al., 2002).

Borri, Corradi and Grazini investigated timber beams that were reinforced using CFRP fabrics or bars. Compared with the control beams, these reinforced beams showed an increase of about 30% in stiffness up to 60% for the CFRP fabric layers reinforced beams. The beams with slotted-in CFRP bars all had a lower stiffness and capacity than the ones reinforced using fabrics (Borri et al., 2005).

Besides, Issa Camille also covered the glulam wood beams with CFRP fabrics. Obtained results indicate that the behavior of reinforced beams is totally different from the un-reinforced ones. The reinforcement changed the mode of failure from brittle to ductile and increased the load-carrying capacity of specimens (Issa Camille, 2005).

Gezer and Aydemir observed the strength ratio of the wrapped and non-wrapped wood material with CFRP. Compression and bending strength of the specially wrapped wood materials was investigated. At the same time, two types of woods were compared in terms of strength ratios. As a result of this study, the increment of compression and three-point bending strengths were determined for wrapped CFRP wood materials. Bending tests showed that samples exhibited an improvement of 65% in smaller cross sections and 15% in larger cross sections. Also, the variation of elastic modulus was analyzed, it was seen that the CFRP material leads to an increase in elastic modulus (E) of the material for both tree types. The wrapped specimen became a very rigid structure under bending compared to the non-wrapped specimen (Gezer, 2010).

Furthermore, a series of different experiments were conducted on timber beams reinforced with different amounts of CFRP sheets (carbon fiber reinforced plastic) followed by a statistical

analysis. A moderate increase of load-bearing capacity and ductility (approx. 30%) and a small increase of elastic stiffness (approx. 16%) may be achieved (Andor et al., 2015). Also, another study showed that the externally strengthening systems of pine timber LVL beams with different grammage basalt and carbon FRP gave rise to structures having higher stiffness and carrying capacity than the initial ones. However, the ultimate displacement experienced was not increased in the reinforced beams. By comparing the three unidirectional fabrics, the best results of ultimate load were obtained with FB280 (280 g/m^2 basalt), followed by FB600 (600 g/m^2 basalt), and finally FC300 (300 g/m^2 carbon), while the ultimate stress of FC300 was higher than that of FB280 and FC210 (De la Rosa Garcia et al., 2013).

Another research investigated an experimental programme based on strengthening laminated wood beams by using two different types of FRP -carbon fiber reinforced polymer (CFRP) and glass fiber reinforced polymer (GFRP) composite- sheets. The results of the study are encouraging with an increment of flexural stiffness up to 45.76% for 5% addition of GFRP composite sheet to the tension side of the beam. For the same percentage each of GFRP the flexural strength increase was 40%, compared to the same unstrengthened beam. For 3.33% addition of CFRP composite sheet to the tension side of the beam the increment in flexural stiffness was 64.12%. The gain in flexural strength for the corresponding percentage addition of CFRP was 50.62%. Thus, carbon fiber reinforced polymer increased the flexural stiffness and strength of timber beams more than glass fiber reinforced polymer (Nadir et al., 2016).

Besides, flexural behaviour of wood beams strengthened with hybrid FRP (HFRP) was carried out by Yang et al., 2013. Strengthening technique consists of adding carbon fiber (CF), high-strength glass fiber (SGF), hybrid CF/glass fiber, and hybrid CF/SGF to elements. Test results indicated that hybrid CF/SGF strengthening showed better ductility and strength compared with other strengthening schemes.

When it comes to shear reinforcement, some authors have analyzed the behavior of reinforced beams to shear stress through sheets arranged transversally and longitudinally to the direction of the wood fiber on the lateral beam sides (Greenland et al., 1999). Another form of shear reinforcement has been carried out with FRP pultruded rods embedded in epoxy resin into holes in the lower beam face (Radford, 2002). This application of the reinforcement is intended to diminish the possible early failure to shear effect that the drying splits may cause on beams subjected to bending.

In joint scale, Silva et al. conducted four-point bending tests on timber lap joints with the CFRP strengthening techniques of near-surface mounted (NSM) and externally bonded (EBR) reinforcement which was sufficient to get the CFRP strain distribution, shear stress distribution

and bond-slip responses (Silva et al., 2004). Wan et al. introduced single lap timber joint shear tests, where bond strength between CFRP and timber element was examined. Different CFRP bond lengths were used and the propagation of debonding cracks was monitored. Failure modes of the joints and effective bond length were identified, based on results. The relationship between failure load and the bond length is directly proportional (Wan et al., 2010).

Table 2. 4: The contributions of FRP reinforced on timber structures

Sources	Reinforced Material	Research Subject
Buell and Saadatmanesh 2005	CFRP fabrics	Strengthened beams in order to analysis the increasement of bending strength and stiffness
Blass et al. 2002	CFRP lamellas	Influence of FRP reinforcement on the bending stiffness and load bearing capability of glulam
Barri et al. 2005	CFRP fabrics and bars	Strengthened beams in order to determine the stiffness and the load-bearing capacity
Issa Camille 2005	CFRP fabrics	Strengthened glulam wood beams strengthened in order to determine the load-bearing capacity and the mode of failure
Gezer 2010	CFRP fabrics	Compression and bending strength of the wrapped wood materials were investigated
Andor et al. 2015	CFRP sheets	Influence of CFRP reinforcement on the predicted elastic stiffness and ductility

De la Rosa Garcia et al. 2013	BFRP and CFRP sheets	Strengthened beams with different grammage materials in order to determine the ultimate load-bearing capacity
Nadir et al. 2016	GFRP and CFRP sheets	Strengthened beams with different materials in order to determine the flexural stiffness and strength
Yang et al. 2013	HFRP sheets	Influence of hybrid reinforcement on the flexural behaviour
Greenland et al. 1999	FRP sheets	Strengthened beams in different directions in order to determine the shear stress
Radford 2002	FRP pultruded rods	Analysis of shear reinforcement in timber beams
Silva et al. 2004	CFRP sheets	Strengthened lap joints under different criteria (EBR and NSM).
Wan et al. 2010	CFRP sheets	Analysis of the effect of bond length in lap joints

3. GLOBAL ANALYSIS

Hımış structures are mainly composed of a timber frame formed by vertical timber posts connected to horizontal timber beams (at top and bottom) and braced by horizontal and diagonal timber elements, made reference to Chapter 2. State of the Art. The walls are filled with masonry with mortar, what contributes to dissipate the seismic energy. The connections

between various frame elements are formed by Mortise-tenon and Lap types of connections, supplemented with steel nails. The damage of timber joints during an earthquake usually leads to failure of the integrity of the structure due to their crucial role, thus it derives into a loss of stability of the entire building. The existence of bracing enhances the strength of the frame during an earthquake. Besides, the configuration of bracings used in timber structure may vary and this directly affects the lateral strength of the structure. In order to assess the seismic behaviour of the whole structure, the behaviour of each member regarding the failure of specific joints and weak parts of the frame are detected using global analysis.

3.1 Definition of Model Parameters

In order to evaluate the internal forces of members in general, a selected frame configuration was analysed by performing dynamic a non-linear implicit analysis. The frame configuration was based on the case study of Aktas, 2007 (Figure 3.1). In Aktas´s study, the frame outer boundaries are defined by wall plates, a foot plate, main posts and the frame interior is divided into smaller compartments by means of horizontal/vertical inner elements, as well as diagonal members, which also help increase inplane lateral load-bearing capacity. A number of frame tests and capacity/demand calculations based on capacity spectrum method were carried out with the aim of assessing and quantifying the seismic resistance of traditional timber hımış frames. The obtained results are discussed to draw important conclusions with regards to how frame geometry and infill/cladding techniques affect the overall performance. Results show that all frames with infill/cladding are incapable of bearing seismic demand in the linear range and they pass into nonlinear state. Therefore, frames do not remain elastic and exhibit certain amount of damage. Also, the average capacity to demand ratio for bare frames in the nonlinear range is reduced from 1.33 to 1.27 (Aktas, 2016).

In the traditional Turkish timber structure, the location of timber joints is totally arbitrary. In this study, lap joints have been located in those positions more exposed to bending in order to analyse the influence of reinforcement in more detail (Figure 3.2). Particularly, these joints are located over the openings (door and window). A numerical model was carried out in a structural frame analysis software, RSTAB which is an ideal tool to calculate internal forces, deformations and support reactions for beam, truss and frame structures. Timber posts and beams have been modelled as linear elastic bars. All nodal points have been considered rigid.

Figure 3. 1: The frame configuration for analysis in Aktas´s study (Aktas, 2016)
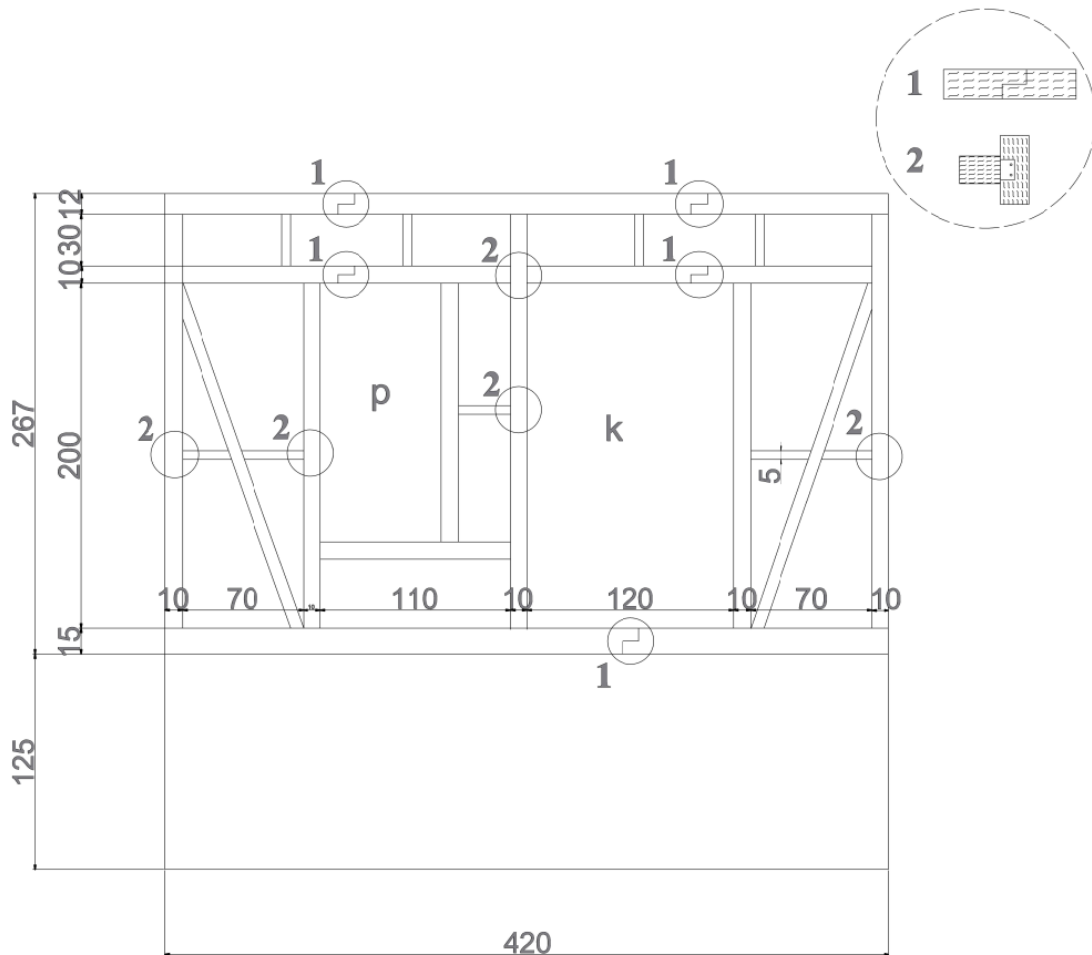
Figure 3. 2: The frame configuration for analysis

The values which have been used for elastic parameters, are given in Table 3.1, and material properties have been obtained from previous experimental tests. The additional necessary

information which did not derive from experimental results, has been obtained from the Joint Committee on Structural Safety probabilistic model code (JCSS, 2006). Other material properties have been estimated based on this model code, given in Table 3.2. Besides, for the infill material, masonry with standard mortar from material libraries has been chosen, which considers masonry according to EN 1996-1-1:Eurocode 6; masonry has been considered as non-linear plastic (Table 3.3). The mechanical behaviour of masonry in compression is clearly non-linea; Limit compression strength is considered as 10 MPa then yielding, while limit tension is 0.1 MPa (Figure 3.3).

Table 3. 1: Elastic parameters of timber from experimental tests

Bending strength (R_m):	72.97 MPa
Bending MOE (E_m):	13648 MPa
Compression strength ($R_{C,0}$):	39 MPa
Compression strength ($R_{C,90}$):	4.12 MPa
Density (ρ_{den}):	500 kg/m^3

Table 3. 2: Elastic parameters of timber from JCSS (2006)

Tension strength ($R_{t,0}$):	43.782 MPa
Tension strength ($R_{t,90}$):	7.5 MPa
MOE tension ($E_{T,0}$):	13648 MPa
MOE tension ($E_{T,90}$):	454.93 MPa
Shear modulus (G_v):	853 MPa
Shear strength (R_v):	6.18 MPa

Table 3. 3: Elastic parameters of masonry

Modulus of elasticity (E):	1500 MPa
Shear modulus (G):	625 MPa
Poisson´s ratio (v):	0.2
Specific weight (γ):	24.04 kN/m^3
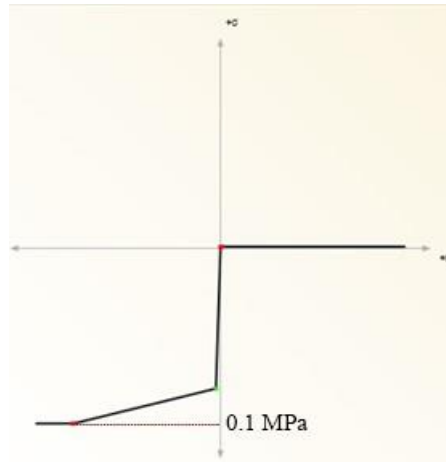
Figure 3. 3: The non-linear plastic curve of masonry

3.2 Dynamic Non-Linear Analysis

It is widely recognized that nonlinear time-history analysis constitutes the most accurate way for simulating response of structures subjected to strong levels of seismic excitation. The dynamic non-linear implicit analysis using the method of response spectrum (spectral analysis) with the time history has been carried out under lateral seismic loads. Velocities and displacements at the end of each time step are obtained by the Newmark method. The basic formula of the Newmark method specifies the relations between displacement, velocity and acceleration vectors and the analysis provides equilibrium of the internal structure forces with the externally applied loads.

The structure has been subjected to seismic load through an accelerogram. The Kocaeli earthquake 1999 accelerogram has been selected for determining the acceleration-time steps. Kocaeli is the targeted seismic zone of Hımış structures in Turkey. Ground motions are reasonably represented to fit the seismicity level of the targeted zone in Figure 3.4. Accelerations during 100 seconds have been applied to frame in 'x' lateral direction. The maximum acceleration is 0.728 m/sec^2 at the time is 27.340 sec in push, while the maximum acceleration is 0.842 m/sec^2 at the time is 28.05 sec in pull.
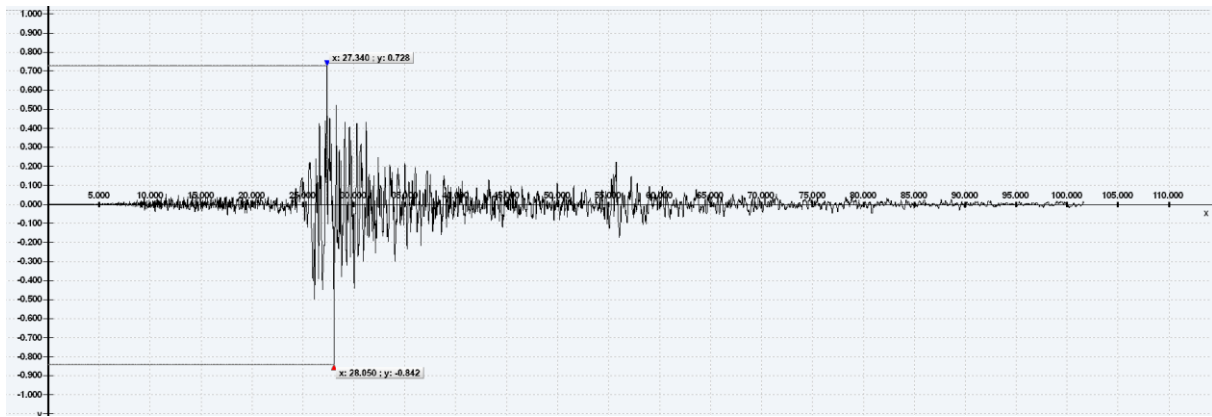
Figure 3. 4: Acceleration

Timber members have been modelled by using bar elements and the masonry infill has been modelled with 2D planer elements. The masonry base has been chosen as a fixed support (Figure 3.5). Two load cases have been defined: dead loads and live loads. Dead loads come from permanent construction material loads comprising the roof, floor, wall, and masonry. Live loads come from use and occupancy of a building. These loads have been calculated as;

Dead Load = 2 kN/m^2 (assumed) x 4 m width of floor x 2 floors = 16 kN/m

Live Load = 2 kN/m^2 (assumed) x 4 m width of floor= 8 kN/m (Figure 3.6-3.7).
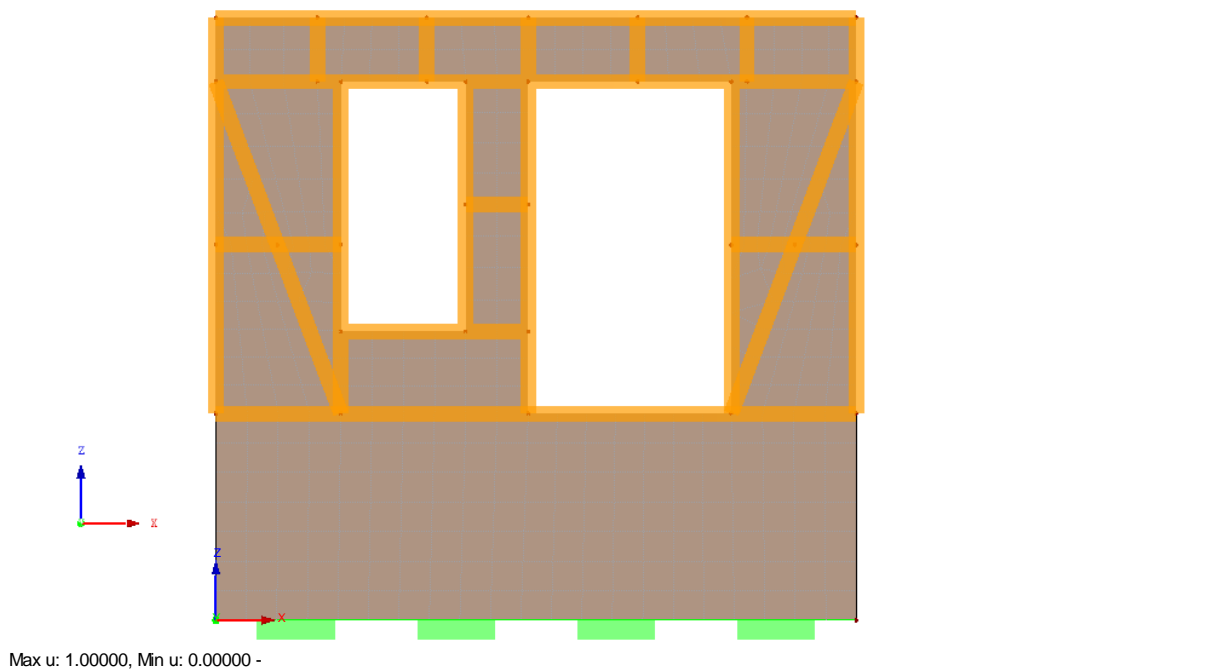
Figure 3. 5: General model of frame
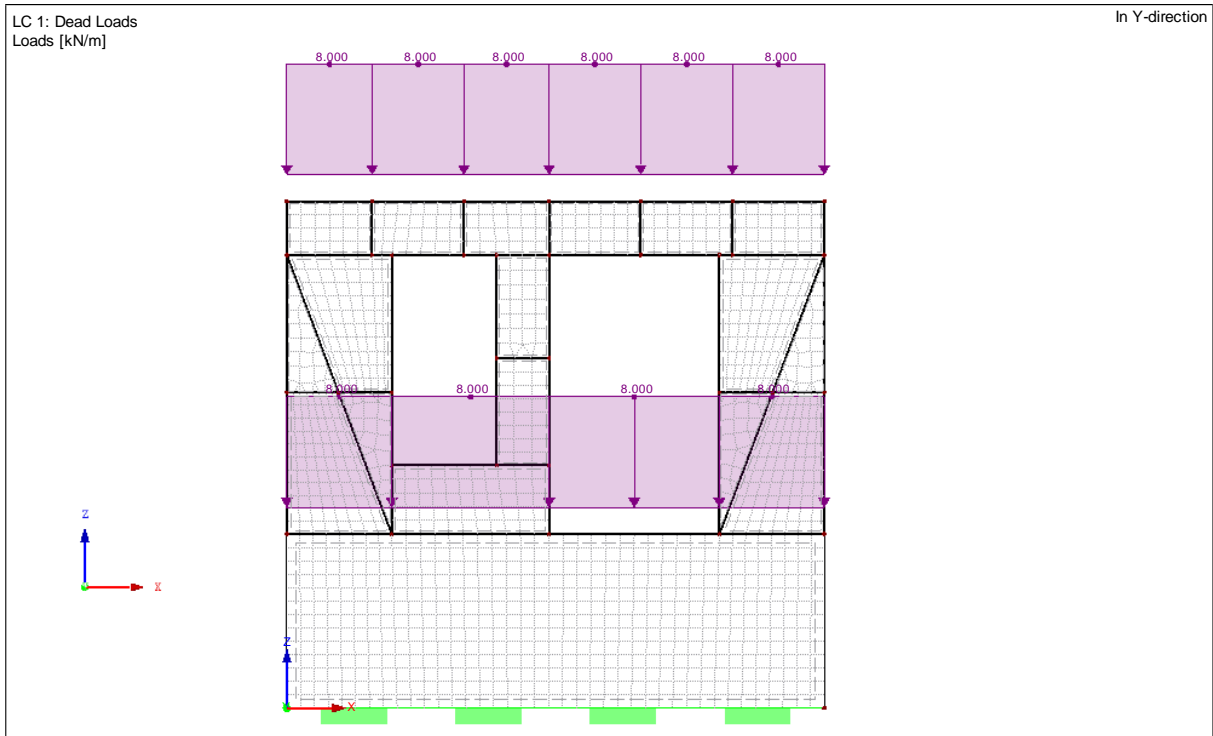
Figure 3. 6: Definition of dead loads
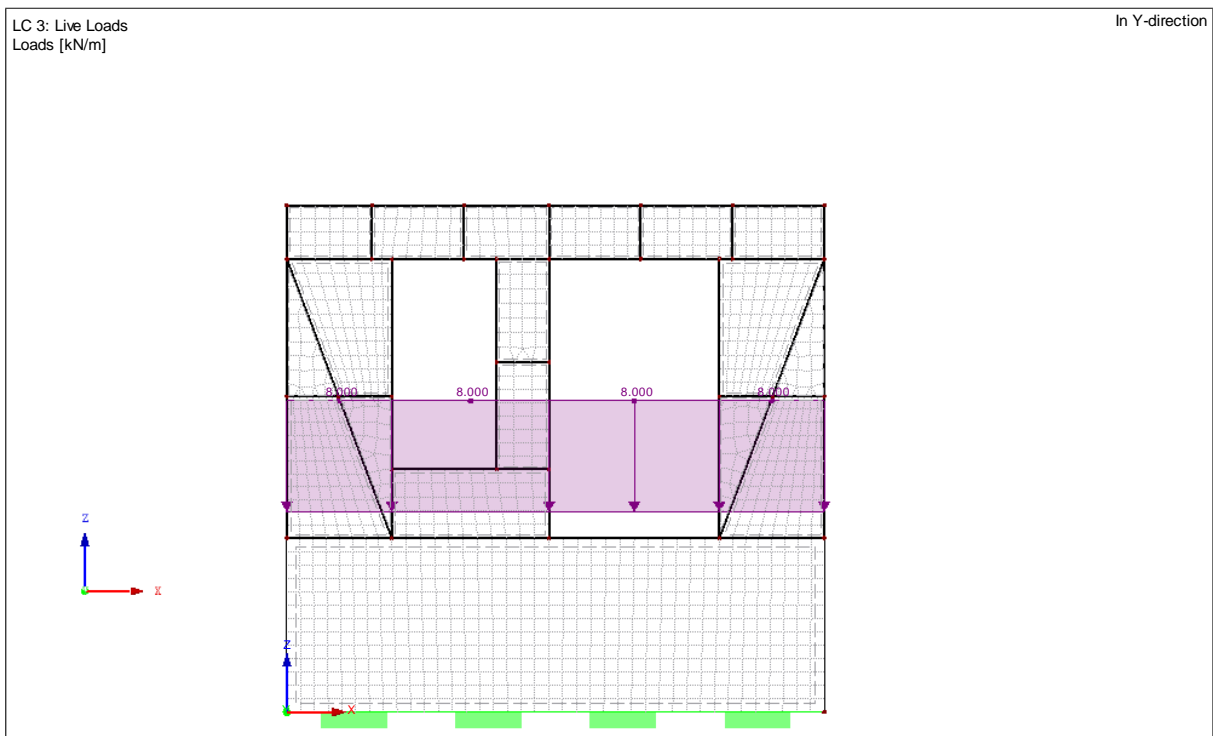
Figure 3. 7: Definition of live loads

3.3 Analysis of Results

After solving a dynamic non-linear analysis, the envelope of normal and shear forces and bending moment, together with the elastic deformed shape, is shown in Figure 3.8-3.10.

26
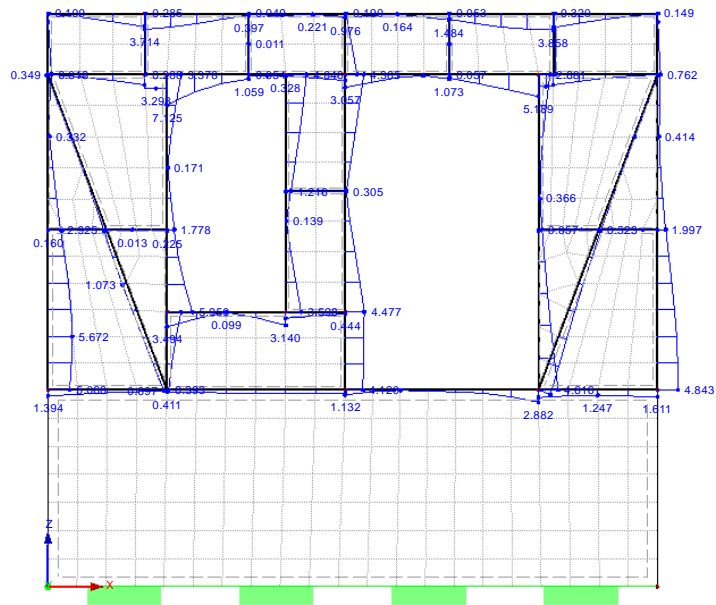
Max N: 7.125, Min N: 0.007 kN

Figure 3. 8: Normal forces

In Y-direction

Max V-z: 1.649, Min V-z: 0.002 kN

Figure 3. 9: Shear forces

27

RC 5: DLC2 - Result Envelope
Members Internal Forces M-y
Result Combinations: Max Values
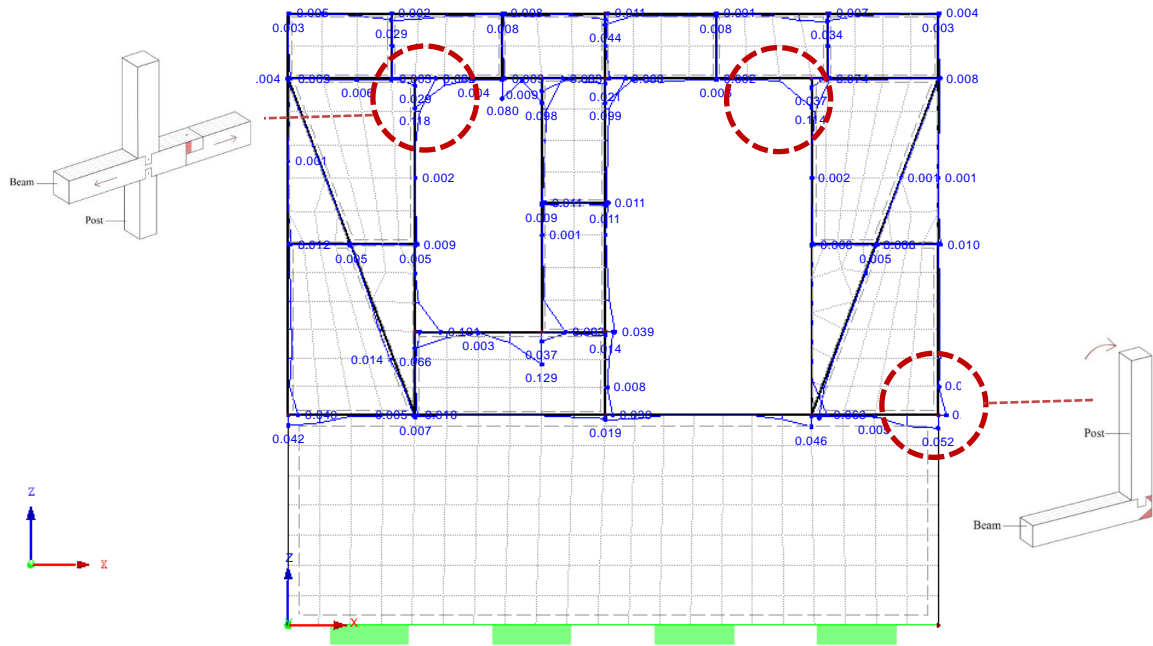
Max M-y: 0.129, Min M-y: 0.000 kNm

Figure 3. 10: Bending moment

RC 5: DLC2 - Result Envelope
Global Deformations u
Result Combinations: Max Values
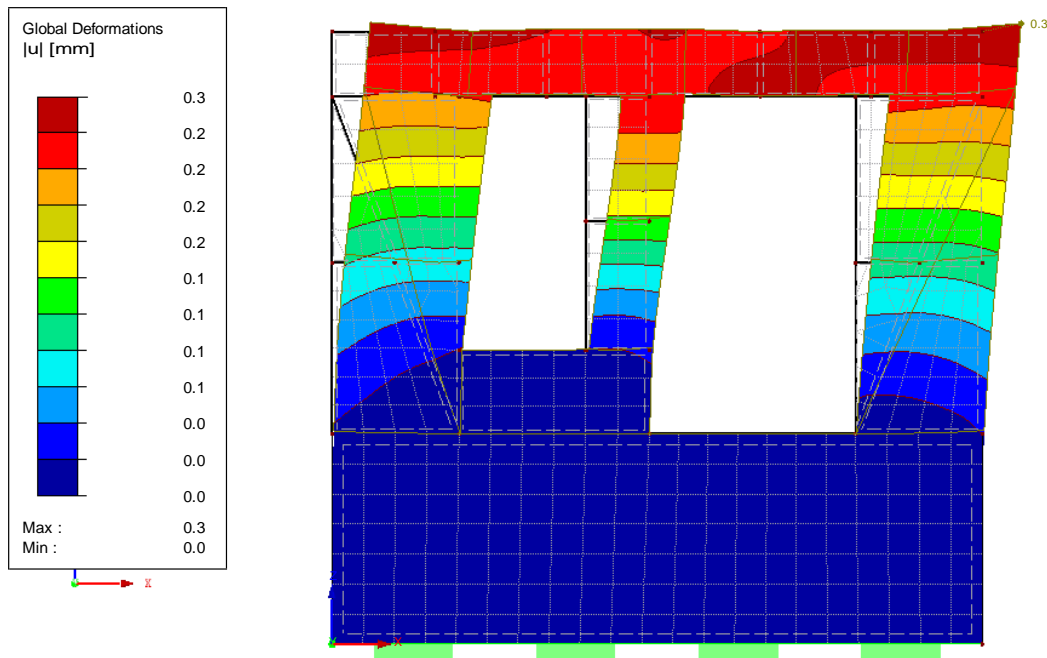
Max u: 0.3, Min u: 0.0 mm
Factor of deformations: 920.00

Figure 3. 11: Global deformations

Results from analysis have proved that the acceleration dependence of connections significantly affects the global response of the system, since they represent important dissipative elements in the frame. Connections have been considered rigid in order to reproduce an ideal behaviour. Joints are crucial during a seismic episode, particularly when infill is not present at opening parts.

A first review of results shows that the Hımış timber frame is significantly rigid and low deformable, with deformations of 0.3 mm (Figure 3.11). The upper part suffers the highest deformation, where the force is applied in the opposite direction. In general, the frame behaves in a rocking mode on further increasing acceleration in the lateral drift demand whereby the lateral capacity has been largely dependent on tension capacity of vertical posts.

The upper beam of opening parts (window, door) are subjected to the maximum compressive forces, as 7.12 kN. Moreover, different behavior is observed at the braces depending on the location. The diagonal element inclined against the applied displacement is under compression while the another one under tension. This diagonal brace (at the right) suffers from pure tension (4 kN) leading to physical separation of elements. Finally, during severe cycles, lower parts of the frame tend to slide off the masonry basement due to heavy shear forces, approximately 1.64 kN. Besides, these nodes allow certain rotation of the post, moment is about 0.052 kN.m. Highlighted areas in Figure 3.10 show higher bending moments in the frame. Maximum bending moments, like 0.129 kN.m can be observed on the window and door openings, where the lap joints are located, thus these parts show the highest bending moments. Furthermore, another high bending moment is seen at the lower part of frame, where the column and beam are usually connected with mortise-tenon joints. Thereafter, the whole structure deforms significantly. Depending on the obtained results of the analysis, internal forces of members and transferring of loads to each node have been detected, thereby the efficiency of the structural connections can be evaluated.

Moreover, the distribution of stresses in sigma x and sigma y on masonry surfaces are given in Figure 3.12-3.13. It is evident that the value of the tensile municipal stresses are over the above limit slightly at the corner of the openings, the limit tension of masonry was defined as 0.1 MPa.

RC 5: DLC2 - Result Envelope
Surfaces Stresses Sigma-x,+
Result Combinations: Max Values
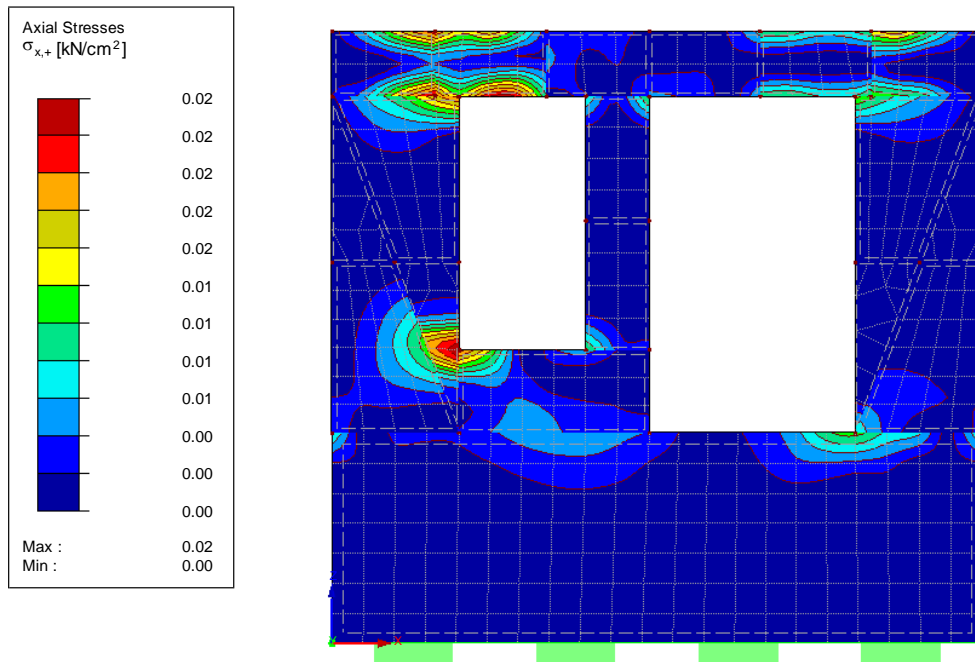
Max Sigma-x,+: 0.02, Min Sigma-x,+: 0.00 kN/cm^2

Figure 3. 12: Axial stresses in sigma-x at masonry surface

RC 5: DLC2 - Result Envelope
Surfaces Stresses Sigma-y,+
Result Combinations: Max Values
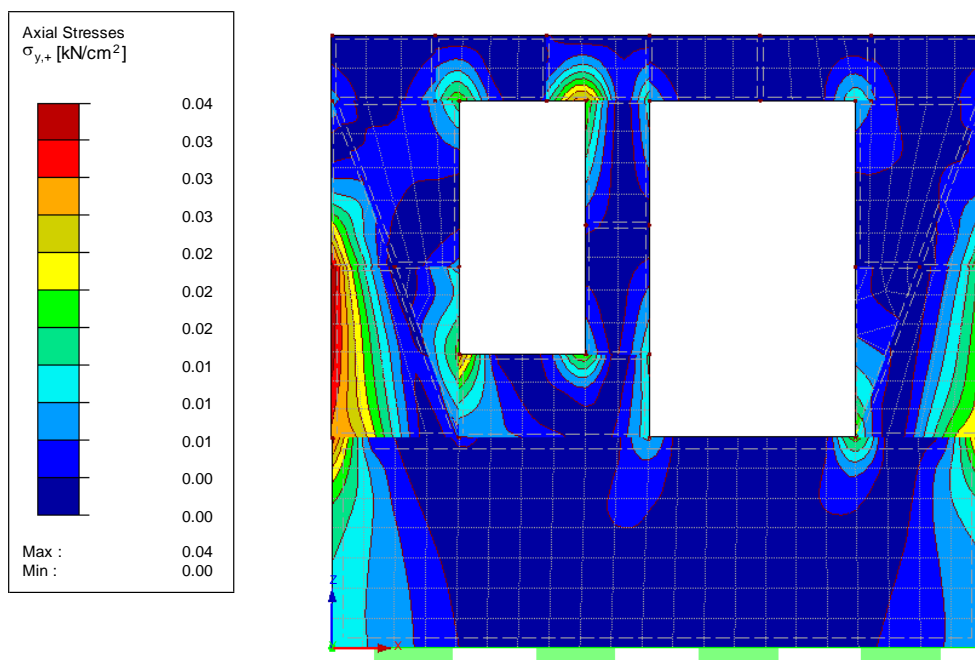
Max Sigma-y,+: 0.04, Min Sigma-y,+: 0.00 kN/cm^2

Figure 3. 13: Axial stresses in sigma-y at masonry surface

3.4 Response Spectrum Analysis

In order to indicate the likely maximum seismic response of an essentially elastic structure, a respond spectrum analysis has been carried out. Response spectrum analysis provides insight into dynamic behaviour of structure. It was carried out with contribution from each natural modes. Modes are inherent properties of a specific structure, and are determined by material properties (mass, damping, and stiffness) and boundary conditions. Each mode is defined by a natural (modal or resonant) frequency, modal damping, and a mode shape. The natural and angular frequencies ω and f as well as the periods T are listed in table 3.4.

Table 3. 4: The parameters of mode shapes

Mode No.	Eigenvalue v [1/s^2]	Angular Frequency ω [rad/s]	Natural frequency f [Hz]	Natural period T [s]
1	11247.050	106.052	16.879	0.059
2	94582.086	307.542	48.947	0.020
3	180791.094	425.195	67.672	0.015
4	243747.516	493.708	78.576	0.013
5	329508.000	574.028	91.359	0.011
6	416756.125	645.567	102.745	0.010

The assigned response spectrum (derived from 1999 Kocaeli Earthquake) is illustrated in the graphic (Figure 3.14).
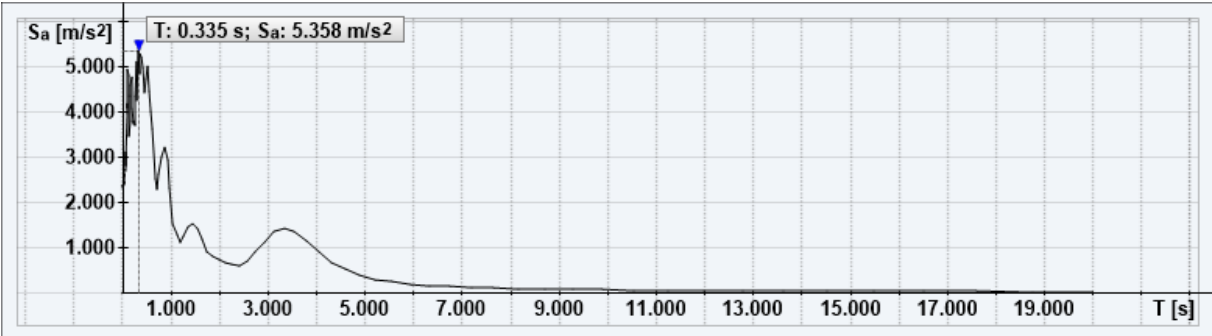
Figure 3. 14: Acceleration spectrum

The frame has been modelled two-dimensional and the acceleration has been recorded at each node of the structure. Six modes in lateral direction have been analyzed (Figure 3.15-3.17). Figure 3.18 that the first mode correspond to large displacements associated with strong excitations, shows 0.8 mm. Considering the peak, period of 0.059 seconds is reached in the first mode of the structure. Internal forces and the distribution of stresses in masonry surfaces are

given in Figure 3.19-3.23. Resulting values are higher than the results from dynamic non-linear time history analysis.
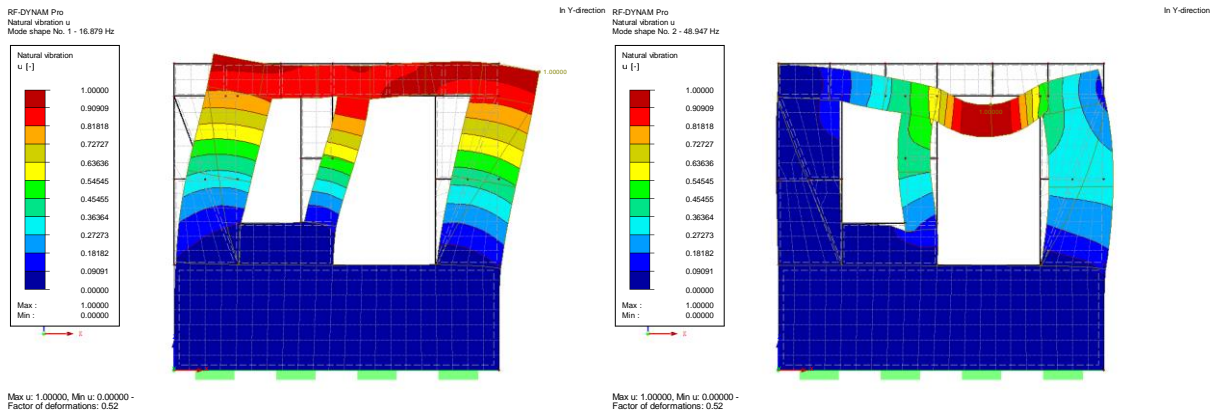
Figure 3. 15: Mode shape 1 and mode shape 2
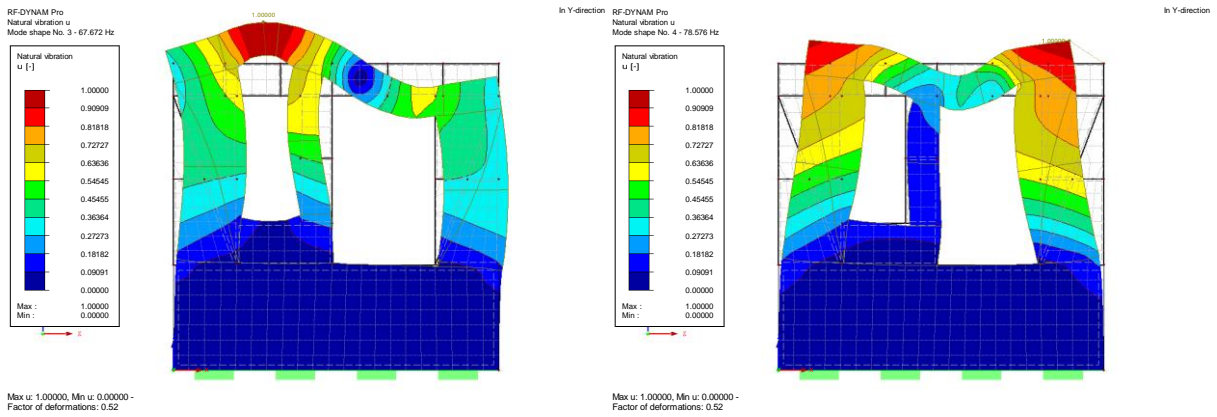
Figure 3. 16: Mode Shape 3 and mode shape 4
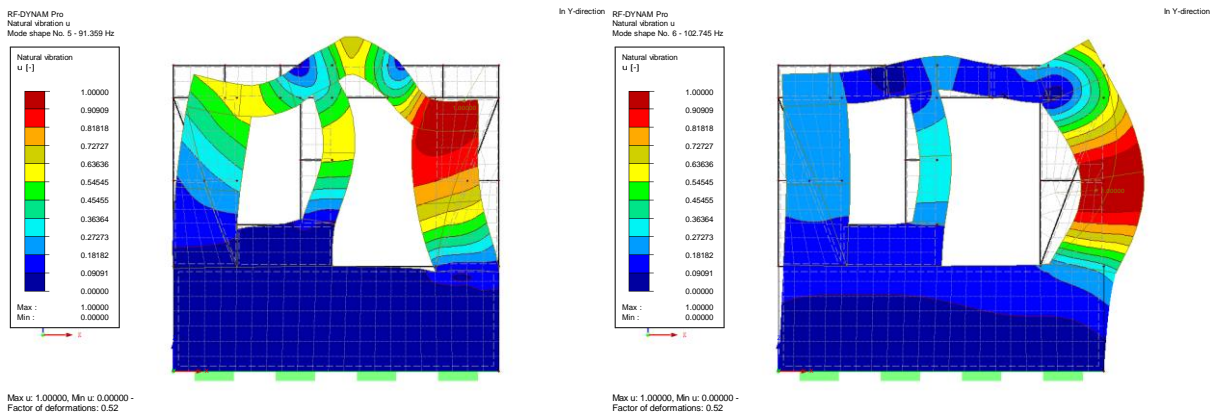
Figure 3. 17: Mode Shape 5 and mode shape 6

RC 6: DLC1, Result Envelope
Global Deformations u
Result Combinations: Max Values
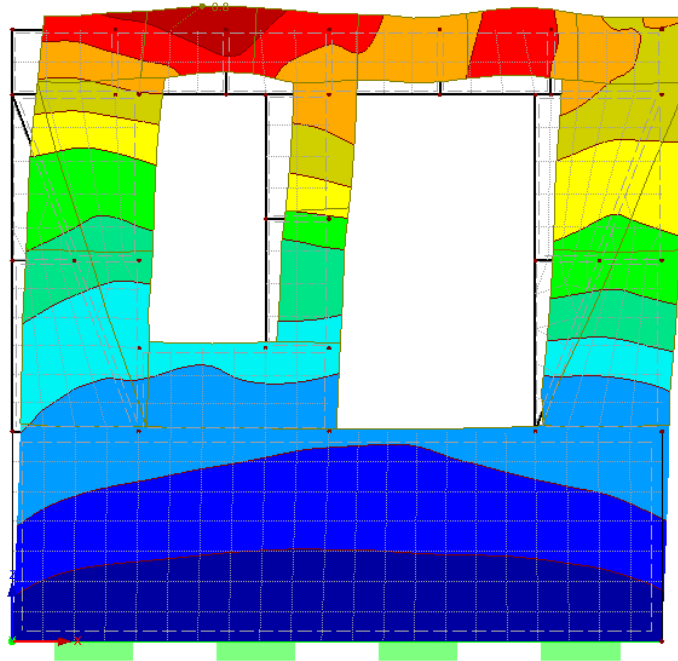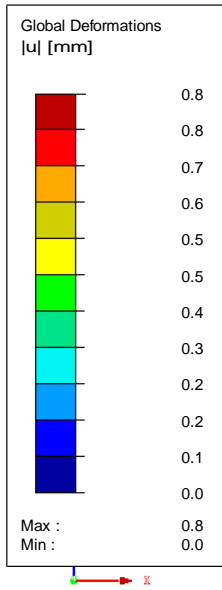
Max u: 0.8, Min u: 0.0 mm
Factor of deformations: 300.00

Figure 3. 18: The deformation in mode shape 1

RC 6: DLC1, Result Envelope
Members Internal Forces N
Result Combinations: Max Values
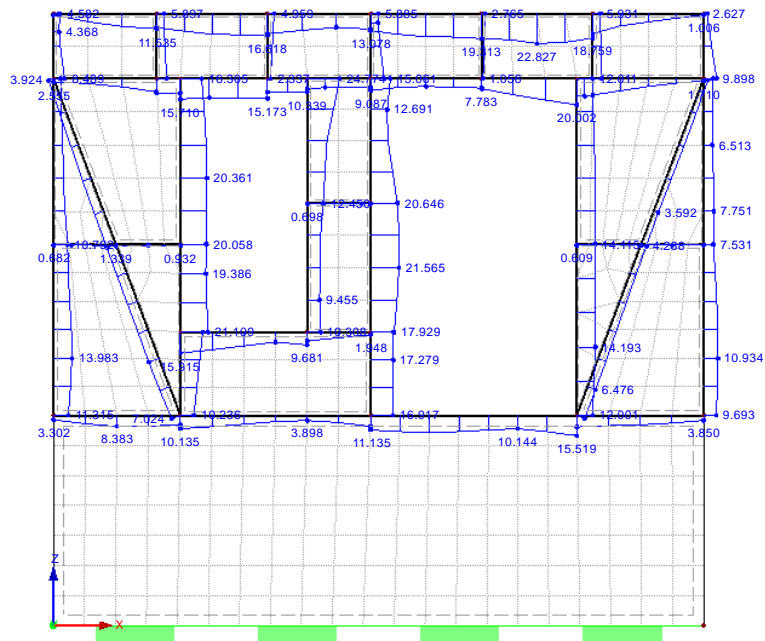
Max N: 24.774, Min N: 0.413 kN

Figure 3. 19: Envelope of normal forces

RC 6: DLC1, Result Envelope
Members Internal Forces V-z
Result Combinations: Max Values
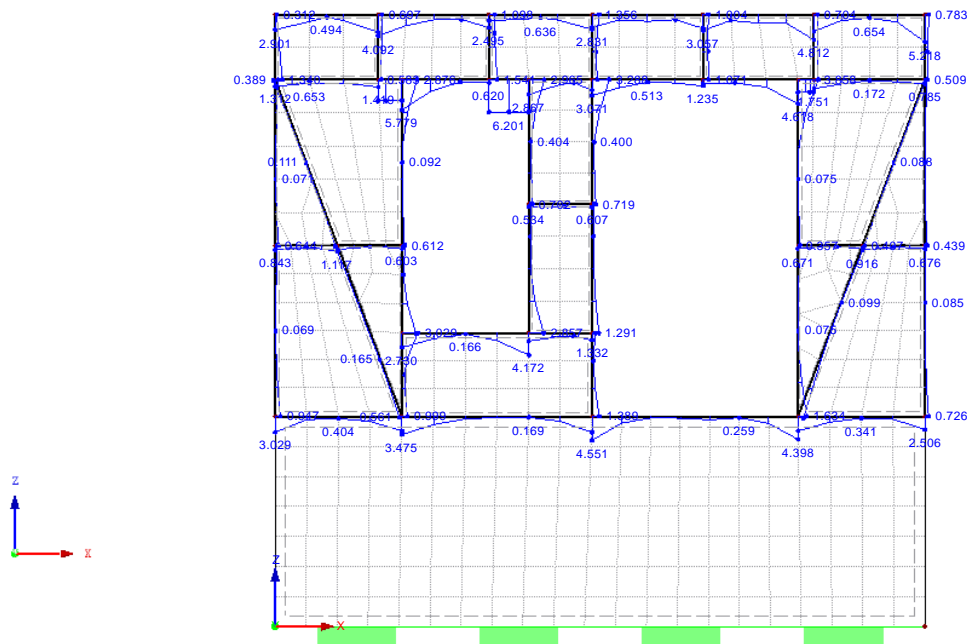
Max V-z: 6.201, Min V-z: 0.058 kN

Figure 3. 20: Envelope of shear forces

RC 6: DLC1, Result Envelope
Members Internal Forces M-y
Result Combinations: Max Values
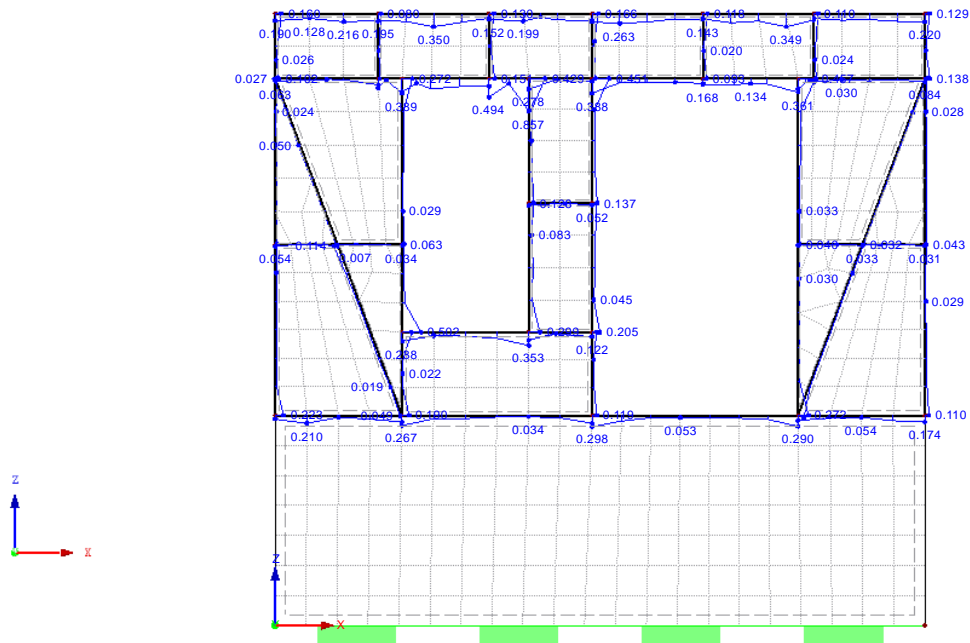
Max M-y: 0.857, Min M-y: 0.005 kNm

Figure 3. 21: Bending moment

RC 6: DLC1, Result Envelope
Surfaces Stresses Sigma-x,+
Result Combinations: Max Values

Axial Stresses
$\sigma_{x,+}$ [kN/cm^2]

	0.06
	0.06
	0.05
	0.05
	0.04
	0.04
	0.03
	0.02
	0.02
	0.01
	0.01
	0.00
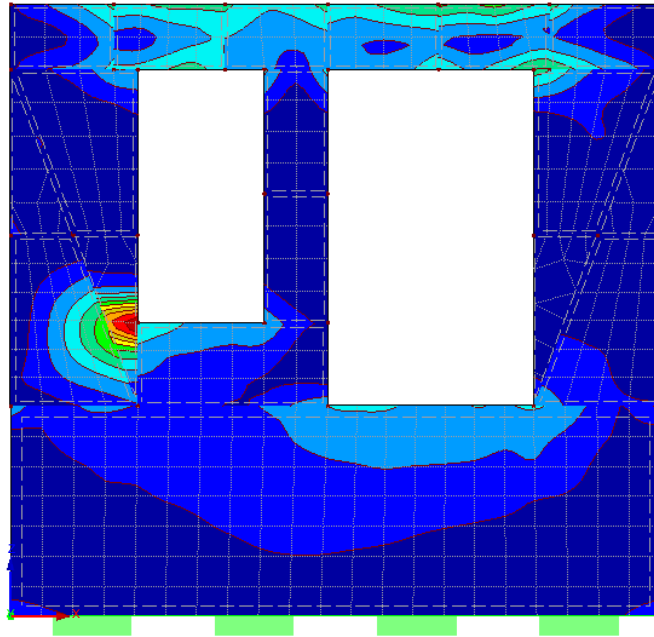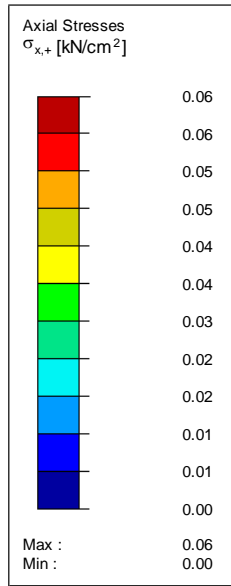
Max : 0.06
Min : 0.00

Max Sigma-x,+: 0.06, Min Sigma-x,+: 0.00 kN/cm^2

Figure 3. 22: The stresses of masonry surfaces in sigma-x

RC 6: DLC1, Result Envelope
Surfaces Stresses Sigma-y,+
Result Combinations: Max Values

Axial Stresses
$\sigma_{y,+}$ [kN/cm^2]

	0.09
	0.08
	0.07
	0.07
	0.06
	0.05
	0.04
	0.04
	0.03
	0.02
	0.01
	0.00

Max : 0.09
Min : 0.00
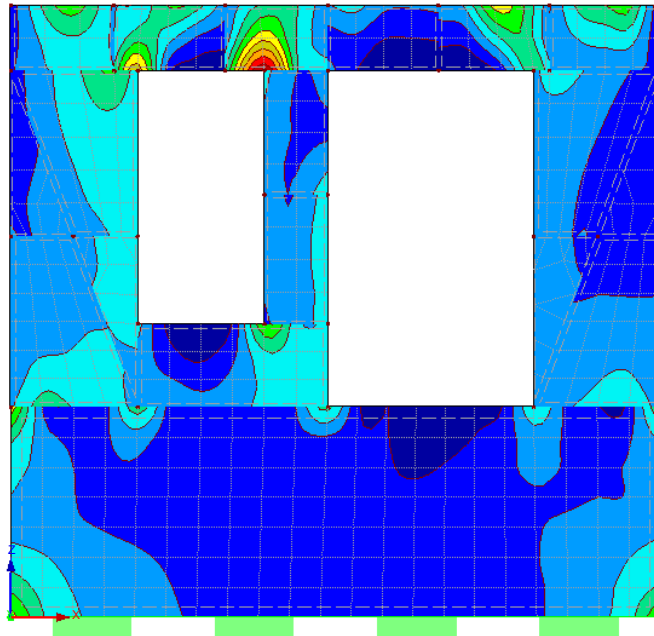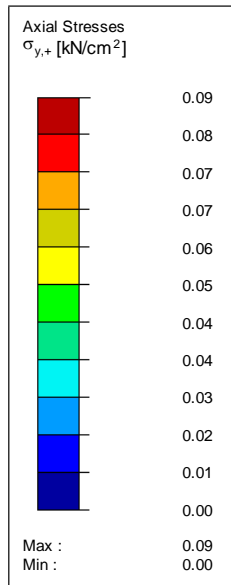
Max Sigma-y,+: 0.09, Min Sigma-y,+: 0.00 kN/cm^2

Figure 3. 23: The stresses of masonry surfaces in sigma-y

According to the results of response spectrum analysis, the obtained deformed shapes are quite different, which are asymmetric on the first, second, third and sixth mode shapes and are symmetric on the fourth and fifth mode shapes. Each mode shape is influenced differently by the position of the joint nodes, just where the highest deformation takes place in the first mode. It has been proved that connections, which are at side of openings, forced excessively in tension. Moreover, maximum stresses in masonry surfaces (sigma-x) can be mostly seen at the corner of openings and the maximum stresses of masonry surfaces (sigma-y) can be detected at the left side of frame, to where the load is applied.

If a general comparison is considered between the response spectrum analysis (RSA) and dynamic time history analysis, it is clearly seen that the response spectrum measures the contribution from each natural mode of vibration to indicate the likely maximum seismic response of structure, while time history analysis requires the solution of the differential equation of motion over time. In dynamic non-linear time history analysis, the maximum stresses which have been measured on masonry surfaces in sigma-x and sigma-y are 0.02 kN/cm2, 0.04 kN/cm^2, while in response spectrum analysis, the maximum stresses of masonry surfaces in sigma-x and sigma-y are 0.06 kN/cm^2, 0.09 kN/cm^2 respectively. Besides, the maximum strains of masonry surfaces in eps-x and eps-y are 0.000001 με, 0.000002 με in dynamic non-linear analysis, while in response spectrum analysis, the maximum strains of masonry surfaces in eps-x and eps-y are 0.00037 με, 0.00053 με respectively. In other words, all values of internal forces in timber members and values of maximum stresses, strains in masonry surfaces are a bit more higher in the response spectrum analysis.

4. EXPERIMENTAL ANALYSIS OF TIMBER JOINTS

Firstly, general mechanical behaviour (elastic and strength properties) of timber based on existing literature is given in order to better understand the behaviour of timber depending on different orientation of the wood fibers (parallel and perpendicular to fibers). Secondly, some characterization tests, usually used for timber joints, have been carried out. These tests have been done under compression in both directions and bending. Compressive strength parallel to

the fiber and perpendicular to the fiber, bending strength, global modulus of elasticity have been calculated with the expressions provided by standard.

Two different types of timber joints (lap joint and mortise-tenon joints) have been analyzed under monotonic and cyclic loading. Subsequently, joints which locally have been strengthened with carbon fiber textile were tested under monotonic and cyclic loadings. The purpose of these tests were to increase the flexural strength and load-bearing capacity of joint. Comparative results between reinforced and un-reinforced specimens are given below graphics. Besides, the failure pattern of specimens have been examined in detail.

4.1 General Mechanical Behaviour of Timber

Timber or wood is an anisotropic material, due to the orientation of the wood fibers and the manner in which a tree increases in diameter as it grows, the properties vary along three axes: longitudinal, radial, and tangential (Figure 4.1). The radial and tangential directions are summed up as the direction perpendicular to grain.
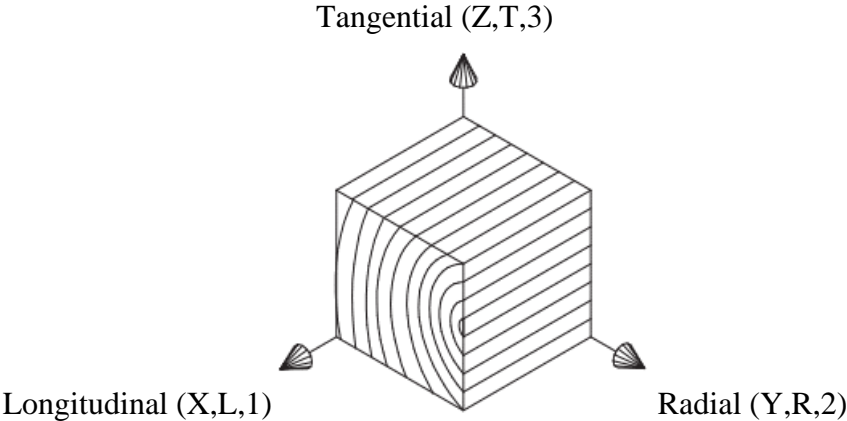
Figure 4. 1: Directions of wood fibers

In order to better understand the directions of the wood fibers, it is necessary to evaluate the mechanical properties of wood, which are the characteristics of material in response to external forces. These are mainly elastic properties, which characterize ductility and strength properties, which characterize resistance to applied loads.

a) Elastic properties: Wood is not an ideally elastic material; deformation does not recovered immediately after unloading; however, residual deformations are generally recoverable over a period of time. It is assumed to behave orthotropic elastic material and 12 constants are required to calculate: three moduli of elasticity (E), three moduli of rigidity (G), and six

Poisson's ratios (μ) (Winandy, 1994). Moduli of elasticity imply that deformations produced by low stress are completely recoverable after loads are removed. Under higher stress levels, plastic deformation or failure occurs. Modulus of elasticity relates the stress applied along one axis to the strain occurring on the same axis. The three moduli of elasticity for wood are denoted E_L, E_R, and E_T to indicate the elastic moduli in the longitudinal, radial, and tangential directions, respectively. The only constant that obtained from bending test results, is E_L. This value (E_L) can be used to determined E_R and E_T based on the elastic ratios for various species. When timber member is loaded axially, the deformation perpendicular to the direction of the load is proportional to the deformation parallel to the direction of the load. The ratio of the transverse to axial strain is called Poisson's ratio. The Poisson's ratios are denoted by μLR, μRL, μLT, μTL, μRT and μTR. The first letter of the subscript refers to direction of applied stress and the second letter to direction of lateral deformation.

The modulus of rigidity, also called shear modulus, indicates the resistance to deflection of a member caused by shear stresses. The three moduli of rigidity denoted by GLR, GLT, and GRT are the elastic constants in the LR, LT, and RT planes, respectively.

b) Strength properties: Strength properties imply the ultimate resistance of a material under loading: compression, tension, bending (flexural) and shear stresses. Generally, by considering all strength properties, wood has less strength value in perpendicular to grain compared to parallel to grain.

When compression is applied parallel to grain, vertical stress takes place by shortening wood cells along their longitudinal axis. Under compression parallel to grain, the failure initially starts when the microfibrils begin to fold within the cell wall, thus slipping occurs between the cells before buckling. Another possible failure under compression parallel to the grain is through pushing the cells into each other, so wood is shortened (Figure 4.2a). When compression is applied perpendicular to grain, stress shortens the wood cells perpendicular to their length, the bending of the horizontal cell walls is preceding the buckling of the vertical cell walls (Figure 4.2b). Timber under compression, beyond the elastic region, irreversible changes in the material can be seen. In other words, it behaves in a highly nonlinear way.

When timber loaded under compression, the response for the three main directions can be characterized by an initial elastic region, followed by a plateau region and finally a region of rapidly increasing stress. Compression in the tangential direction gives a smooth stress–strain curve which a rise softly throughout the plateau, whereas compression in the radial direction tends to give a slightly irregular stress plateau and to be characterized by a small drop in stress after the linear elastic region. Tangential and radial yield stresses are similar (Holmberg, 1999).

Yield stress in the longitudinal direction is considerably higher than that in radial and tangential directions and the plateau region (Figure 4.3). Under tension parallel to the grain, wood behaves really good. The brittle failure which occurs by a complex combination of two modes: cell-to-cell slippage and cell wall failure, can be also seen.

In contrast to tension parallel to grain, wood is relatively weak when loaded under tension perpendicular to the grain. Stresses in this direction act perpendicular to the cell lengths and produce splitting along the grain, which lead to significant effect on structural integrity. After a slight plastic deformation, the wood starts to split and a sudden drop in load carrying capacity occurs (Figure 4.3). The tensile strength perpendicular to grain is aprx. 1%-5% of the tensile strength parallel to grain (BS EN 338: 2009).

(a)   (b)
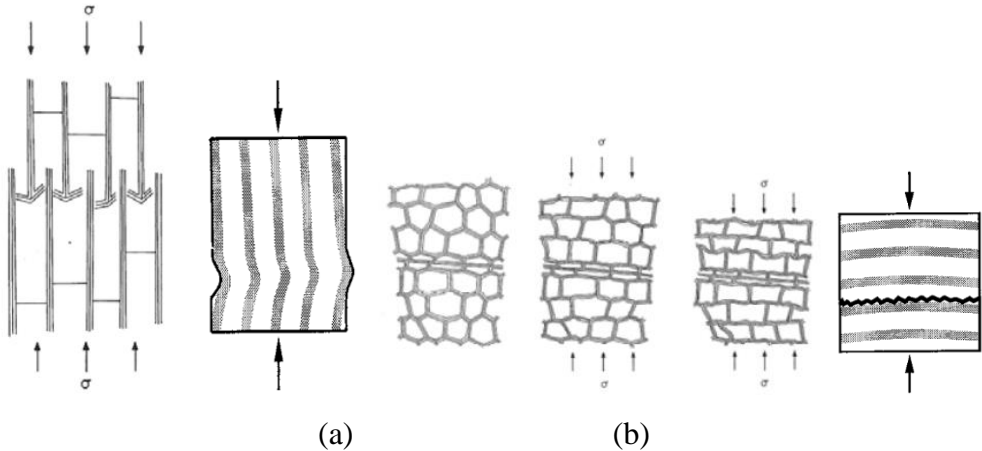
Figure 4. 2: Compression failure modes of the wood in parallel to grain (a) and perpendicular to the grain (b) (Gibson, 1997).
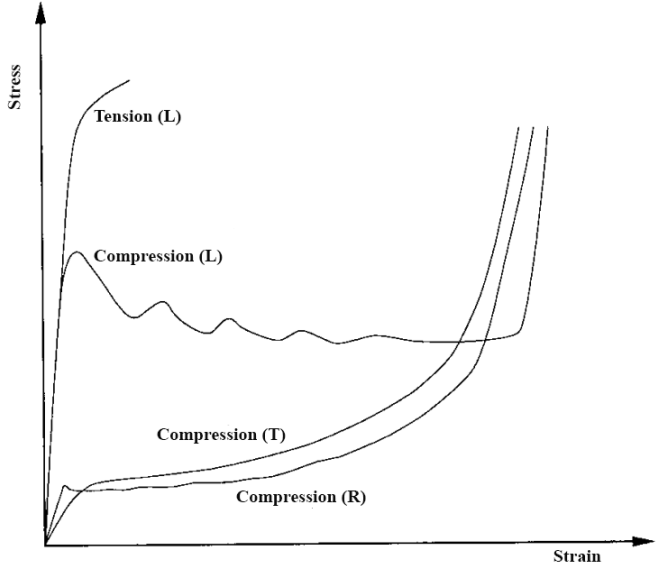
Figure 4. 3: Typical stress–strain curves for timber loaded in compression in the longitudinal, radial and tangential directions and for tension in the longitudinal direction (Holmberg, 1999).

Bending properties are critical, particularly when timber material is used as a beam. When a force applied to perpendicular the beam creates compression stress on this side and also creates tension stress in the extreme fibers on the opposite side. Thus, there is a tendency to compress the fibers in compression side and to elongate the fibers in the tension side. The stress distributed from the outside faces towards the center of neutral axis (American Wood Council, 1993). Due to tensile and compressive strengths parallel to grain are different from each other, the strength in bending is less than in tension but more than in compression. In other words, the weak part of the beam in bending loading, is tension side. There is also tendency to create shearing stress through the section of beam, when the timber beam exposed to bending loads. The largest shear stress usually occurs along the neutral axis on the plane at which the induced stress changes from compression to tension. Generally, shear failures are explosive brittle failures. The rolling shear stress was defined as the shear stress in the radial-tangential (RT) plane of wood which was perpendicular to the longitudinal grain direction. Besides, the strength and stiffness of shear in radial-tangential plane of wood is significantly lower than those of the longitudinal plane (Nie, 2015).

4.2 Timber Characterization Tests

Before carrying out the experimental timber joint tests, timber which has been used, has been analyzed in order to determine the mechanical properties of material. The tests were carried out at the Laboratory of Materials in Escuela Politécnica Superior de Edificación de Barcelona (EPSEB). The following are the results of laboratory tests performed on specific timber specimens subjected to compression and bending loads.

4.2.1. Compression parallel to the grain

The type of wood which has been used for specimens belongs to softwood species, namely pine. The size of timber specimens were manufactured according to the standard EN 408:2010. Thus, specimens shall be of full cross section, and shall have a length of 6 times the smaller cross-sectional dimension (Figure 4.4). A total of 3 specimens with 45x70 mm of cross section (bxl) and height 90 mm (h), were subjected under compression parallel to the grain (Figure 4.5). Before characterization, the moisture content of three specimens was accurately measured, approximately 9.9%, 10.1% and 9.7% respectively.
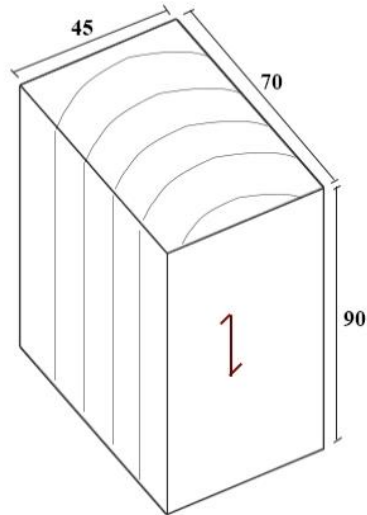
Figure 4. 4: The dimension of specimens for compression test parallel to the grain
(Dimensions are presented in mm)
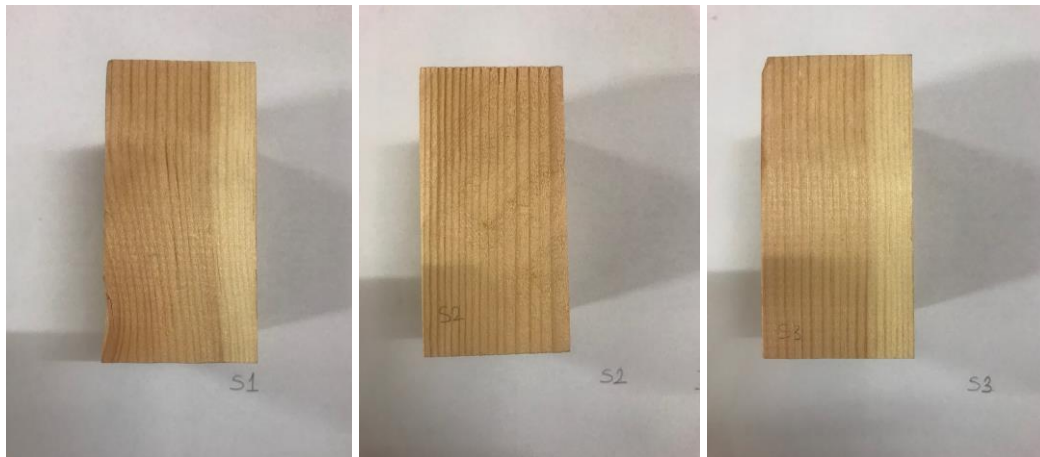
Figure 4. 5: Three specimens for compression test parallel to the grain

Experimental tests have been performed with an automatic press with maximum capacity of 300 kN and strain rate sensitivity about 0,01 mm.

According to EN 408:2010, load was applied at a constant loading-head movement so that the maximum load is reached within (300±120) s. The load was applied continuously with constant velocity 3kN/min until failure (Figure 4.6). Load and deformation were recorded in a computer and later stored as excel files.
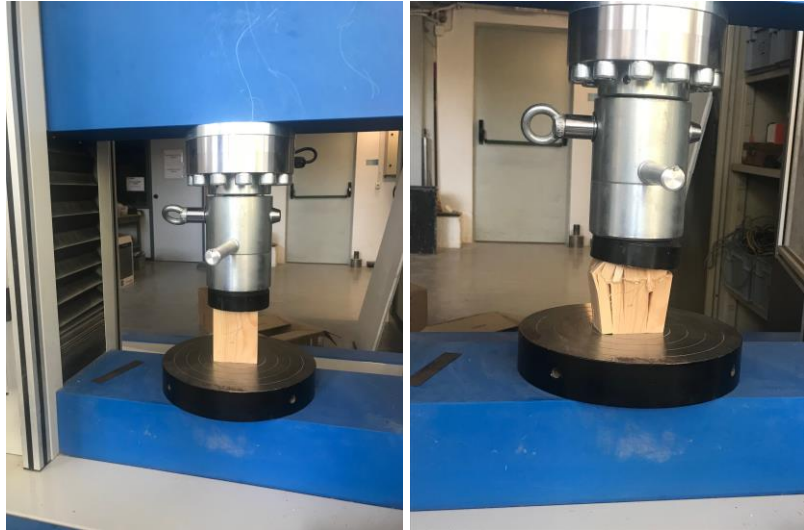
Figure 4. 6: Compression test parallel to the grain

Load-deformation curve for compression parallel to the grain for three specimens are given in Figure 4.7. The stress-strain behavior under compression parallel to the grain is characterized by a decrease after reaching the ultimate load. At the ultimate load, the weakest cell starts to collapse followed by the adjacent cells to guarantee that crushing band occurs. The collapse, which is a stability failure of the cell walls, leads to the loss of the load capacity of the cell. The load drops down to a level between 40 and 50% of the ultimate load. On average, the load slightly decreases in a ductile manner followed by a significant softening. Specimens 1 and 3 show less load capacity than specimen 2 due to the existence of knot in timber (Figure 4.7).
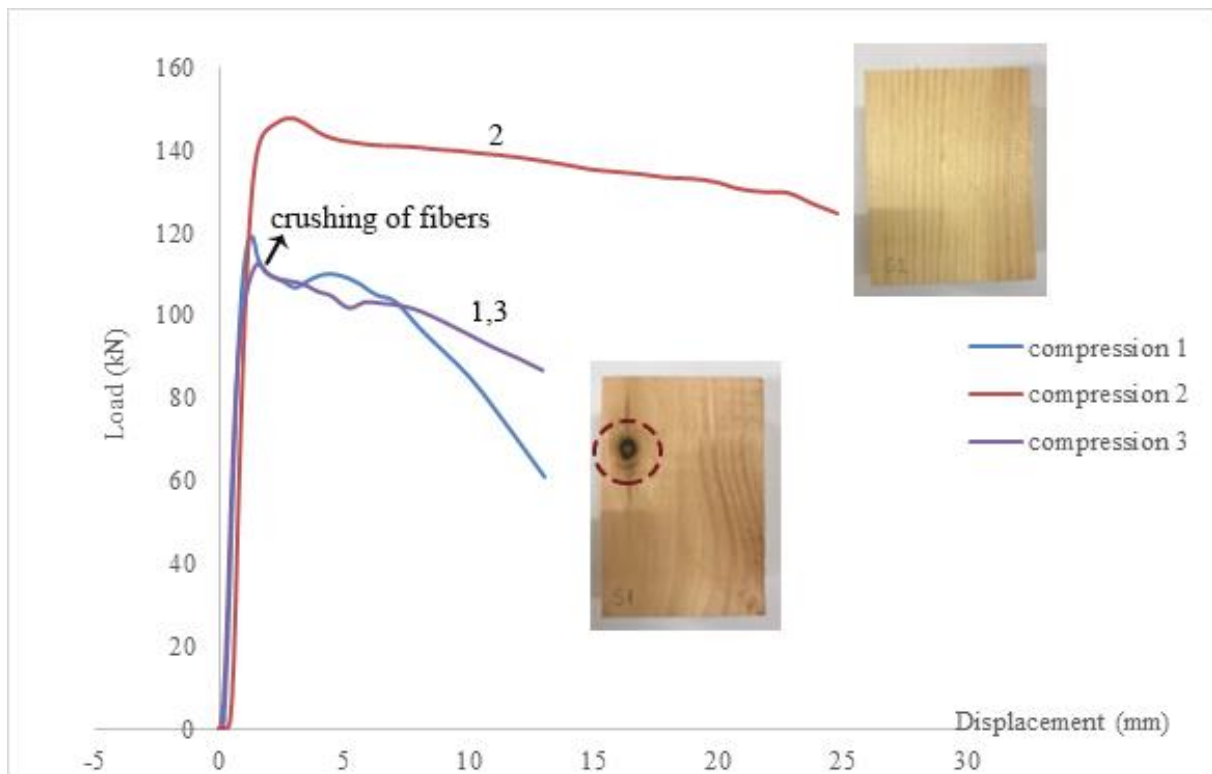
Figure 4. 7: Load-deformation curve for compression test parallel to the grain

In ASTM D143-14, compression failure patterns of wood were classified according to its shape as shown in Fig 4.8. The results of failure modes were evaluated with this standard.
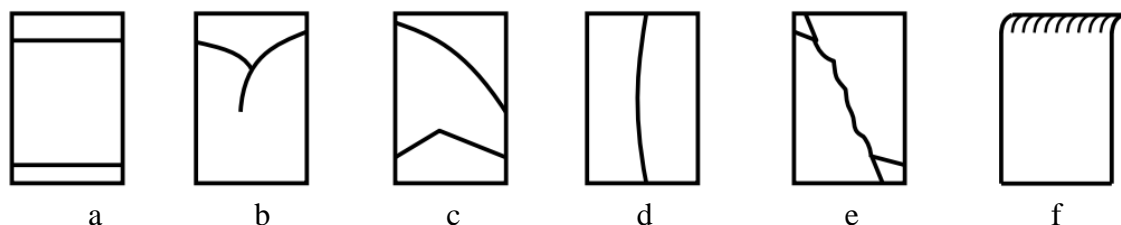
Figure 4. 8: Compression failure patterns, a) Crushing, b) Wedge split, c) Shearing d) Splitting, e) Compression and shear parallel grain, f) Brooming or end-rolling, (ASTM D143-14).

After tests, the failure patterns were examined based on the classification of failure patterns in standard ASTM D143-14. In the first and third specimens, ´crushing and oblique shearing´ can be detected, while in the second specimen ´crushing´ at end local is clearly seen. When the plane of rupture is horizontal, crushing occurred. Besides this, because of the initial eccentricity the plane rupture makes an angle of aprx. 45^0, the oblique shear formed in the middle of specimens-1 and 3 (Figure 4.9a-c). At the end of specimen-2 within 30mm, end local pressure

occurred and wood fibers were instable due to compression and a transverse fold formed in the specimen surface (Figure 4.9b).

a   b   c
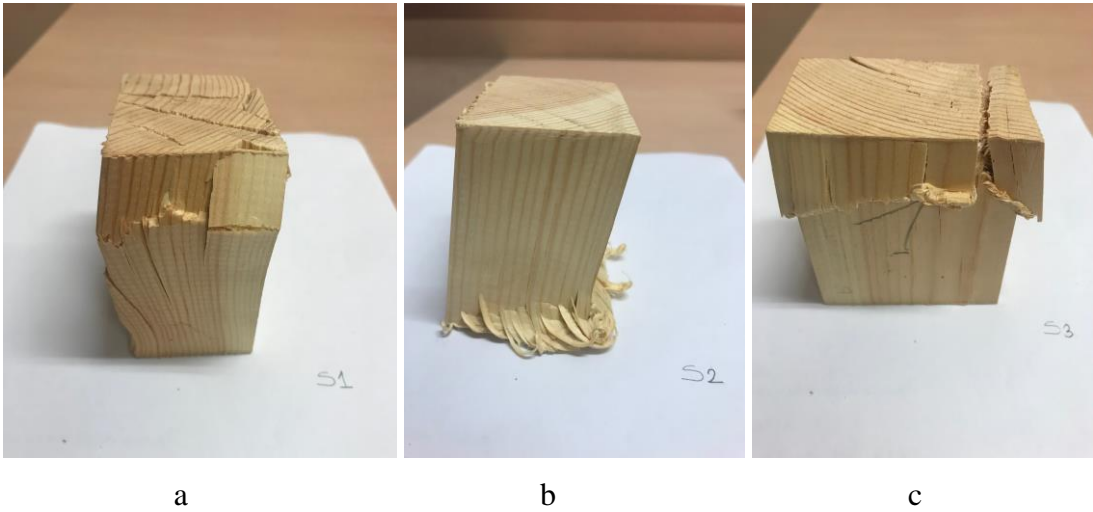
Figure 4. 9: The failure patterns of compression tests parallel to the grain

In order to determine the compressive strength of timber, the equation 4.1 from EN 408:2010 was used. The average compressive strength of three specimens was calculated as 39 N/mm².

$$f_{c,0} = \frac{F_{max}}{A} \qquad (4.1)$$

fc,0   compressive strength parallel to the grain, in newtons per square millimetre;

A cross-sectional area, in square millimetres;

$Fmax$ maximum load, in newtons

$$f_{c,0} = \frac{123kN * 1000}{45 * 70mm} = 39\,N/mm^2$$

4.2.2. Compression perpendicular to the grain

The dimensions of timber specimens have been considered according to Table 2 in standard EN 408:2010 (Figure 4.10). A total of 3 specimens with a cross section of 45x70 mm (bxl) and 90 mm height (h), have been subjected under compression test perpendicular to the grain (Figure 4.11). Before characterization, the moisture content of the three specimens has been accurately measured, approximately 10.5%, 10.3% and 9.5% respectively.
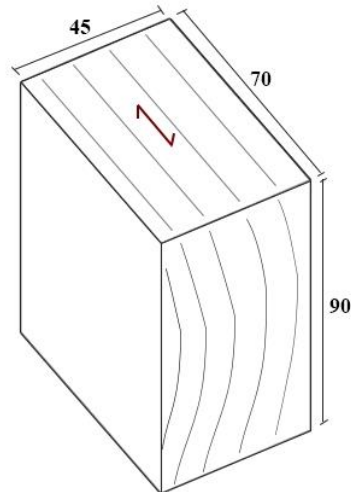
Figure 4. 10: The dimension of specimens for compression test perpendicular to the grain
(Dimensions are presented in mm)
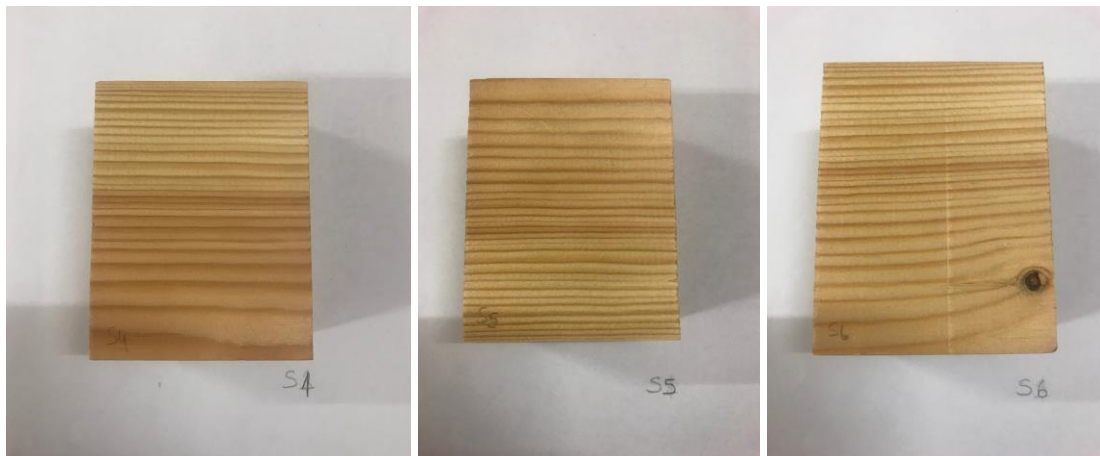
Figure 4. 11: Three specimens for compression test perpendicular to the grain

According to EN 408:2010, the load has been applied at a constant loading-head movement adjusted in order that maximum load is reached within (300±120) s. The load has been applied continuously with constant velocity 3kN/min until failure (Figure 4.12).

When a load is perpendicularly applied to the cells (grains), the thin walled tubes are affected laterally and become squeezed together with the increase of compression stresses, this leads to the collapse. This behavior continues until all the fibers are fully crushed. When all fibers are crushed together it is possible to once again increase the loads and it is difficult to define a failure level. Load-deformation curve for compression perpendicular to the grain for three specimens are given in Figure 4.13. Timber is markedly ductile with a continual increment of load after yielding and an additional hardening after 45 to 55% deformation. Specimen 3 shows less load capacity than specimens 1 and 2, due to the existence of a knot in timber (Figure 4.13).
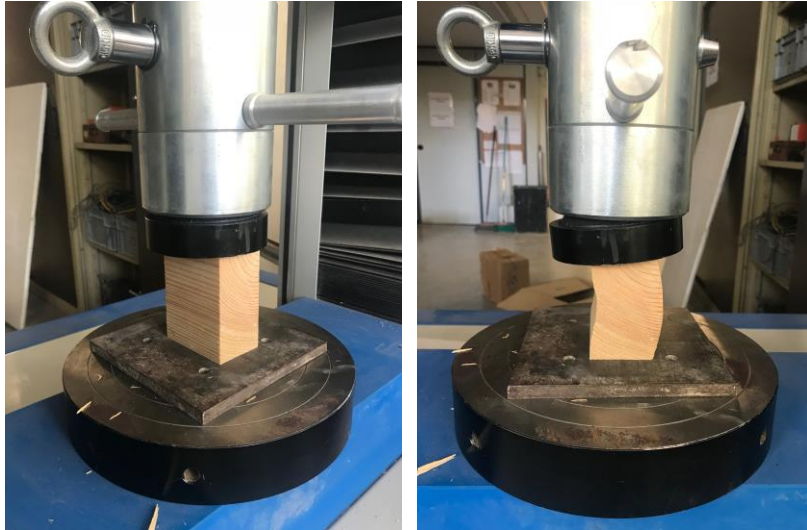
Figure 4. 12: Compression test perpendicular to the grain
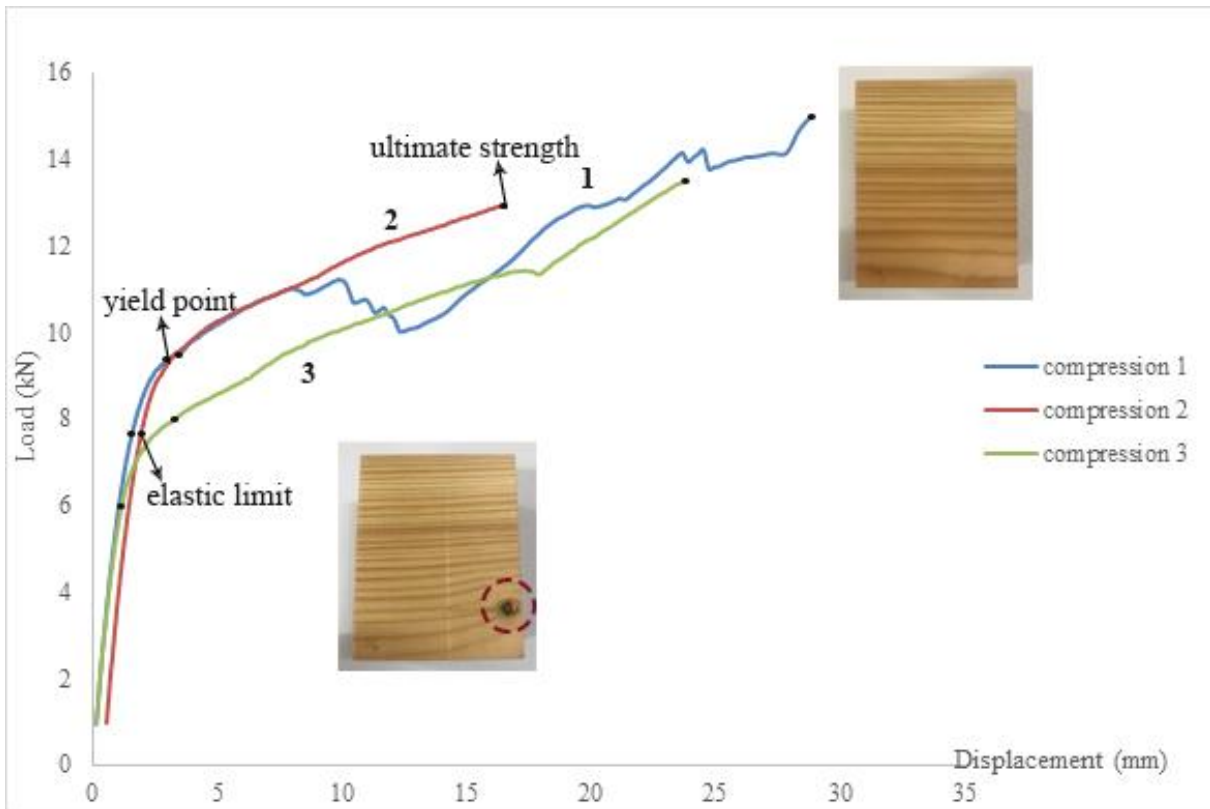
Figure 4. 13: Load-deformation curve for compression test perpendicular to the grain

It is important to note that the compressive strength in the direction perpendicular to the grain is less than 10% of the strength in the direction parallel to the grain.

After the tests, the failure patterns have been examined. In the first specimen, ´rolling shear´ can be detected, while in the second and third specimens, ´densification and buckling´ is

observed. When a load is applied perpendicular to annual rings, tend to buckle total by leading to rolling shear failure (Figure 4.14a) and also exhibits crushing of annual rings with corresponding densification (Figure 4.14b-c).

| a | b | c |
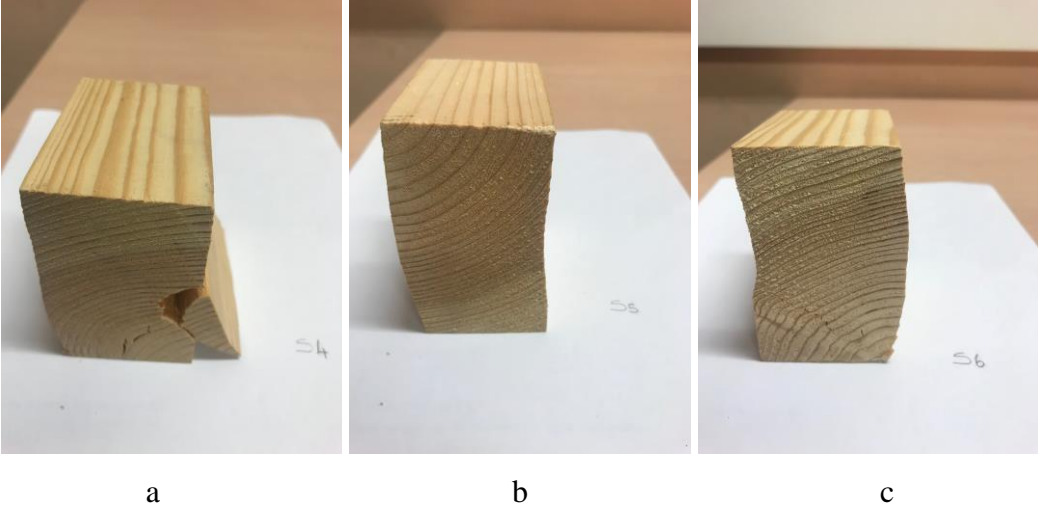
Figure 4. 14: The failure patterns of compression tests perpendicular to the grain

In order to calculate the compressive strength of timber , the equation 4.2 from EN 408:2010 has been used. The average compressive strength perpendicular to the grain of three specimens has been calculated as 4,12 N/mm² which is 9 times less than compressive strength parallel to the grain.

$$f90 = \frac{F_{max}}{A} \tag{4.2}$$

*f*c,90   compressive strength perpendicular to the grain, in newtons per square millimetre;

A   cross-sectional area, in square millimetres;

Fmax   maximum load, in newtons;

$$f90 = \frac{13kN * 1000}{45 * 70mm} = 4,12\,N\big/mm^2$$

4.2.3. Bending

To determine the local modulus of elasticity, global modulus of elasticity and static bending (flexural) strength of wood, four point bending tests have been carried out according to EN 408:2010. According to the standard, the specimen shall have a minimum length of 19 times the depth of the section. A total of 3 specimens were tested, with a cross section of 90 mm × 90 mm (b × h) and 1800 mm length (Figure 4.15). The specimen shall be symmetrically loaded under two bending points with a span of 18 times the depth as shown in configuration of experiment.
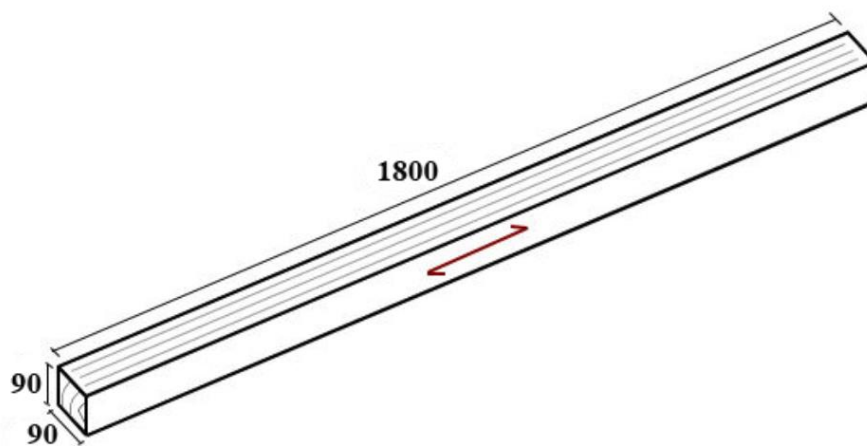
Figure 4. 15: The dimension of specimens for bending tests

(Dimensions are presented in mm)

The specimen has been simply supported. Small steel plates of length not greater than one-half of the depth of the specimen have been inserted between the piece and the loading heads or supports to minimize local indentation (Figure 4.16).
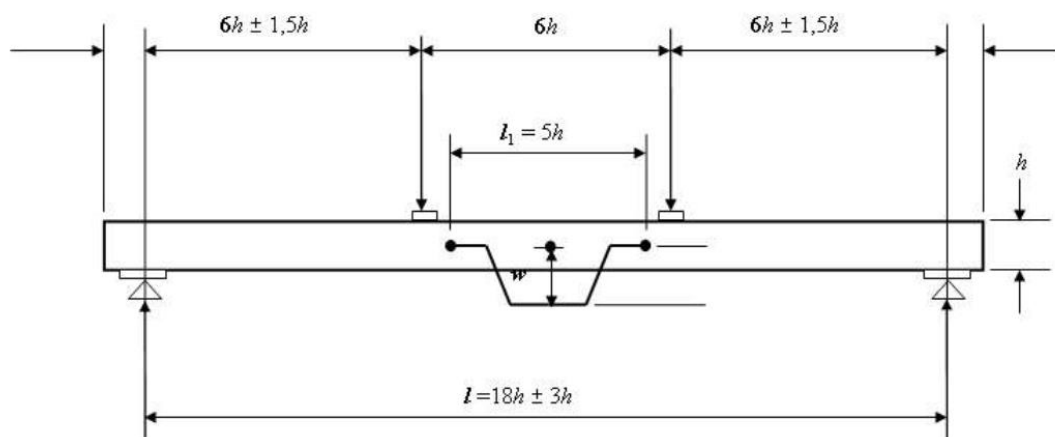
Figure 4. 16: Test arrangement for measuring local modulus of elasticity in bending

(EN 408).

Previously, in order to determine the local modulus of elasticity, timber beams have been subjected to four point flexural loading, by using a 1000 kN displacement control hydraulic jack. Constant velocity of load application was imposed to 12 mm/min. Two Linear Variable Differential Transformers (LVDT) having a resolution of 0.1 mm, were used for monitoring the vertical deflections at the mid-span under the mid points of two side faces of the beam (Figure 4.17). The deformation (*w*) shall be taken as the average of measurements on both side faces at the neutral axis and shall be measured at the centre of a central gauge length of five times the depth of the section. According to EN 408:2010, to determine the local modulus of elasticity, the maximum load applied shall not exceed 0,4 F_{max}. Besides, at the load/deformation graph within the range of elastic deformation, the section 0,1 F_{max} and 0,4 F_{max} is used for a regression analysis. In order to calculate the local modulus of elasticity, the equation 4.3 was used.

$$E_{m,l} = \frac{a * l^2 * (F2 - F1)}{16I * (W2 - W1)} \qquad (4.3)$$

Em,1   local modulus of elasticity, in newtons per square millimetres;

F2-F1   an increment load, in newtons on the regression line;

W2-W1   increment of deformation, in mm corressponding to *F2-F1*;

 a   distance between a loading position and the nearest support, in millimetres;

l   length (aprx. 5h) for the determination of modulus of elasticity, in millimetres;

I   moment of inertia, in millimetres to the fourth.

The load-deformation graph has been obtained from test results (Figure 4.18). The regression line has been obtained between 0.1 Fmax- 0.4 Fmax loads and the deformations corresponding to them. The regression value was calculated with 988,96 N/mm from diagram, hereby the average local modulus of elasticity of three specimens has been calculated as 1236,2 N/mm^2.

$$E_{m,l} = \frac{540 * 450^2 * 988,96}{16 * 5467500} = 1236,2\,N\!/mm^2$$

Figure 4. 17: The test set up for measuring local modulus of elasticity in bending
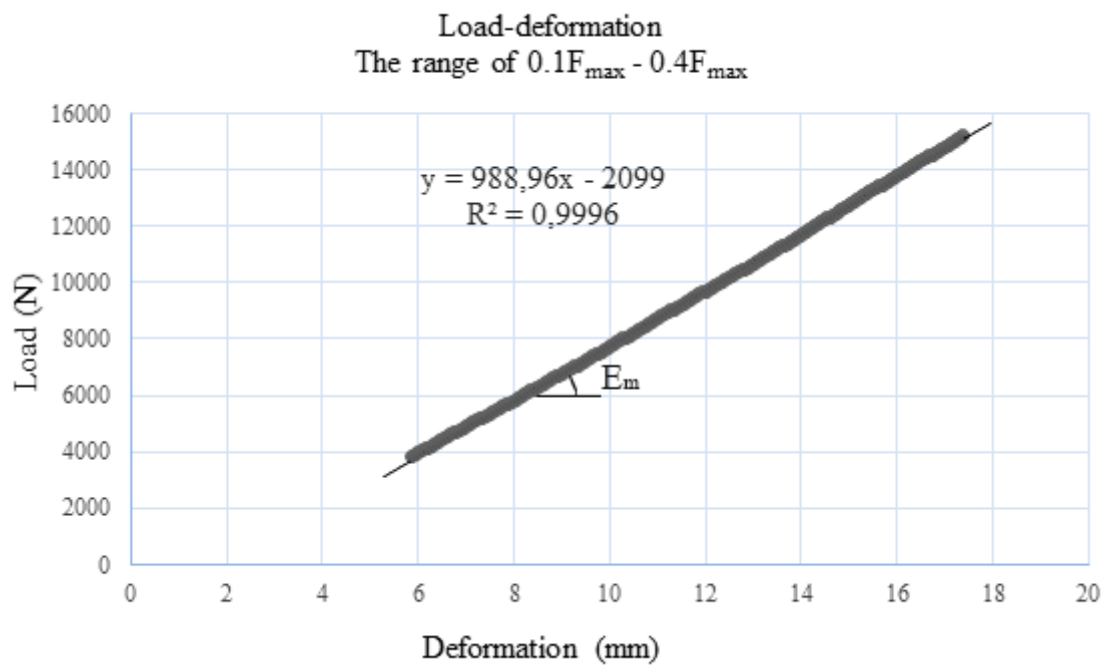
Figure 4. 18: Load-deformation curve for the range of 0.1 F_{max}-0.4 F_{max}

Secondly, in order to determine the global modulus of elasticity, same specimens have been subjected to four point flexural loading until the failure. According to standards, the test piece shall be symmetrically loaded in bending at two points over a span of 18 times the depth (Figure 4.19-4.20). The test set up is the same as the local modulus of elasticity test, except of the position of measurement. The deformation was measured at the centre of the span and from the centre of the tension edge (Figure 4.21). Constant velocity of load application has been imposed to 12 mm/min.
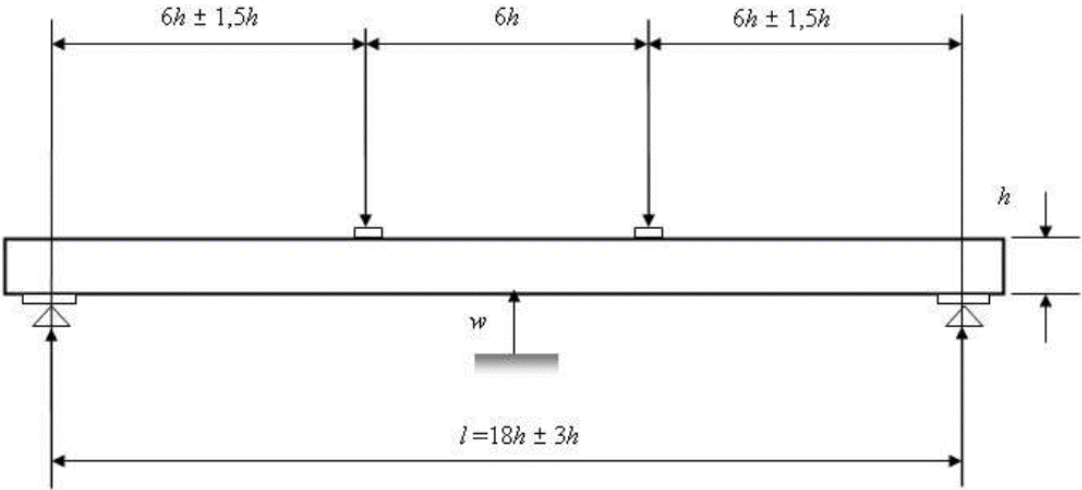
Figure 4. 19: Test arrangement for measuring global modulus of elasticity in bending (EN 408)
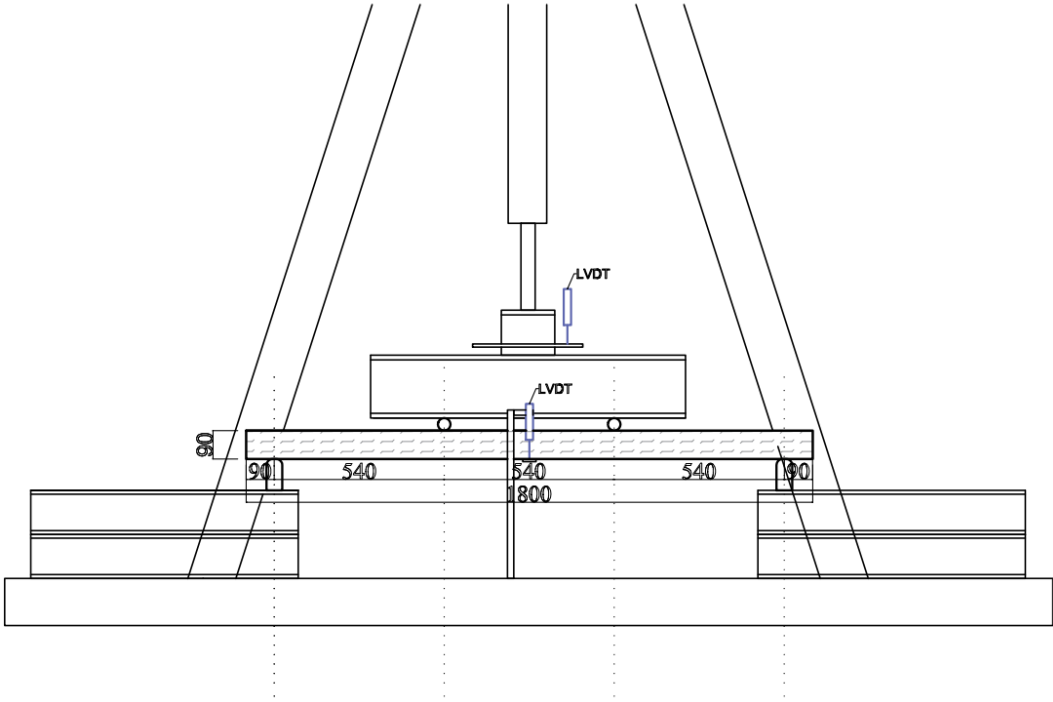
Figure 4. 20: The configuration of bending tests (Dimensions are presented in mm)

Figure 4. 21: The test set up for measuring global modulus of elasticity in bending

The load-deformation graph was obtained from test results (Figure 4.22). The obtained diagram mainly consists in three principal phases: A first phase with an initial linear elastic behaviour followed by a second phase of nonlinear behaviour in which the maximum loading is reached. It can be seen the upper surface starts to crush while the lower part starts to crack. In the last phase, a reduction of the load which is applied, is observed until the total rupture of the specimens. The strain is at an important rate when the failure occurs.

The slope of the linear part of the curves is defining the bending stiffness; the higher slope is the higher bending stiffness. Ultimate load-bearing capacity is defined by the load at which the curve turns into horizontal. Specimen 2 shows the smallest bending stiffness and load-bearing capacity than other specimens due to the existence of knot. Knot led to reduce the properties of timber.

Besides, in order to calculate the global modulus of elasticity, the equation 4.4 has been used.

$$Em, g = \frac{3al^2 - 4a^3}{2bh^3 * \left(2\dfrac{W2 - W1}{F2 - F1} - \dfrac{6a}{5Gbh}\right)} \tag{4.4}$$

Em,g   global modulus of elasticity, in newtons per square millimetre;

F2-F1   an increment load in newtons on the regression line;

W2-W1   increment of deformation in mm corresponding to *F2-F1*.

G   shear modulus, in newtons per square millimetre.

$$Em, g = \frac{3*540*450^2 - 4*540^3}{2*90*90^3 * \left(2\dfrac{1}{988,96} - \dfrac{6*540}{5*650*90*90}\right)} = 13647,648\,N/mm^2$$
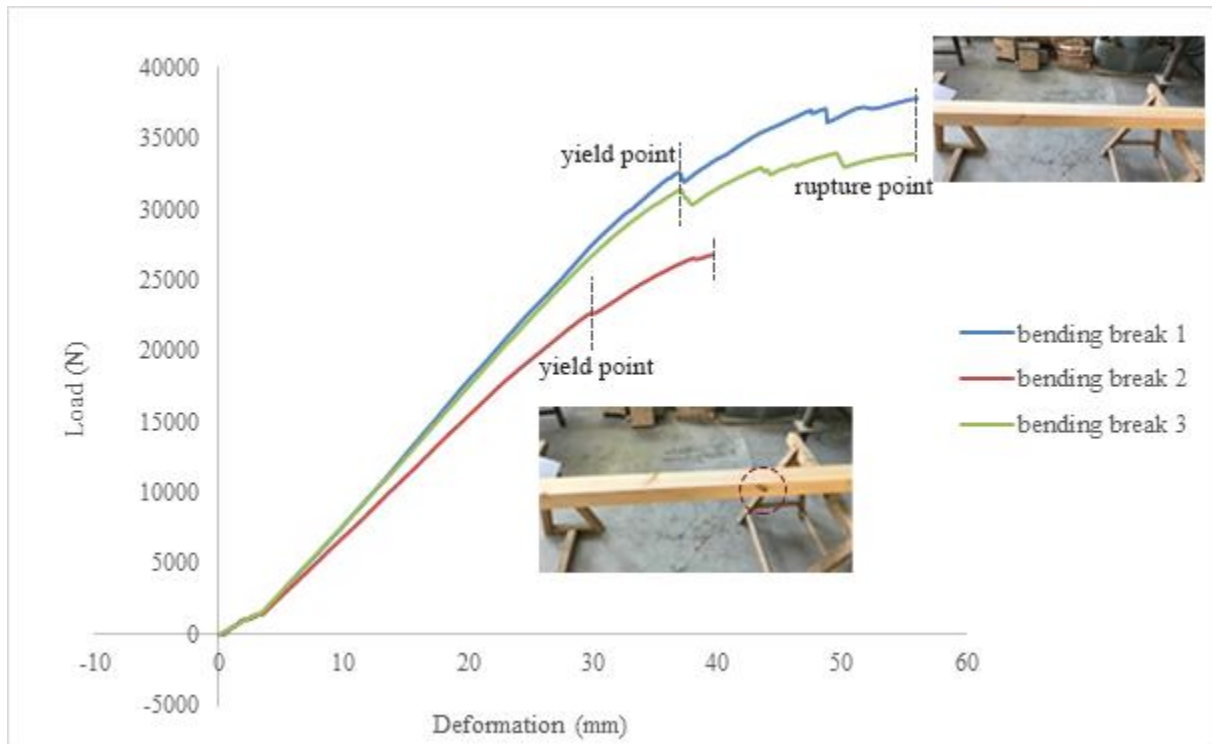
Figure 4. 22: Load-deformation curve for bending test

For the 3 specimens, the average ultimate load which has been obtained, is around 32000 N. In order to calculate the bending strength, the equation 4.5 has been used.

$$f_m = \frac{3Fa}{bh^2} \tag{4.5}$$

53

*f*m	bending strength, in newtons per square millimetre;
F	load, in newtons;
a	distance between loading position and the nearest support, in millimetres,
b	width of cross section, in millimetres,
h	depth of cross section, in millimetres.

$$f_m = \frac{3*32840*540}{90*90^2} = 72,97 \; N/mm^2$$

In ASTM D143-14, bending failure patterns of wood are classified according to its shape as shown in Fig 4.23. The analysis of the failure modes have been evaluated with according to standard.
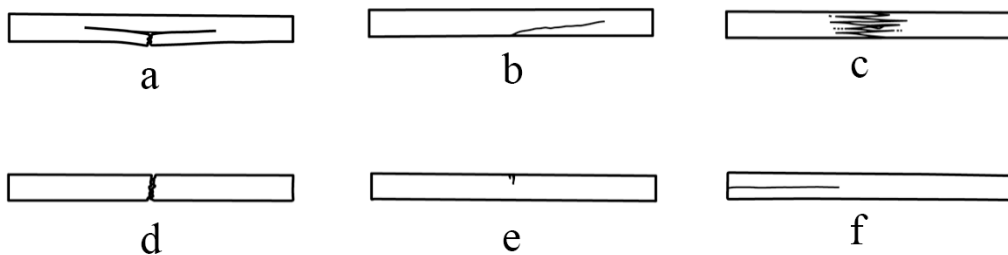
Figure 4. 23: Compression failure patterns a) Simple tension, b) Cross grain tension, c) Splintering tension, d) Brash tension, e) Compression, f) Horizontal shear (ASTM D143-14)

After carrying out the tests, the failure patterns have been examined based on the classification of ASTM D143-14. In the first and third specimens, ´simple tension failure´ can be detected, while in the second specimen ´cross grain tension and compression failure´ can be clearly seen (Figure 4.24-26). Timber beam was deformed due to bending, particularly in the middle of the span. In all of 3 specimens, the cracks were detected in the tension side. In addition, shear cracks were detected around a knot in the second specimen (Figure 4.25).

Figure 4. 24: The failure pattern of first specimen under bending

Figure 4. 25: The failure pattern of second specimen under bending
due to the influence of having knot

Figure 4. 26: The failure pattern of third specimen under bending

4.2.4. Discussion of test resuts

The characterization test results show that timber beams tend to fail in a sudden such as experienced under bending, tensile or buckling failures. This is mainly due to the brittle behaviour of wood under tension parallel to the grain, tension perpendicular to the grain and shear. Only compressive failure exhibits large plastifications, by allowing sustained load over an extended deformation range. This effect provides ductility which is beneficial for structures, which may experience more deformations. Mechanical properties of selected timber, which is pine, are given from the test results (Table 4.1).

Table 4. 1: The mechanical properties of timber from experiment results

Density (ρ)	500 kg/m^3
Compressive strength parallel to grain (fc,0)	39 N/mm^2
Compressive strength perpendicular to grain (fc,90)	4,12 N/mm^2
Bending strength (fm)	72,97 N/mm^2
Global modulus of elasticity (Em,g)	13647,648 N/mm^2

4.3 Lap Joint Tests

A set of monotonic tests of unreinforced specimens have been performed in order to describe the behaviour of lap joints which is used for beam-beam connections in Turkish timber house (The details are given in part 2.2). Subsequently, joints locally strengthened with carbon fiber textile have been tested under monotonic and cyclic loadings. The purpose of these tests is to increase the flexural strength and load-bearing capacity of the joint. Besides, carbon fiber textile may prevent the premature seperation of components of the joint under loading.

4.3.1. Monotonic tests on unreinforced specimens

To determine the load-deformation behaviour of lap joint under monotonic loading, four point bending tests have been carried out according to BS EN 26891 (Timber structures- Joints made with mechanical fasteners- General principles for the determination of strength and deformation characteristics). A total of 2 lap joint specimens have been tested, by using the dimensions of 90 mm × 90 mm in cross-section (b × h) and 1800 mm length (Figure 4.27). Two screws with dimensions of Ø4.5 mmx h:80 mm have been used for connection introduced with an angle of 45^0 angles (Figure 4.27). In table 4.2, the specimens are abbreviated with codes. In the code, ´LP` shows the type of joint, such as; lap joint. Besides, ´M` and ´C` indicate monotonic and cyclic loads. Following, the three specimens are shown as ´A`, ´B` and ´C`. Last letter ´R` in the code indicates that CFRP reinforcement exists on the specimen. The specimens have been loaded under two point bending over a span of 18 times the depth according to the loading procedure in standard (Figure 4.28)
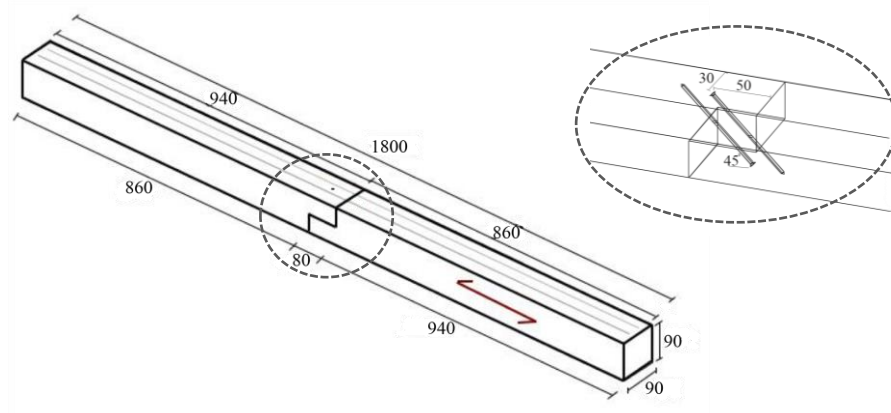
Figure 4. 27: Dimensions of specimens in monotonic tests
(Dimensions are presented in mm)

57

Table 4. 2: The codes of specimens for tests

Codes	Height (cm)	Width (cm)	Length (cm)	Bending Strength (MPa)	Reinforcement with CFRP
LJM1800A	90	90	1800	72	-
LJM1800B	90	90	1800	72	-
LJM1800AR	90	90	1800	72	+
LJM1800BR	90	90	1800	72	+
LJC1800AR	90	90	1800	72	+
LJC1800BR	90	90	1800	72	+
LJC1800CR	90	90	1800	72	+

Monotonic load   type of specimen (A, B, C)

LJM1800AR —reinforcement

Lap joint   length
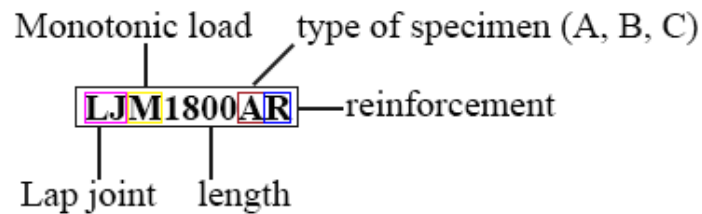
Two LVDT with sensitivity of 0.1 mm, have been used for monitoring the vertical deflections at mid-span under the mid points of two side faces of the beam. The load has been distributed in 2 points with two cylinders of a diameter of Ø4 mm. At the same time, two metal semicylinders at the supports have been used.

The loading procedure of test has been obtained from BS EN 26891:1991 (Figure 4.29). According to the standard, the load is applied up to 0,4 Fest and maintained for 30 s. Then the load is reduced to 0,1 Fest and maintained for 30 s. Thereafter, the load is increased until the ultimate load. The test is stopped when the ultimate load is reached. Following, the estimated maximum load, Fest, 1000 N has been taken on the basis of previous bending experiments. The load has been applied up to 0.4 Fest, which corresponds to 400 N, maintaned for 30 sec. Then, the load has been reduced to 0.1 Fest, which corresponds to 100 N, maintaned for 30 sec at this value. Thereafter, the load has been increased until the ultimate load (Figure 4.29). Constant velocity of load application has been imposed to 10 mm/min.

Figure 4. 28: The set up for monotonic test
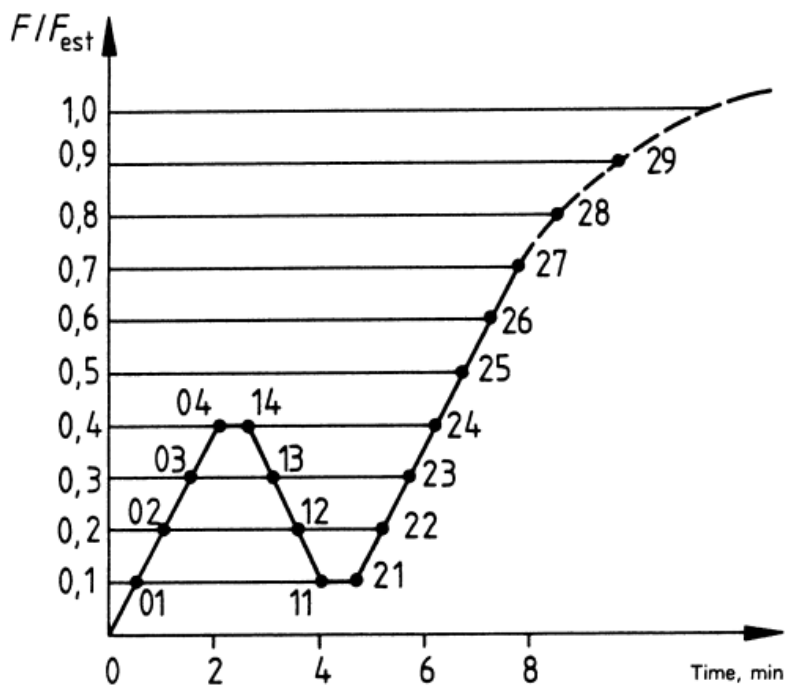
Figure 4. 29: The loading procedure of monotonic test (BS EN 26891:1991)

When the timber beam deforms under bending, the deformation has been caused by moment and changing geometry (Figure 4.30). In addition to tensile and compressive stresses, shear also take place. The deformation is a result of normal and shear stresses in the beam cross section. The load-deformation diagram has been obtained directly from test results (Figure 4.31).

The curves which are presented in Figure 4.31 show a quite elastic behaviour until the maximum strength; this point when a slip occurs, there is loss of friction by inducing a rapid decrease of resistance. Thus, the brittle behaviour is followed by an inelastic phase. Finally, a total loss of friction occurs with the failure of the connection. The screws have bent under stresses and at the same time have been pulled out from the wood.

By comparing the force-displacement curves obtained from the two tests of specimens, under the same loading conditions, only an increment of the maximum force and corresponding elastic limit displacement can be pointed out (Figure 4.31). Regarding the stiffness, it remains constant and similar in both cases. The yield point after the elastic limit for the first specimen (LJM1800A) is higher than for the second specimen (LJM1800B). Second specimen ((LJM1800B) shows more ductile behaviour due to local compression of wood and the behavioral difference of screws. Screws pressed the timber locally and finally has led to 23% less load-bearing capacity than in specimen 1 (LJM1800A).

The mode of failure of joints with screw connectors has been relatively brittle; the brittleness of the failure mode becomes evident due to the sudden drop of the load after the peak load. The failure mode in specimens with screws has been associated with localised crushing of the timber and bending of the screws. The components of joint have separated in tension zone of timber with a depth of approximately 5 mm (Figure 4.32).
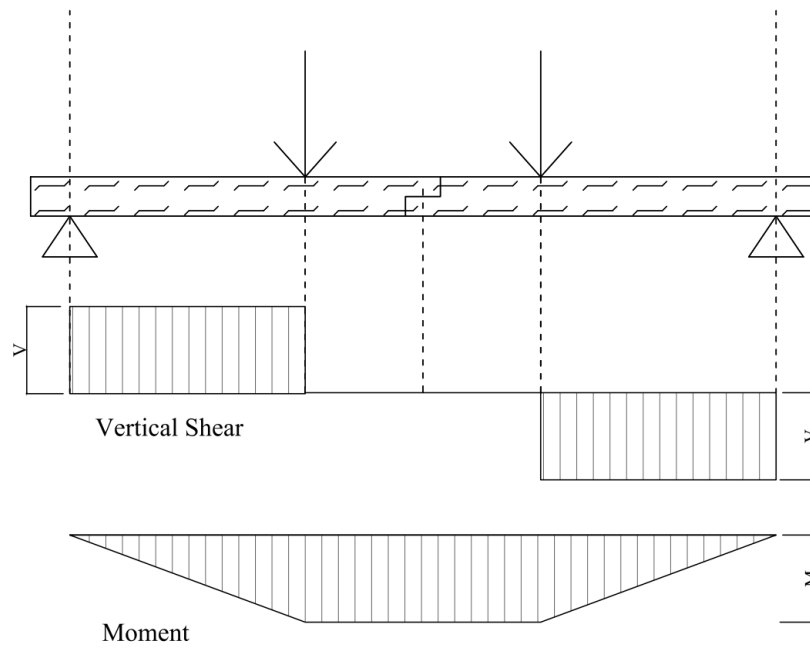
Figure 4. 30: Distribution of stress of bending test under monotonic load
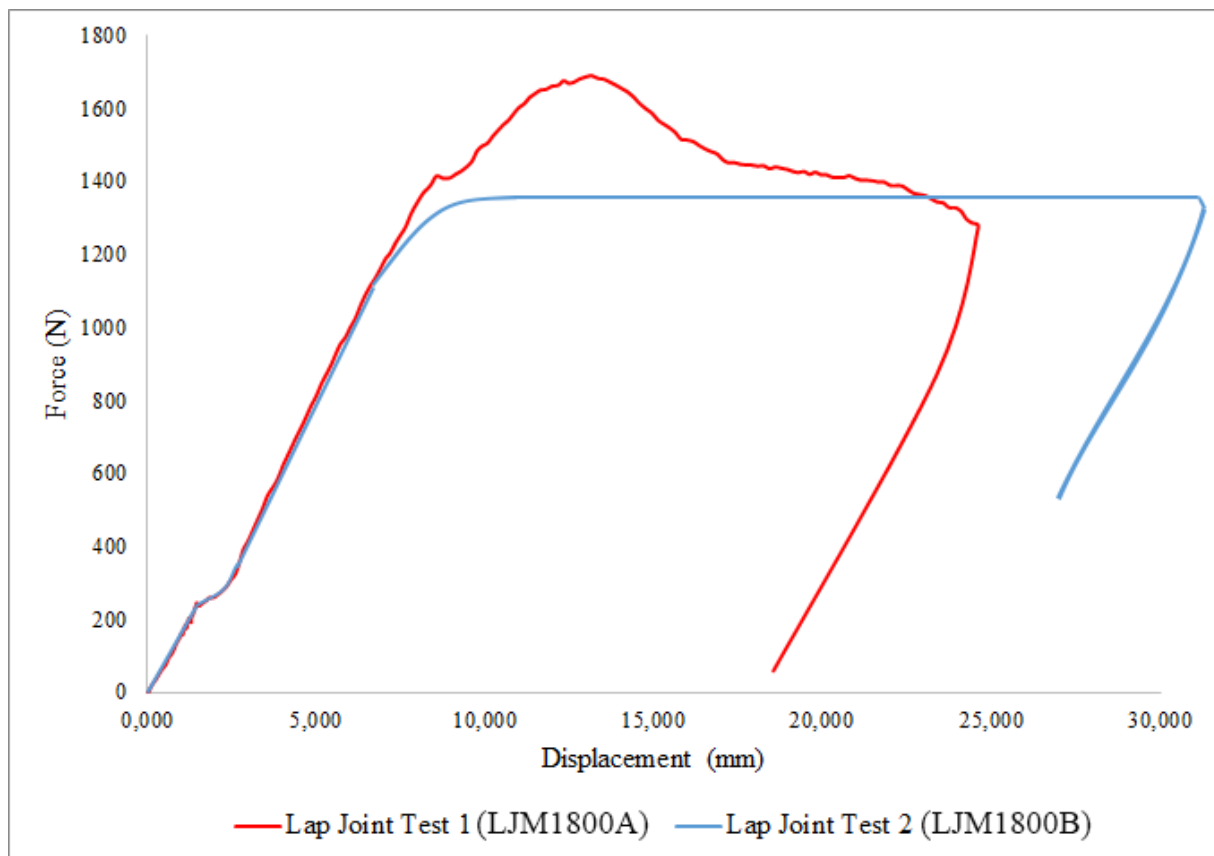
Figure 4. 31: Load-deformation curve of monotonic tests

Figure 4. 32: The failure pattern of two specimens under monotonic loading

4.3.2. Monotonic tests on reinforced specimens

A total of 2 lap joint specimens, with dimensions of 90 mm × 90 mm of cross-section (b × h) and 1800 mm length, have been reinforced with undirectional carbon fiber textile. High strength carbon fiber textile has been wrapped all around the timber specimen, as 400 mm wideness (Figure 4.33). It has been bonded parallel to the longitudinal direction of the beam in one layer with two component epoxy. The epoxy, named MasterBrace P 3500, is composed by two parts A (resin) and B (hardener). The mix ratio is 3:1 (Part A to Part B) by volume. Each component were carefully measured and then added part B (hardener) to part A (resin) (Figure 4.34). Technical data of carbon fiber textile and epoxy are given in Table 4.2 and 4.3.

Firstly, the initial resin coat with a thickness of 1 mm has been applied with a brush. Subsequently, the unidirectional CFRP fabric reinforcement with a thickness of 5 mm has been placed parallel to the longitudinal direction of the beam and finally a finishing layer of the same epoxy resin with a thickness 1 mm has been applied again (Figure 4.35). The curing time is 48 hours.
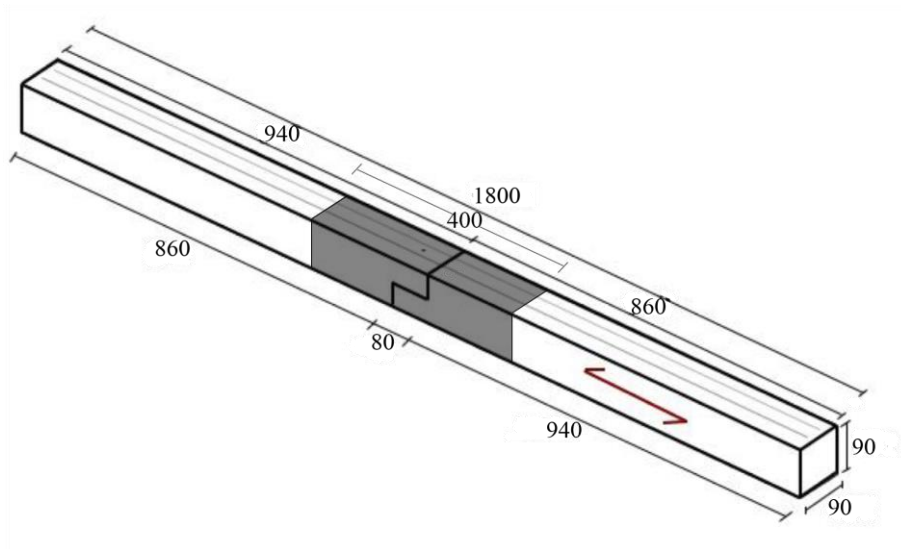
Figure 4. 33: Dimensions of reinforced specimens in monotonic test
(Dimensions are presented in mm)

Figure 4. 34: The selected epoxy and carbon fiber textile for reinforcement

Table 4. 3: The technical data of carbon fiber textile (Ticem)

Property	Average value	ASTM test method
Tensile strength	630 MPa	D3039
Tensile modulus	42000 MPa	D3039
Elongation at break	1.5 %	D3039
Nominal layer thickness	0,5 mm	-

Table 4. 4: The technical data of epoxy (BASF)

Property	Average value	ASTM test method
Adhesion strength on carbon	2.87 MPa	D4541:95e1
Tensile strength	35 MPa	D638:00
Tension strain at yield	2.0 %	D638:00
Tension elastic modulus	717 MPa	D638:00
Flexural strength	24.1 MPa	D790:01
Flexural modulus	595 MPa	D790:01
Compressive strength	28.3 MPa	D695:96
Compressive modulus	670 MPa	D695:96

Figure 4. 35: General view of reinforced specimens for monotonic test

Timber reinforced specimens have been subjected to four point flexural loading, using a 1000 kN displacement control hydraulic jack. Two LVDT with a sensitivity of 0.1 mm, have been mounted for monitoring the vertical deflections at the mid-span under the mid points of two side faces of the beam (Figure 4.36). The loading steps were similar to monotonic tests on unreinforced specimens. The estimated maximum load, Fest, 1000 N has been taken on the

basis of previous bending experiments. The load has been applied up to 0.4 *F*est, which corresponds to 400 N, maintaned for 30 sec. Then, the load has been reduced to 0.1 *F*est, which corresponds to 100 N, maintaned for 30 sec at this value. Thereafter the load was increased until the ultimate load. Constant velocity in the load application has been imposed to 10 mm/min.
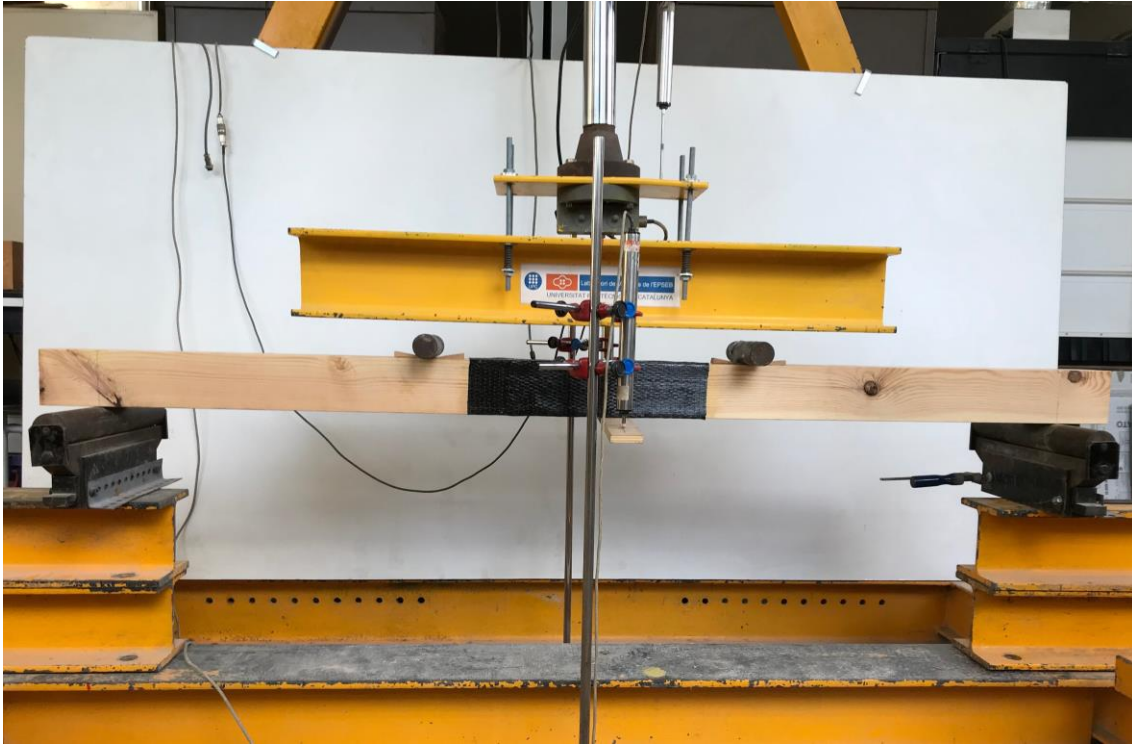
Figure 4. 36: General view of the set up for monotonic test on reinforced specimen

The load-deformation diagram has been obtained from test results (Figure 4.37). The curves show that beam exhibited more essentially linear elastic behaviour up to the failure. The averaged maximum force is approximately 9 times more than in the unreinforced specimen. After a loss of friction, a rapid decrease of the resistance takes place. Thus, the brittle behaviour is replaced by an inelastic phase. Finally, a total loss of friction occurs with the general failure of the connection. Carbon fiber textile reinforced beams revealed less ductile behavior compared to the un-reinforced beams. The CFRP reinforcement derived into a global increment of the maximum load at failure, from 1400 N to 13000 N, which represents an increase of 830 percent.

It should be noticed that the rupture of the strengthened timber beams occurred due to the first crack of the solid timber in the tensile region. Failure has been initiated at the joint in tension zone due to screw buckling. Even though the components of the joint have been separated in tension zone, the joint still resisted to the increment of load by means of high tensile strength

of carbon fiber textile. When the specimen has reached the peak of load, the complete failure has occurred. Carbon fiber textile has separated from the timber surface (Figure 4.37-4.38). In addition, crack has been formed as horizontal in the first specimen (LJM1800AR) due to shear stress (Figure 4.38).
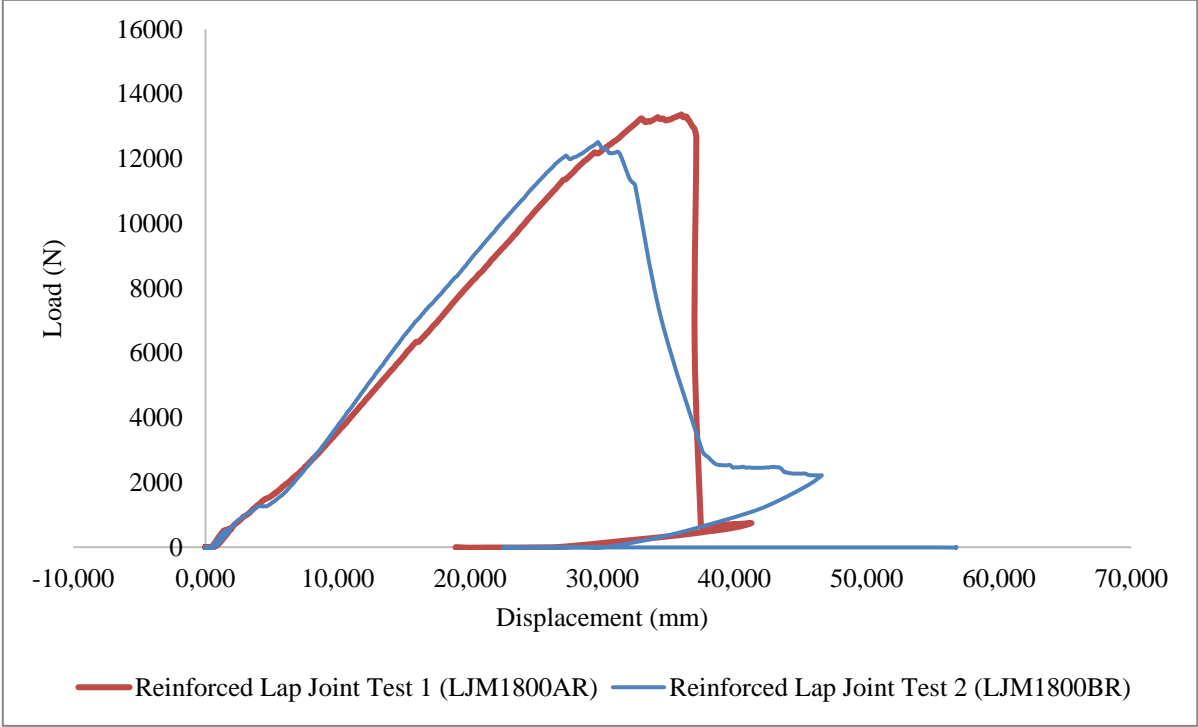
Figure 4. 37: Load-deformation curve of monotonic tests on reinforced specimens

Figure 4. 38: Failure pattern of reinforced specimen (LJM1800AR) under monotonic loading
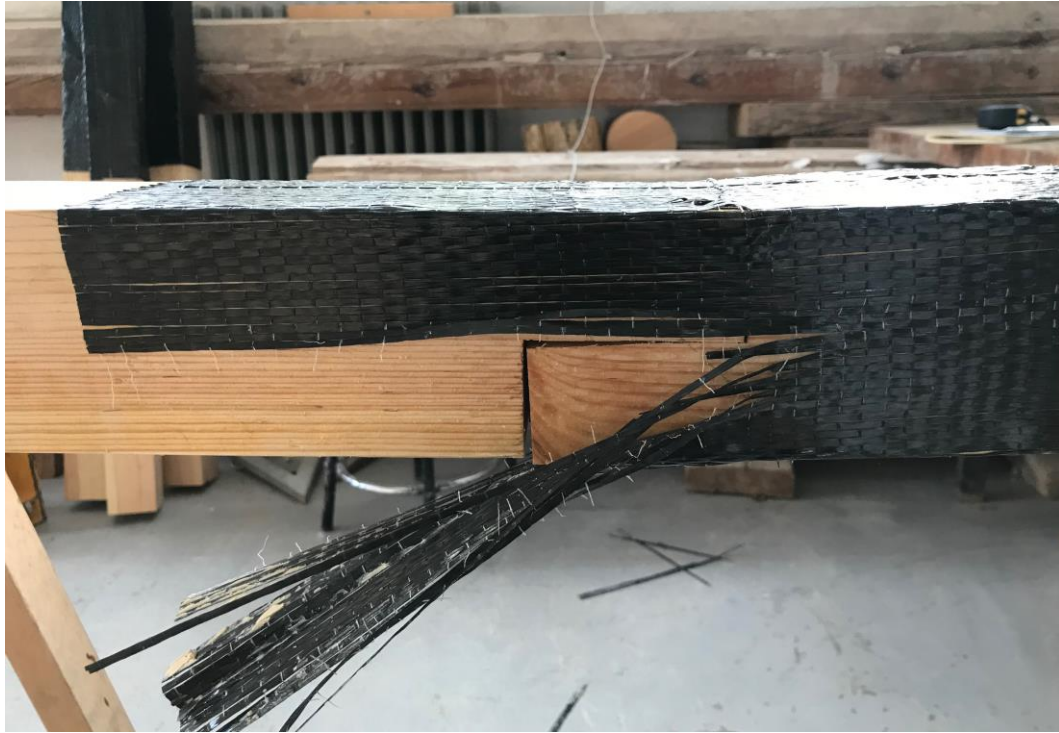
Figure 4. 39: The failure pattern of second reinforced specimen (LJM1800BR) under monotonic loading

4.3.3. Cyclic tests of reinforced specimens

A total of 3 lap joint specimens, with the same dimensions of 90 mm × 90 mm of cross-section (b × h) and 1800 mm length, reinforced with undirectional carbon fiber textile have been subjected to unidirectional cyclic vertical loads. Two LVDT with a resolution of 0.1 mm, have been used for monitoring vertical deflections at mid-span under the mid points of two side faces of the beam (Figure 4.40).

The loading protocol given in `BS EN 12512:2001 Timber structures-Test methods-Cyclic testing of joints made with mechanical fasteners` was used for displacement controlled unidirectional cyclic tests (4.41). Estimated yield slip has been determined as Vy=32 mm from monotonic tests and target displacements have been calculated by using this value (Table 4.4). First two target displacements have been applied in one cycle only. Further target displacements have been applied in three different cycles.

Firstly, in the 1st cycle, the load has been compression, until a slip of 25% of the estimated yield slip Vy. The value of maximum displacement has been taken from the previous monotonic tests on lap joints and estimated yield slip was determined as Vy=32 mm. Then, the specimen has been unloaded. At 2nd cycle, the load has been applied in compression until reading a slip

of 50% of Vy and it has been unloaded to zero-slip. At 3th, 4th, 5th cycles, the specimen has been loaded in compression until reading a slip of 75% of Vy. In the following set of three next cycles, the load has been applied in three different steps, 100% and 200% of Vy. The load-displacement diagram of the specimen is given in Figure (4.42).
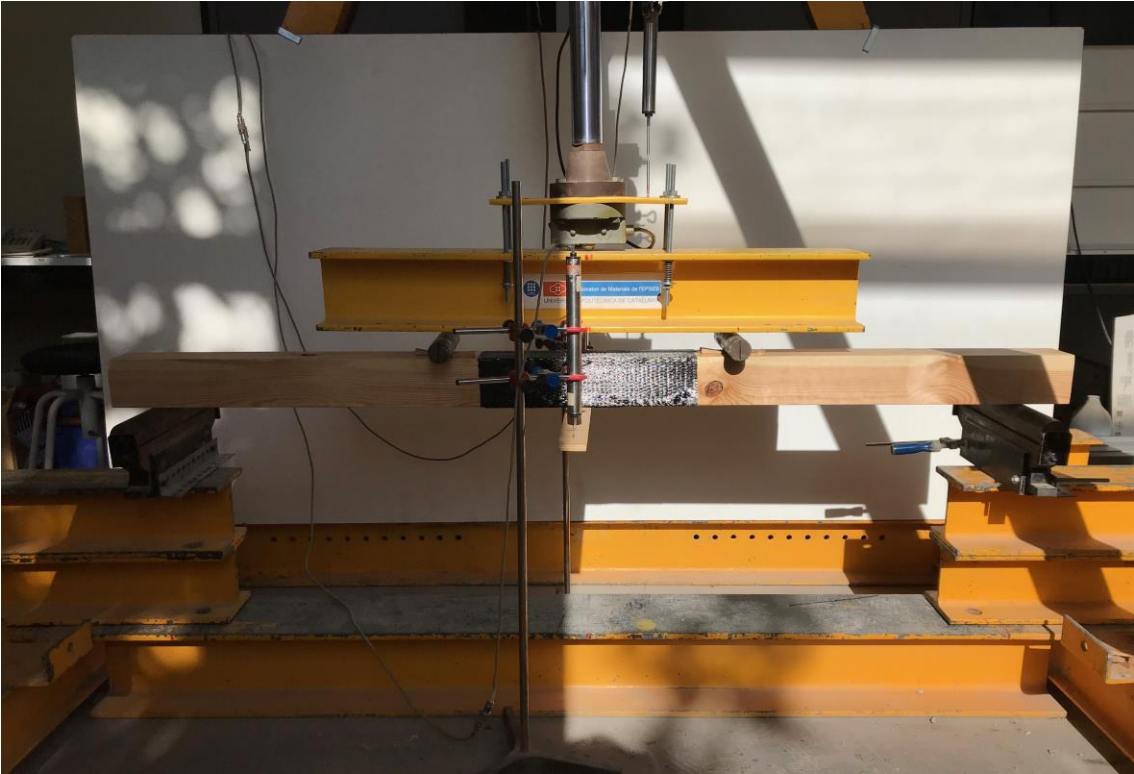
Figure 4. 40: Test set up for cyclic test on reinforced specimen

Key

V	Slip
t	Time
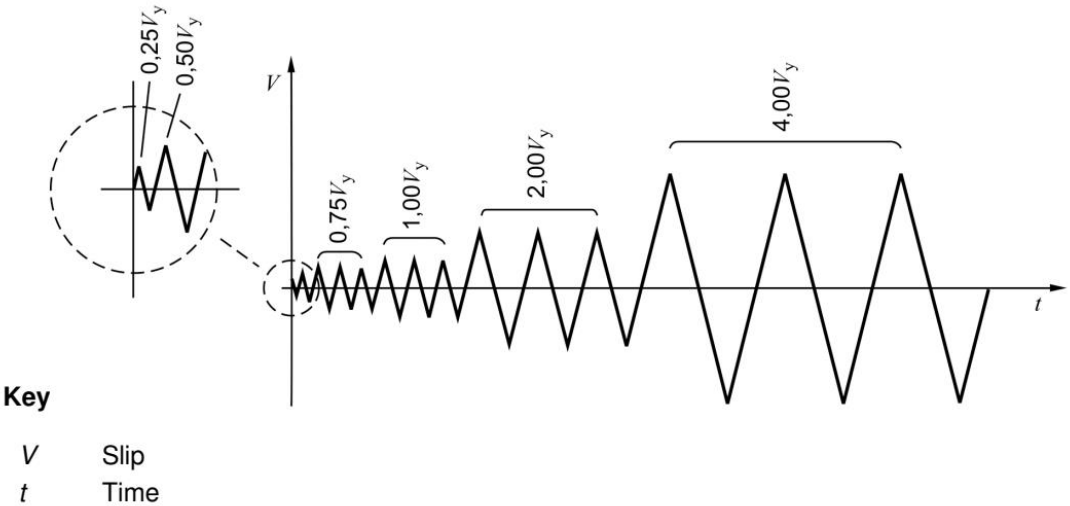
Figure 4. 41: The loading procedure of cyclic test proposed by BS EN 12512:2001

Table 4. 5: Loading steps of cyclic tests

Load steps	Number of cycles	Target displacement ratio (Vy=32 mm)	Target displacement (mm)
1	1	0,25Vy	8
2	1	0,50Vy	16
3-4-5	3	0,75Vy	24
6-7-8	3	1,00Vy	32
9-10-11	3	2,00Vy	64

Failure of all three specimens has occurred at 1,00Vy load level (6th step). Maximum load and top displacements of specimen-1, specimen-2 and specimen-3 are 11721 N and 32 mm, 14930 N and 35 mm, 10627 N and 35 mm for pushing, respectively. Plastic strain has resulted in permanent deformation under loading and it has not recovered upon unloading (Figure 4.43). The total strain (ε_T) is composed two components: an elastic strain (ε_e) and plastic strain (ε_p). For each cycle, load- displacement diagram and plastic strains are given in Figure 4.44 and Figure 4.45.
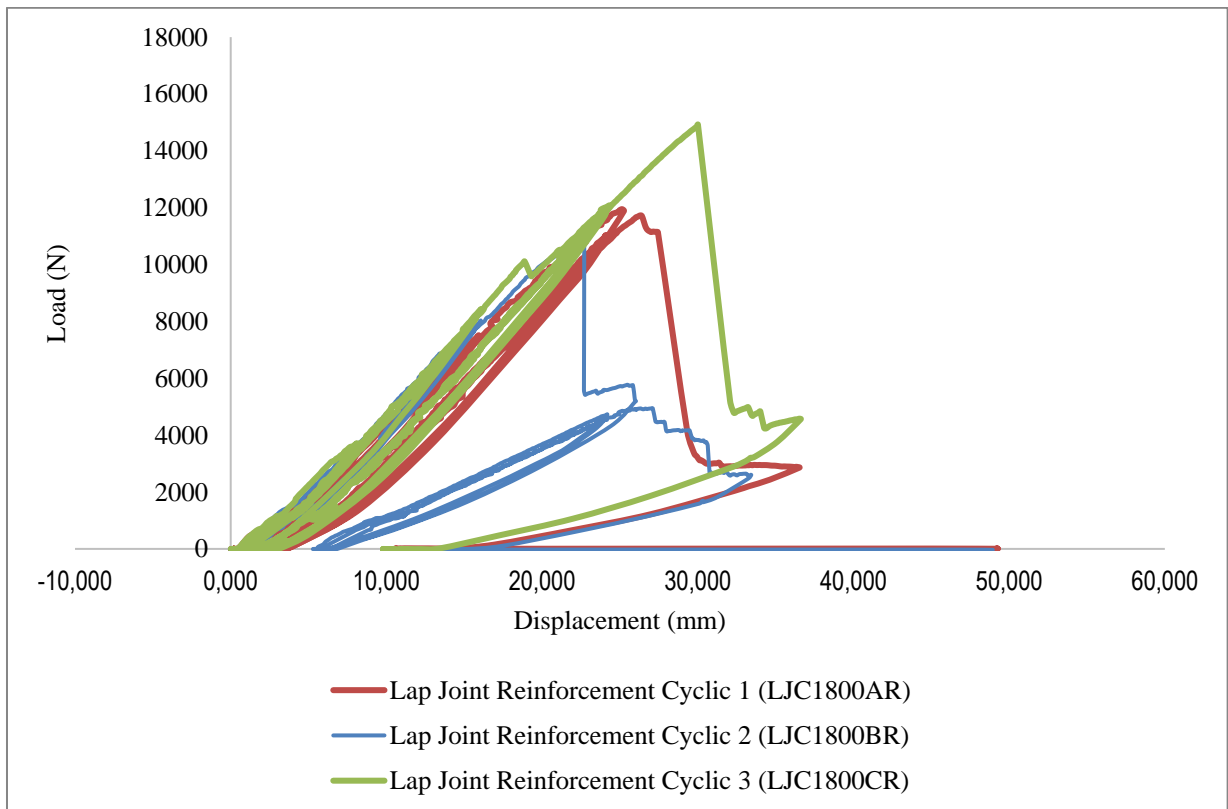
Figure 4. 42: Load-deformation curve of cyclic tests on reinforced specimens
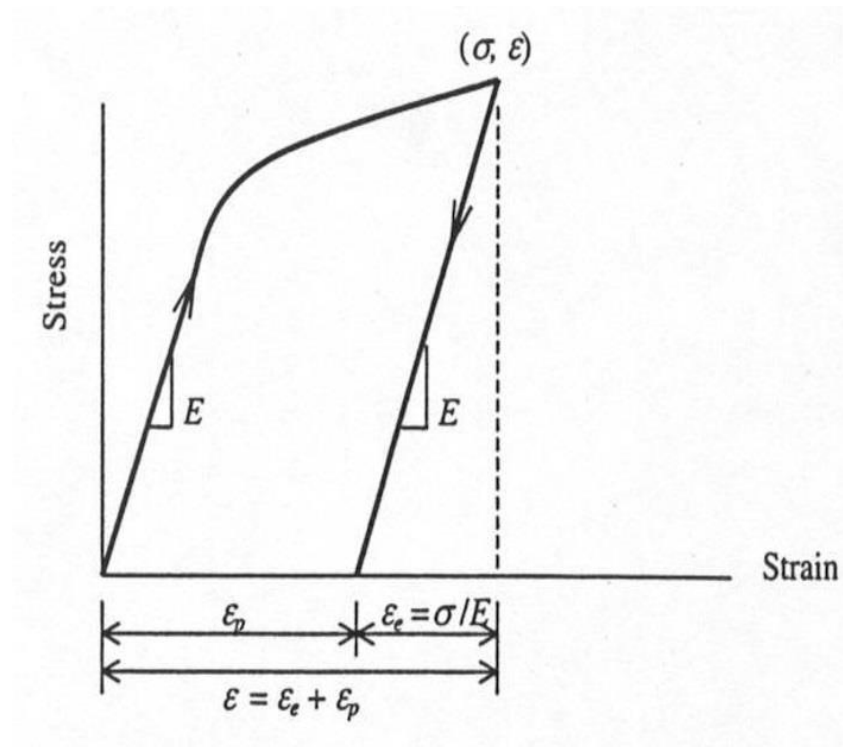
Figure 4. 43: Graphical relationship between total strain, permanent strain and elastic strain
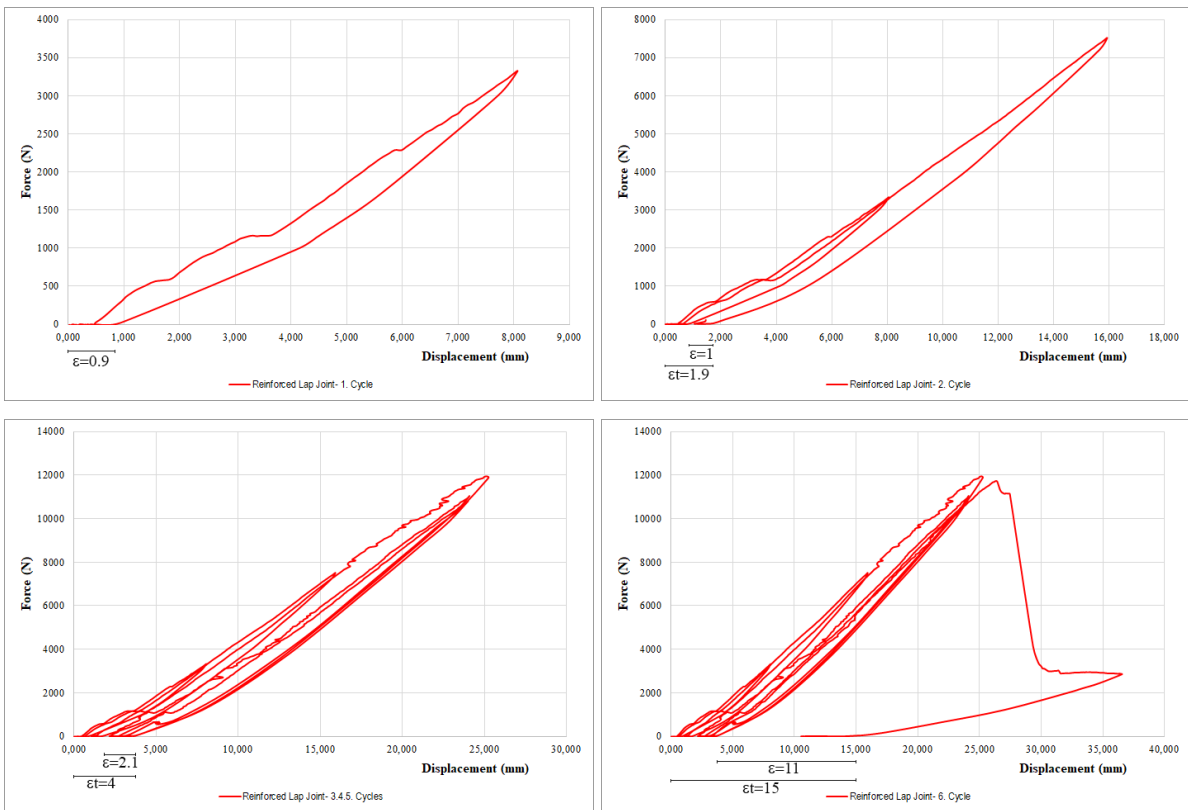
Figure 4. 44: Load-deformation curves of specimens at each cycle
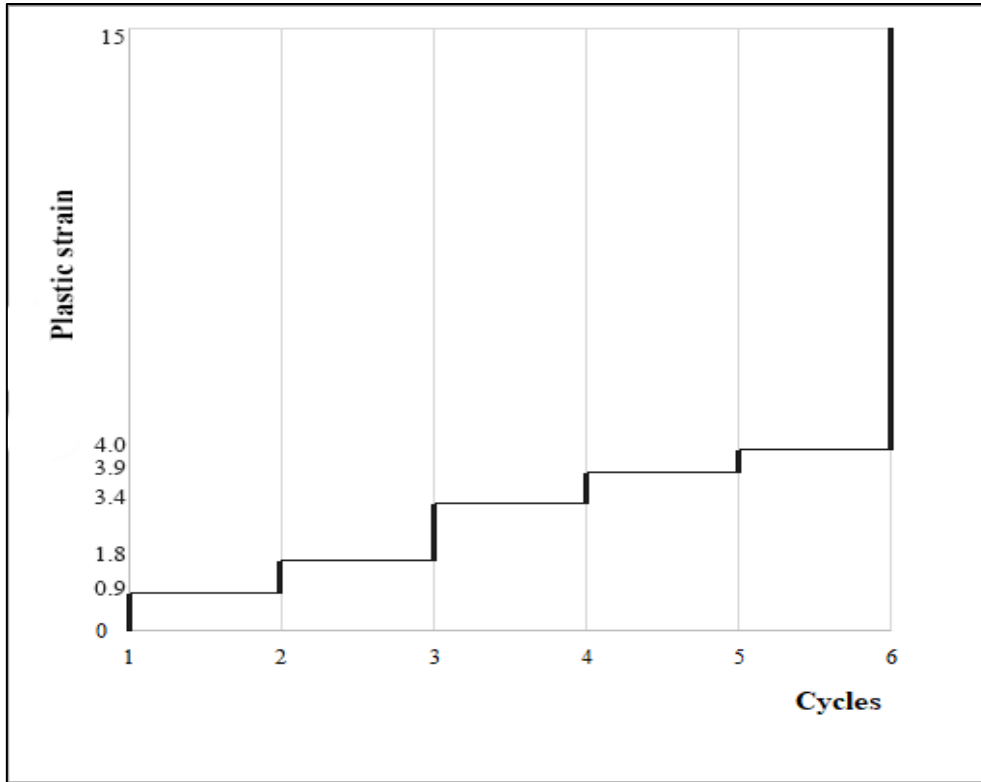
Figure 4. 45: Plastic strain-cycles diagram of reinforced specimens

Besides, the modulus of elasticity has been calculated by using equation 3.6 for each cycle.

$$E = \frac{L^3 F}{4bh^3 d} \tag{4.6}$$

L   length of span, in millimetre;

h   height of beam, in millimetre;

b   width of beam, in millimetre;

F   load, in newton;

d   deflection, in millimetre;

For specimens, the modulus of elasticity has been calculated as E_1=1758 N/mm²; E2=3575 N/mm²; E3,4,5=2709 N/mm²; E6=507 N/mm² at cycle 1 (Vy=8 mm), cycle 2 (Vy=16 mm), cycles 3,4,5 (Vy=24 mm), cycle 6 (Vy=32 mm) respectively (Figure 4.46). Modulus of elasticity is a measure of the stiffness or rigidity of a material. The modulus of elasticity has decreased with an increasing number of cycles. Thus, the general knowledge confirms that cyclic loading weakens the material and reduces its strength.

71

In the last loading steps, timber seperated substantially. Sharp decrements of load have occurred in the last cycles (1,00Vy), while the rupture of carbon fiber textile has become clearly visible. At that point, test has been completed since specimens do not resist the load any more.
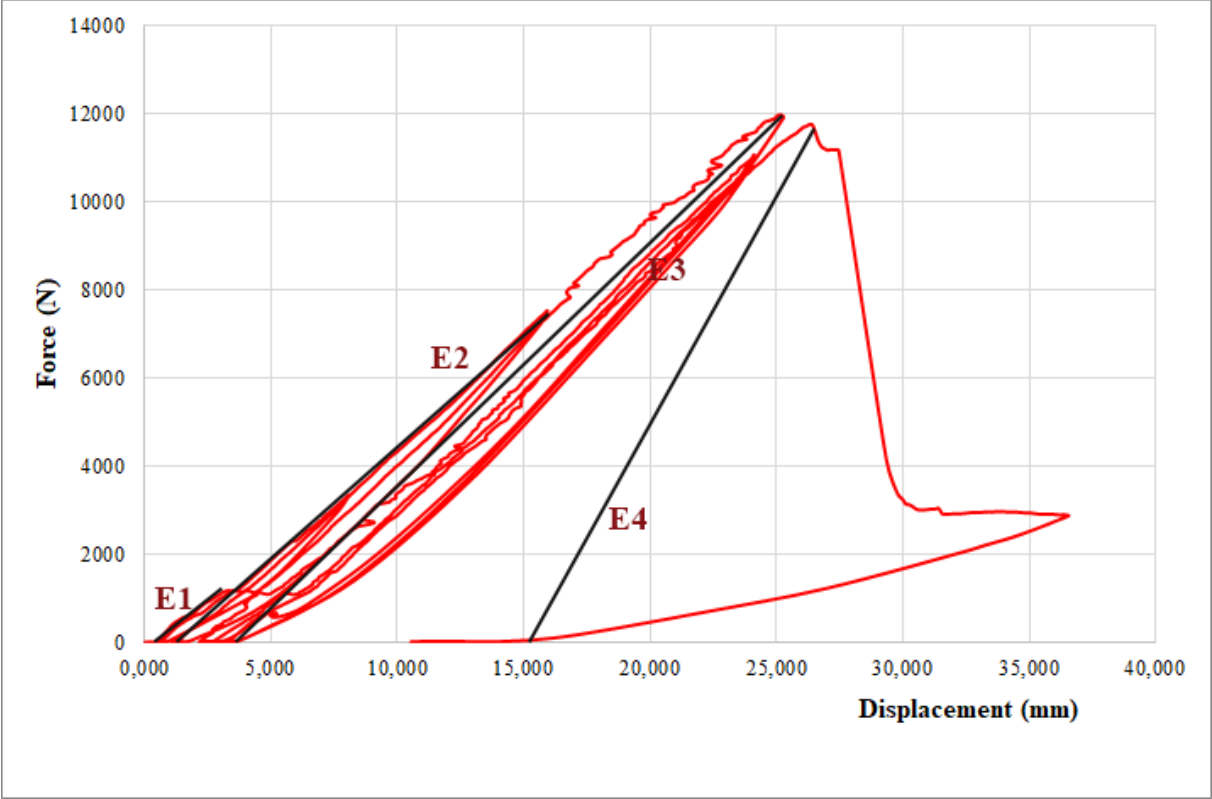
Figure 4. 46: Damage affecting the modulus of elasticity in tested specimens

After carrying out the tests, failures has detected for assessment of the resistance of the timber. Failure patterns have been examined based on the classification of failure patterns in standard ASTM D143-14. The 3 specimens have failed due to combined shear- tension failure modes (Figure 4.47-4.49). The tension stress has led to a brittle failure due to the rupture of the wood fibres, as shown in first reinforced specimen (LPC1800AR). The horizontal shear cracks have been initiated within LR plane at the joint of the beam. In other words, shear failure has been marked by an increase in split length and the development of more cracks which has separated the beam into two parts along the parallel to the longitudinal direction (in specimens LPC1800BR and LPC1800CR).
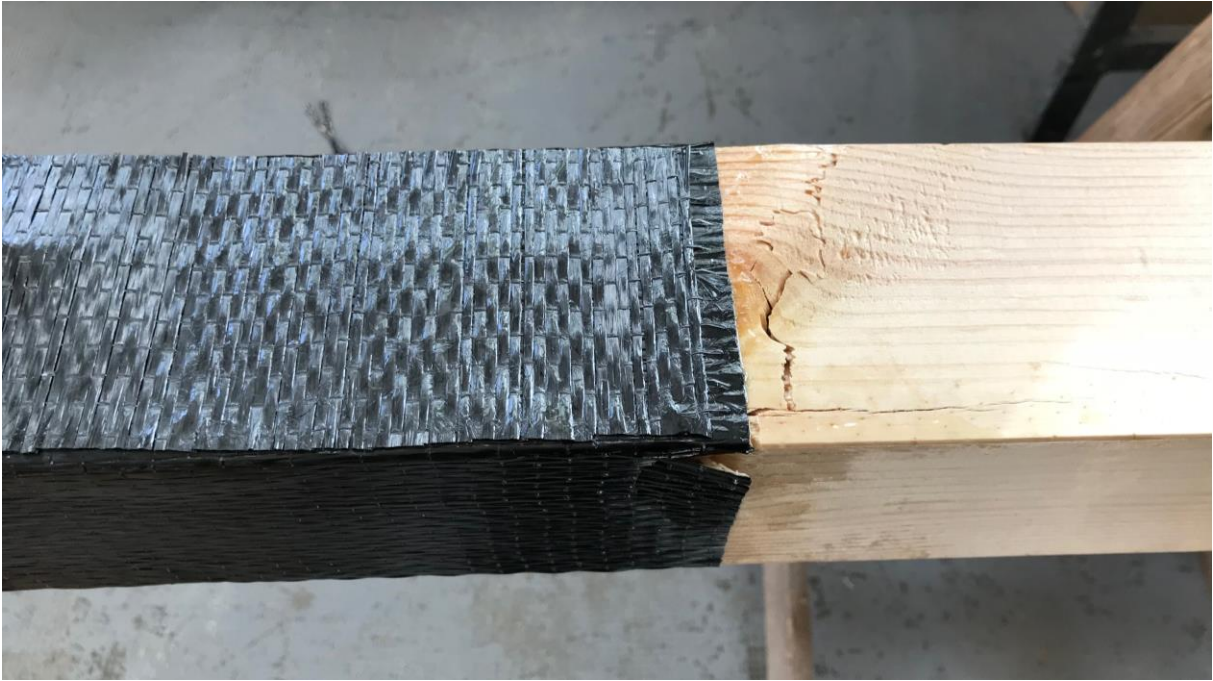
Figure 4. 47: A failure mode due to tensile stress of first reinforced specimen (LPC1800AR)

Figure 4. 48: Shear failure in second reinforced specimen (LPC1800BR) under cyclic loading

Figure 4. 49: Shear failure of third reinforced specimen (LPC1800CR) under cyclic loading

4.3.4. Discussion of test results

The test results show that monotonic tests on unreinforced specimens were mainly influenced by the screws, which would increase the load carrying capacity of the connection. Furthermore, the strengthening of timber joint under bending with CFRP had a beneficial effect on the load-bearing capacity and on the rigidity of the reinforced specimens. The comparison between the reinforced and unreinforced specimens under monotonic loading, confirms that carbon fiber textile led to higher stiffness and strength in the joints. It can be observed that load and deformation capacities of reinforced specimens are higher than unreinforced specimens. The CFRP reinforcement caused an increase in the average maximum load at failure from 1400 N to 13000 N, which represents an increase of 830 percent. Besides, at load-deformation curve of reinforced specimen, sudden drop after the ultimate load is seen, which shows brittle behavior. It should be pointed out the maximum load is approximately similar in monotonic and unidirectional cyclic tests on reinforced specimens. The average of maximum load and top displacement of reinforced specimens are 12000 N and 35 mm under monotonic loading, while 11713 N, 36 mm under cyclic loading. In other words, even if the types of loading are different, the maximum load and displacements of the specimens with CFRP are similar.

4.4 Mortise Tenon Joint Tests

A set of monotonic tests of unreinforced specimens have been performed in order to describe the behaviour of mortise tenon joint which is commonly used between beam and column members in Turkish traditional timber house. There are numerous examples of this type of joint. Tenon joints members that usually form an "L" or "T" type configuration. The joint comprises two components: the mortise hole and the tenon tongue (Figure 4.50). These joints were implemented with metal fasteners such as; nails, screws or bolts and their ability to carry the loads was achieved through friction. Moreover, various reinforcement techniques such as; metal plates (strips, stirrup), glued composites (glass or carbon fibres textiles) and glued-in rods are used.

In this study, joints which are locally strengthened with carbon fiber textile have been tested under monotonic and cyclic loading. The purpose of these tests is to increase the flexural strength and load-bearing capacity of these joints. Besides, carbon fiber textile may prevent premature seperation of joint components under loading.
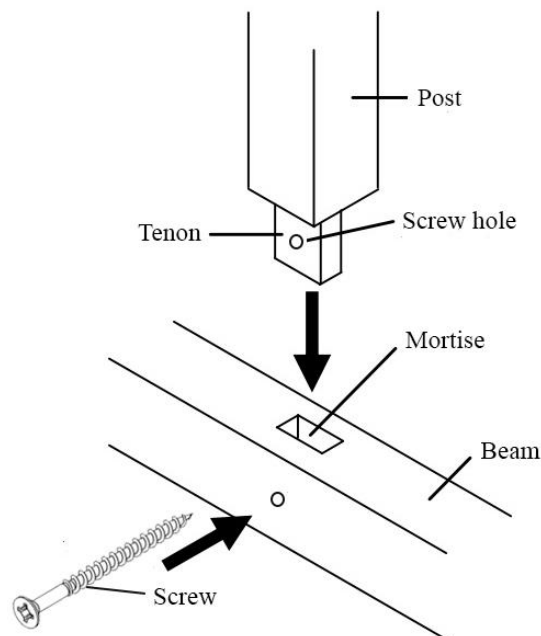
Figure 4. 50: Mortise tenon joint with screw

Joints are assumed to be ideally rigid or pinned in some simplified analysis. It is quite obvious that the assumption of pinned joints is conservative, provided that the joints have enough ductility, in a way their rotation may develop. In fact, most joints in real wood structures are more or less flexible or semi-rigid. The slope of the moment-rotation curves to the elastic curves

change as the joint is loaded (Figure 4.51a). The moment is dependent on the function of relative rotation between structural elements which are loaded (Figure 4.51b).

<div align="center">a   b</div>
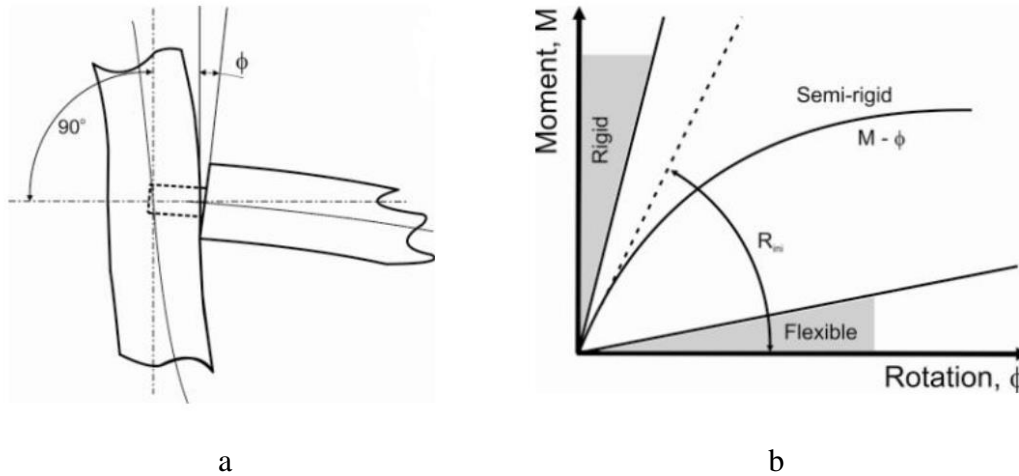
Figure 4. 51: Semi-rigid joint (a), moment-rotation curves (b)

4.4.1. Monotonic tests on unreinforced specimens

A total of 3 pine specimens with 10% moisture content, have been used in T-type mortise-tenon joint, with the dimension of 90x90x500 mm beam and 90x90x1000 mm post member (bxhxl) (Figure 4.52). The dimension of 30x40x50 mm tenon (bxhxl) is connected to mortise hole with 2 lateral screws (Ø4.5 mmx h: 80 mm). The post of each specimens has been horizontally placed and bolted to steel reaction wall which has dimensions of 1000x1000 mm triangle shape using HEB 180 profile. Thus, the post has kept the original vertical position. The load has been concentrated in one point through a rectangle metal plate which has the dimension of 1x4x7 mm (bxhxl). Loaded end of the beam has been at a distance of 480 mm from the face of the post. One LVDT having a resolution of 0.1 mm, has been installed for monitoring the vertical deflections at the corner points of lower side of the beam. The tests of specimens have been carried out under monotonic loading and test set up is shown in Figure 4.53.

The loading procedure of test has been obtained from BS EN 26891:1991 (Figure 4.54). According to the standard, the load is applied up to 0,4 Fest and maintained for 30 s. Then the load is reduced to 0,1 Fest and maintained for 30 s. Thereafter, the load is increased until the ultimate load. The test is stopped when the ultimate load is reached. Following, the estimated maximum load, Fest, 1000 N was taken on the basis of previous bending experiments. The load has been applied up to 0.4 Fest, which corresponds to 400 N, maintained for 30 sec. Then, the load was reduced to 0.1 Fest, which corresponds to 100 N, maintaned for 30 sec at this value.

Thereafter the load has been increased until reading the ultimate load. Constant velocity in the application of load has been imposed to 10 mm/min.
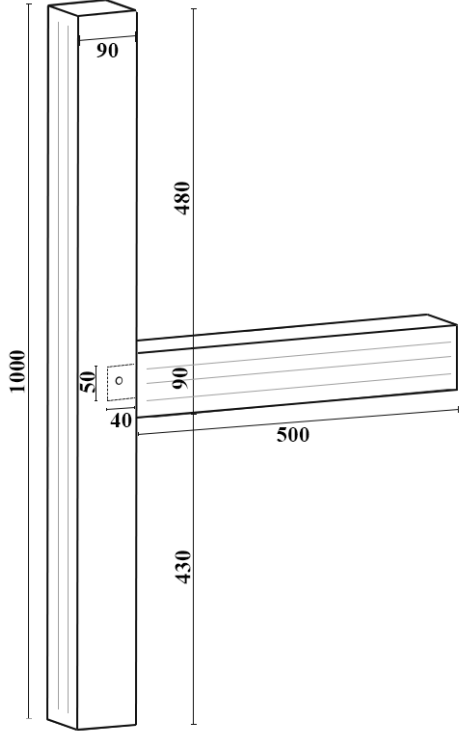
Figure 4. 52: Dimensions of specimens for monotonic loading

(Dimensions are presented in mm)
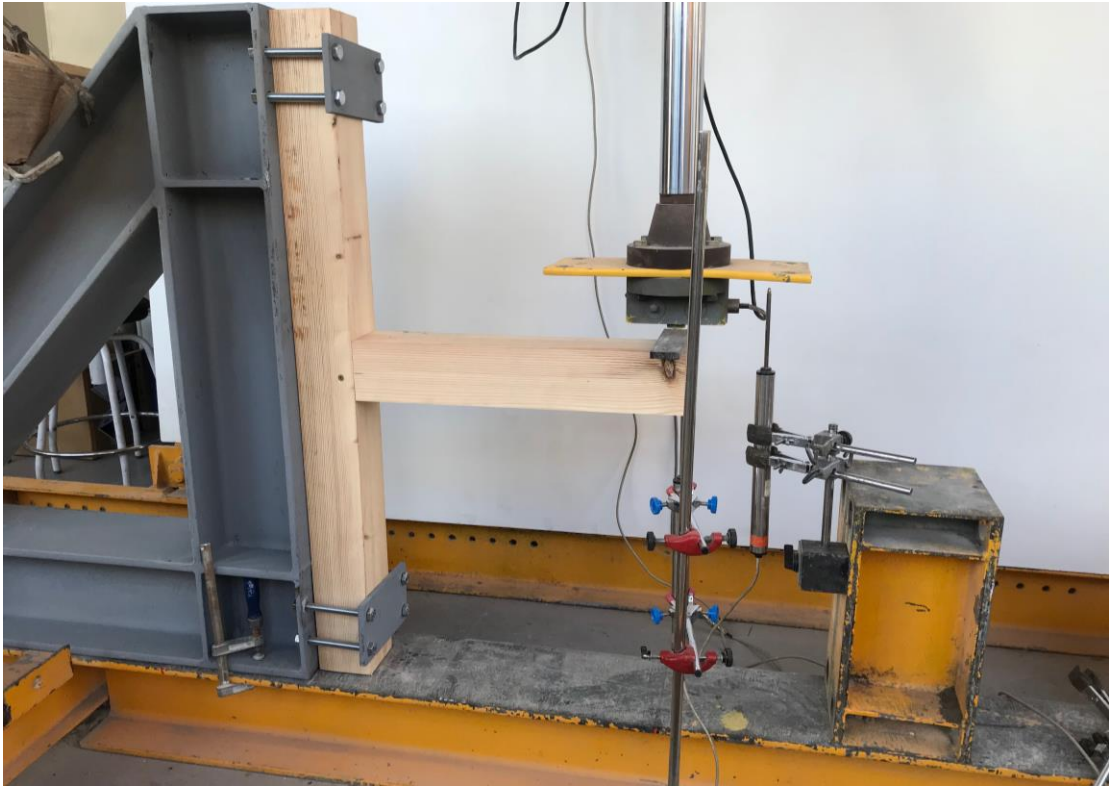
Figure 4. 53: Test set up for monotonic loading

As a pin-jointed connection, the tenon member rotated around the corner of the tenon shoulder once a bending moment is applied to a single screw connection. Resistance to bending is provided by lateral strength and stiffness of the screw. The effective centre of rotation is at the corner of the tenon shoulder creating an effectively solid hinge point (Hassan, 2008). Moment rotation is the value of force at the load (P1) times the distance of d1 and equals to force at screw (P2) times the distance of d2 (Figure 4.55).

$$M = P1 \times d1 = P2 \times d2 \tag{4.7}$$
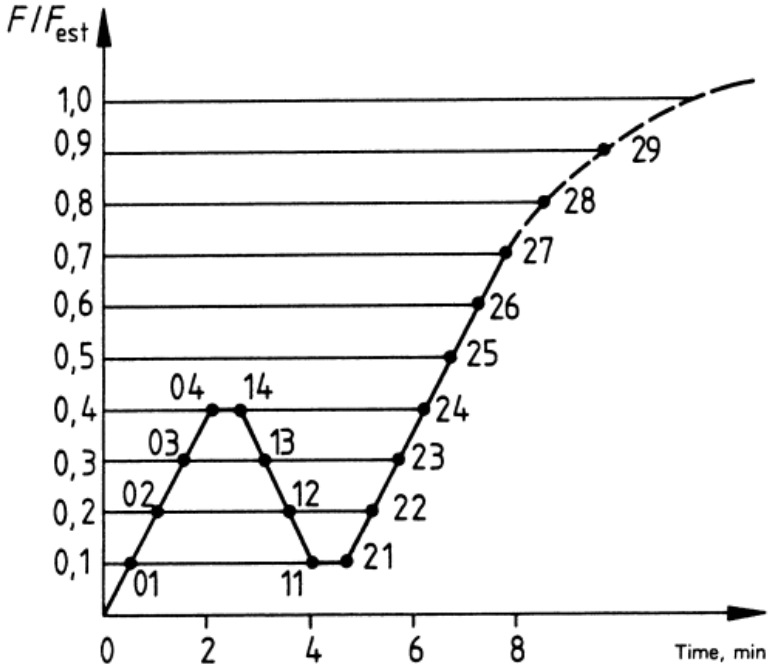
Figure 4. 54: The loading procedure of monotonic test (BS EN 26891:1991)
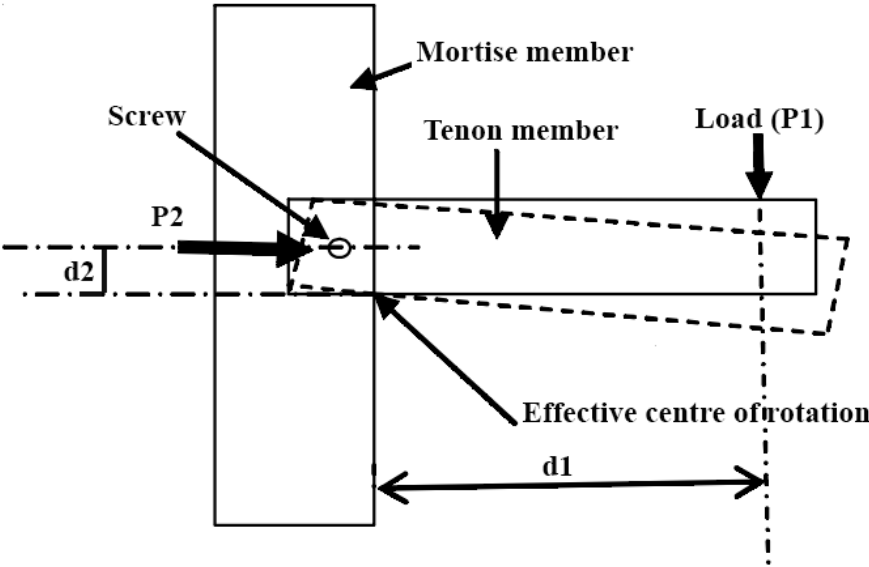
Figure 4. 55: The effective centre of rotation for mortise-tenon joint (Hassan, 2008)

78

Typical load-displacement curves in the three tested specimens measured is shown in Figure 4.56. Initially, the response is linear and elastic, where a linear increment of displacement corresponds to a linear increment of load. When the load reached 800 N, yielding took place in three specimens. Later, a nonlinear load-displacement curve has occurred and smooth plateau associated with tenon end crushing of mortise. The seperation between tenon and mortise has gradually seen and screws have bent under combined stresses. All specimens showed ductile behaviour under bending loading. Finally, a total loss of friction occurred with the global failure of the connection.

One of the conclusions is that the maximum bending load and displacement are similar for two specimens, corresponding to approximately 1200 N and 95 mm. The third one showed the maximum bending load and displacement, 1160 N and 90 mm with lower rotational stiffness than others. When considering the distance from the load point to the centre of rotation is 480 mm, bending moment has been calculated as 595.2 N.m.
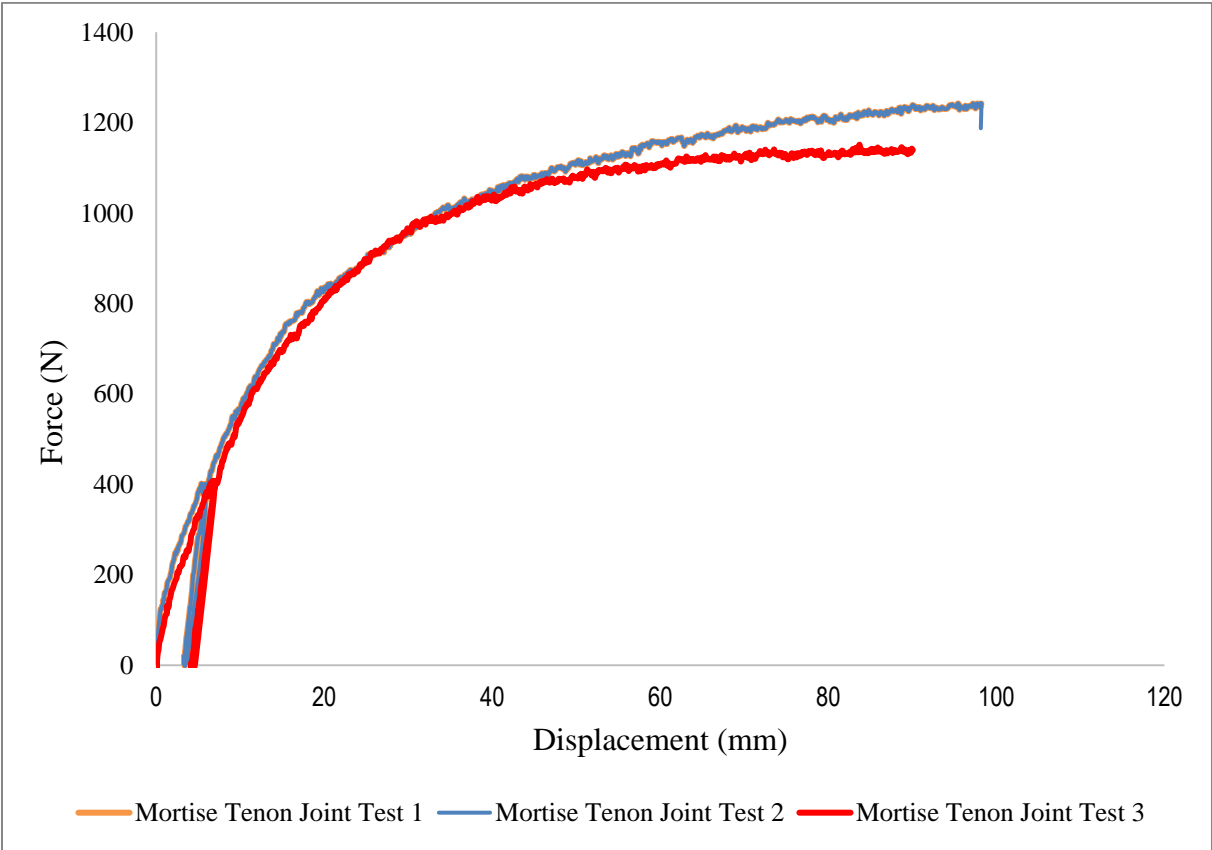
Figure 4. 56: Load-deformation curves of monotonic tests

The experiments revealed that at early stages of loading, tenon and mortise have squeezed each other on contact surfaces, thus the specimens squeaked. Then, the tenon member has started to rotate. The upper tenon surface has slipped outside the mortise and has moved downwards,

while the bottom of tenon surface has slipped inside of the mortise. With the increase of loading, the nonlinear compressive deformation has been observed on the interfaces. Finally, the tenon has been partially pulled out (aprx. 25 mm) and the joint failed since the vertical displacement is excessively large (Figure 4.57).

Figure 4. 57: The failure pattern of three specimens under monotonic loading

4.4.2. Monotonic tests on reinforced specimens

A total of 3 mortise tenon joint specimens, with the same dimension of 90x90x500 mm beam, 90x90x1000 mm post member (bxhxl) have been subjected to monotonic vertical loads (see Figure 4.58). The dimension of 30x40x50 mm tenon (bxhxl) is connected to mortise hole with 2 lateral screws (Ø4.5 mmx h:80 mm). They have been reinforced with undirectional carbon fiber textile. High strength carbon fiber textiles have been bonded to the upper surface of joint, as 90x200 mm with L shaped. It has been bonded parallel to the longitudinal direction of the beam in single layer with two components epoxy. Furthermore, two CFRP textiles have been bonded with 45^0 angle to two lateral surfaces of the specimens with a dimension of 100x200 mm (Figure 4.58-4.59). The epoxy, which name is MasterBrace P 3500, is composed by two parts: A and B. The component A is basically an epoxy resin, and Component B is a hardener. By mixing both components, the reaction starts, which is the responsible for hardening. Components A and B have been mixed in the ratio prescribed by the manufacturer that is 3:1 (Part A to Part B) by volume. Each component were carefully measured and then added part B (hardener) to part A (resin) (Figure 4.60). The viscosity of the adhesive plays a very important

role in the workability which in turn affects the overall quality of the process. Technical data of carbon fiber textile and epoxy are given in Table 4.3 and 4.4 (in previous part of lap joint).
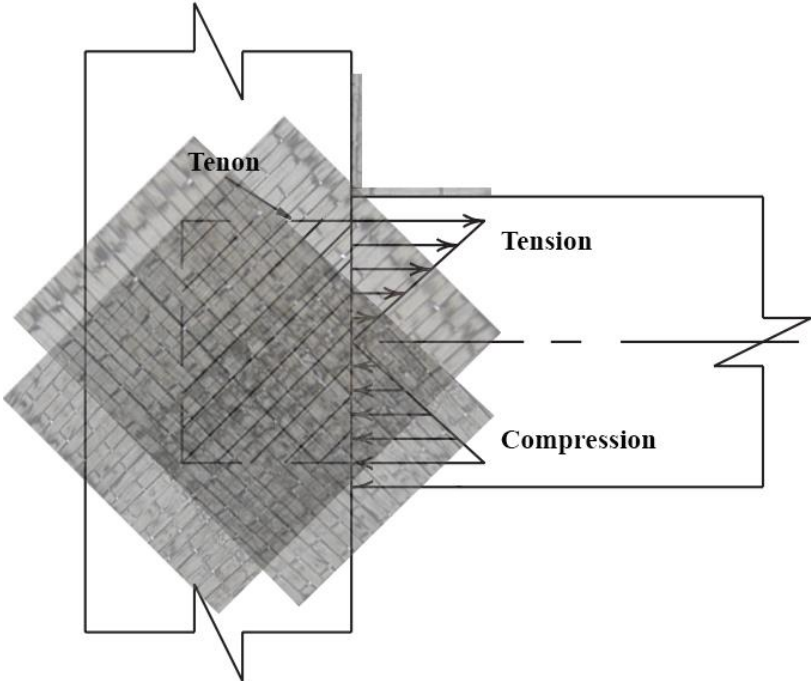
Figure 4. 58: The places of CFRP in specimens
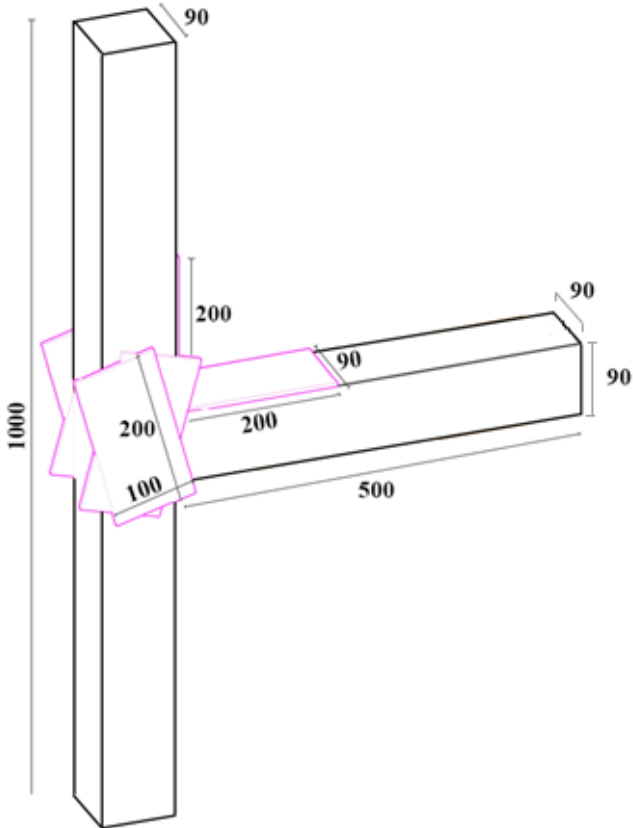
Figure 4. 59: The dimension of reinforced specimens for monotonic test
(Dimensions are presented in mm)

Figure 4. 60: The selected epoxy and carbon fiber textile for reinforcement

First of all, the initial resin coat of thickness 1 mm has been applied with a brush on upper surface which is the tension zone of timber specimen. Subsequently, the unidirectional fabric reinforcement with a thickness of 5 mm has been placed parallel to the longitudinal direction of the joint and finally a finishing layer of the same epoxy resin of thickness 1 mm has been applied again. Besides, two CFRP textiles were bonded in 45^0 angle to each others on lateral surfaces of specimens (Figure 4.61). The curing time was 48 hours.

After the preparation of specimens, the post of each specimens was vertically placed and bolted to steel reaction wall which has the dimension of 1000x1000 mm triangle shape using HEB 180 profile. The loads concentrated on one point with rectangle metal plate with a dimension of 1x4x7 mm (bxhxl). Timber reinforced specimens have been subjected to one point flexural loading, at the end of beam the distance of 480 mm from the post. The load has been applied by one loading cell, powered by a maximum capacity of 1000kN hydraulic jack. One LVDT with sensitivity of 0.1 mm, has been used for monitoring the vertical deflections at the corner points of lower side of the beam (Figure 4.62).

Figure 4. 61: The reinforced specimens for monotonic test
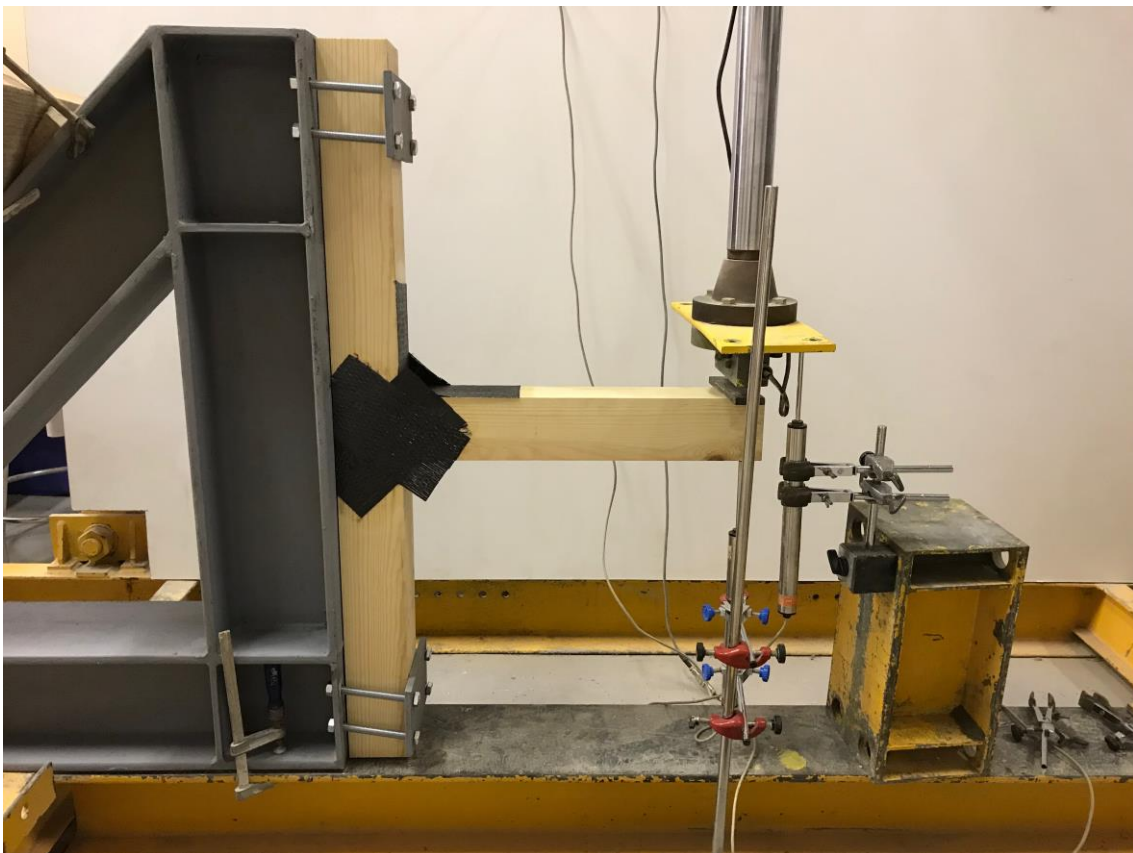
Figure 4. 62: Test set up for monotonic test on reinforced specimen

Loading steps have been chosen similar to monotonic tests on unreinforced specimens. The estimated maximum load, Fest, 1000 N has been taken on the basis of previous bending experiments. The load was applied up to 0.4 Fest, which corresponds to 400 N, maintained for 30 sec. Then, the load has been reduced to 0.1 Fest, which corresponds to 100 N, maintained for 30 sec at this value. Thereafter the load was increased until the ultimate load. Constant velocity of load application has been imposed to 10 mm/min.

The load-deformation curve has been obtained from test results (Figure 4.63). The behaviour of the three specimens has been quite similar, even though the ultimate values of strength varied. The curves show how beams exhibited more essentially linear elastic behaviour up the failure. The average maximum force is approximately 3 times more than unreinforced specimen. After a loss of friction, there is rapid decrease of capacity. Thus, the brittle behaviour is replaced by an inelastic phase. Finally, a total loss of friction takes place with the failure of the connection. Carbon fiber textile reinforced beams revealed more brittle behavior compared to the un-reinforced beams. The CFRP reinforcement caused an increment of the average maximum load at failure from 1200 N to 3600 N, which represents an increase of 300 percent. It is worth to highlight that the failure of the strengthened timber joints occurred due to the separation of joint components in the tensile region. Failure has been initiated at the joint in tension zone due to rotation of tenon member. Even though joint components have been separated in tension zone, it still resisted to the increment of load by help of high tensile strength of carbon fiber textile. When the specimen reaches the maximum peak of load, the carbon fiber textile yielded and separated from the timber surface. CFRP worked as a binder holding two timber members and provided continuity together until the ultimate deformation, that was average of three specimens, 90 mm. In other words, CFRP reinforcements have led to progressive/gradual failure of joint rather than sharp failure. The failure pattern of specimens 1 and 2 are mostly detected as the rupture of CFRP sheet after the rotation of timber tenon. For the specimen 3, the seperation of sheet has been seen in the lateral surface most likely due to deficient of bonding (Figure 4.64).
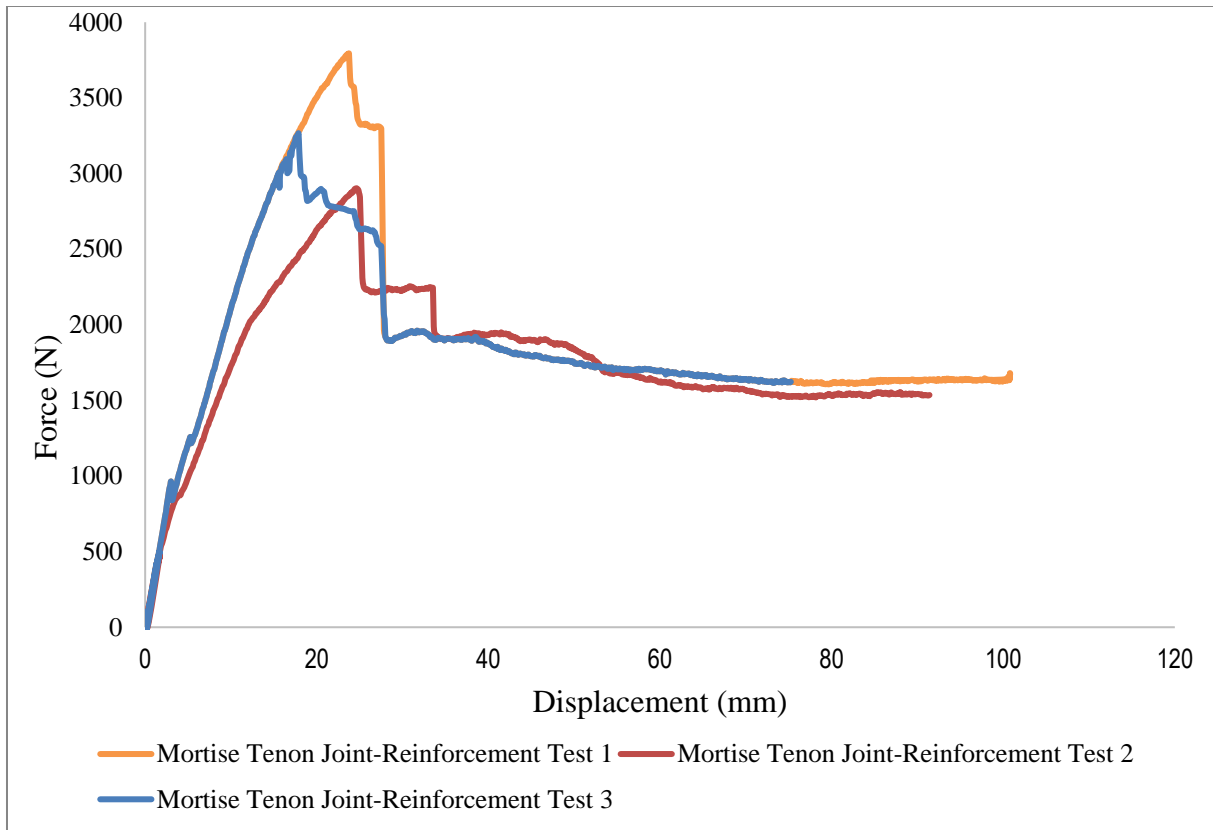
Figure 4. 63: Load-deformation curve of monotonic tests on reinforced specimen

Figure 4. 64: The failure pattern of three reinforced specimens under monotonic loading

4.4.3. Cyclic tests on unreinforced specimens

A total of 3 mortise tenon joint specimens, with the dimension of 90x90x500 mm beam, 90x90x1000 mm post member (bxhxl) have been subjected to unidirectional cyclic vertical loads. The dimension of 30x40x50 mm tenon (bxhxl) is connected to mortise hole with 2 lateral screws (Ø4.5 mmx h:80 mm).

After the preparation of specimens, the post of each specimen has been vertically placed and bolted to steel reaction wall which has the dimension of 1000x1000 mm triangle shape using HEB 180 profile. The loads concentrated on one point with rectangle metal plate which has the dimension of 1x4x7 mm (bxhxl). Timber reinforced specimens have been subjected to one point flexural loading, at the end of beam the distance of 480 mm from the post. The load has been applied by one loading cell, powered by a maximum capacity of 1000kN hydraulic jack. One LVDT with sensitivity of 0.1 mm, has been used for monitoring the vertical deflections at the corner points of lower side of the beam (Figure 4.65).

The loading protocol given in `BS EN 12512:2001 Timber structures-Test methods-Cyclic testing of joints made with mechanical fasteners` has been used for displacement controlled unidirectional cyclic tests (4.66). The loads have been applied until the specified displacements. Estimated yield slip has been determined as Vy=80 mm from monotonic tests and target displacements have calculated using this value (Table 4.6). First two target displacements (0.25Vy and 0.50Vy) have been applied for only one cycle. Further target displacements (0.75Vy, 1.00Vy, 2.00Vy and 4.00Vy) were applied as three sets of cycles.

Firstly, at 1st cycle, applied the load under compression, until a slip of 25% of the estimated yield slip Vy is reached. The value of Vy has been evaluated by calculation as 0.25Vy=20 mm. Then, the specimens were unloaded. At 2th cycle, the load was applied in compression up to a slip of 50% of Vy which corresponded to 40 mm and it unloaded to zero-slip. At 3th, 4th, 5th cycles, specimens were loaded in compression up to a slip of 75% of Vy, 60 mm. At following set of three cycles the load has been applied three times, 100% and 200% of Vy. Failure of all three specimens occured at 2,00Vy load level (9th step). Typical load-displacement curves for three specimens measured during cyclic loading is shown in Figure 4.67. The average of maximum load and top displacements of three specimens is 1115 N and 71 mm. For each of cycles, load-top displacement diagram and plastic strains are given in Figure 4.68 and Figure 4.69. Plastic strain has resulted in permanent deformation under loading and it has not recovered upon unloading (Figure 4.69). The total strain (ε_T) is composed two components: an elastic strain (ε_e) and plastic strain (ε_p).

When considering the distance from the load point to the centre of rotation is 480 mm, the moment resistance of joint was calculated as M (kN·m) = 0.48F. One displacement transducer (D1, m) has been installed below the face of the beam to measure the vertical displacement of the beam and to measure the rotation of the joint, rotation (rad) = D1/0.48. Then, the rotational stiffness was determined M (kN·m) / rotation (rad) for each cycle. For the specimens, rotational stiffness has been calculated as k1=9.26 kN·m/rad; k2=7.11 kN·m/rad; k3,4,5=5.16 kN·m/rad;

k6,7,8=3.79 kN·m/rad at cycle 1 (Vy=20 mm), cycle 2 (Vy=40 mm), cycles 3,4,5 (Vy=60 mm), cycles 6,7,8 (Vy=80 mm) respectively. The equivalent rotational stiffness decreases gradually for all specimens with the increasing of rotation.

Figure 4. 65: The set up for cyclic test on unreinforced specimens
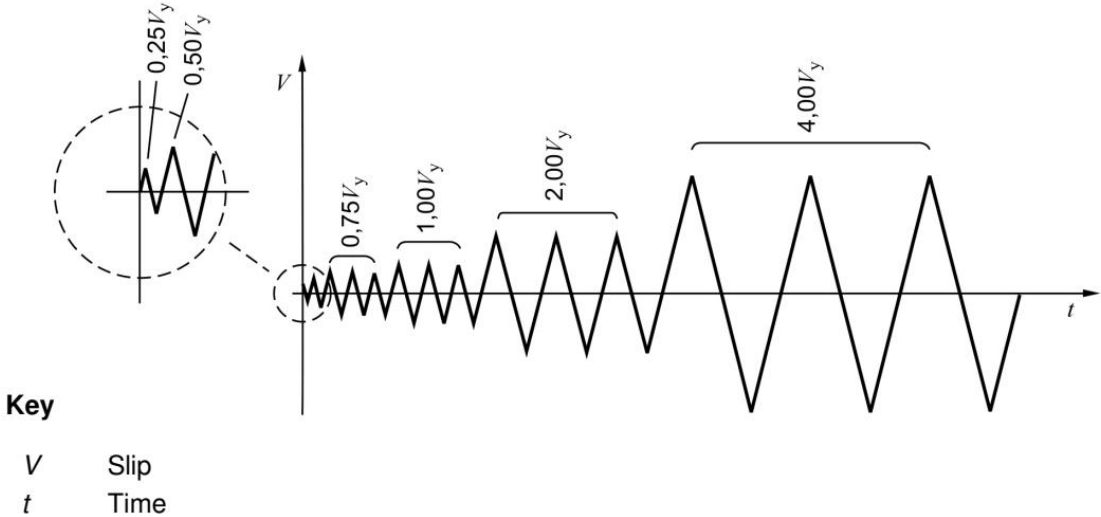
Figure 4. 66: The loading procedure of cyclic test (BS EN 12512:2001)

Table 4. 6: Loading steps of cyclic tests

Load steps	Number of cycles	Target displacement ratio (Vy=80 mm)	Target displacement (mm)
1	1	0,25Vy	20
2	1	0,50Vy	40
3-4-5	3	0,75Vy	60
6-7-8	3	1,00Vy	80
9-10-11	3	2,00Vy	160
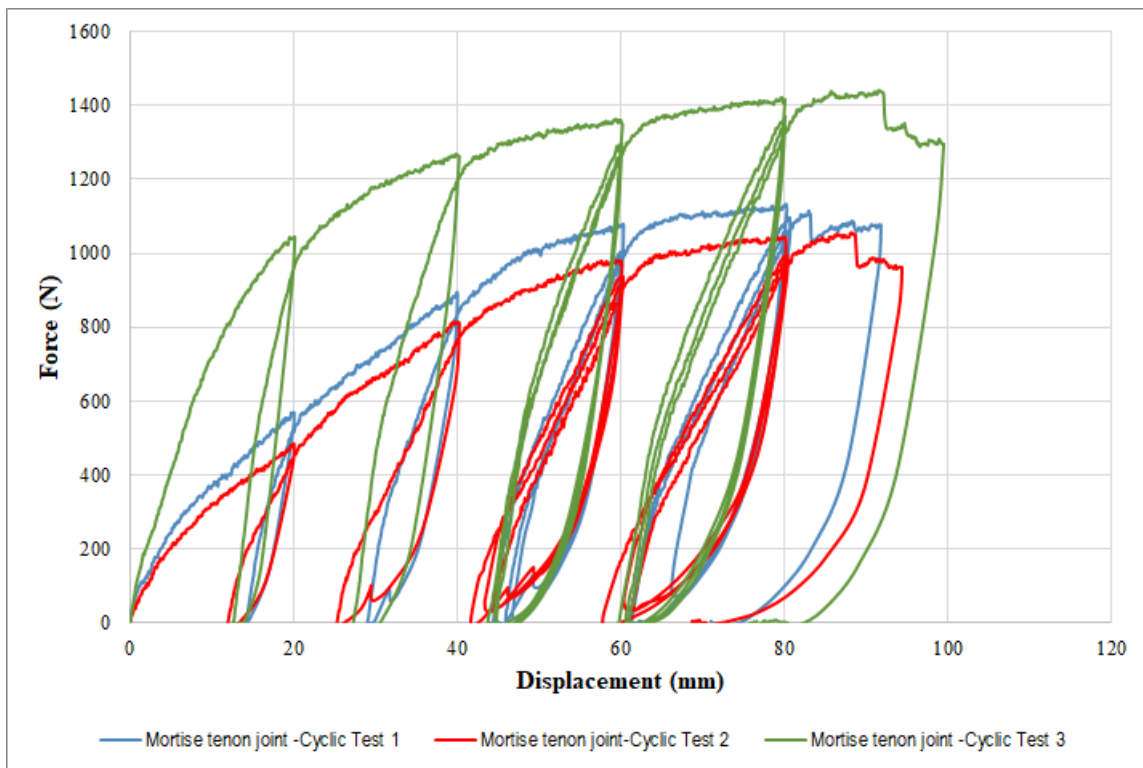
Figure 4. 67: Load-deformation curve of cyclic tests on unreinforced specimens

Graphically, modulus of elasticity is defined as a slope of the stress-strain diagram (Figure 4.70). E1 indicates the initial modulus of elasticity that is calculated with linear portion of stress-strain. The lines of other modulus of elasticities (E2, E3, E4, E5), which describe unloading process of material, is parallel with the linear part of stress-strain diagram. The modulus of elasticities have descreased by increasing of deflection in beam under loads. Besides, decreasing modulus of elasticity has been calculated by using the equation 4.6 for each cycles.

$$E = \frac{L^3 F}{4bh^3 d} \tag{4.6}$$

L   length of span, in millimetre;

h   height of beam, in millimetre;

b   width of beam, in millimetre;

F   load, in newton;

d   deflection, in millimetre;

For the specimens, modulus of elasticity has been calculated as E1=19.39 N/mm2; E2=28 N/mm2; E3,4,5=26 N/mm2; E6,7,8=21 N/mm2 at cycle 1 (Vy=20 mm), cycle 2 (Vy=40 mm), cycles 3,4,5 (Vy=60 mm), cycles 6,7,8 (Vy=80 mm) respectively (Figure 4.70).
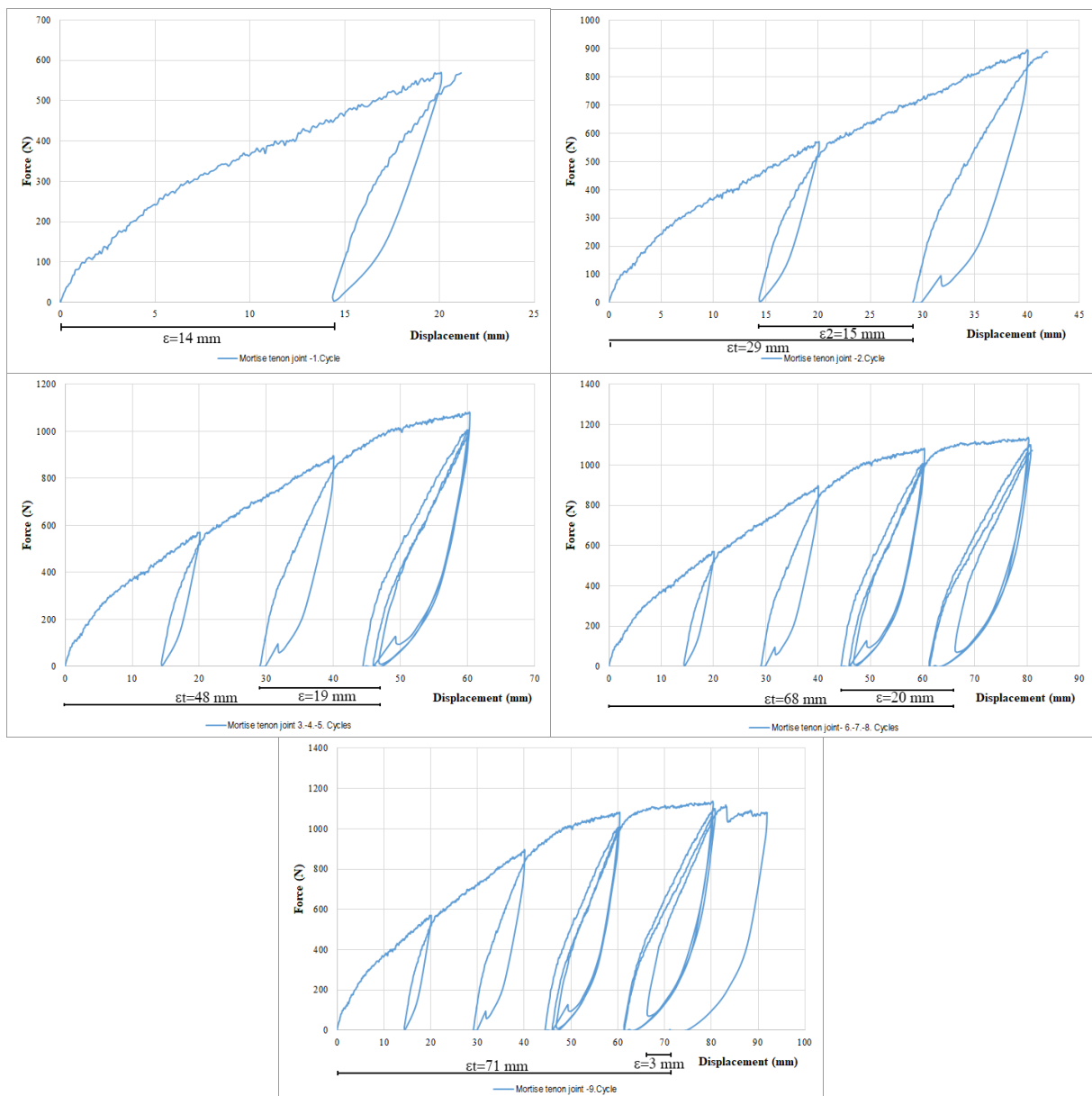
Figure 4. 68: Complete load-deformation curves of specimens
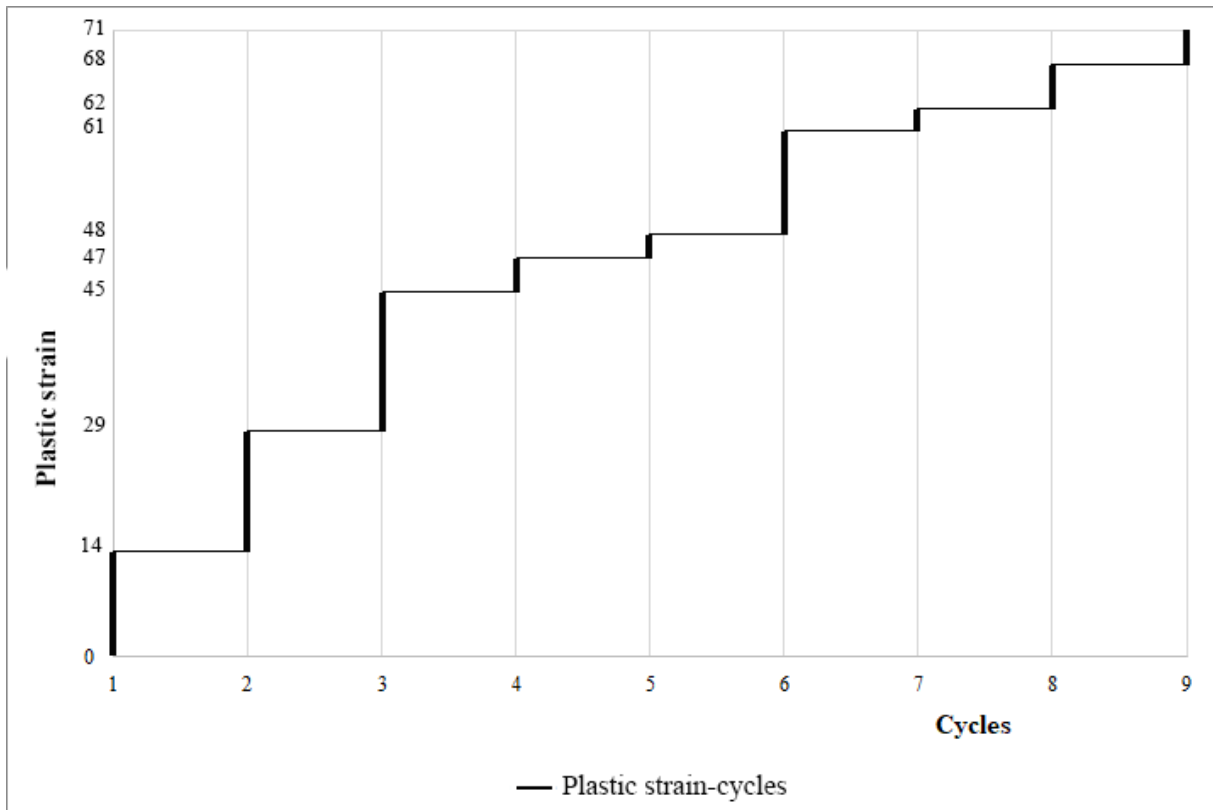
Figure 4. 69: Plastic strain-cycles diagram of unreinforced specimens
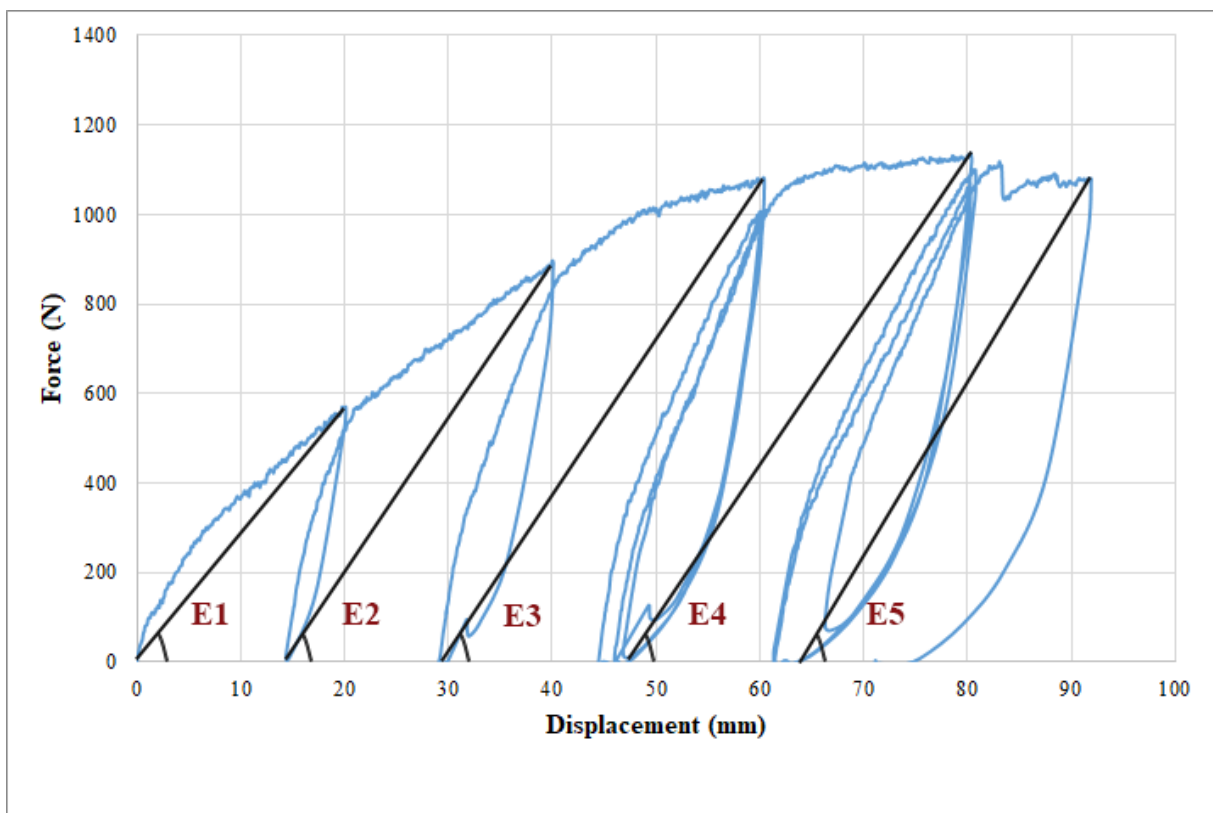
Figure 4. 70: Degradation of modulus of elasticity in specimens

In order to determine the global modulus of elasticity of timber under bending loads, the section of the graph between 0,1 Fmax and 0,4 Fmax for a regression analysis is used. The slope of graph gives the global modulus of elasticity (EN 408). Generally, for the numerical calculations of timbers, the value of E_m is use rather than initial modulus of elasticity, E_0 (Figure 4.71). In the graph; F2-F1: is an increment of load in newtons on the regression line with a correlation coefficient of 0,99 and w2-w1 is the increment of deformation in millimetres corresponding to F2-F1.
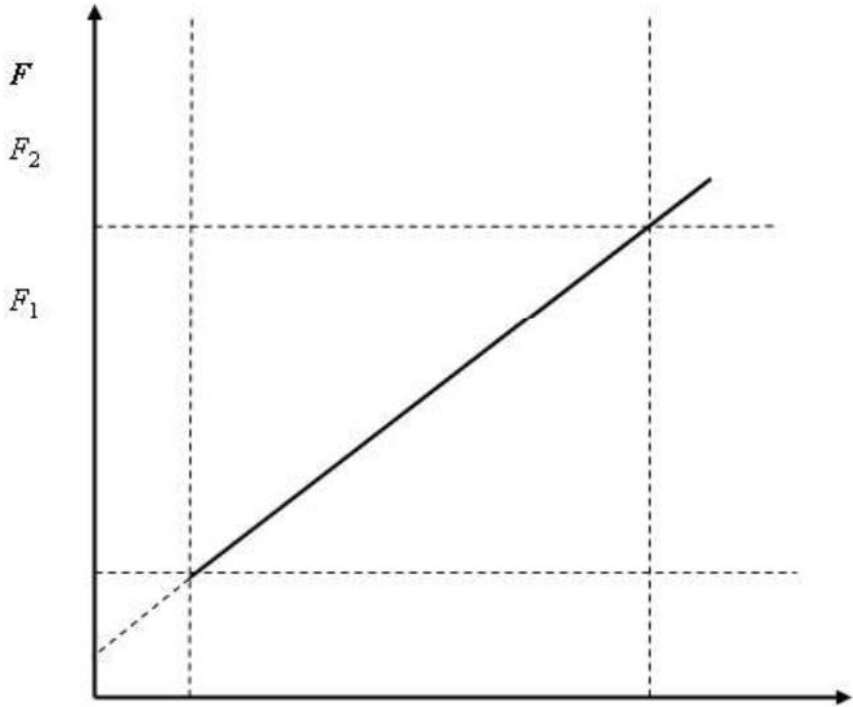
Figure 4. 71: Load-deformation graph within the range of elastic deformation (EN 408)

When joints have been subjected to cyclic loading, the beam has been pushed outwards the actuator. The lower contact surface of the tenon and the mortise has squeezed each other simultaneously. A sound of creaking has occurred between the compression contact surface continuously during the tests due to squeezing of timber fibers and interface friction as the rotation increased. With the increased displacements, significant plastic compression deformation has occurred on the contact surfaces and could not restore and turn back to the first state after unloading. It resulted in a gap between tenon and mortise. For all specimens, the failure were seen around 91 mm, when the specimens have been pushed to cycle (2Vy) 160mm. Failure patterns are detected as tenon pull out from mortise hole (Figure 4.72).

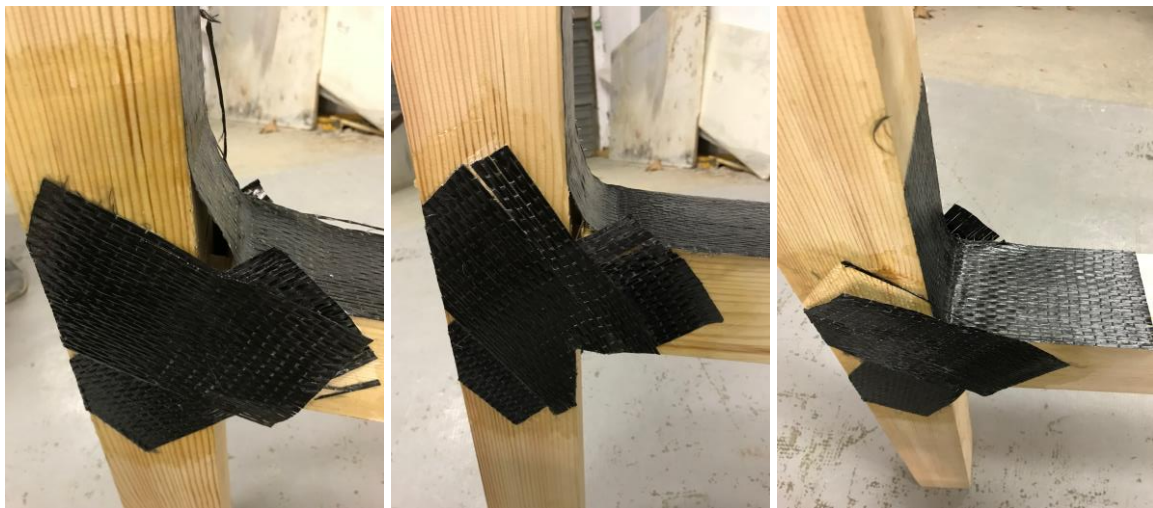**Figure 4. 72:** Failure pattern of three specimens under cyclic loading

4.4.4. Cyclic tests on reinforced specimens

A total of 3 mortise tenon joint specimens, with the same dimension of 90x90x500 mm beam, 90x90x1000 mm post member (bxhxl) have been subjected to unidirectional cyclic vertical loads. The dimension of 30x40x50 mm tenon (bxhxl) is connected to mortise hole with 2 lateral screws (Ø4.5 mmx h:80 mm). They were reinforced with undirectional carbon fiber textile. High strength carbon fiber textiles has been bonded to the upper surface of joint, as 90x200 mm with L shaped. It has been bonded parallel to the longitudinal direction of the beam in one layer with two component epoxy. Furthermore, two CFRP textiles have been bonded at 45^0 angle to two lateral surfaces of specimens with a dimension of 100x200 mm. The technical data of carbon fiber textile and epoxy are given in Table 4.3 and 4.4 (in previous part of lap joint).

After the preparation of specimens, the post of each specimens was vertically placed and bolted to steel reaction wall which has the dimension of 1000x1000 mm triangle shape using HEB 180 profile. The loads, which distributed in one point with rectangle metal plate, has the dimension of 1x4x7 mm (bxhxl). Timber reinforced specimens have been subjected to one point flexural loading, at the end of beam the distance of 480 mm from the post. The loading has been applied by one loading cell which powered by maximum capacity of 1000kN hydraulic jack. One LVDT with sensitivity of 0.1 mm, has been mounted for monitoring the vertical deflections at the corner points of lower side of the beam (Figure 4.73).
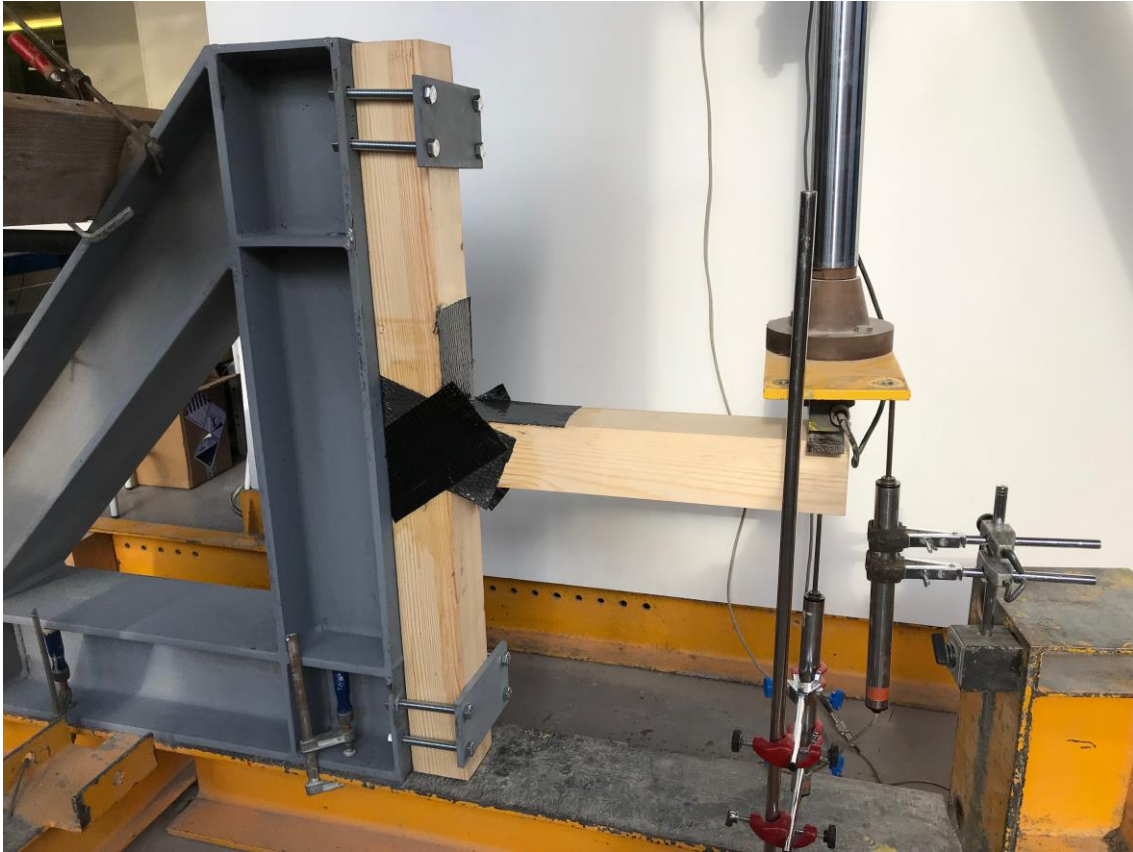
Figure 4. 73: The set up for cyclic test on reinforced specimens

The loading protocol is given in Figure 4.66 (at previous part, 4.4.3. Cyclic tests on unreinforced specimens). Estimated yield slip has been determined as Vy=16 mm and target displacements have been calculated by using this value (Table 4.7). The first two target displacements were applied for only one cycle. Further target displacements have been applied as three sets of cycles. First, at 1st cycle, the load applied in compression, until a slip of 25% of the estimated yield slip Vy is reached. The value of Vy has been evaluated by calculation as 0.25Vy=4 mm. Then, the specimen has been unloaded. At the 2nd cycle, the load has been applied in compression up to a slip of 50% of Vy which corresponded to 8 mm and it unloaded to zero-slip. At 3th, 4th, 5th cycles, it has been loaded in compression up to a slip of 100% of Vy, 16 mm. At following set of three cycles the load has been applied three times, 200% of Vy, 32 mm. The failure of all three specimens have occured at 4,00Vy load level (9th step). Typical load-displacement curves for three specimens which have been measured during cyclic loading is shown in Figure 4.74. The average of maximum load and top displacements of three specimens is 3625 N and 55.8 mm. For each of cycles, load-top displacement diagram and plastic strains are given in Figure 4.75 and Figure 4.76. Plastic strain has resulted in permanent

93

deformation under loading and it has not recovered upon unloading (Figure 4.75). The total strain (ε_T) is composed two components: an elastic strain (ε_e) and plastic strain (ε_p).

Table 4. 7: Loading steps of cyclic tests for reinforced specimens

Load steps	Number of cycles	Target displacement ratio (Vy=16 mm)	Target displacement (mm)
1	1	0,25Vy	4
2	1	0,50Vy	8
3-4-5	3	1,00Vy	16
6-7-8	3	2,00Vy	32
9-10-11	3	4,00Vy	64
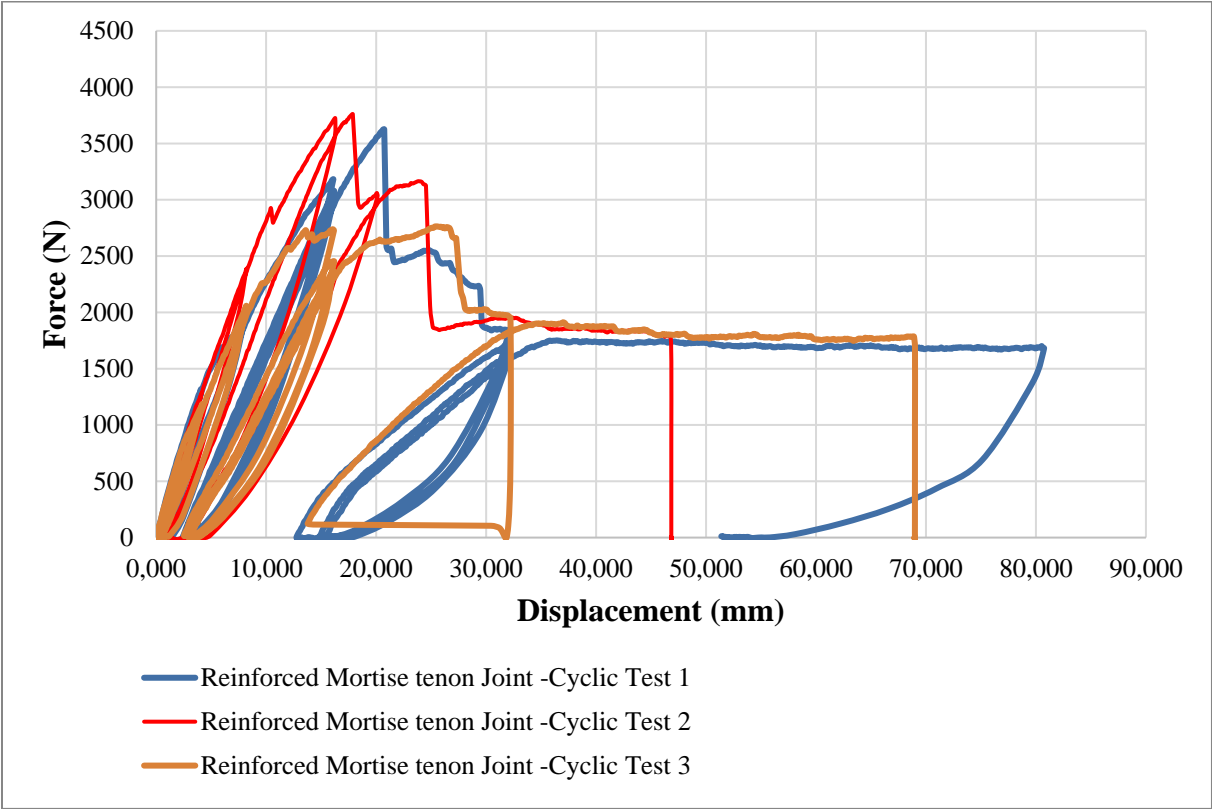
Figure 4. 74: Load-deformation curve of cyclic tests on reinforced specimens
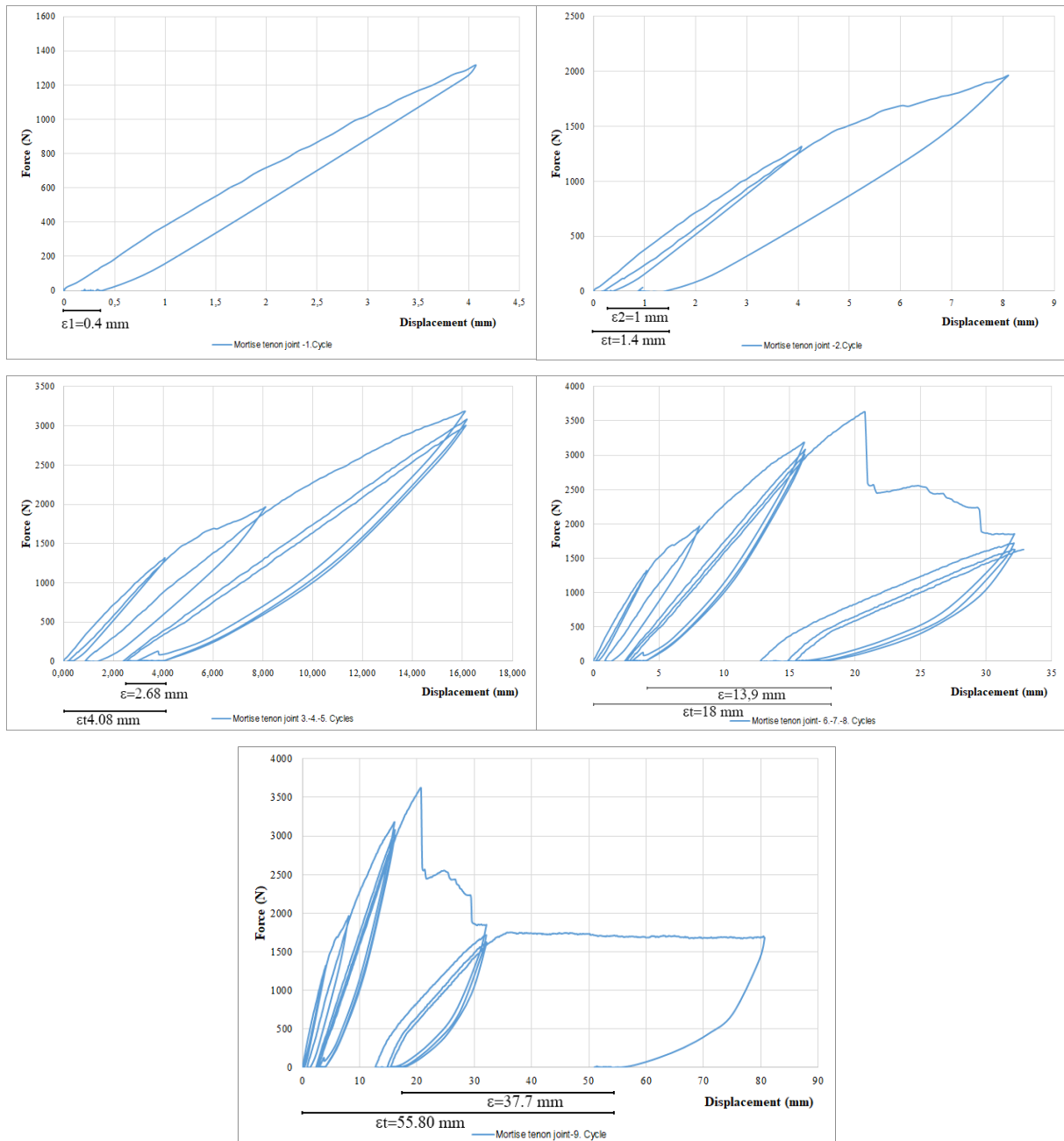
Figure 4. 75: Complete load-deformation curves of reinforced specimens

When the distance from the load point to the centre of rotation is 480 mm, the moment resistance of joint has been calculated as M (kN·m) $= 0.48F$. One displacement transducer (D1, m) has been installed below the face of the beam to measure the vertical displacement of the beam and to measure the rotation of the joint, rotation (rad) = D1/0.48. Then, the rotational stiffness has been determined M (kN·m) / rotation (rad) for each cycle. For reinforced specimens, rotational stiffness has been calculated as k_1=787 kN·m/rad; k_2=324 kN·m/rad; $k_{3,4,5}$=190 kN·m/rad; $k_{6,7,8}$=23.78 kN·m/rad, k_9=6.95 kN·m/rad at cycle 1 (Vy=4 mm), cycle 2 (Vy=8 mm), cycles 3,4,5 (Vy=16 mm), cycles 6,7,8 (Vy=32 mm), cycle 9 (Vy=64 mm)

95

respectively. The equivalent rotational stiffness decreases gradually in all specimens as rotation increases.

Besides, decreasing modulus of elasticity has been calculated by using the equation 4.6 for each cycle. For reinforced specimens, modulus of elasticities were calculated as E_1=1569 N/mm^2; E_2=938 N/mm^2; $E_{3,4,5}$=558 N/mm^2; $E_{6,7,8}$=58.25 N/mm^2; E_9=21.25 N/mm^2 at cycle 1 (Vy=4 mm), cycle 2 (Vy=8 mm), cycles 3,4,5 (Vy=16 mm), cycles 6,7,8 (Vy=32 mm), cycle 9 (Vy=64 mm) respectively (Figure 4.77).
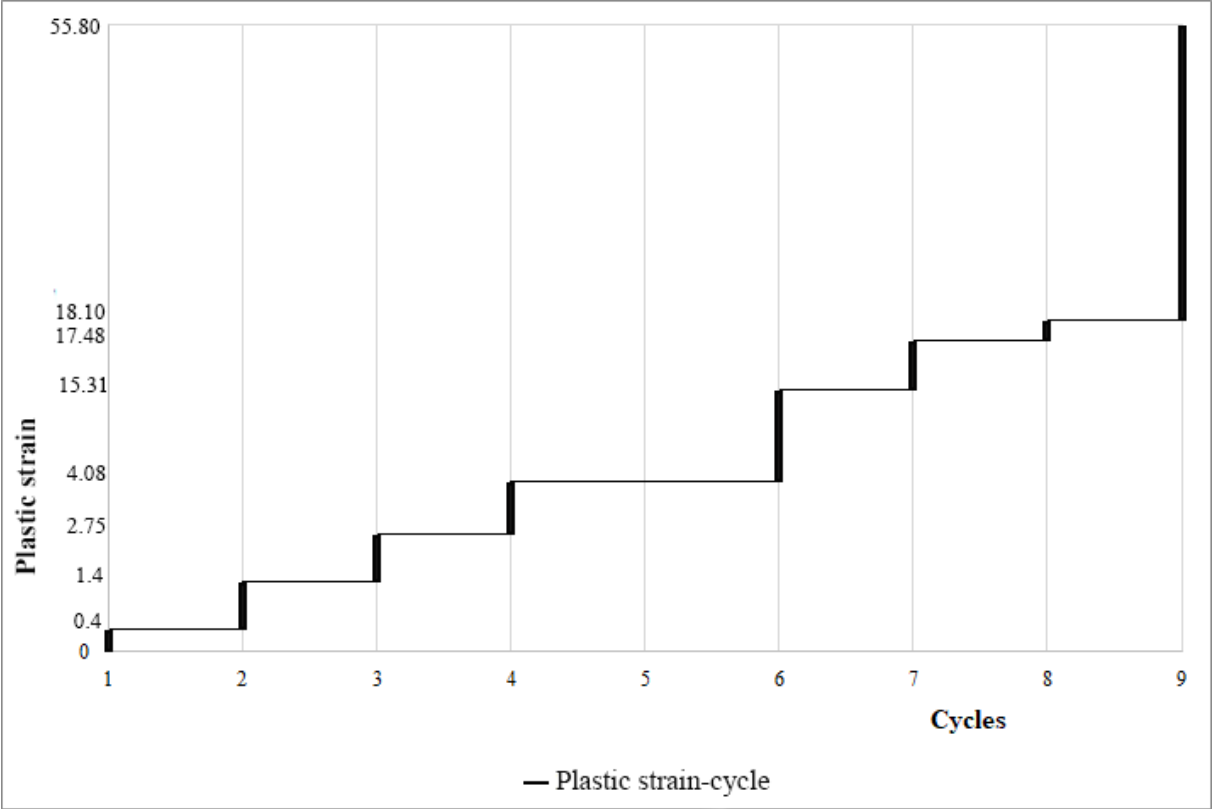
Figure 4. 76: Plastic strain-cycles diagram of reinforced specimens

When reinforced specimens subjected to cyclic loading under pushing, the lower contact surface of the tenon and the mortise has squeezed each other simultaneously. The significant plastic compression deformation occurred on contact surfaces. Failure has been initiated at the joint in tension zone due to rotation of tenon member. Tenon and the mortise members started to separate from each other. Even though the joint has been separated in tension zone, it still resisted to the increment of load by help of high tensile strength of carbon fiber textile. When the specimen has reached the maximum load, carbon fiber textile has separated from the timber surface. CFRP has provided continuity of timber members together until the failure. In other

words, CFRP reinforcements lead to progressive/gradual failure of joint rather than abrupt failure. For all specimens, the ultimate failure has been seen detected at 80 mm. The irrecoverable deformation of specimens is 55.80 mm. The modes of failure for reinforced specimens are detected as the rupture of CFRP sheet after the rotation of timber tenon (Figure 4.78).
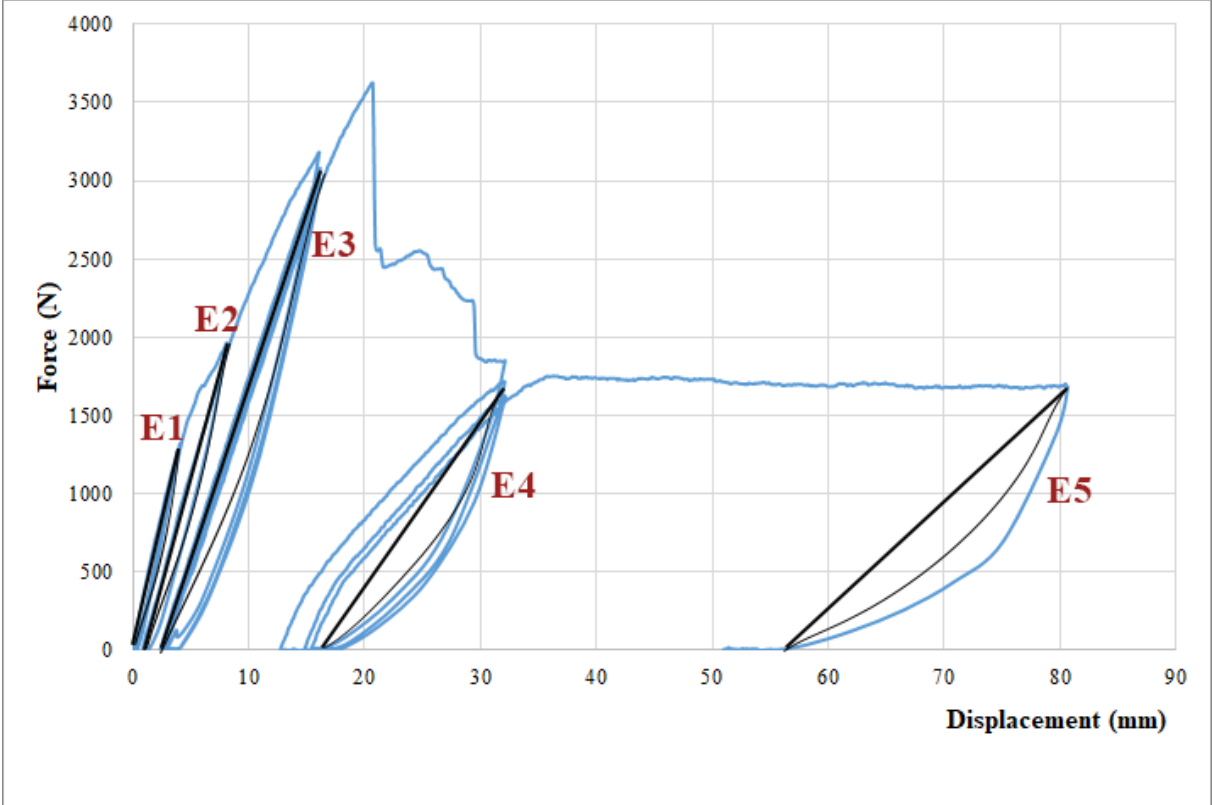
Figure 4. 77: Degradation of modulus of elasticity in reinforced specimens
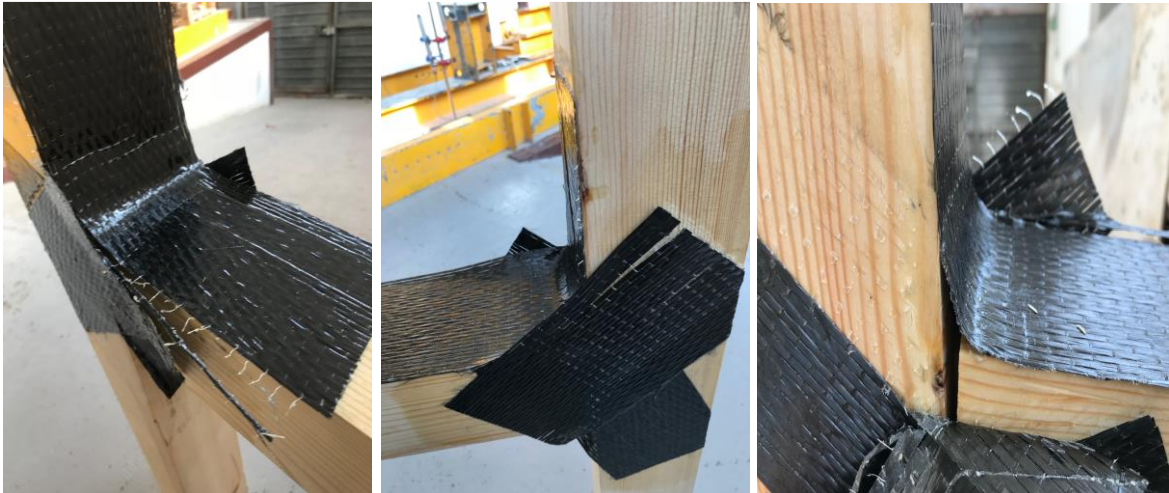
Figure 4. 78: The modes of failure for three reinforced specimens under cyclic loading

4.4.5. Discussion of test results

Test results show that unreinforced specimens have been mainly influenced by the quality of interlocking of the connection, which has increased the load carrying capacity of the screw. Furthermore, the strengthening of timber joints under bending with CFRP has had a beneficial effect on the load-bearing capacity and on the rigidity of the reinforced specimens. The comparison between reinforced and unreinforced specimens under loading, confirms that carbon fiber textile has led to higher stiffness and strength of the joints.

In monotonic tests, the CFRP reinforcement has allowed an increment of the average maximum load from 1200 N to 3600 N, which represents 300 percent more. Besides, at load-deformation curve of reinforced specimen, a sudden drop after the ultimate load is seen, which shows a clear brittle behavior. Even though the failure of CFRP, the joint system still worked and loaded until the ultimate strain. After the peak point of load, with or without CFRP in both conditions, specimens have resisted to load until the deformation, 90 mm. However, in the plateau part of curves the value of load is 1700 N with CFRP while it is 1000 N without CFRP. In other words, under monotonic loading, CFRP provides an increment of load bearing capacity of the joint. Also, the irrecoverable deformations are similar, 90 mm, for the both of unreinforced and reinforced specimens under monotonic loading.

In cyclic tests, the CFRP reinforcement provided the increment of the average maximum load from 1115 N to 3625 N. Furthermore, the rotational stiffness of unreinforced specimens were calculated as $k1=9.26$ kN·m/rad; $k2=7.11$ kN·m/rad; $k3,4,5=5.16$ kN·m/rad; $k6,7,8=3.79$ kN·m/rad at cycle 1 ($Vy=20$ mm), cycle 2 ($Vy=40$ mm), cycles 3,4,5 ($Vy=60$ mm), cycles 6,7,8 ($Vy=80$ mm) respectively. For the reinforced specimens, rotational stiffness have been calculated as $k1=787$ kN·m/rad; $k2=324$ kN·m/rad; $k3,4,5=190$ kN·m/rad; $k6,7,8=23.78$ kN·m/rad, $k9=6.95$ kN·m/rad at cycle 1 ($Vy=4$ mm), cycle 2 ($Vy=8$ mm), cycles 3,4,5 ($Vy=16$ mm), cycles 6,7,8 ($Vy=32$ mm), cycle 9 ($Vy=64$ mm) respectively. The rotational stiffness of reinforced specimens is higher than the unreinforced specimens which has led to more brittle behaviour. The rotational behavior of the damaged mortise tenon joints is semi-rigid. When the reinforced specimens have been pushed to 32 mm (cycle 6), it reached the maximum load, CFRP ruptured and sudden drop from 3625 N to 1800 N has been seen. Then, after three cycles more, the reinforced specimens showed ductile behaviour. It continued with constant load (1780 N) until the ultimate strain, 80 mm. Permanent deformation is detected as 71 mm in unreinforced specimen, while it is 55 mm in reinforced specimen. It can be observed that CFRP provided the reduction of deformation as 23% and the increasement of load bearing capacity

325% under cycle loading. Besides, the modulus of elasticity has been calculated for each cycle. For the unreinforced specimens, modulus of elasticity has been calculated as $E1=19.05$ N/mm^2; $E2=14.61$ N/mm^2; $E3,4,5=10.66$ N/mm^2; $E6,7,8=7.8$ N/mm^2 at cycle 1 (Vy=20 mm), cycle 2 (Vy=40 mm), cycles 3,4,5 (Vy=60 mm), cycles 6,7,8 (Vy=80 mm) respectively. For the reinforced specimens, modulus of elasticity has been calculated as $E1=1569$ N/mm^2; $E2=667$ N/mm^2; $E3,4,5=370$ N/mm^2; $E6,7,8=48.49$ N/mm^2; $E9=14.34$ N/mm^2 at cycle 1 (Vy=4 mm), cycle 2 (Vy=8 mm), cycles 3,4,5 (Vy=16 mm), cycles 6,7,8 (Vy=32 mm), cycle 9 (Vy=64 mm) respectively. It can be stated that the modulus of elasticity has been increased with CFRP reinforcement.

All joint specimens have experienced similarly failure pattern under loading. Significant plastic compression deformation have occurred on the contact surfaces between tenon and mortise, and tenon pull-out increased as the rotation increased. In other words, the modes of failure for unreinforced specimens are detected as tenon pull out from mortise hole, whereas the failure pattern of reinforced specimens are detected as the separation of the timber members and then rupture of CFRP sheet after the rotation of timber tenon. Without strengthening, the joint is not able to prevent the failure causes by high load (detachment of the connected elements) and the amount of energy dissipated is very small. CFRP strengthening technique was efficient in the improvement of the hysteretic behaviour of the connections.

5. NUMERICAL ANALYSIS

The finite element model (FEM) is suitable tool for the analysis of the behaviour of structural elements. The numerical results must be always calibrated on existing experimental results. In this chapter, a 3D numerical model has been calibrated by using the experimental results from monotonic and cyclic tests of timber joints. The model was created using ANSYS 18.1.

5.1 Material Model

Timber is a clear anisotropic material in terms of engineering elastic models, wood is usually treated as an orthotropic in the system of so called anatomic cylindrical coordinates corresponding to the longitudinal, L, radial, R, and transversal, T, directions. The orthotropic

behavior of material requires values of three Youngs moduli, E, three shear moduli, G, and six Poissons ratios, ν, in total, up to nine elastic constants.

A suitable way to represent wood as a 3D continuum material, is to use Hooke's generalized law as given in Equation 5.1. The constitutive law describes the dependency between stress and strain.

$$\varepsilon = C \times \sigma \tag{5.1}$$

The elastic flexibility tensor C is defined as 6×6 matrix in Voigt's notation in Equation 5.2 for orthotropic materials and organizes the moduli of elasticity E and shear G along with Poisson's ratio ν. The orthotropic directions L, T and R correspond to the longitudinal, transverse and radial timber local axes, respectively. It is assumed that the longitudinal axis direction is parallel to the grain of the timber material, while the transverse and radial axes lay in the cross-section plan and act in the direction perpendicular to the grain.

$$C = \begin{bmatrix} \dfrac{1}{E_L} & -\dfrac{\nu_{LR}}{E_R} & -\dfrac{\nu_{TL}}{E_T} & 0 & 0 & 0 \\[2mm] & \dfrac{1}{E_R} & -\dfrac{\nu_{TR}}{E_T} & 0 & 0 & 0 \\[2mm] & & \dfrac{1}{E_T} & 0 & 0 & 0 \\[2mm] & & & \dfrac{1}{G_{LR}} & 0 & 0 \\[2mm] & & & & \dfrac{1}{G_{LT}} & 0 \\[2mm] & & & & & \dfrac{1}{G_{RT}} \end{bmatrix} \tag{5.2}$$

The numerical values for the elastic parameters that have been used are given in Table 5.1. The reference material properties were obtained from previous experimental tests (given in Chapter 4.2 Timber characterization tests). The additional information necessary which was not derived from experimental results was obtained using the Joint Committee on Structural Safety probabilistic model code (JCSS, 2006). Other material properties which are estimated, are based on the reference material properties. Expressions for the expected values E and the coefficient of variation COV are given in Table 5.2.

Table 5. 1: Elastic parameters from experimental tests

Bending strength (R_m):	72.97 MPa
Bending MOE (E_m):	13648 MPa
Compression strength ($R_{C,0}$):	39 MPa
Compression strength ($R_{C,90}$):	4.12 MPa
Density (ρ_{den}):	500 kg/m^3

Table 5. 2: Relation between reference properties and other properties (JCSS, 2006)

Property	Expected values $E[X]$	Coefficient of variation $COV[X]$
Tension strength ($R_{t,0}$)	$E[R_{t,0}] = 0.6\, E[R_m]$	$COV[R_{t,0}] = 1.2\, COV[R_m]$
Tension strength ($R_{t,90}$)	$E[R_{t,90}] = 0.015\, E[\rho_{den}]$	$COV[R_{t,90}] = 2.5\, COV[\rho_{den}]$
MOE tension ($E_{t,0}$)	$E[E_{t,0}] = E[E_m]$	$COV[E_{t,0}] = COV[E_m]$
MOE tension ($E_{t,90}$)	$E[E_{t,90}] = E[E_m]/30$	$COV[E_{t,90}] = COV[E_m]$
Compression strength ($R_{c,0}$)	$E[R_{c,0}] = 5\, E[R_m]^{0.45}$	$COV[R_{c,0}] = 0.8\, COV[R_m]$
Compression strength ($R_{c,90}$)	$E[R_{c,90}] = 0.008\, E[\rho_{den}]$	$COV[R_{c,90}] = COV[\rho_{den}]$
Shear modulus (G_v)	$E[G_v] = E[E_m]/16$	$COV[G_v] = COV[E_m]$
Shear strength (R_v)	$E[R_v] = 0.2\, E[R_m]^{0.8}$	$COV[R_v] = COV[R_m]$

According to coefficient of variations, other material properties are calculated (Table 5.3).

Table 5. 3: Elastic parameters from JCSS (2006)

Tension strength ($R_{t,0}$):	43.782 MPa
Tension strength ($R_{t,90}$):	7.5 MPa
MOE tension ($E_{T,0}$):	13648 MPa
MOE tension ($E_{T,90}$):	454.93 MPa
Shear modulus (G_v):	853 MPa
Shear strength (R_v):	6.18 MPa

As observed in the experimental campaign, timber do not show significant plasticity behavior before failure occurred and thus no plasticity rules were accounted for the analytical study. In order to fully understand the behavior of wood connections when subjected to loading and to predict the collapse, a definition of failure mode needs to be applied to models.

Two main failure types were identified:

• ductile behaviour in compression parallel and perpendicular to the grain,
• brittle behaviour in tension perpendicular to the grain and shear parallel to grain.
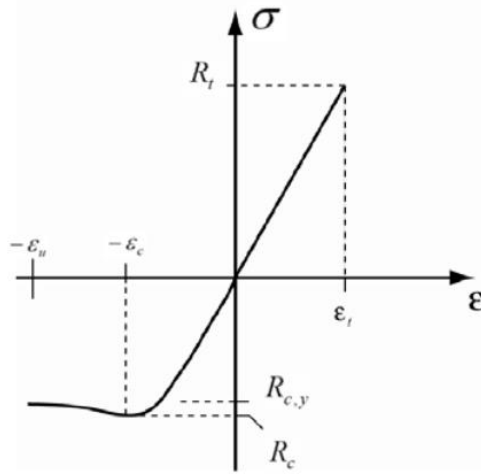
Figure 5. 1: Linear elastic-plastic stress strain curve (Glos, 1981)

In Figure 5.1, an idealised stress-strain relationship under axial load is shown for timber specimens, according to Glos (1981). In tension there is a linear relationship described by the modulus of elasticity E_t. In compression the relation is described by the initial modulus of elasticity E_c, the compression strength R_c , the asymptotic final compression strength R_c, y, the strain ε_c at maximum stress and the ultimate strain ε_u. The following empirical relation is assumed:

$$\sigma(\varepsilon) = \frac{\varepsilon + k_1 \varepsilon^N}{k_2 + k_3 \varepsilon + k_4 \varepsilon^N} \quad \text{for} \quad -\varepsilon_u \leq \varepsilon \leq 0 \qquad (5.3)$$

$$E_t \varepsilon \qquad \qquad \text{for} \quad 0 \leq \varepsilon \leq \varepsilon_t$$

These parameters (k_1, k_2, k_3, k_4) are used to determine relationship between: $R_{c,y}$ and R_c

$$k_1 = \frac{R_{c,y}}{(N-1).E_c.\varepsilon_c^{N-1}(1 - R_{c,y} / R_c)}$$

$$k_2 = \frac{1}{E_c}$$

$$k_3 = \frac{1}{R_c} - \frac{N}{(N-1).E_c.\varepsilon_c}$$

$$k_4 = \frac{k_1}{R_{c,y}}$$

Typical values for the parameters are:

$$R_{c,y} / R_c \approx 0.8 \quad \varepsilon_c = 0.8 - 1.2\% \quad \varepsilon_u \approx 3\varepsilon_c \quad N=7$$

As all structural materials, timber eventually fails if subjected to increasing stress. Failure can be defined in various ways, but here focus on stress based failure criteria and fracture mechanics.

5.2 Failure Criteria

Failure is commonly assessed by linear elastic stress analysis with a stress based criterion. Three commonly failure criteria used for timber: the maximum stress criterion, the Norris criteria and the Tsai-Wu criterion (Larsson, 2017).

The most frequently used failure criterion for anisotropic brittle materials is ´the maximum normal stress criterion´, which states that the material fails when any of the stresses exceeds the material strength in the principal direction. As a single stress component reaches its strength, failure occurs according to Equation 5.4 as given for 3D analysis.

$$\max\left\{\frac{|\sigma_{LL}|}{f_{Li}}, \frac{|\sigma_{RR}|}{f_{Ri}}, \frac{|\sigma_{TT}|}{f_{Ti}}, \frac{|\tau_{LR}|}{f_{LR}}, \frac{|\tau_{LT}|}{f_{LT}}, \frac{|\tau_{RT}|}{f_{RT}}\right\} - 1 = 0 \tag{5.4}$$

The strengths with respect to normal stresses may have different values regarding compression or tension ($i = c$; t).

Timber exhibits a progressive failure process as it becomes loaded. When the material is subjected to loading, the matrix controlled modes of failure can occur. The material stiffness is instantly reduced based on damage variables. After a certain point, the material experiences enough damage by means of local failure, thus the material resists no longer the load. A progressively decreasing stiffness path was used in the model. The allowable values of tensile matrix stiffness reduction and compressive matrix stiffness reduction are between 0 and 1 (where 0= no reduction in material stiffness in the affected more after damage initiation and 1= complete stiffness loss in the affected mode). The progressively decreasing stiffness was simulated and while tensile matrix stiffness reduction was taken as %80, compressive matrix stiffness reduction was taken as %20.

5.3 Numerical Modelling of Lap Joint

Timber material has been modelled with a constitutive model based on elastic orthotrophy with maximum stress failure criterion. The lap joint is connected via two screws in the model. A

basic elastic-plastic material model with bilinear isotropic hardening is used for steel of screws, assuming the von Mises yield criterion. Material parameters used for this model are given in Table 5.4, (ASME BPV Code ,1998).

Table 5. 4: Material properties of steel (ASME BPV Code, 1998)

Density :	7850 kg/m3
Young´s modulus:	2E+05 MPa
Young´s modulus Z direction:	1529 MPa
Poisson´s ratio:	0,3
Bulk modulus:	1,6667 E+11 Pa
Shear modulus:	7,6923E+10 Pa
Yield strength:	250 MPa

5.3.1. Geometric constraints, mesh and loading

The geometry of finite element model, loading, boundry conditions and material axes are shown in Figure 5.2. Subsequently, a vertical displacement of 60 mm has been applied, with a constant movement rate, at the two loading points. It is noted that the self-weight of the wood element and standard earth gravity are considered in the analyses as well. While one support has been pinned, the other has been roller support which allows to move in x direction.
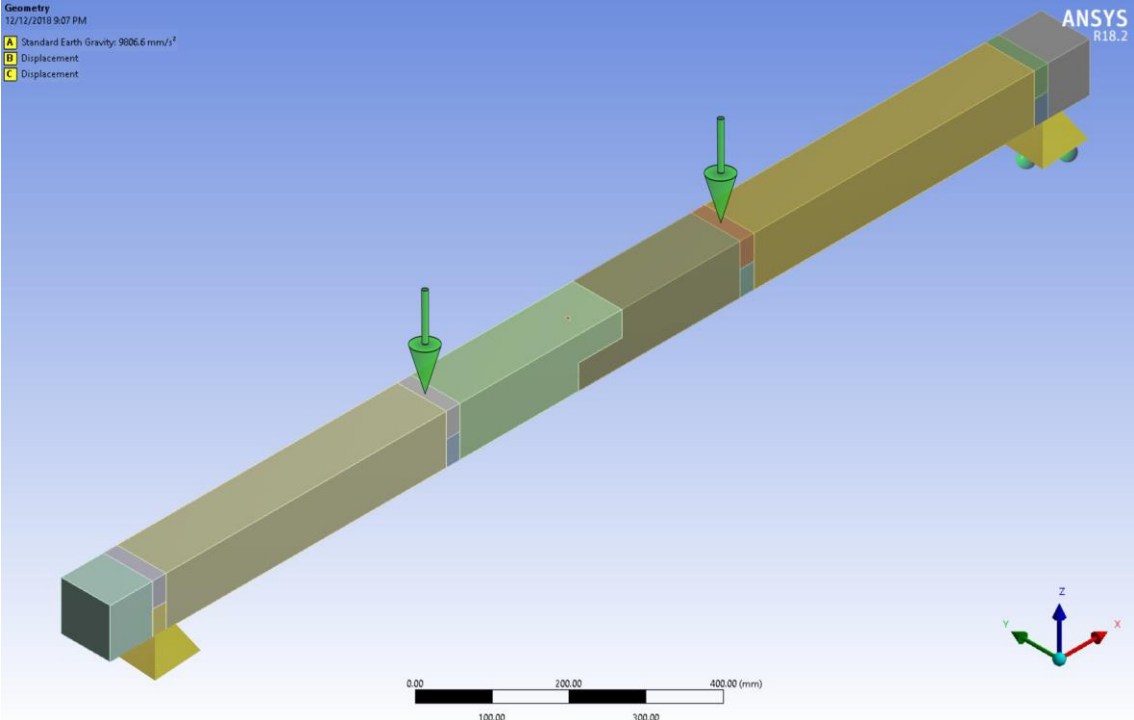
Figure 5. 2: Finite element model geometry

The adopted finite element mesh has been created using total 24525 solid elements and 41568 nodes. (Figure 5.3). In the analysis SOLID 186 element and SOLID 187 element are used (Figure 5.4). SOLID 186 is a higher order 3D 20-node solid element with quadratic displacement behavior. The element is defined by 20 nodes having three degrees of freedom per node: translations in the nodal x, y, and z directions.

SOLID 187 element is a higher order 3D, 10-node element. It has a quadratic displacement behavior and is well suited to modeling irregular meshes. The element has been defined by 10 nodes having three degrees of freedom at each node: translations in the nodal x, y, and z directions. The element supports plasticity, hyperelasticity, creep, stress stiffening, large deflection, and large strain capabilities.

Contacts between timber-timber and timber-steel elements have been defined using 3-D contact surface elements (CONTA174) associated with the 3-D target segment elements (TARGE170). CONTA 174 is used to represent contact and sliding between 3D target surfaces and a deformable surface defined by this element.
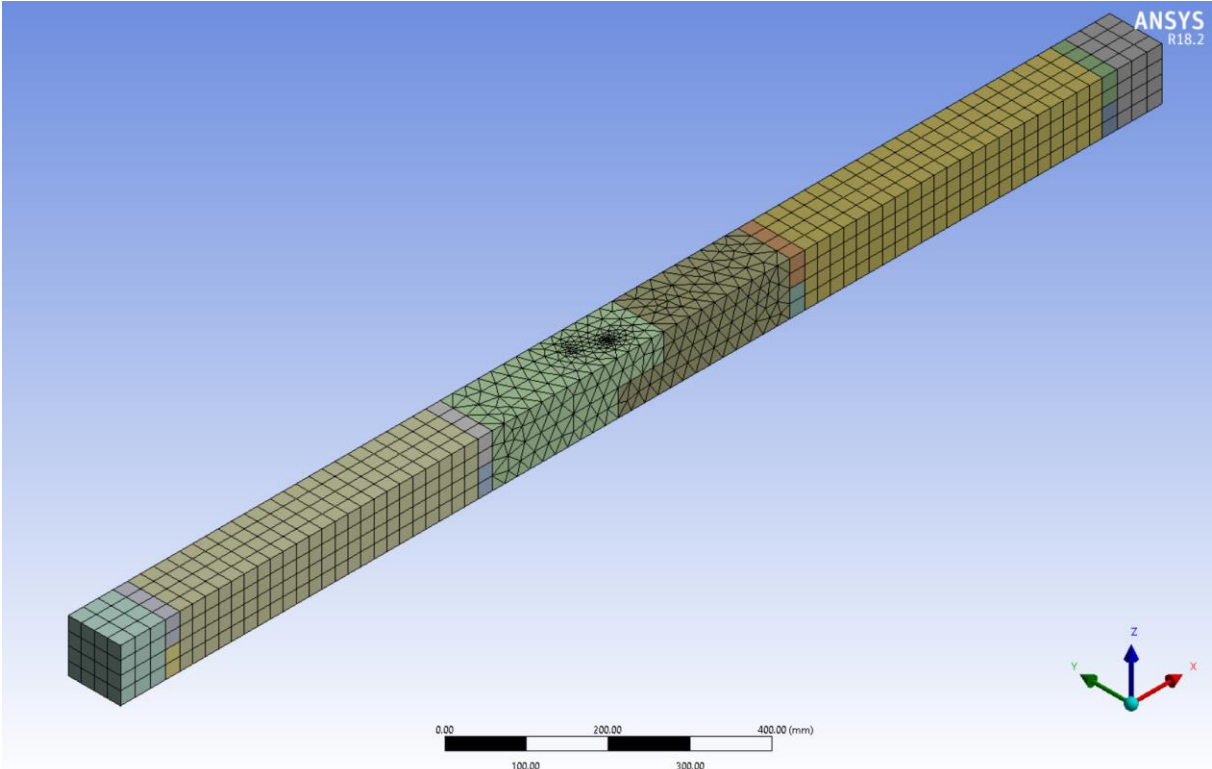
Figure 5. 3: Finite element mesh
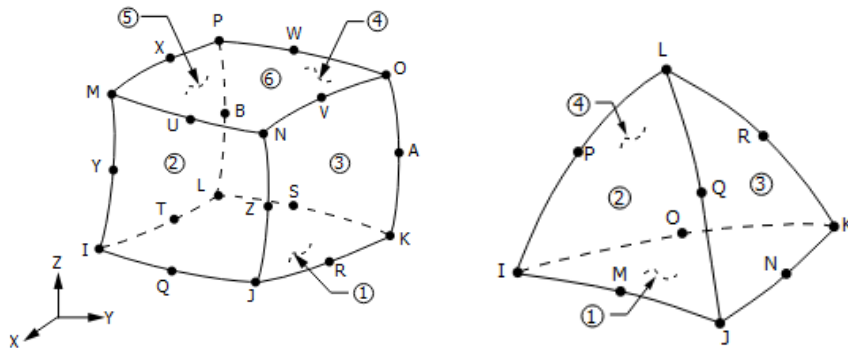
Figure 5. 4: SOLID 186 and SOLID 187 element types, respectively

Note that the stiffness of the frame wall mostly depends on the contact status (both faces touching or not). Therefore, at each contact surface, isotropic Coulomb friction is considered by using coefficients of friction of 0.2 and 0.4 for timber-steel and timber-timber contact, respectively (BS 5975 1996).

5.3.2. Analysis of the unreinforced model under monotonic loading

Assuming the values above, the model of the timber beam with lap joint has been calibrated, by applying a monotonic load to the top of the model in displacement control. Figure 5.5 shows the numerical load-displacement curve with the experimental monotonic results.
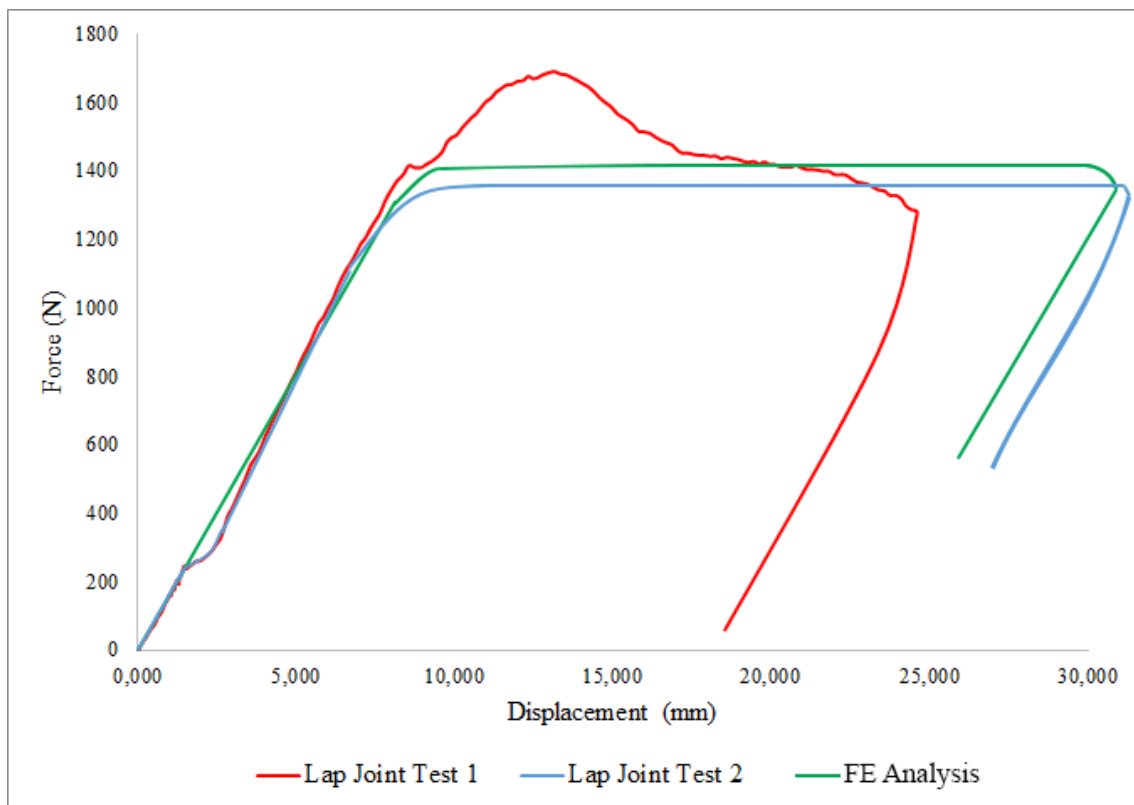
Figure 5. 5: Load displacement curves under monotonic loads

106

A significant fitting between experimental and numerical results is observed both in terms of stiffness and lateral resistance. When the load reaches the peak of load, the joint starts to separate by showing ductile behaviour until the whole collapse. The maximum displacement has been about 25 mm in average. Figure 5.6 presents the directional deformation (Z axis) and maximum deformation of the test. Concentrated normal stresses parallel to grain are shown in Figure 5.7. In particular, the maximum compressive stress take place around screws, which led to local crushing in timber. Besides, the supports and load introduction are exposed to high compressive stress levels. The maximum tension stress is observed at the lower part of the joint. The lap joint is a weak joint type under bending. At first stage of loading at lower bending moment levels, the joint starts rotating by finishing with plastic deformations within the screws and local damage in timber in direct vicinity of screws. Load-deflection behavior of the beam with lap joint is majorly affected by the interaction of the screws with timber; in other words: friction coefficient between the two materials. In the analysis, a value of 0.2 for the friction coefficient was considered for timber-steel contact. The failure mode in specimens with screws is clearly associated with local crushing of timber derived from bending of the screws (Figure 5.8-5.9).
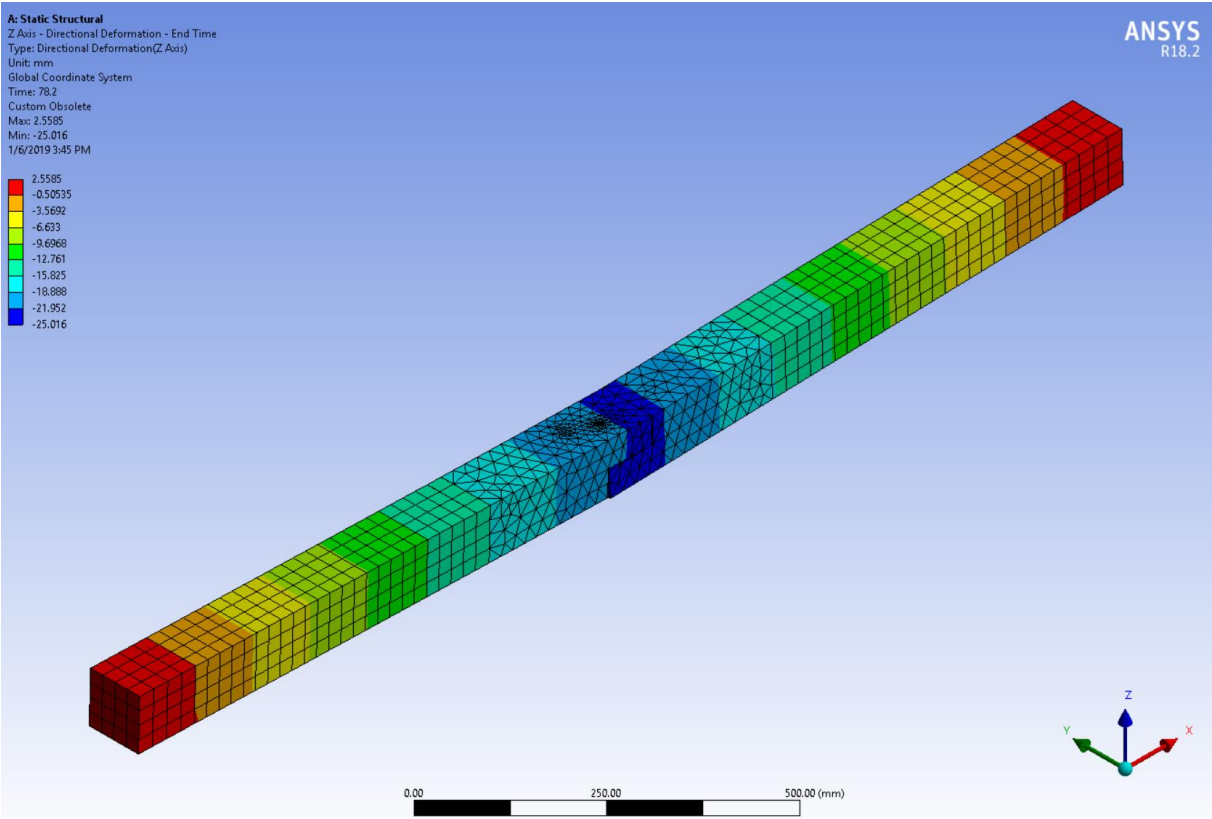
Figure 5. 6: Directional deformation
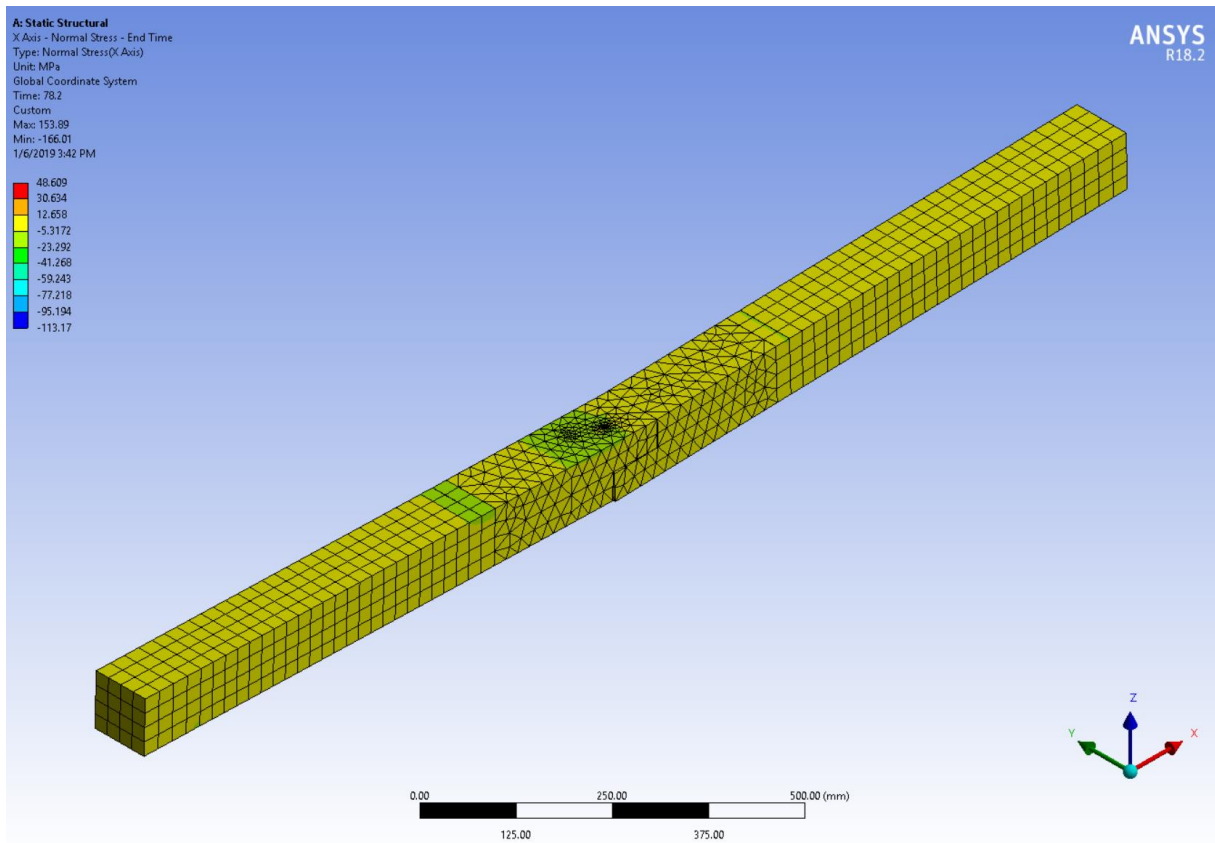
Figure 5. 7: Normal stress distribution
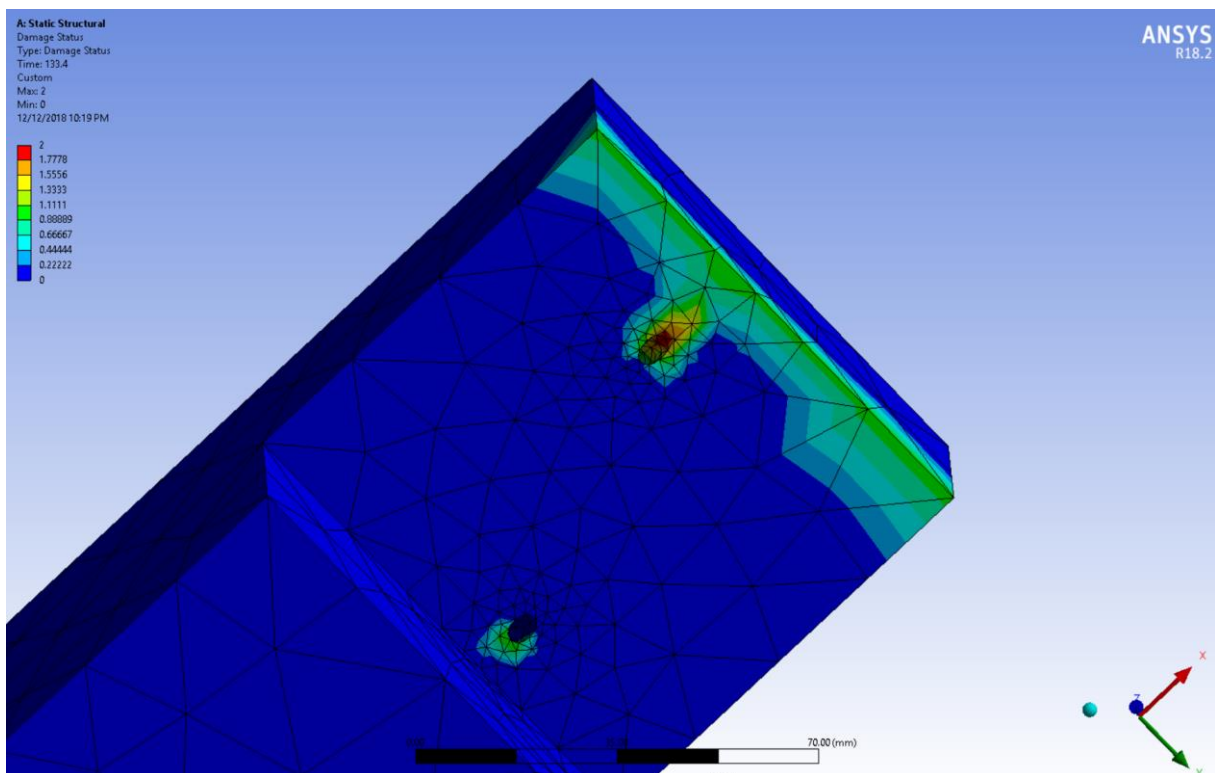
Figure 5. 8: Damage status in place of screws
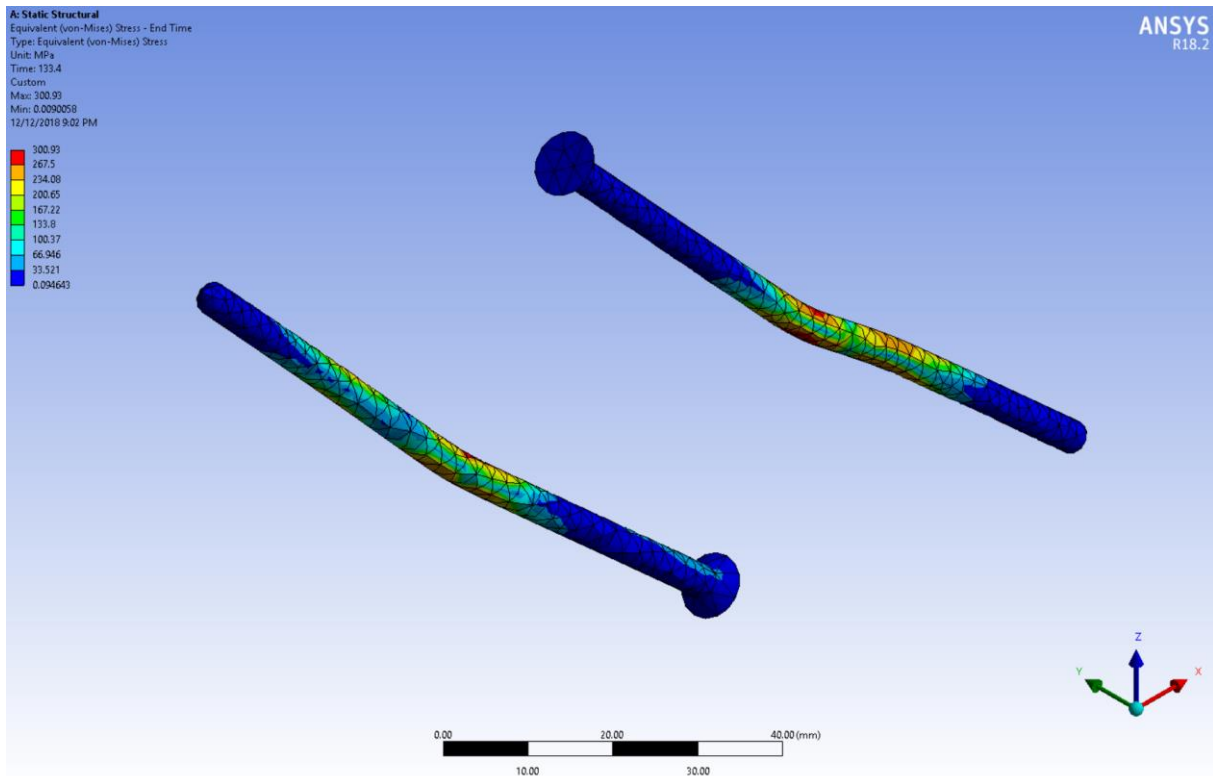
Figure 5. 9: Damage status of screws

5.3.3. Analysis of the reinforced model under monotonic loading

A numerical approach of timber beams strengthened with carbon fiber reinforced polymer (CFRP) composites is shown here. To predict the behavior of timber beam strengthened with CFRP composites, a three dimensional computational model was developed using the general-purpose FEA program ANSYS. Timber and CFRP composites were modeled as an elastic orthotropic constitutive model until failure.

FRP composites are supposed to be bonded on the joint of timber beams, as 400 mm wideness in order to enhance load-carrying capacity. As a solid element types SOLID 186 element and SOLID 187 element were used for timber. The CFRP layer, thickness 0,5 mm, is also meshed with the same element type, SOLID 186 (Figure 5.10). The elastic properties of carbon fiber reinforced polymer (CFRP) is given in table 5.5.
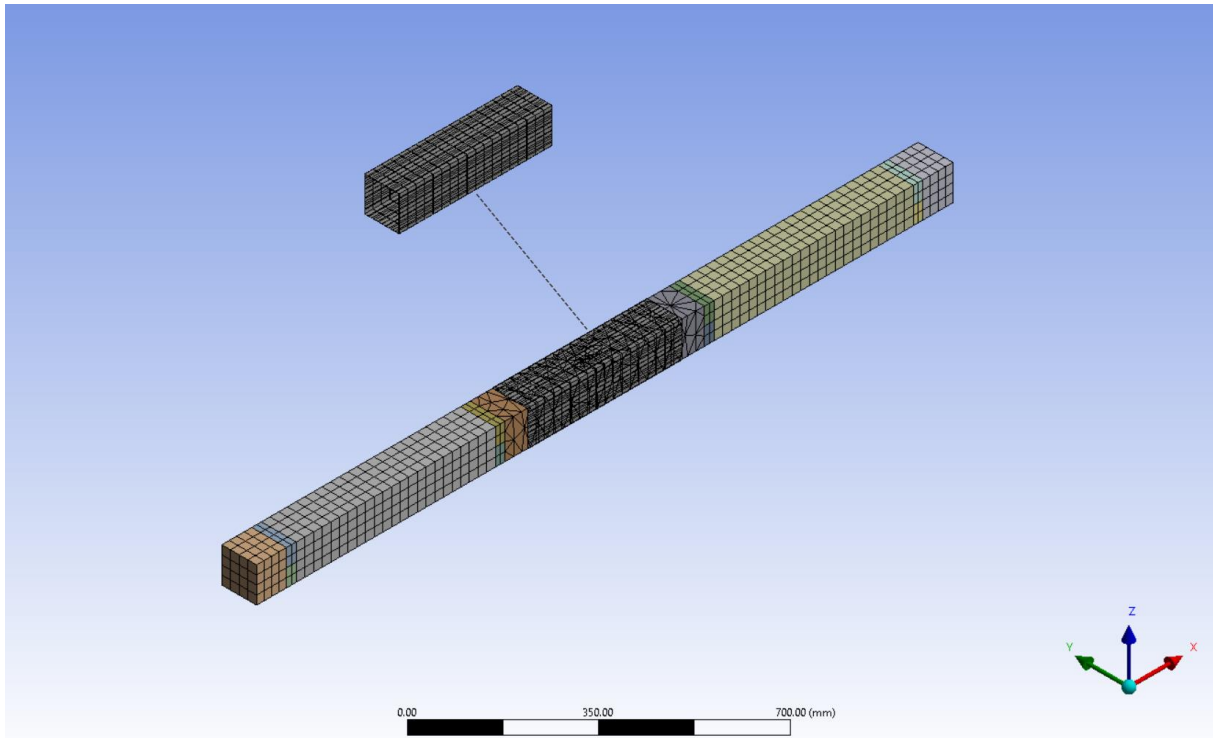
Figure 5. 10: Finite element mesh of beam strengthened with CFRP composites

Table 5. 5: Elastic parameters of CFRP (Ticem)

Young´s modulus X direction:	42000 MPa
Young´s modulus Y,Z directions:	8600 MPa
Tensile strength ($R_{T,0}$):	630 MPa
Tensile strength ($R_{T,90}$):	29 MPa
Compression strength ($R_{C,0}$):	1082 MPa
Compression strength ($R_{C,90}$):	100 MPa

Between each contact surface, the coefficients of friction have been considered as 0.2 and 0.4 for timber-steel and timber-timber contact. As an adhesive layer, between timber and carbon fiber reinforced polymer, bonded contact was defined. A vertical displacement of 60 mm with a constant amplitude, has been applied to the beam model until the established failure criteria were satisfied. The CFRP element has been modelled as it ruptures when the maximum axial stress exceeds the tensile and compressive strength of the composite. As the progressive decreasing stiffness, tensile matrix stiffness reduction and compressive matrix stiffness reduction were taken as the value of 1 (which means complete stiffness loss). Figure 5.11 shows

the numerical load-displacement curve after reinforcement with the experimental monotonic results.
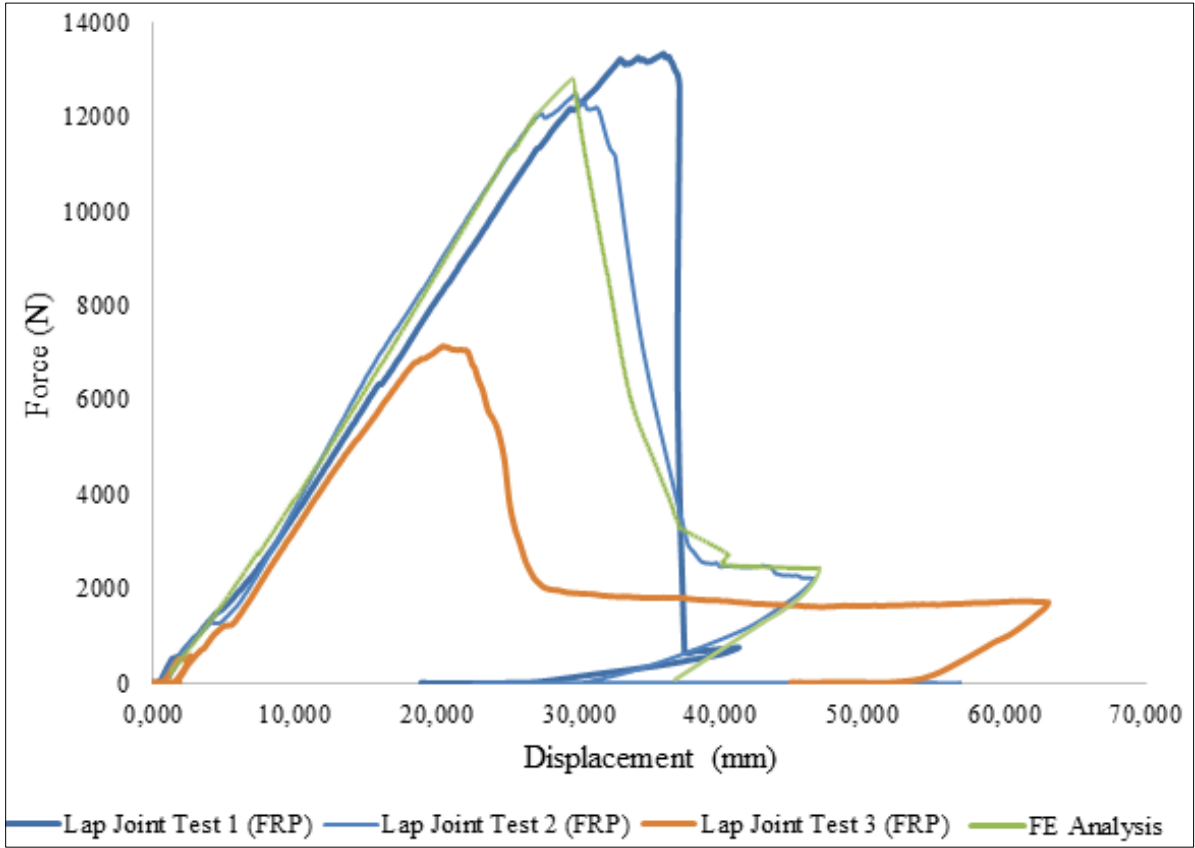
Figure 5. 11: Load displacement curves of the strengthening beams under monotonic loads

It is observed that the results of FE analysis correlate well with those experimental results. The model captures the behaviours of the strengthened beams of experiments. Particularly with specimen 2, they have similar responses of initially elastic before undergoing a non-linear softening phase and the maximum load point. The response of the beams was essentially linear until the failure. After that, due to the high stiffness of CFRP material, sharp crack and brittle behaviour has been seen in the strengthening beams. The strengthened beam reaches a maximum load of 12 kN at a displacement of about 40 mm.

Figure 5.12 shows the stress distribution in the strengthening beam. It is clearly seen that stress is mainly concentrated along the CFRP sheet, due to a higher stiffness. Maximum compressive stress, approximately 238 MPa, is concentrated at the upper part of the beam which exposed the loads. Maximum tension stress, approximately 788 MPa, is concentrated at the lower part of the beam. When the maximum axial stress exceeded the tensile strength of the composite, the strengthened beam collapsed by the tension side. However with the CFRP sheet, the whole

timber beam could still provide a certain bending capacity. Finally, CFRP ruptured and separated from timber beam. Slip between the wood and the adhesive did not take place.
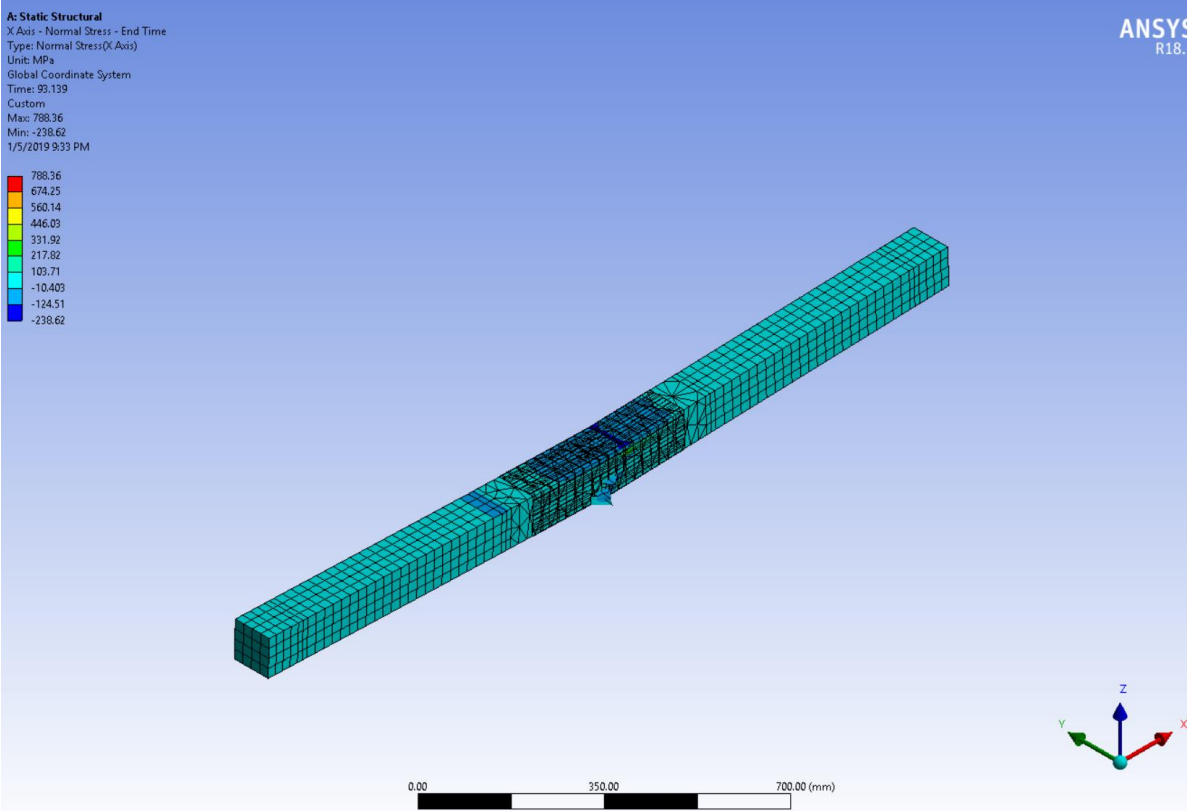
Figure 5. 12: Normal stress distribution of the strengthening beam
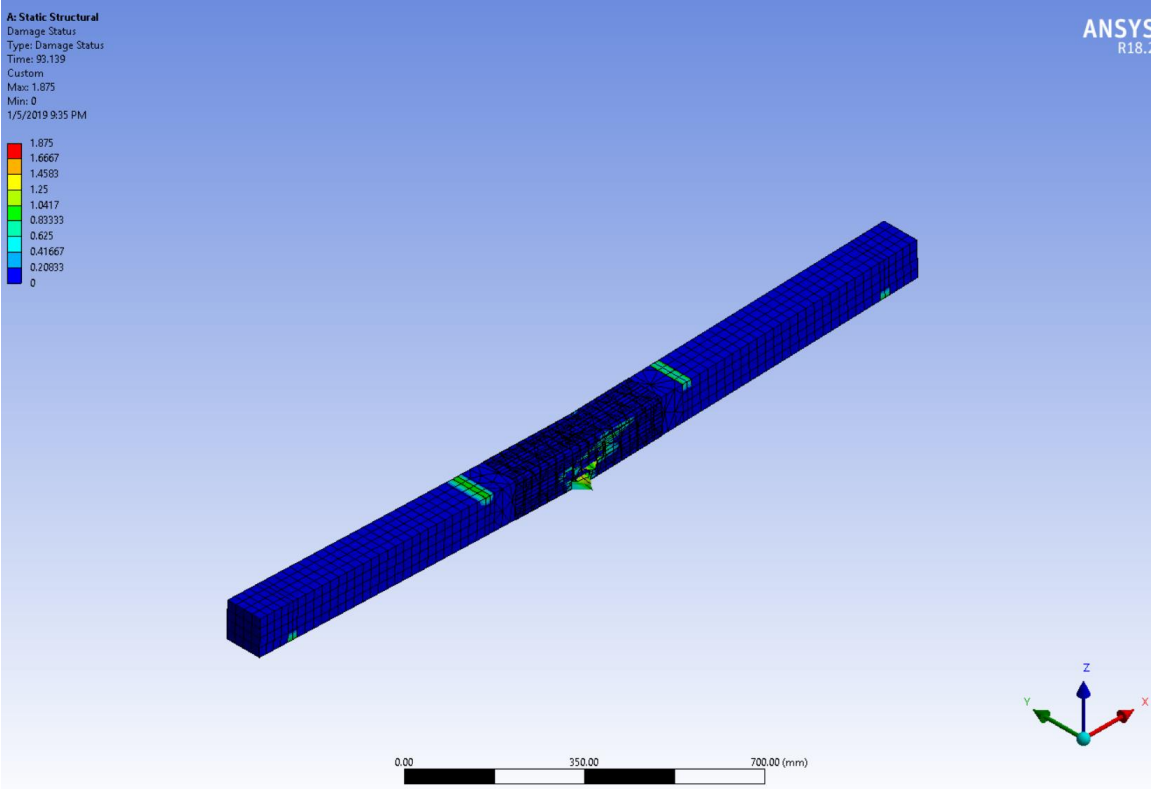
Figure 5. 13: Damage status (0-1) of the strengthening beam

Two distinct collapse modes of the strengthened timber beams are observed, namely, the timber fracture at a flexure-critical region (near midspan) and at the CFRP composites where stress concentrations occurred (Figure 5.13). The damage status is defined with values of 0,1 and 2. (0: undamaged, 1:partially damaged, 2:completely). The fiber tensile damage in the range of 0-1 has been detected under part of beam. Besides, the elastic modulus of the CFRP material increased the load-carrying capacity of the strengthened timber beams and also governed the failure mode of the beams.

5.3.4. Comparison of analysis results

It can be clearly seen that the strengthening enhances the load carrying ability of the beam with lap-joint. The maximum load and top displacement of unstrengthened specimen are 14000 N and 25 mm, while 12000 N, 40 mm for strengthened specimen. The CFRP shows an increase of the ultimate load by about 800% and a change of failure mode is observed with greater ductility. The tension failure in wood in bending is brittle, for this reason, CFRP layers bonded on the tension side of the beam. The overall aim is then to increase the flexural strength and stiffness, and achieve a ductile compression failure mode. CFRP sheet improves the flexural capacity and rigidity of timber beam.
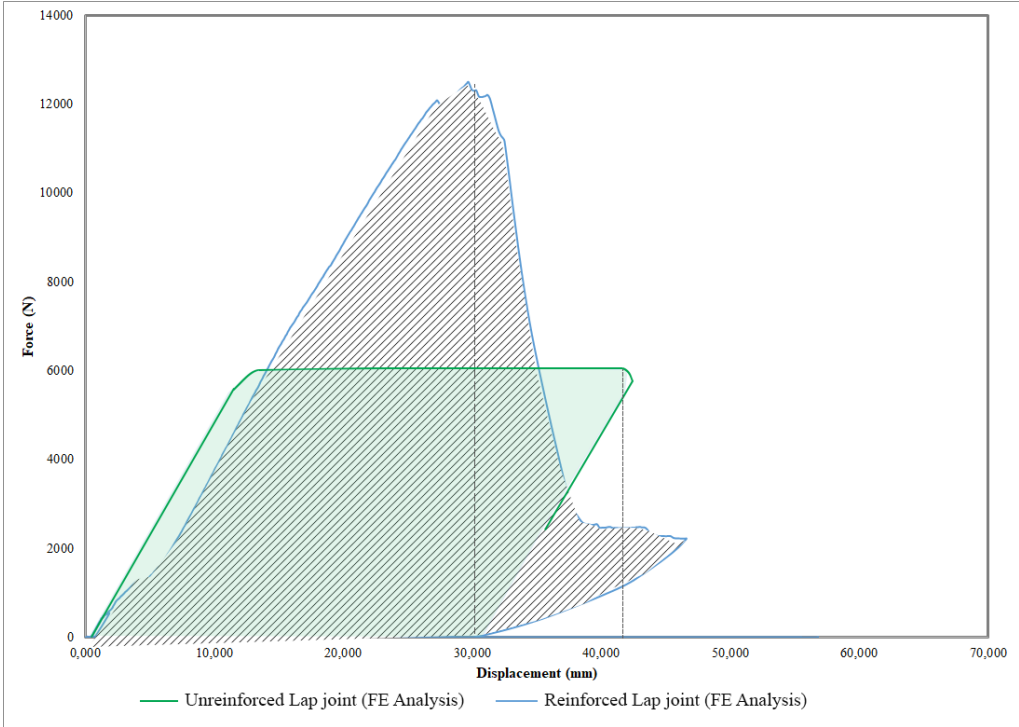
Figure 5. 14: The comparison of the unreinforced and reinforced specimen in FE analysis

Ductility index obtained from energy method which is calculated by the area under the curves. Reinforced beam exhibits high ductility index and the main reason was due to higher range of inelastic region in the compression zone (Figure 5.14). It is very obvious that the reinforced beam reachs high ultimate load compare to the unreinforced beam, even though it yields to low ultimate deflection, it has high total energy and ductility.

5.4 Numerical Modelling of Mortise Tenon Joint

Timber material has been modelled with a constitutive model based on elastic orthotrophy with maximum stress failure criterion. The mortise tenon joint is connected via two screws in the model. A basic elastic-plastic material model with bilinear isotropic hardening is used for steel of screws, assuming the von Mises yield criterion. Material parameters used for this model are given in previous chapter in Table 4.4, (ASME BPV Code ,1998).

5.4.1. Geometric constraints, mesh and loading

The geometry of finite element model, loading, boundry conditions and material axes are shown in Figure 5.15. Subsequently, a vertical displacement of 60 mm is applied, with a constant movement rate, at the one loading point. It is noted that the self-weight of the wood element and standard earth gravity are considered in the analyses as well. The back side of column member is selected as a fixed support which restrain both rotation and translation.
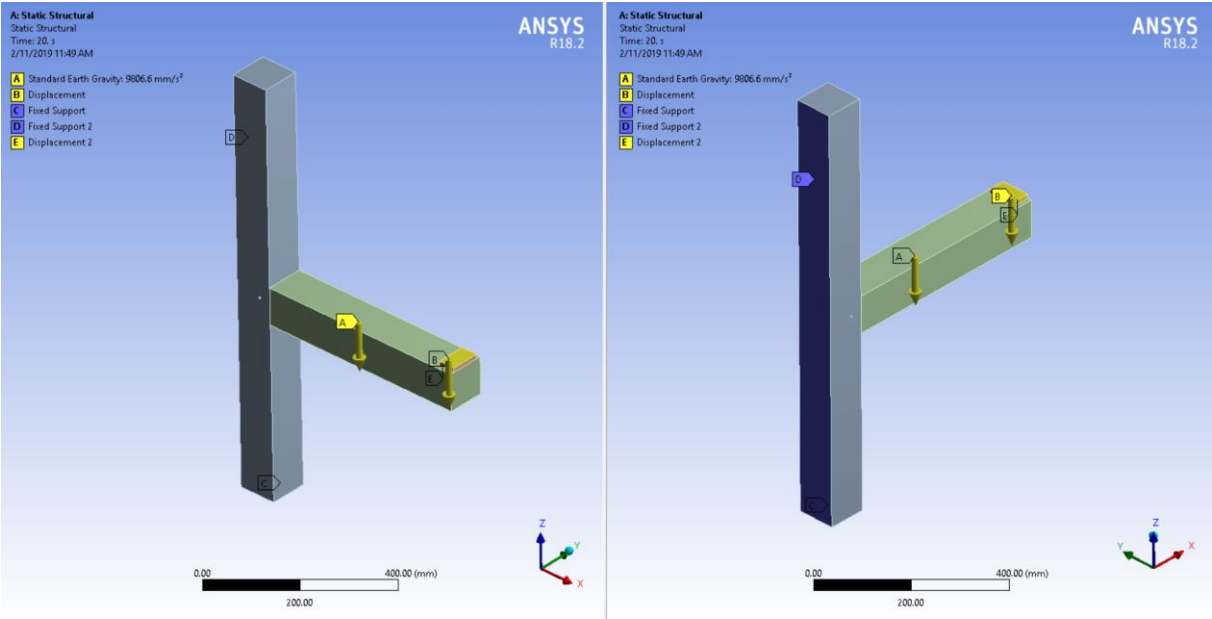
Figure 5. 15: Finite element model geometry

The adopted finite element mesh is created using total 24536 solid elements and 38989 nodes. (Figure 5.16). In the analysis SOLID 186 element and SOLID 187 element are used. SOLID 186 is a higher order 3D 20-node solid element with quadratic displacement behavior. The element is defined by 20 nodes having three degrees of freedom per node: translations in the nodal x, y, and z directions.

SOLID 187 element is a higher order 3D, 10-node element. It has a quadratic displacement behavior and is well suited to modeling irregular meshes. The element is defined by 10 nodes having three degrees of freedom at each node: translations in the nodal x, y, and z directions. The element supports plasticity, hyperelasticity, creep, stress stiffening, large deflection, and large strain capabilities.

The contacts between timber-timber and timber-steel elements are defined using 3-D contact surface elements (CONTA174) associated with the 3-D target segment elements (TARGE170). CONTA 174 is used to represent contact and sliding between 3D target surfaces and a deformable surface defined by this element.
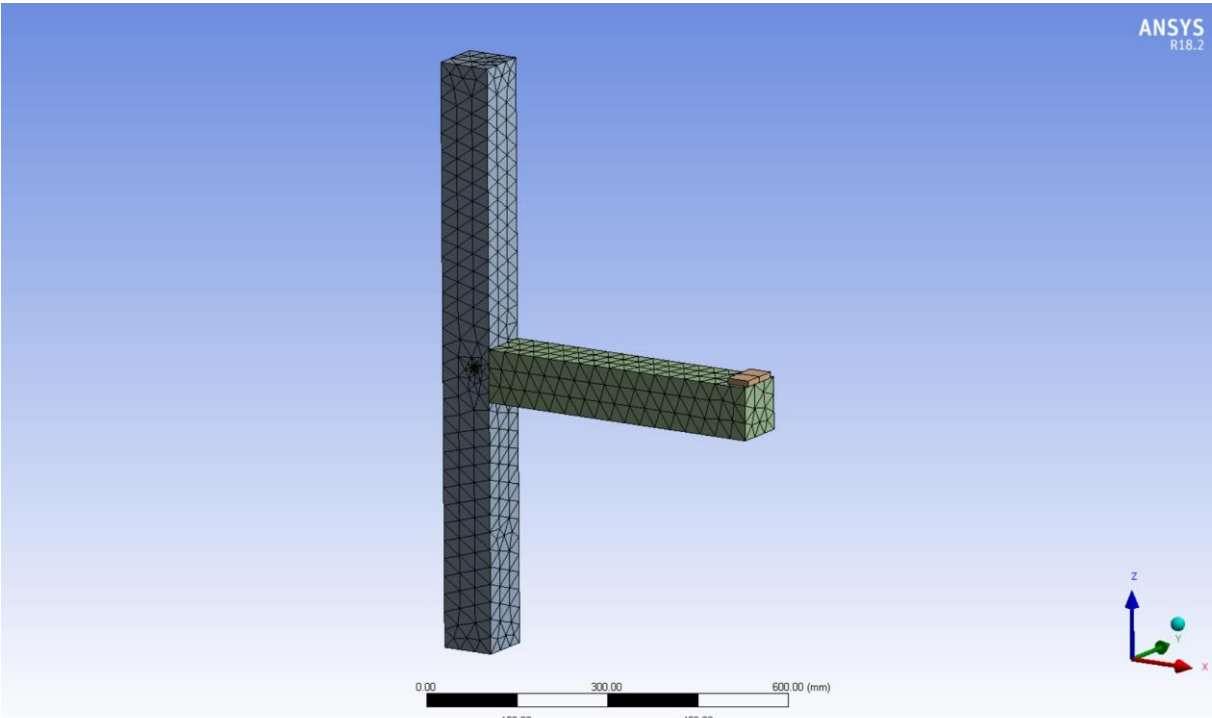
Figure 5. 16: Finite element mesh

Note that the stiffness of the frame wall mostly depends on the contact status (both faces touching or not). Therefore, at each contact surface, isotropic Coulomb friction is considered

using coefficients of friction of 0.2 and 0.4 for timber-steel and timber-timber contact, respectively (BS 5975 1996).

5.4.2. Analysis of the unreinforced model under monotonic loading

Assuming the values at above, the model of the timber beam and column with mortise tenon joint was calibrated, applying a monotonic load to the top of the model in displacement control. Figure 5.17 shows the numerical load-displacement curves with the experimental monotonic results and finite element analysis result.

Figure 5. 17: Load-displacement curves under monotonic loads

A significant fitting between experimental and numerical results is observed both in terms of stiffness and lateral resistance. Initially, the response is linear elastic, where a linear increase in displacement corresponds to a linear increase in load. When the load reaches near 1020 N, the yield occurs. Later, a non linear load-displacement curve developed and smooth plateau associated with tenon end crushing on the mortise. The maximum displacement has been about 80 mm in average. Figure 5.18 presents the directional deformation (Z axis) and maximum deformation of the test. Concentrated normal stresses parallel to grain are shown in Figure 5.19. In particular, the maximum compressive stress take place around screws, which led to local

crushing in timber. Besides, the load introduction is exposed to high compressive stress levels, while the maximum tension stress is observed at the upper part of the tenon. Load-deflection behavior of the beam with mortise tenon joint is majorly affected by the interactions of the screws with timber and also the interaction of mortise with tenon; in other words: friction coefficient between different surfaces. In the analysis, values of 0.2 and 0.3 for the friction coefficients of steel-timber and timber-timber have been considered. When the seperation of tenon from the mortise member has occured, the screws have bent under acting forces stresses. The failure modes in specimen are local crushing of tenon and bending of the screws (Figure 5.20-5.21). The damage status is defined with values of 0,1 and 2. (0: undamaged, 1:partially damaged, 2:completely). The fiber tensile damage in the range of 0-1 has been detected in tenon of beam (Figure 5.20). The compressive damage in the range of 0-1 has been detected at screws (Figure 5.21).
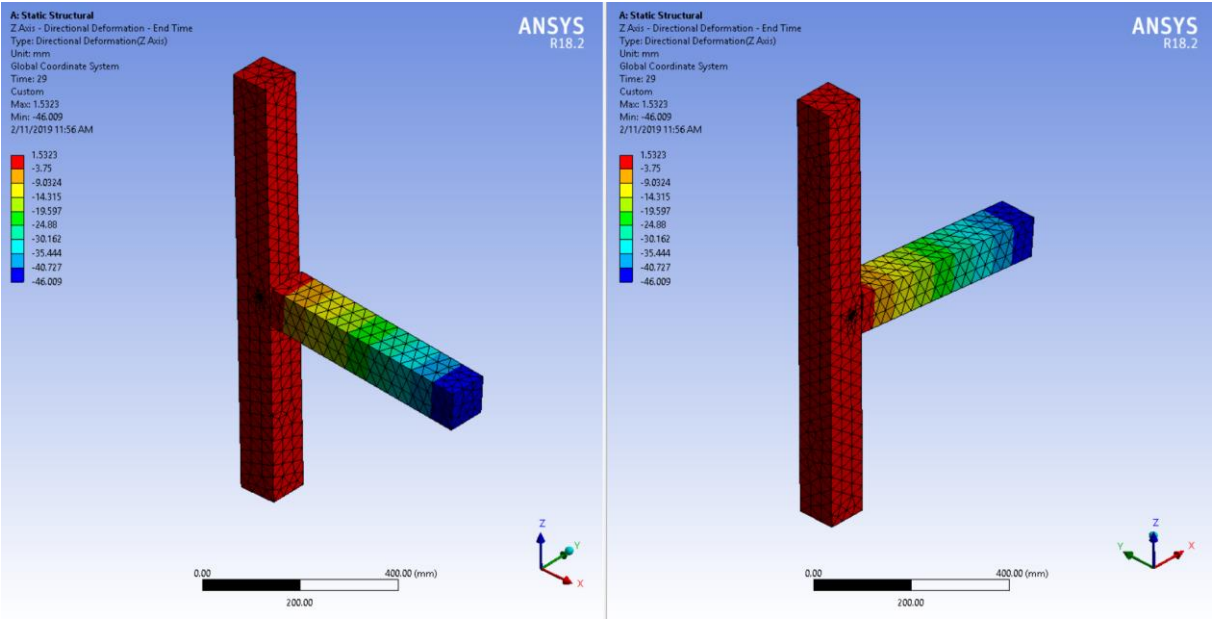
Figure 5. 18: Directional deformation (Z axis)
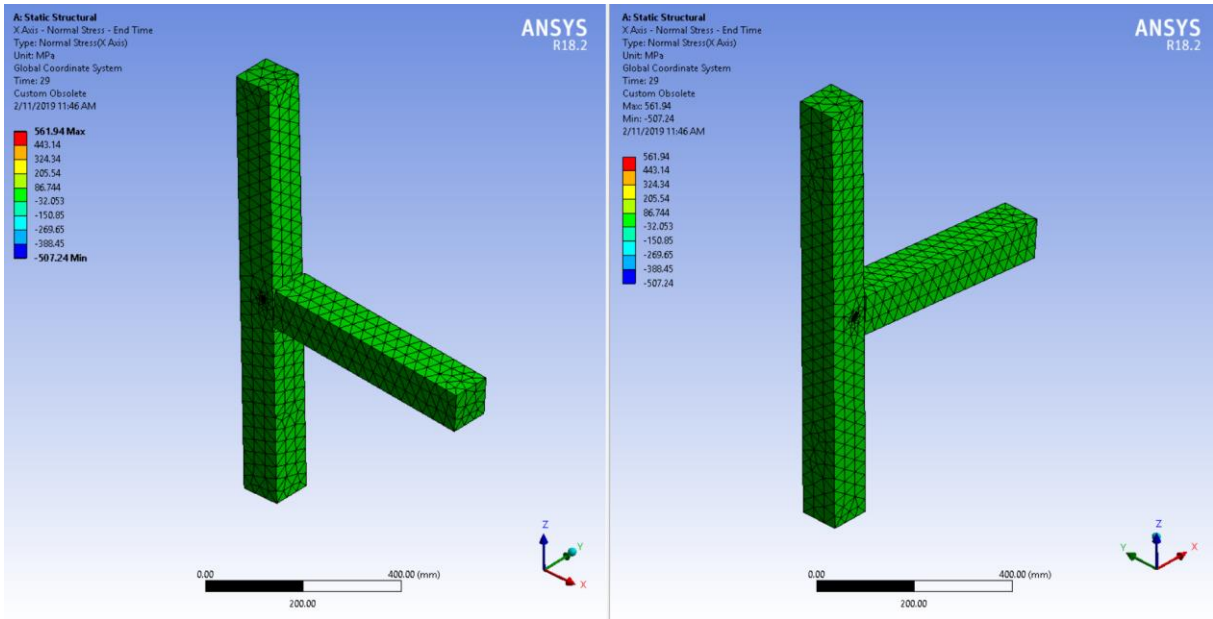
Figure 5. 19: Normal stress distribution
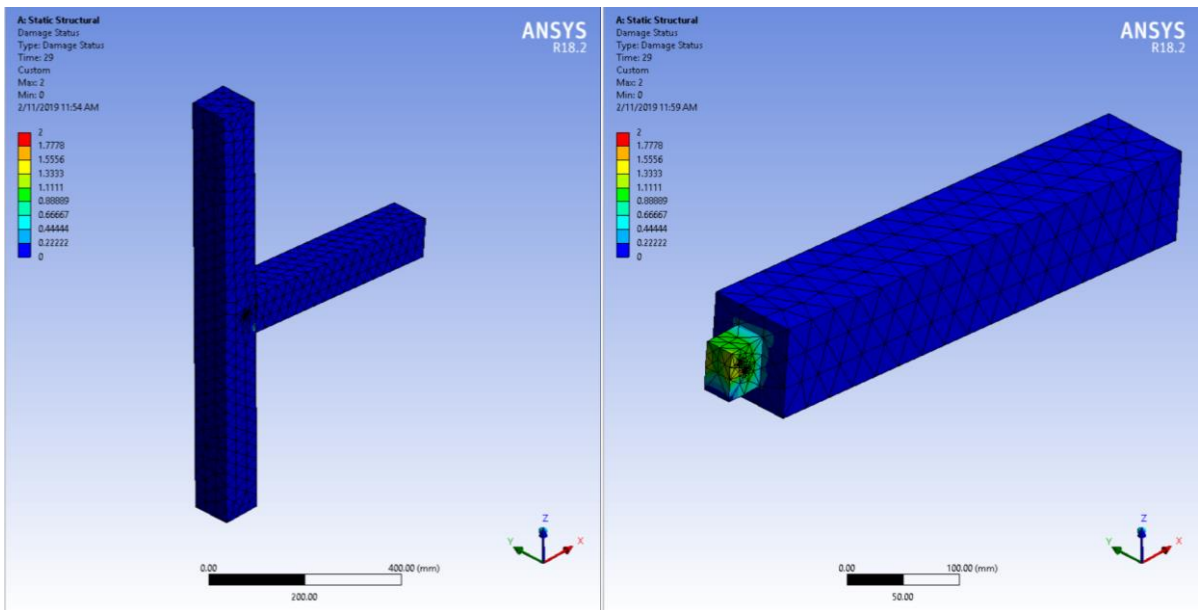
Figure 5. 20: Damage status (0-1) of timber tenon
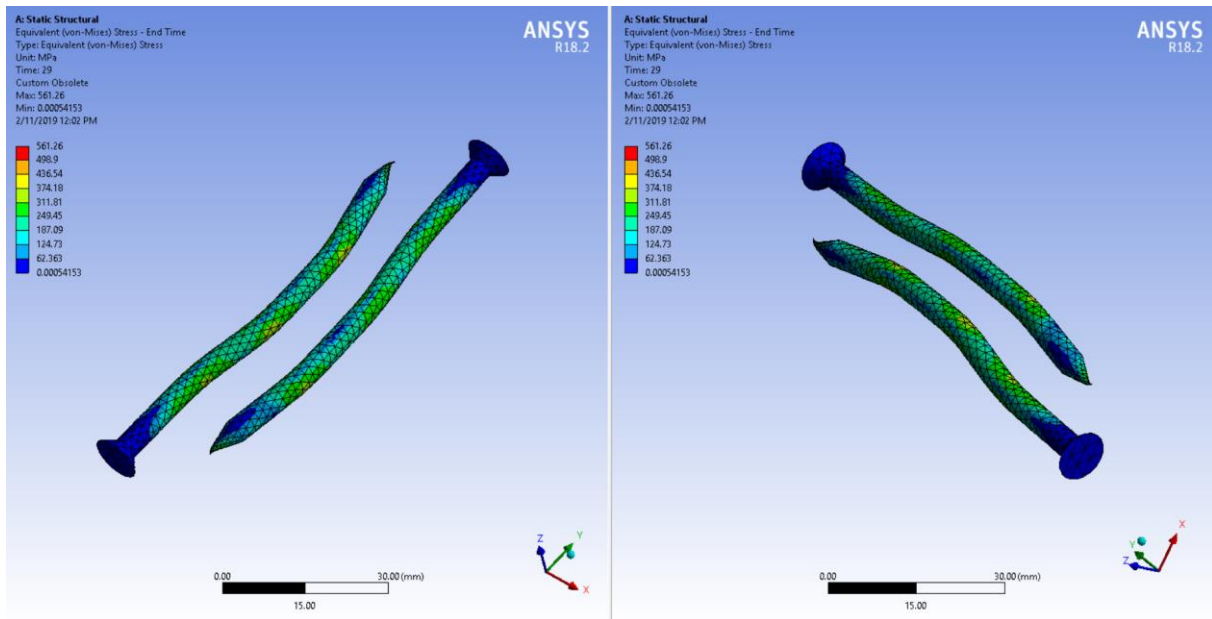
Figure 5. 21: Damage status (0-1) of screws

5.4.3. Analysis of the reinforced model under monotonic loading

In order to understand the behavior of timber beam and column connection, strengthened with CFRP composites, a three dimensional computational model have been developed using the general-purpose FEA program ANSYS. Timber and CFRP composites have been modelled as an elastic orthotropic constitutive model until failure. FRP composites are supposed to be bonded on the upper surface of joint, as 90x200 mm with L shaped. Furthermore, two CFRP textiles are supposed to be bonded as 45^{0} angle to two lateral surfaces of joint with the dimension of 100x200 mm to enhance load-carrying capacity (Figure 5.22).

The adopted finite element mesh is created using total 24536 solid elements and 38989 nodes. (Figure 5.23). As a solid element types SOLID 186 element and SOLID 187 element were used for timber. The CFRP layer, thickness 0,5 mm, is also meshed with the same element type, SOLID 186. The elastic properties of carbon fiber reinforced polymer (CFRP) is given in table 5.5 (in previous part 5.3.3).
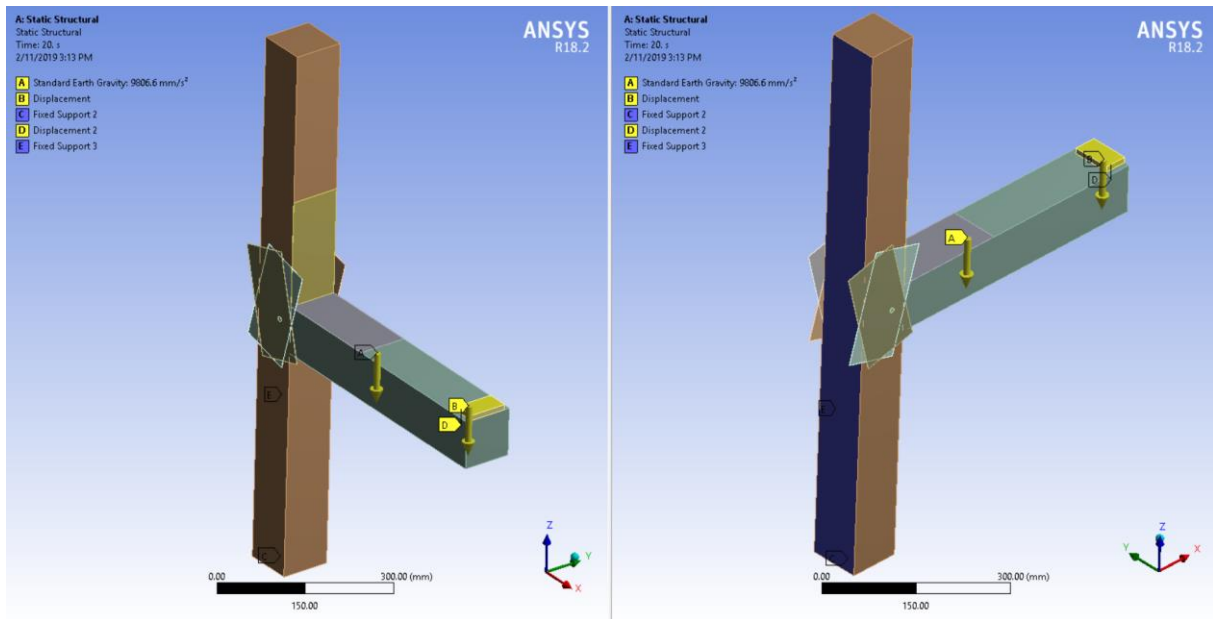
Figure 5. 22: Finite element model geometry of joint strengthened with CFRP
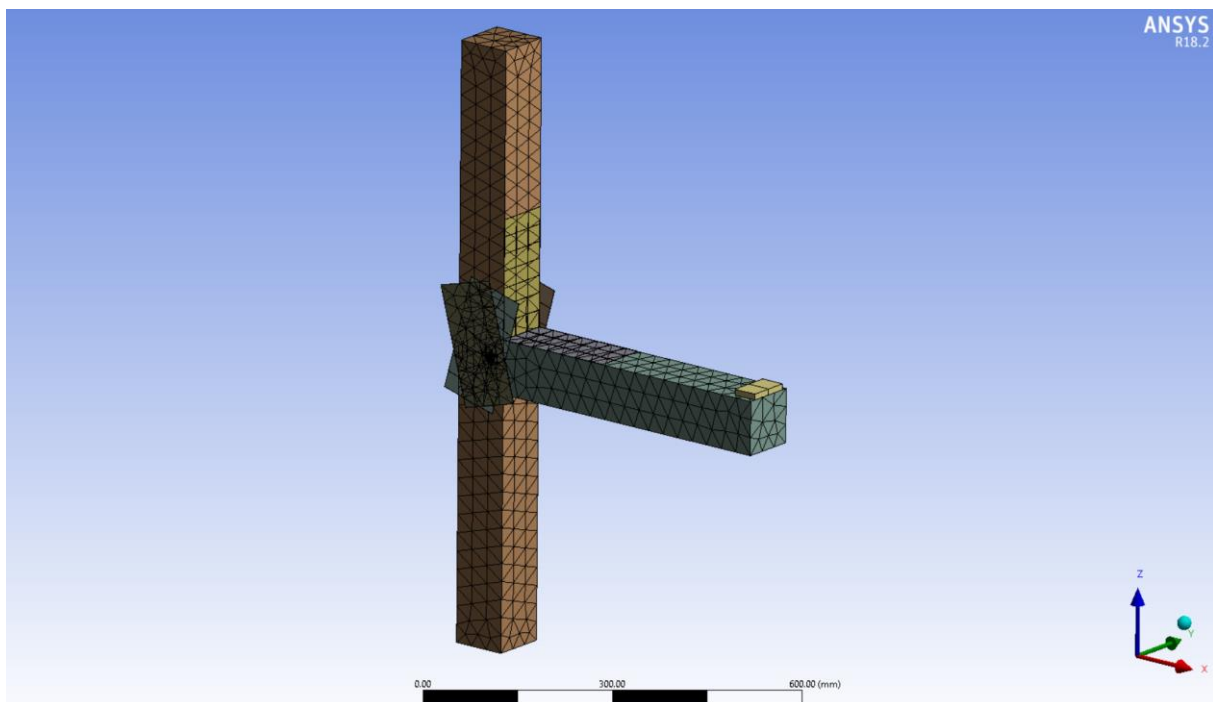
Figure 5. 23: Finite element mesh of reinforced joint

Between each contact surface, the coefficients of friction have been considered as 0.2 and 0.4 for timber-steel and timber-timber contact. As an adhesive layer between timber and carbon fiber reinforced polymer, bonded contact has been defined. A vertical displacement of 60 mm with a constant amplitude, has been applied to the beam model until the established failure criteria were satisfied. The CFRP element has been modelled as when the maximum axial stress exceeds the tensile and compressive strength of the composite, it could lead to the rupture. As

the progressive decreasing stiffness, tensile matrix stiffness reduction and compressive matrix stiffness reduction have been taken as 1 (which means complete stiffness loss). Figure 5.24 shows the numerical load-displacement curves after reinforcement with the experimental monotonic results and finite element analysis result.
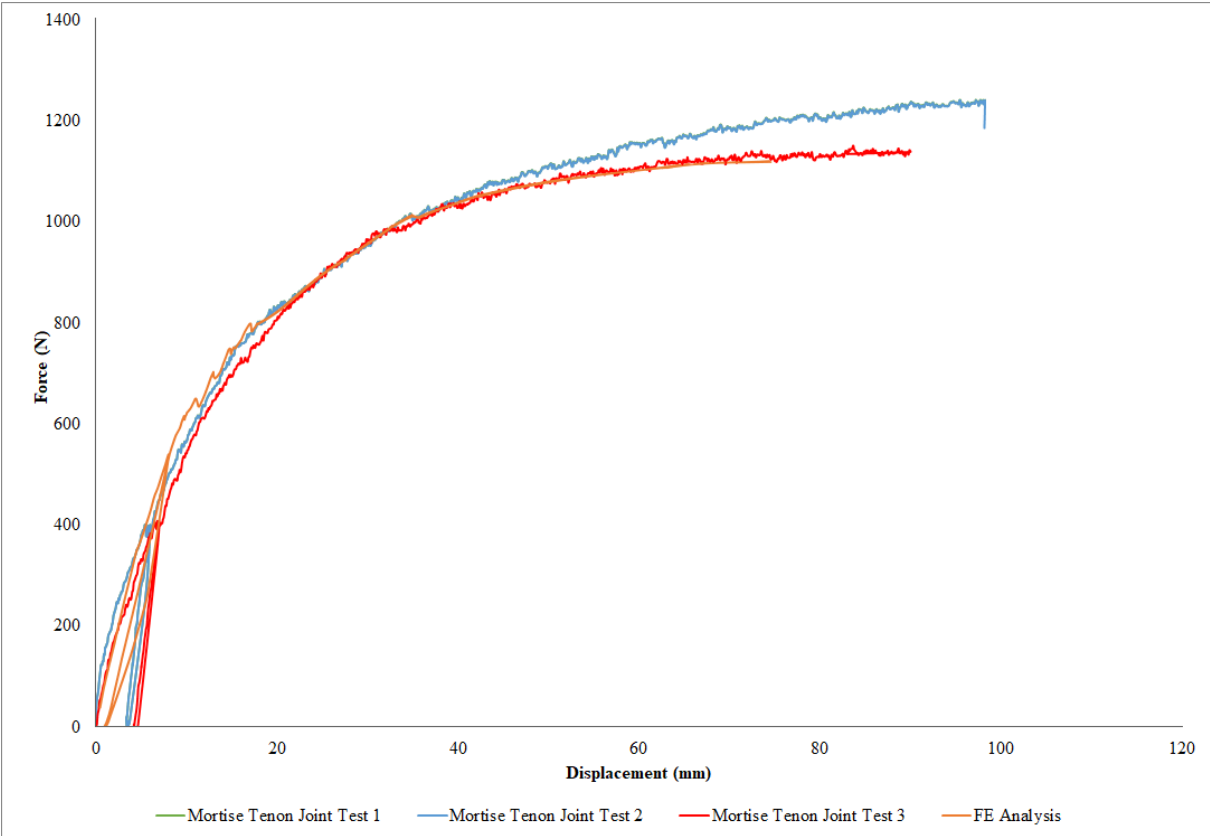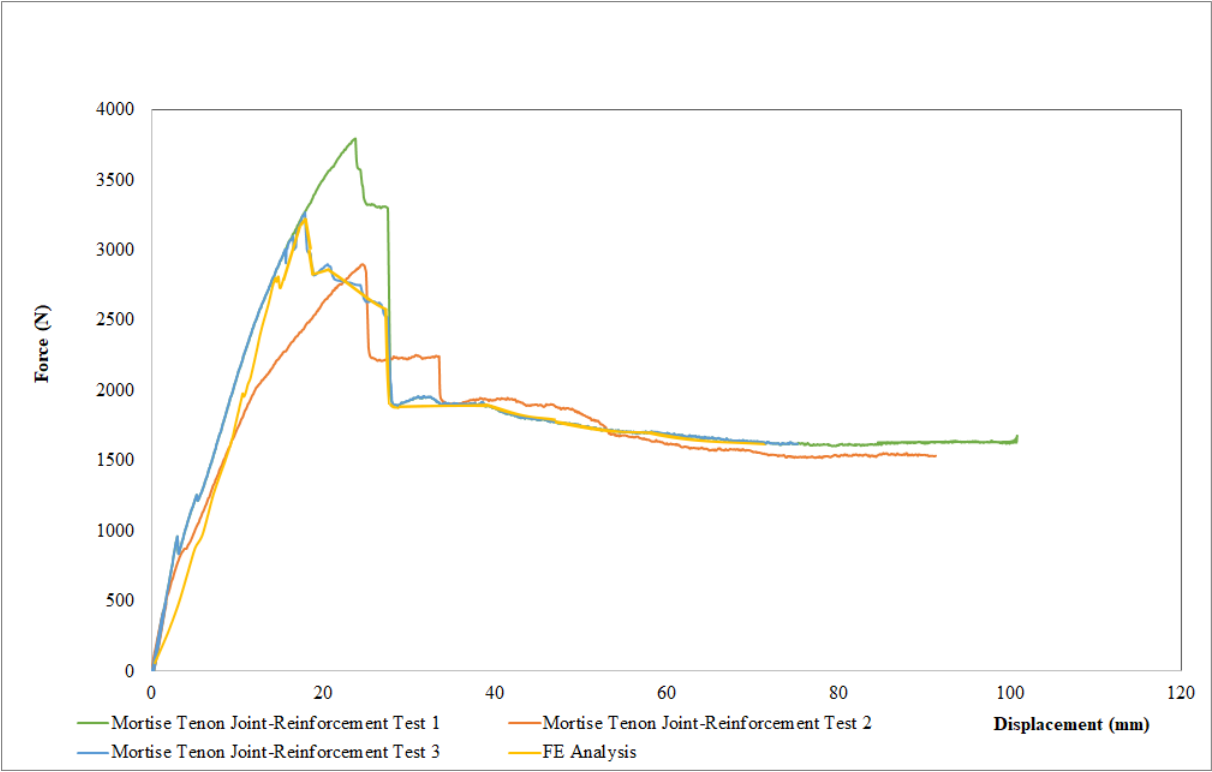

Figure 5. 24: Load-displacement curves of the strengthening joints under monotonic loads

It is observed that the results of FE analysis correlate well with those experimental results. The developed model captures the behaviours of the strengthened specimens of experiments. Particularly with specimen 3, they have similar inelastic behaviour and the maximum load point. The response of the joints has been essentially linear until failure has occurred. After that, due to the high stiffness of CFRP material, sharp crack and brittle behaviour has seen in the strengthened beams. The strengthened joint reaches a maximum of 3.2 kN at a displacement of about 80 mm. The directional deformation (Z axis) is given in Figure 5.25.

Figure 5.26 shows the stress distribution in the strengthened beam. It is clearly seen the stress is mainly concentrated along the CFRP sheet, due to the higher stiffness. Maximum compressive stress, approximately 155 MPa, is concentrated at the upper part of the beam which exposed the loads. Maximum tension stress, approximately 625 MPa, is concentrated at the lower part of the beam.

It should be noticed that the failure of the strengthened timber joints occurred due to the seperation of joint components in the tensile region. Failure was initiated at the joint in tension zone due to rotation of tenon member. Even though the joint components have been separated in tension zone, it still resisted to the increase load by help of high tensile strength of carbon fiber textile. When the specimen reached the maximum load, carbon fiber textile pulled out from the timber surface. CFRP has worked as a binder holding two timber members and has provided continuity together until the ultimate deformation. A distinct collapse mode of joint is detected as the rupture of CFRP sheet at a lateral surface of joint after the rotation of timber tenon (Figure 5.27-5.29). Besides, when the seperation of tenon from the mortise member was occured, the screws bent under stresses (Figure 5.30). The damage status is defined with values of 0,1 and 2. (0: undamaged, 1:partially damaged, 2:completely). The fiber tensile damage in the range of 0-1 has been detected in tenon member and on surface of CFRP sheets (Figure 5.27-29). The compressive damage in the range of 0-1 has been detected at screws (Figure 5.30).
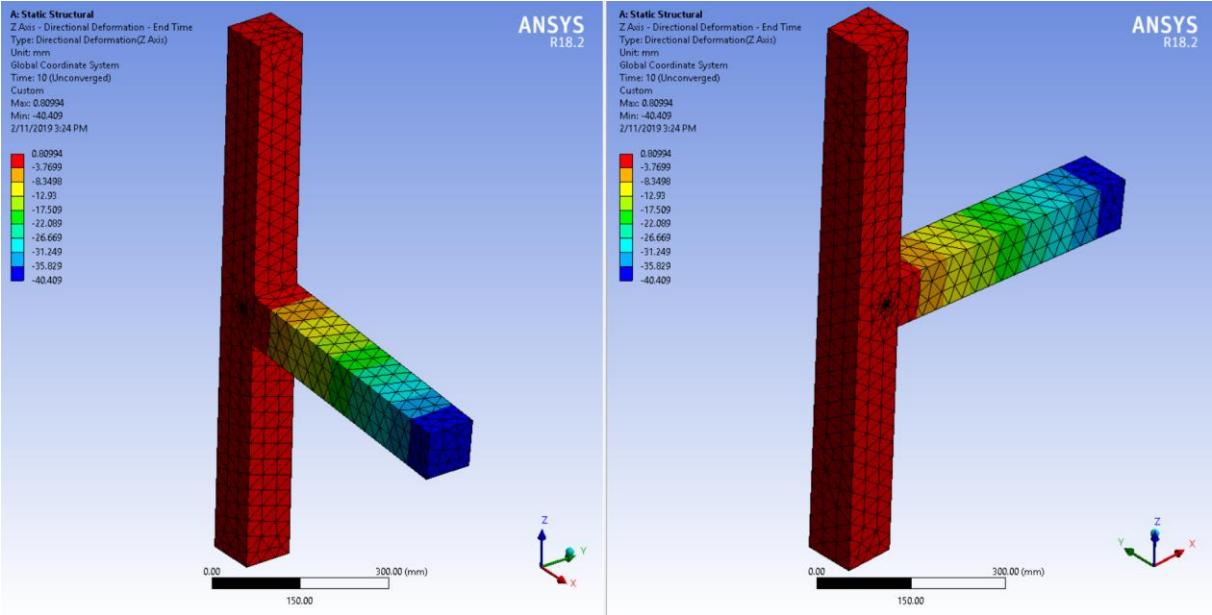
Figure 5. 25: Directional deformation (Z axis) of the strengthening joint
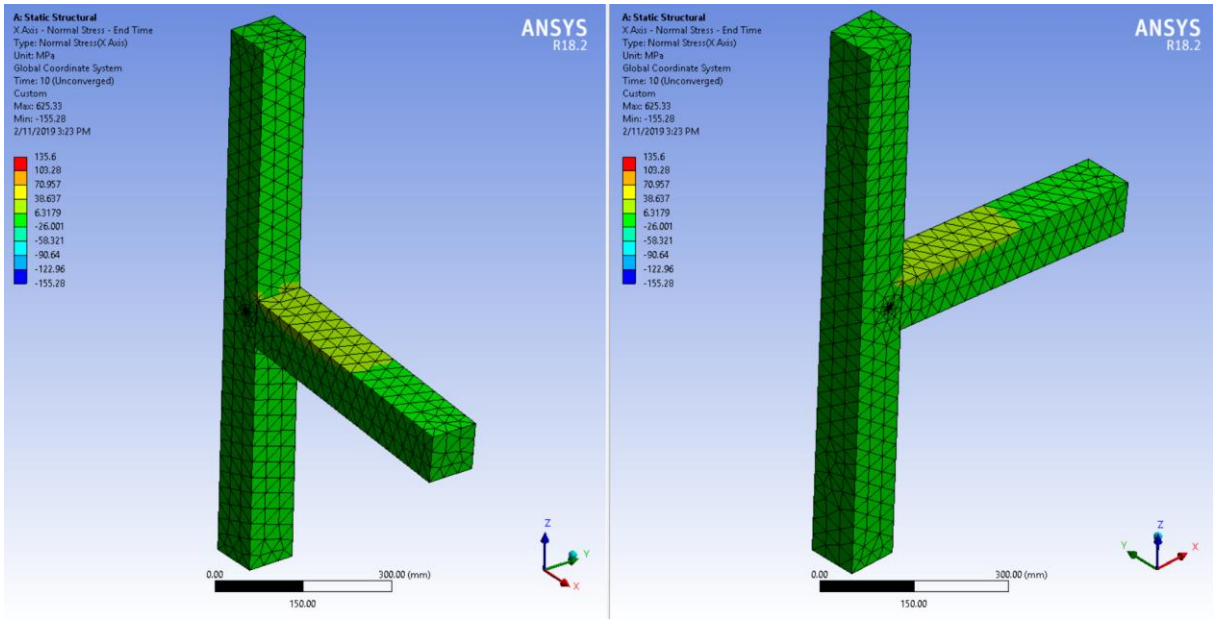
Figure 5. 26: Normal stress distribution of the strengthening joint
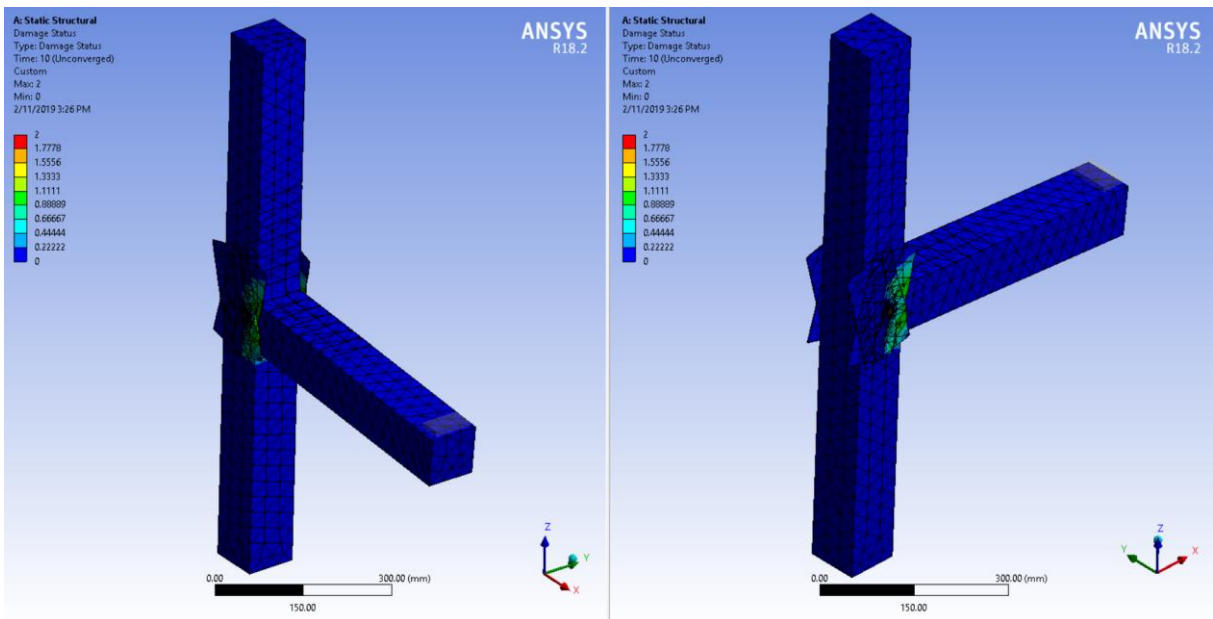
Figure 5. 27: Damage status (0-1) of the strengthening joint
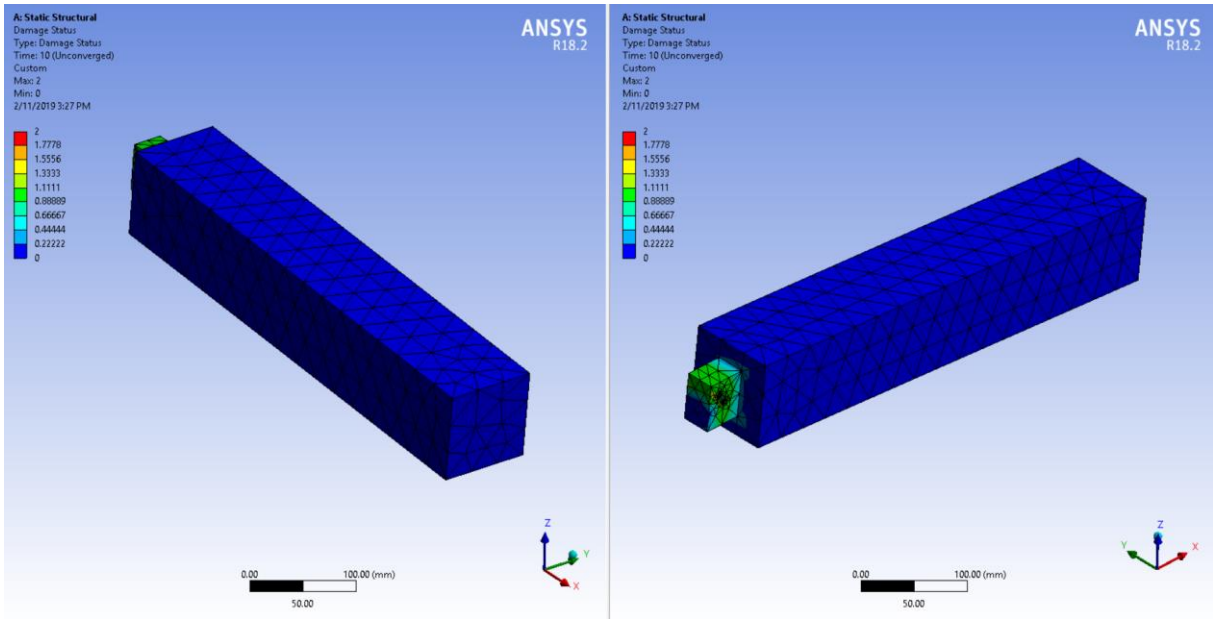
Figure 5. 28: Damage status (0-1) of the tenon in tension zone
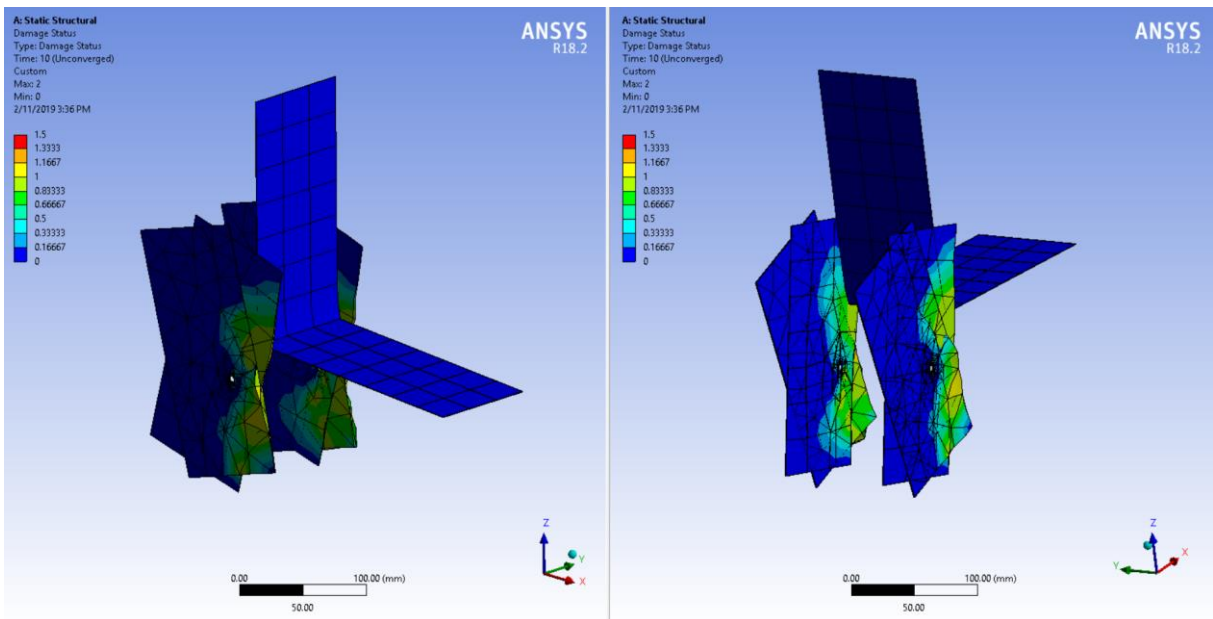
Figure 5. 29: Damage status (0-1) of CFRP
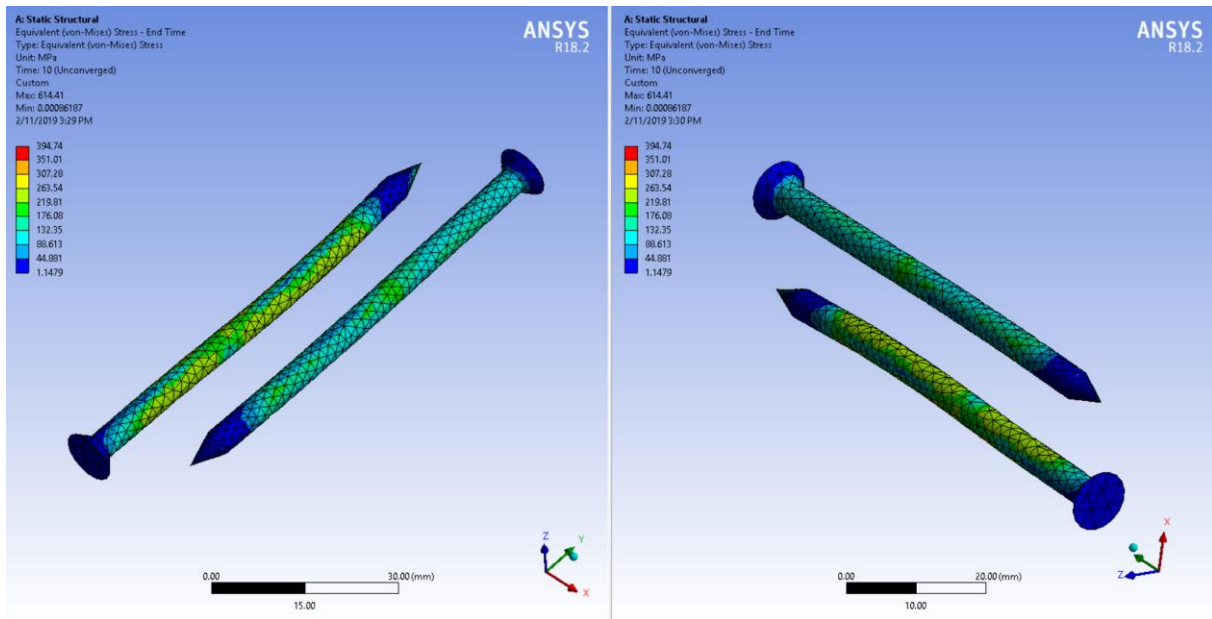
Figure 5. 30: Damage status (0-1) of screws

5.4.4. Comparison of analysis results

It can be clearly seen that the strengthening enhances the load carrying ability of the mortise tenon joint. The maximum load and top displacement of unstrengthened specimen are 1020 N and 90 mm, while 3200 N, 75 mm for strengthened specimen. The CFRP shows an increase of the ultimate load by about 313% and a change of failure mode is observed with greater ductility. The tension failure of wood under bending is brittle, for this reason, CFRP layers bonded on the tension side of the joint. The overall aim is then to increase the flexural strength and stiffness, and achieve a ductile compression failure mode. CFRP sheet improves the flexural capacity and rigidity of the timber beam (Figure 5.31). Ductility index obtained from energy method which is calculated by the area under the curves. Reinforced joint exhibits high ductility index and the main reason is due to higher range of inelastic region in the compression zone. It is very obvious that the reinforced joint reaches high ultimate load compare to other joint, eventhough yields to low ultimate deflection, it has high total energy and ductility.
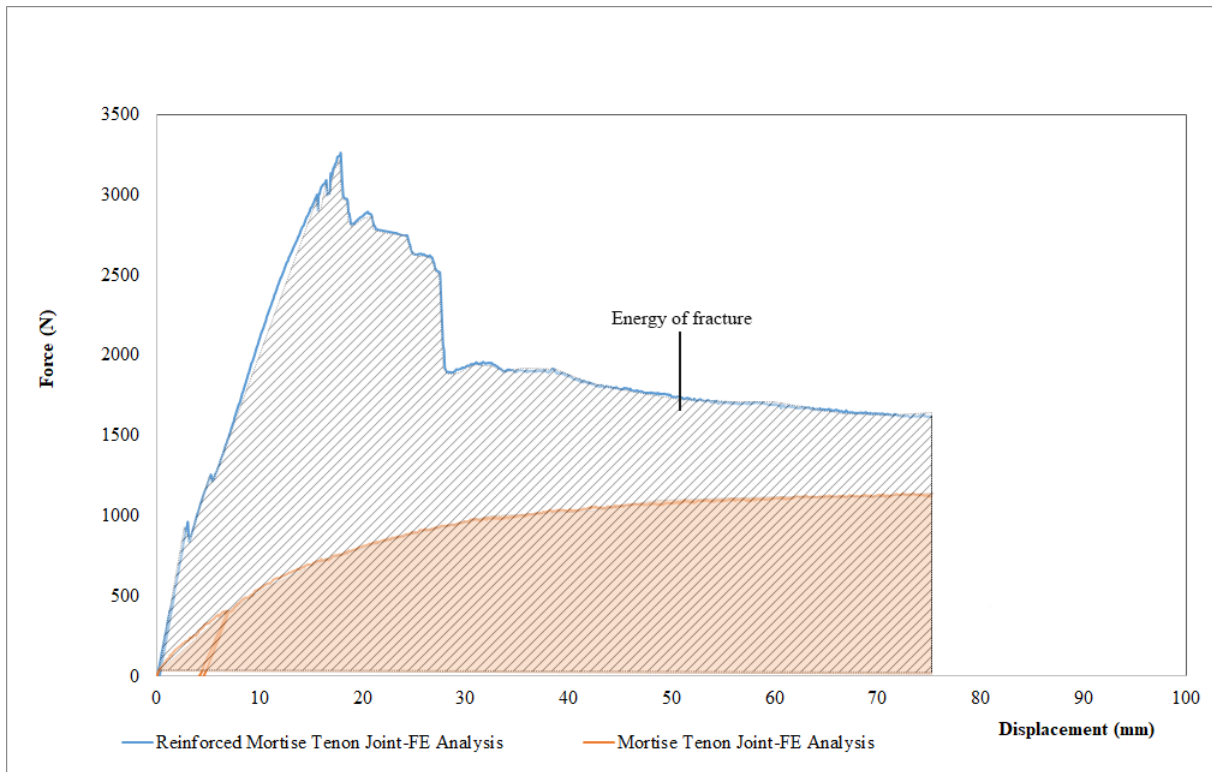
Figure 5. 31: The comparison of the unreinforced and reinforced specimen in FE analysis

6. GLOBAL SEMI-RIGID ANALYSIS

In the case of existing timber structures to be rehabilitated and reinforced, a realistic interpretation of the global structural behaviour is a primary need. In typical structural configuration of timber construction, the commonly used hinge models are inadequate; because in real structures, where joints have moment resisting capability, the equilibrium conditions may not be reached analytically. The semi-rigid modelling of timber connections, using nonlinear moment-rotation laws and hysteretic rules, intends to represent the behaviour of timber structures with a comparable level of detail for all the structural components. The original and strengthened traditional timber connections are modelled using a nonlinear spring element available in a structural frame analysis software, RSTAB in order to analyze the internal forces, deformations and support reactions of frame in terms of global scale.

6.1 Definition of Model Parameters

In order to evaluate the internal forces of members and deformation in existing structure and reinforced structure, a selected frame configuration has been analysed under lateral loads (Figure 6.1). The frame configuration is based on the work (Aktas, 2007). The timber posts and beams have been modelled as isotropic linear elastic bars. The mechanical characterization of the materials is obtained through experimental testing on two types of joint. The numerical values for the elastic parameters that have been used are given in Table 6.1. The reference material properties were obtained from experimental tests. The additional information necessary which was not derived from experimental results, was obtained using the Joint Committee on Structural Safety probabilistic model code (JCSS, 2006). Other material properties are estimated based on this model code, given in Table 6.2. Besides, for the infill material, masonry with standard mortar from the material libraries of program, that creates masonry according to EN 1996-1-1:Eurocode 6, has been modelled as isotropic plastic (Table 6.3). The mechanical behaviour of masonry under compression is non-linear (Figure 6.2). Limit compression strength is considered as 10 MPa then yielding, while limit tension is 0.1 MPa (made reference to Chapter 3, Figure 3.3).

Figure 6. 1: The frame configuration for analysis

127
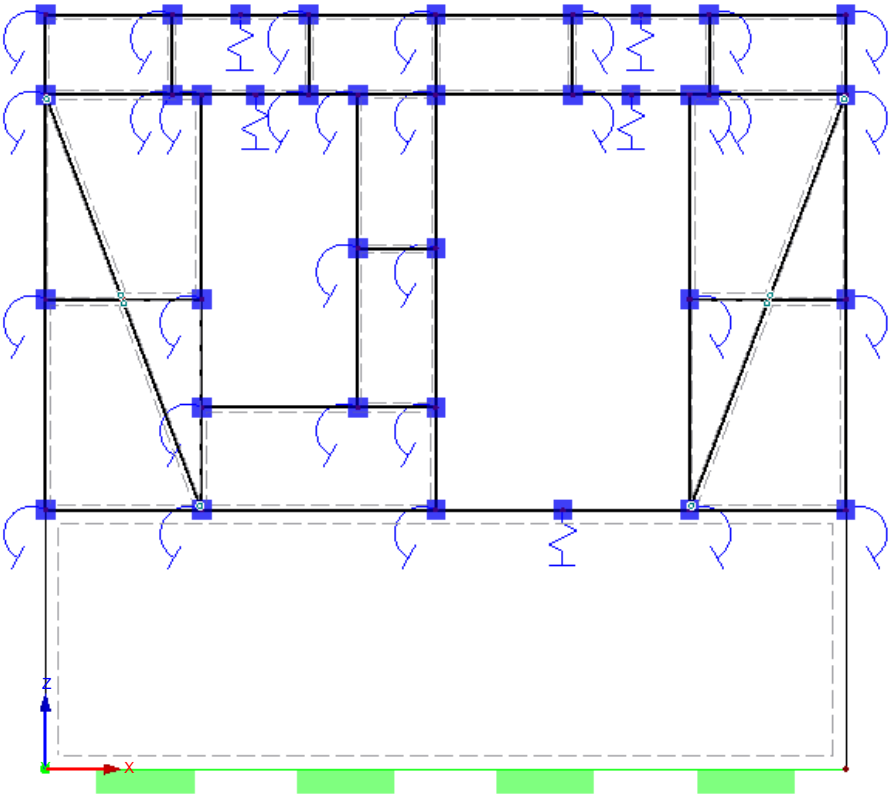
Table 6. 1: Elastic parameters of timber from experimental tests

Bending strength (R_m):	72.97 MPa
Bending MOE (E_m):	13648 MPa
Compression strength ($R_{C,0}$):	39 MPa
Compression strength ($R_{C,90}$):	4.12 MPa
Density (ρ_{den}):	500 kg/m^3

Table 6. 2: Elastic parameters of timber from JCSS (2006)

Tension strength ($R_{t.0}$):	43.782 MPa
Tension strength ($R_{t.90}$):	7.5 MPa
MOE tension ($E_{T,0}$):	13648 MPa
MOE tension ($E_{T,90}$):	454.93 MPa
Shear modulus (G_v):	853 MPa
Shear strength (R_v):	6.18 MPa

Table 6. 3: Elastic parameters of masonry

Modulus of elasticity (E):	1000 MPa
Shear modulus (G):	416.5 MPa
Poisson´s ratio (v):	0.2
Specific weight (γ):	24.52 kN/m^3
Specific weight (γm):	1
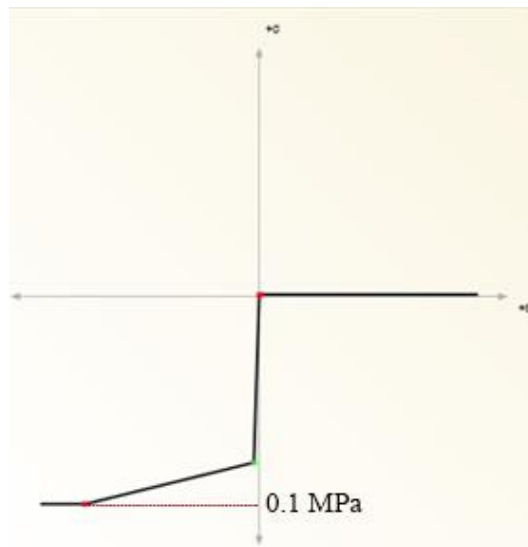
Figure 6. 2: The non-linear curve of masonry

Plastic deformation capability, ductility and energy dissipation are important concepts that determine seismic behaviour of structure. Selected spring model must reflect the ductility and energy dissipation capacity of the system. In order to represent the behaviour of semi-rigid joints, spring models have been derived from the average of force-displacement curves of three lap joint specimens and the average of moment-rotation curves of three mortise-tenon joint specimens under monotonic bending load (Chapter 4. Experimental analysis). Thus, two non-linear curves have been obtained from regression curve of specimens (Figure 6.3-6.4). Non-linearity effects concentrated hinges were applied to the joints. Stiffnesses of connections which have been obtained from experiments, were progressively added at the joints. In total, three spring stiffness values were adopted to the nodals:

1. Hinge1 where lap joints between the beam and beam have been considered as semi-rigid.

2. Hinge2 where mortise-tenon connections between the beam and column have been considered as semi-rigid.

3. Hinge3 where connections between the diagonal (brace) and the main frame have been considered pinned.

The translational spring is introduced at Hinge1 and rotational spring for the non-linear analysis of Hinge2. Properties of nonlinear hinges have been defined according to the force displacement and the moment-curvature, following diagrams presented at Figure 6.3 and Figure 6.4. Besides, the connection between the diagonals and the main frame as pinned. To this term, the rotational degree of freedom is released.
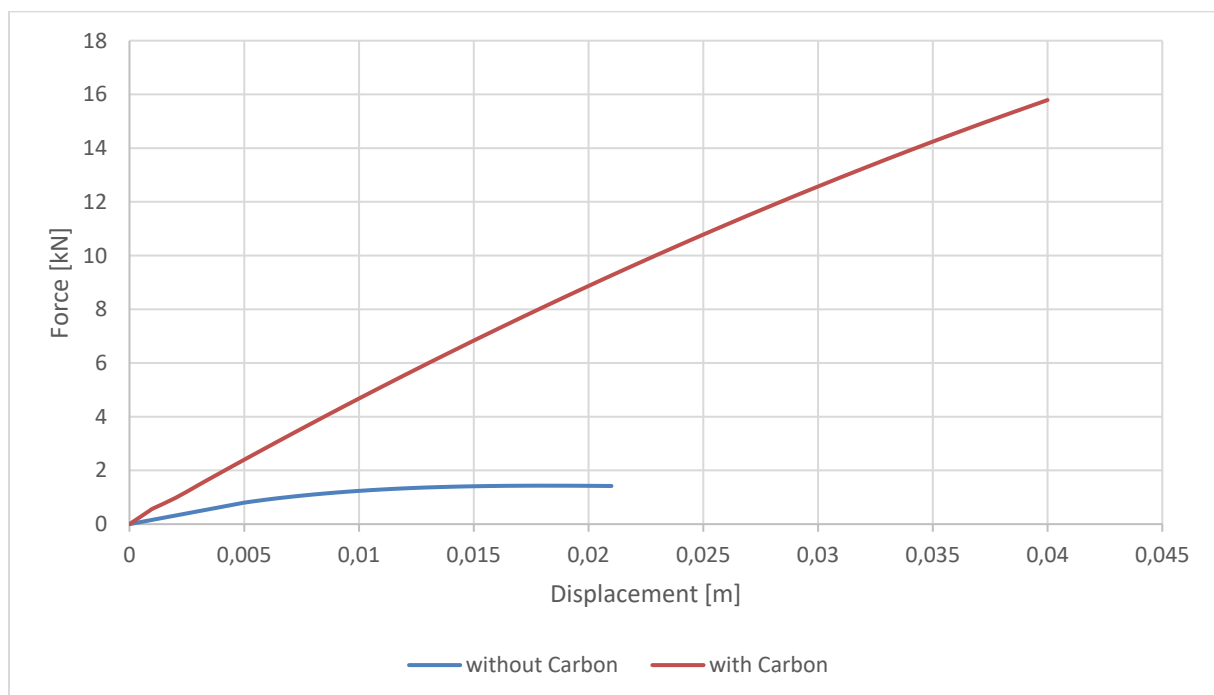
Figure 6. 3: The translational spring of lap joint
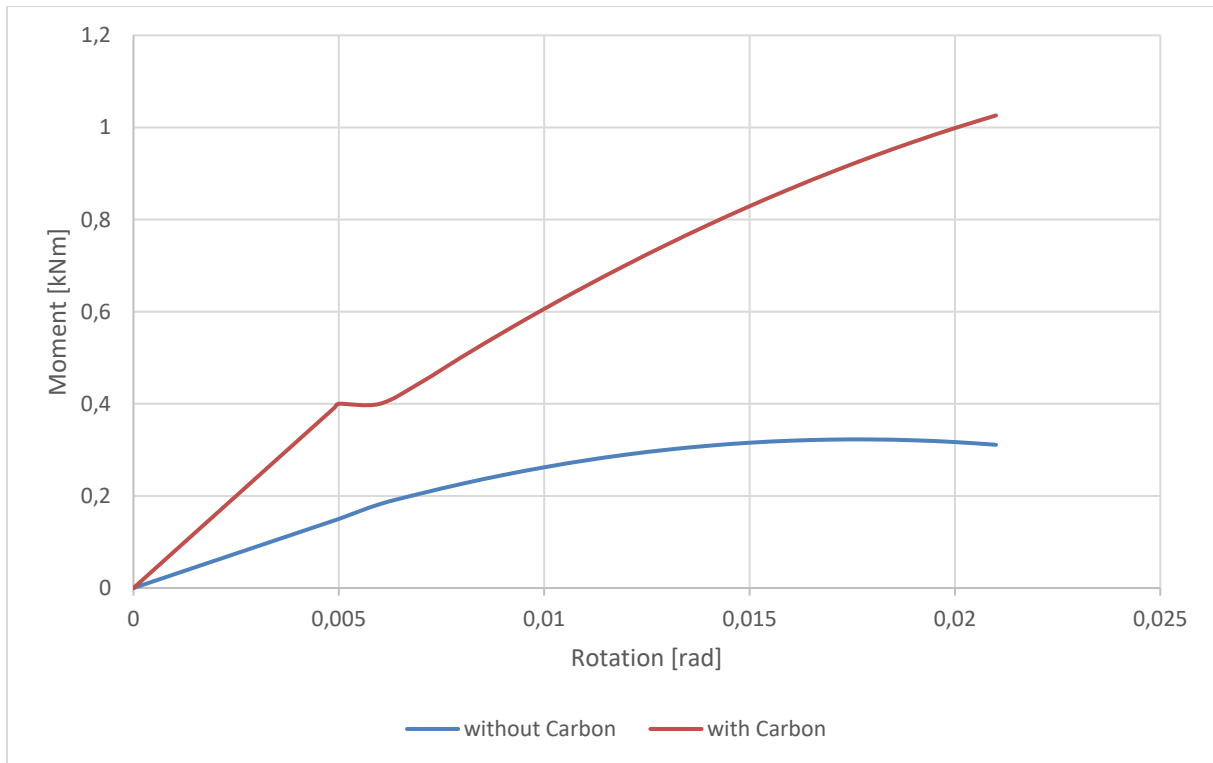
Figure 6. 4: The rotational spring of mortise-tenon joint

In Figure 6.4, the reason of the rupture of the curve of joint with CFRP (red curve) is that during the experiments the carbon fiber textile yielded and separated from the timber surface due to rotation of tenon member. Even though, the carbon fiber textile failed, CFRP has worked as a binder holding two timber members and provided continuity together until the ultimate deformation, thus the moment-rotation of the joint continued to rise after rupture.

6.2 Lateral Load Analysis

Two load cases have been defined: dead loads and live loads. Dead loads consist of the permanent construction material loads comprising the roof, floor, wall, and masonry, that is 1,35 G=10.8 kN/m. Live loads come from the use and occupancy of a building, that is 1,50 Q=12 kN/m.

(G=2 kN/m2, q= 2 kN/m2, l=4 m). The following load combination, depends on Eurocode 6, was considered 1,35 G + 1,50 Q + 1,00 E (in which live load, Q, snow load, S, earthquake load, E). Horizontal loads proportional to the weight of the structure have been used so to simulate seismic action on the structure. So that, different values of horizontal loads have applied at the top of frame until maximum 144 kN. In order to present the capacity curve of the model relationship between the loads and displacements, the loads of 9, 18, 27, 36, 45, 54, 63, 69, 72,

81, 90, 108, 126, 144 kN have been applied. As a boundary conditions, the masonry base has been chosen as fixed support, which restrained in vertical and horizontal directions (Figure 6.5).
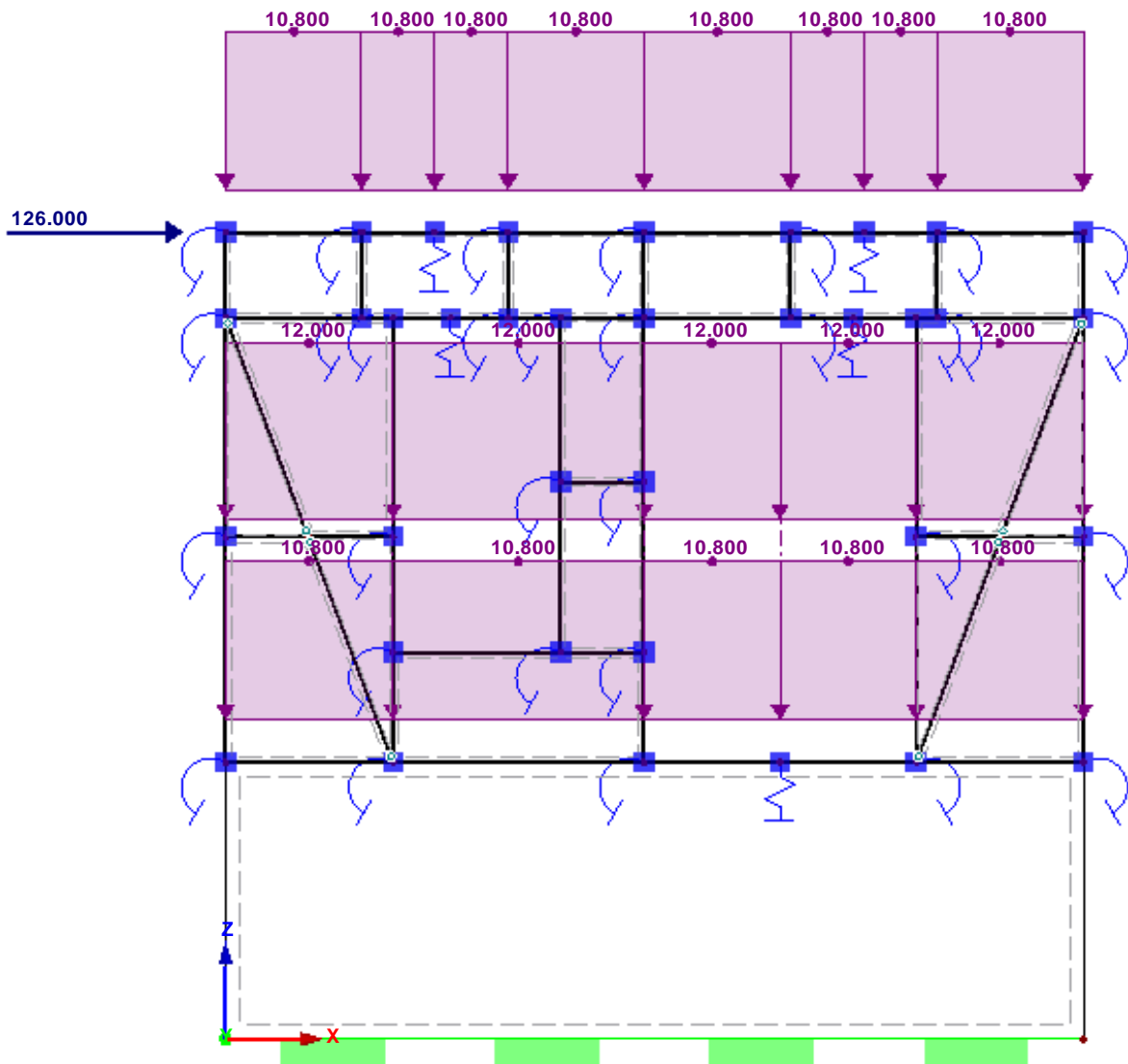
Figure 6. 5: Load cases in the frame

6.3 Analysis Results of Unreinforced and CFRP Reinforced Structures

Maximum deformation and normal forces took place at the upper storey, to direction of the applied lateral loads in both unreinforced and reinforced conditions.

After lateral load analysis, the envelope of normal and shear forces and bending moment, together with the elastic deformed shape, are shown in Figure 6.6-6.11. The high compression forces are seen upper beam of the frame, where the lap joint exists. After the reinforcement with CFRP, the compression forces decreased %10. Moreover, the base timber plate (lower beam) suffer high tension forces, where the mortise-tenon joint and diagonal joint come together. A

%12 of reduction has seen after reinforcement of the structure. Besides, the diagonal members (braces) are modelled as pinned and only normal forces (compression forces at left one, tension forces at right one) are obtained like constant stress distribution along the length of members (Figure 6.6-6.7). High shear forces have been detected at the intersection of base timber plate and masonry ground floor, where mortise-tenon and lap joints are located. The values of shear forces for both unreinforced and reinforced frames are not so different, the effect of reinforcement on the structure is insufficient (Figure 6.8-6.9). Furthermore, high bending moment has been seen at the left of base timber plate, where lap joints connect the beams. Also, the corners of door and window which are exposed to high bending, particularly in the place of mortise-tenon joints, that connect column and beam members. The reinforcement of joints with CFRP, has reduced the bending moment of joints, approximately %25 (Figure 6.10-6.11).

 A review of results shows that the Hımış timber frame is significantly low deformable under lateral loads, which is maximum 29 mm. The upper part suffering highest deformation is the face in the opposite direction of the applied force. After changing existing joints by semi-rigid joints, the deformation of frame decreased to 17 mm (Figure 6.12-6.15).
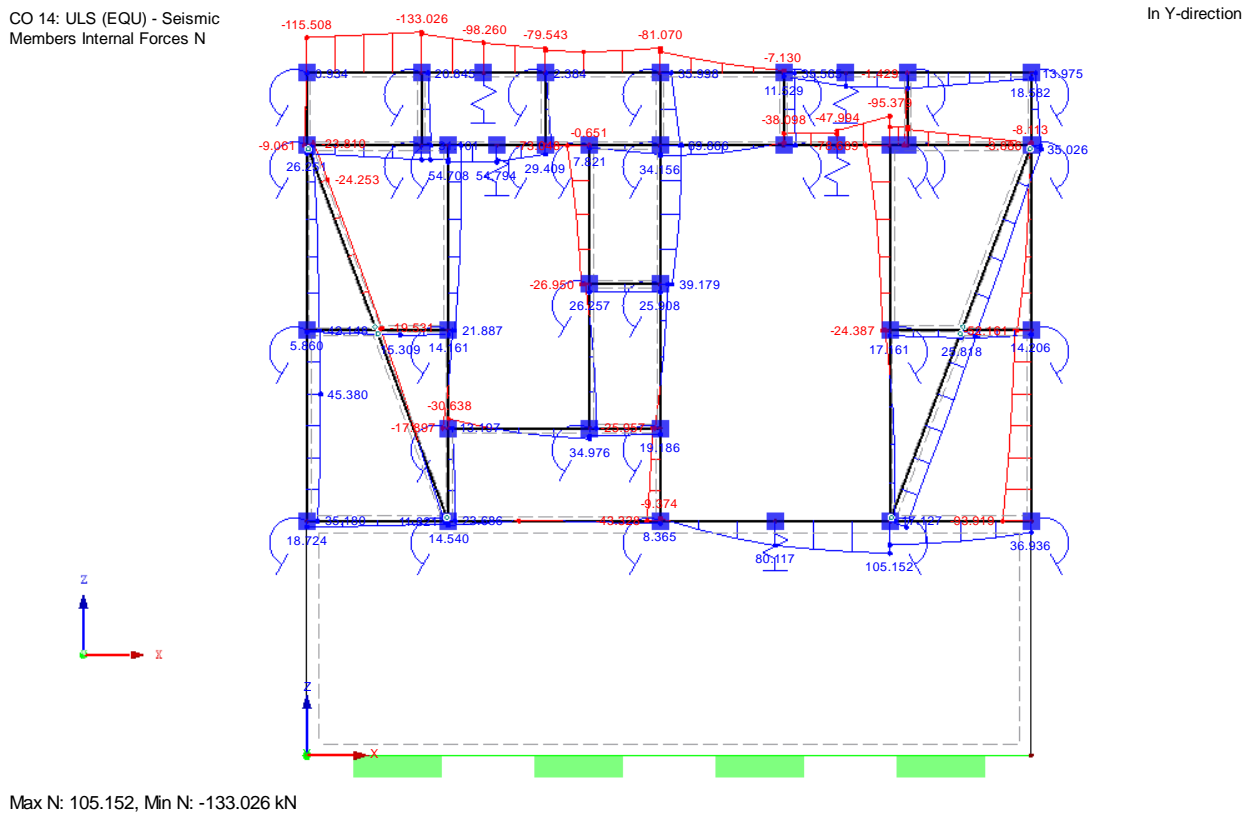
Figure 6. 6: Normal forces of unreinforced frame

CO 14: ULS (EQU) - Seismic
Members Internal Forces N

Figure 6. 7: Normal forces of reinforced frame
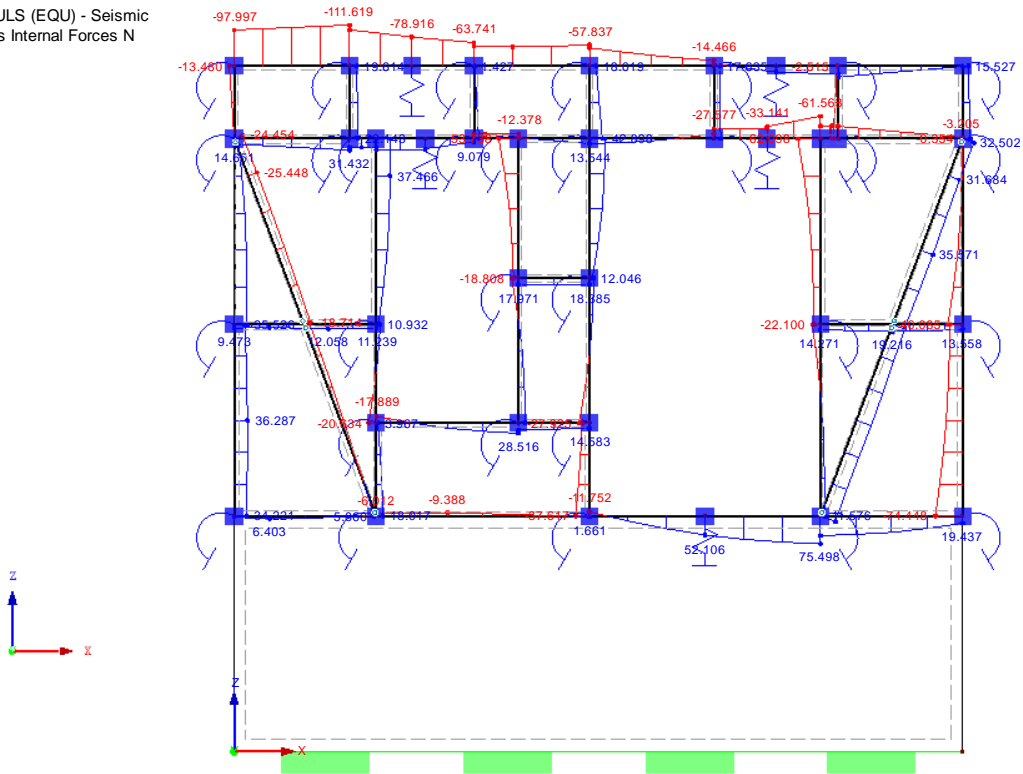
Max N: 75.498, Min N: -111.619 kN

CO 14: ULS (EQU) - Seismic
Members Internal Forces V-z
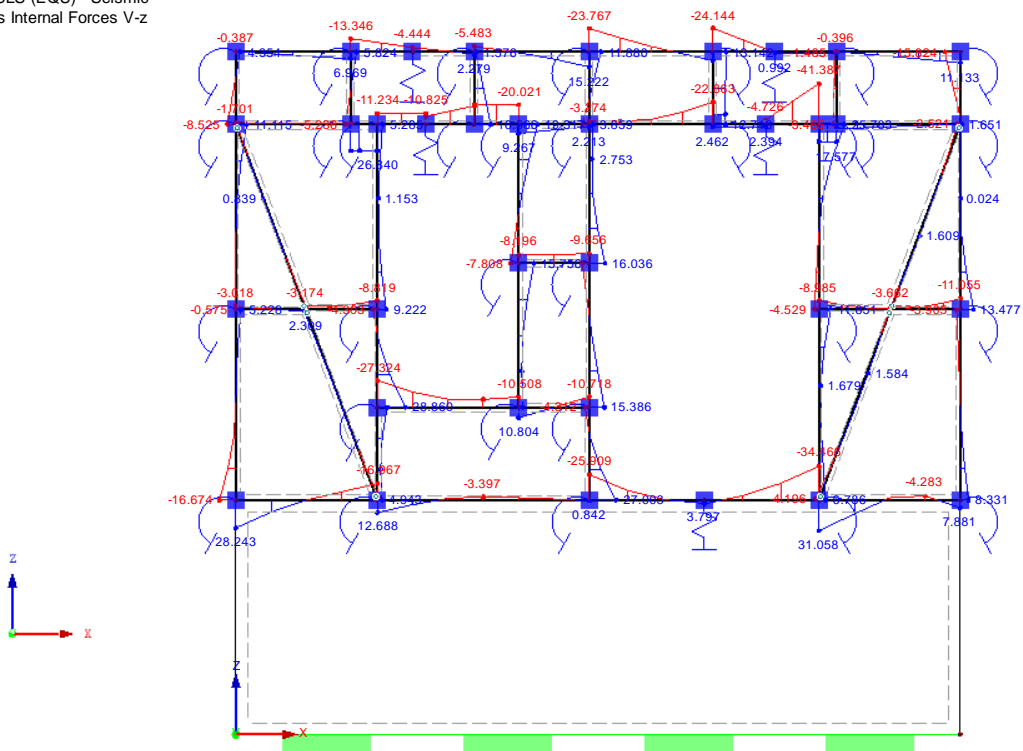
Max V-z: 31.058, Min V-z: -41.387 kN

Figure 6. 8: Shear forces of unreinforced frame

CO 14: ULS (EQU) - Seismic
Members Internal Forces V-z
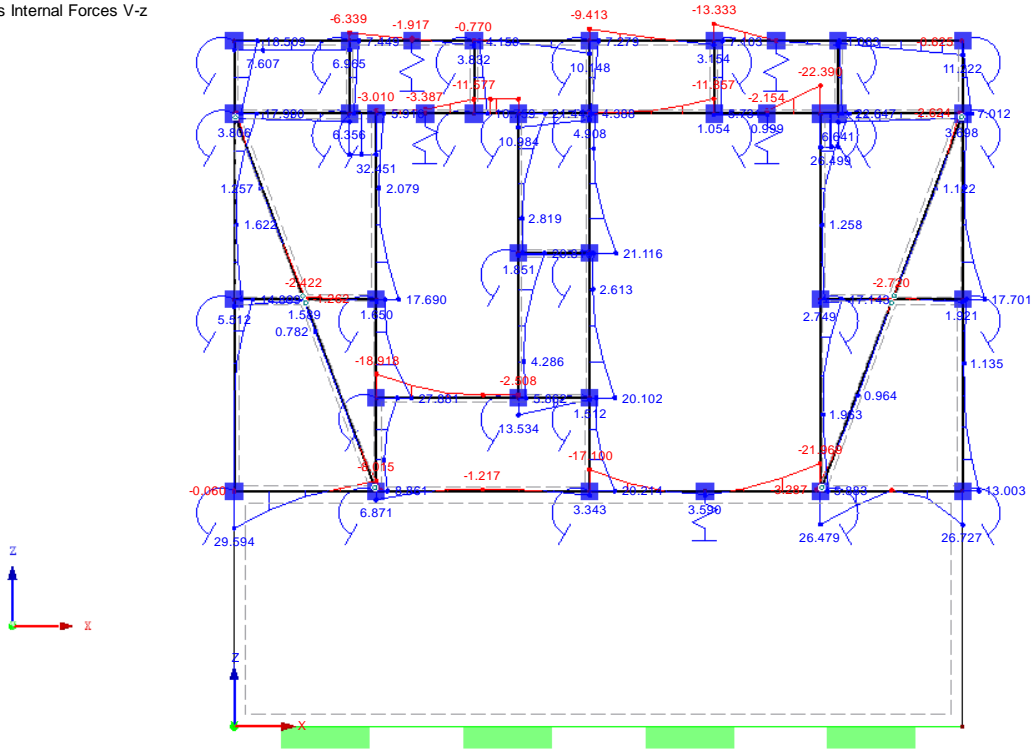
Max V-z: 32.451, Min V-z: -22.390 kN

Figure 6. 9: Shear forces of reinforced frame

CO 14: ULS (EQU) - Seismic
Members Internal Forces M-y
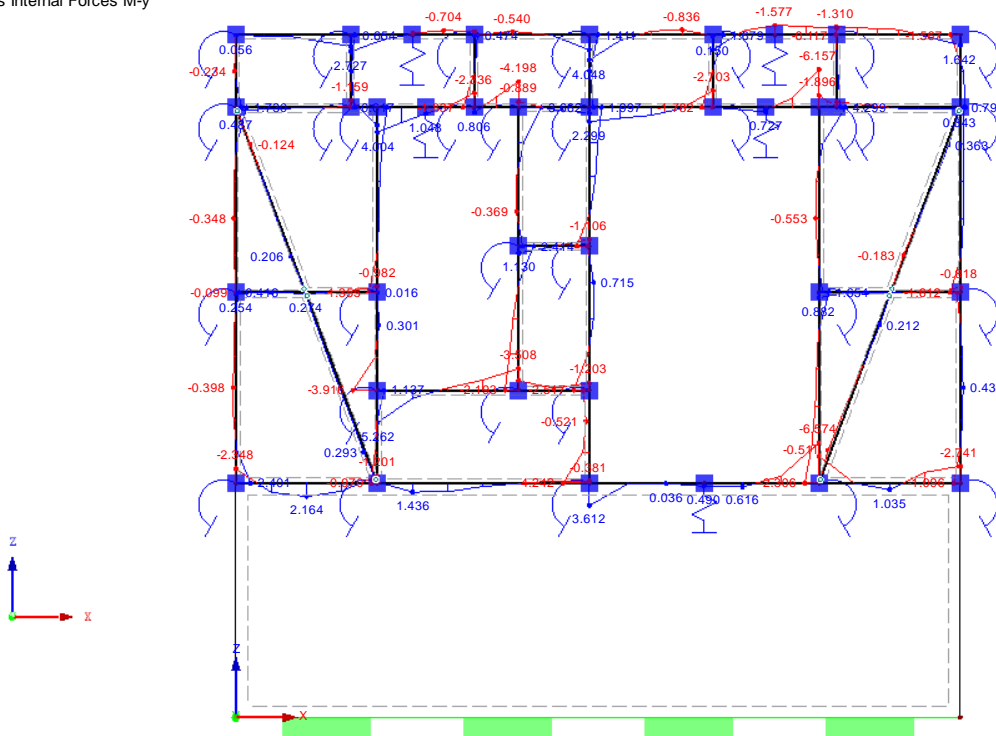
Max M-y: 5.262, Min M-y: -6.574 kNm

Figure 6. 10: Bending moment of unreinforced frame
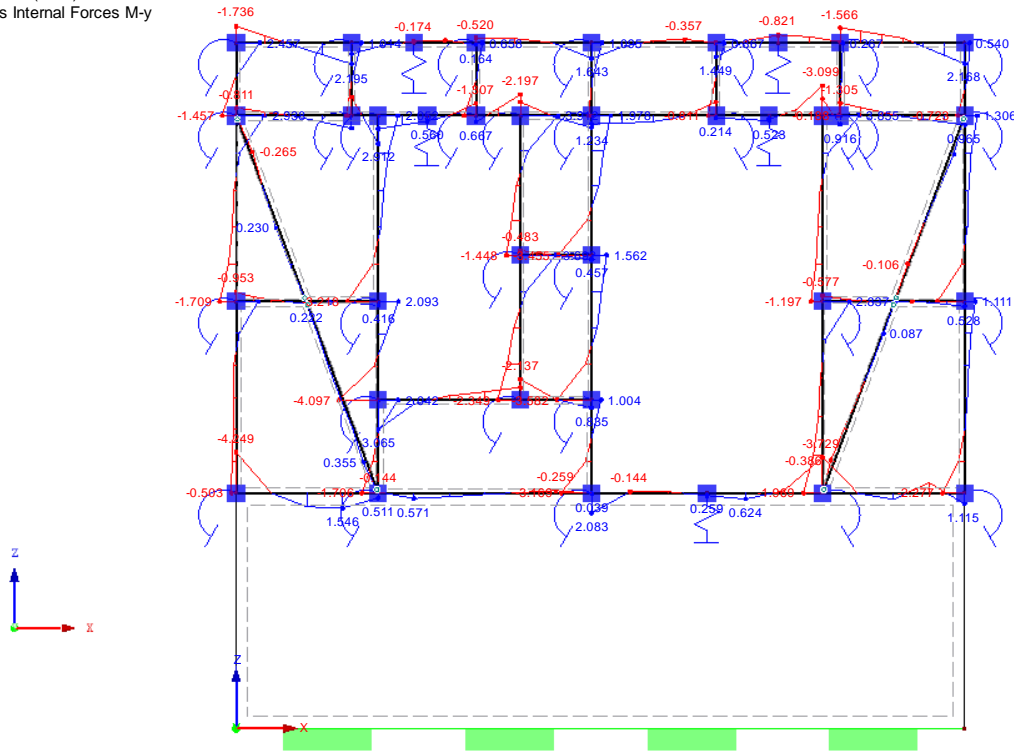
Max M-y: 3.912, Min M-y: -4.249 kNm

Figure 6. 11: Bending moment of reinforced frame
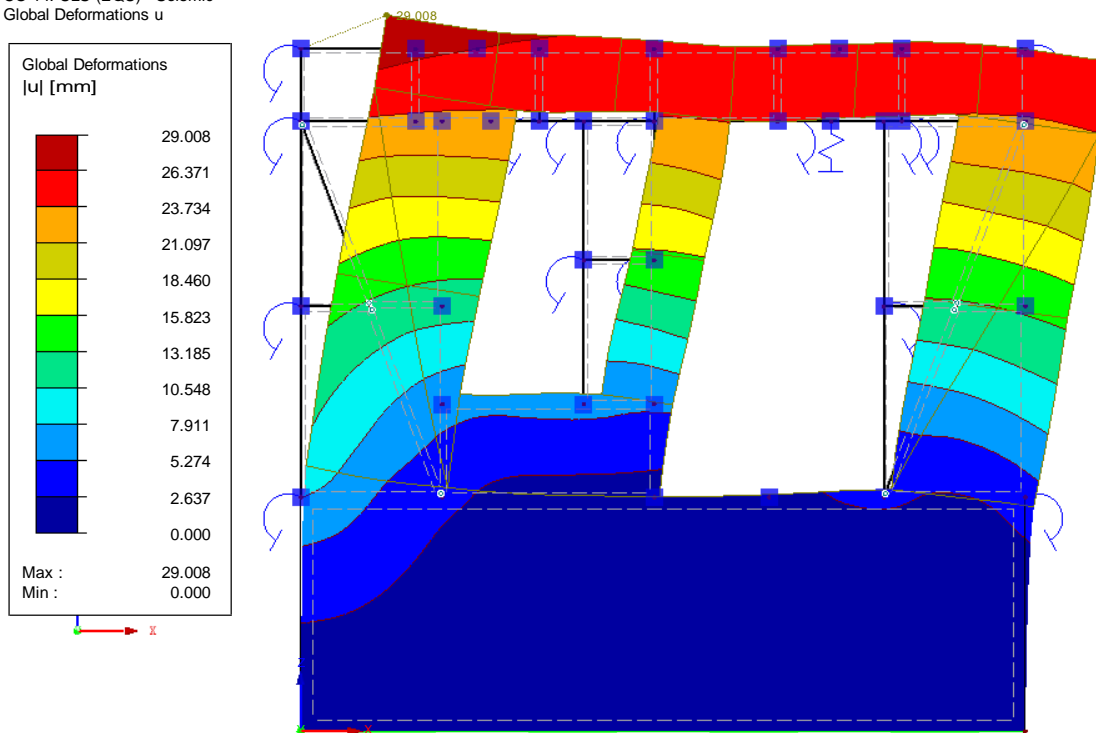
Max u: 29.008, Min u: 0.000 mm
Factor of deformations: 18.00

Figure 6. 12: Global deformation of unreinforced frame

CO 14: ULS (EQU) - Seismic
Global Deformations u

Global Deformations
|u| [mm]

	17.715
	16.105
	14.494
	12.884
	11.273
	9.663
	8.052
	6.442
	4.831
	3.221
	1.610
	0.000

Max : 17.715
Min : 0.000
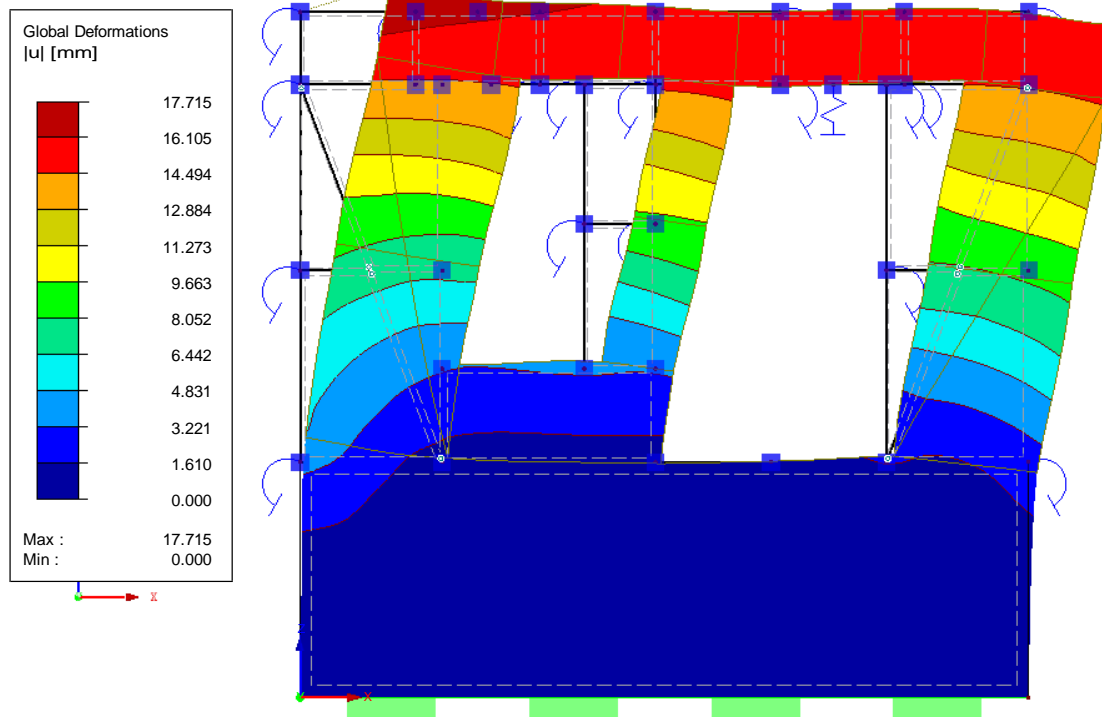
Max u: 17.715, Min u: 0.000 mm
Factor of deformations: 30.00

Figure 6. 13: Global deformation of reinforced frame

CO 14: ULS (EQU) - Seismic
Global Deformations u-X

Global Deformations
u$_X$ [mm]

	26.988
	24.535
	22.081
	19.628
	17.174
	14.721
	12.267
	9.814
	7.360
	4.907
	2.453
	0.000
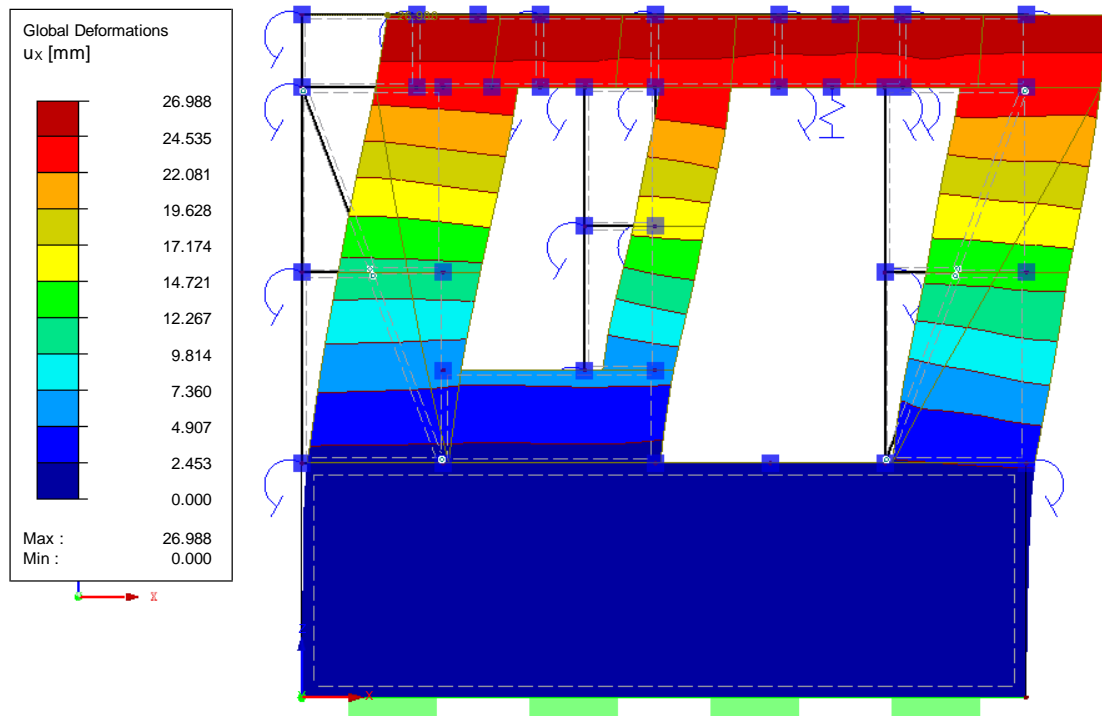
Max : 26.988
Min : 0.000

Max u-X: 26.988, Min u-X: 0.000 mm
Factor of deformations: 18.00

Figure 6. 14: Global deformation-x direction of unreinforced frame

CO 14: ULS (EQU) - Seismic
Global Deformations u-X

Global Deformations
u_X [mm]

	16.923
	15.385
	13.846
	12.308
	10.769
	9.231
	7.692
	6.154
	4.615
	3.077
	1.538
	0.000
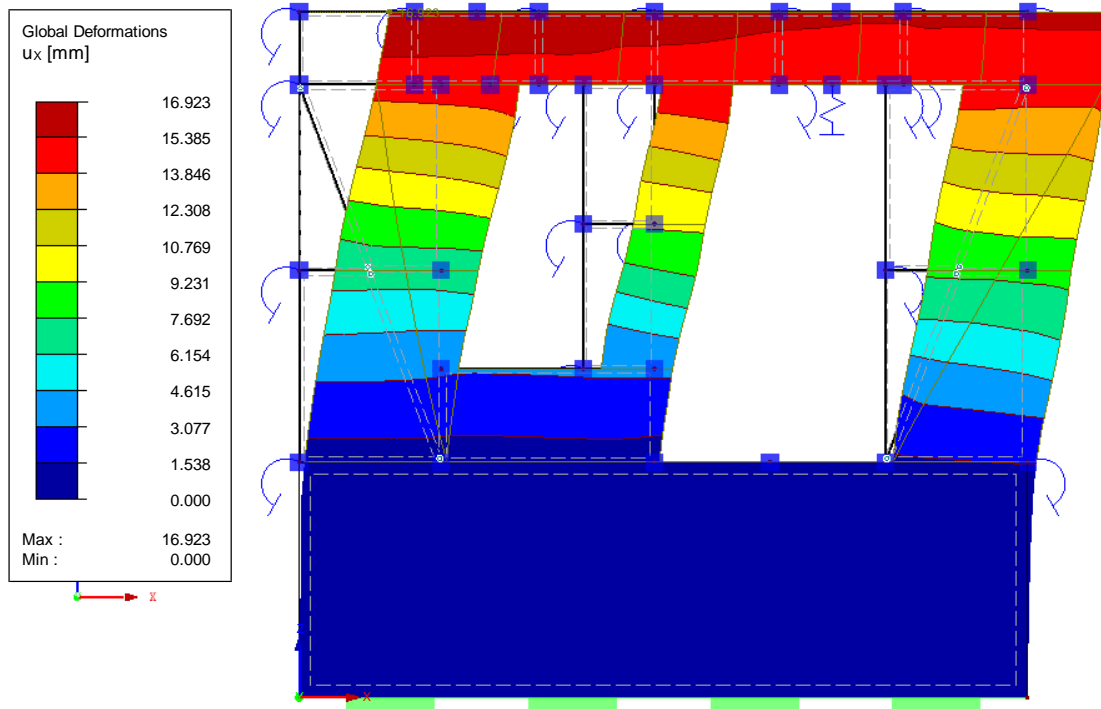
Max : 16.923
Min : 0.000

Max u-X: 16.923, Min u-X: 0.000 mm
Factor of deformations: 30.00

Figure 6. 15: Global deformation-x direction of reinforced frame

CO 14: ULS (EQU) - Seismic
Members Stresses Sigma-x

Stresses
Sigma-x [kN/cm^2]

	3.33
	2.61
	1.88
	1.15
	0.43
	-0.30
	-1.02
	-1.75
	-2.47
	-3.20
	-3.92
	-4.65
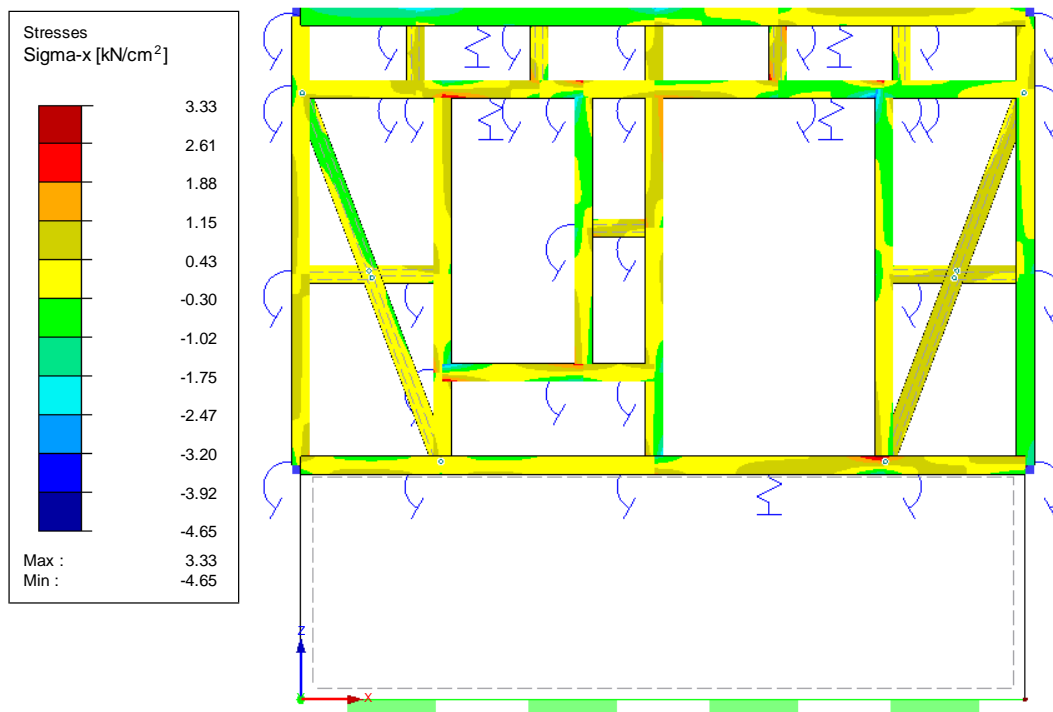
Max : 3.33
Min : -4.65

Max Sigma-x: 3.33, Min Sigma-x: -4.65 kN/cm^2

Figure 6. 16: Normal stresses of timber in unreinforced frame

137

CO 14: ULS (EQU) - Seismic
Members Stresses Sigma-x
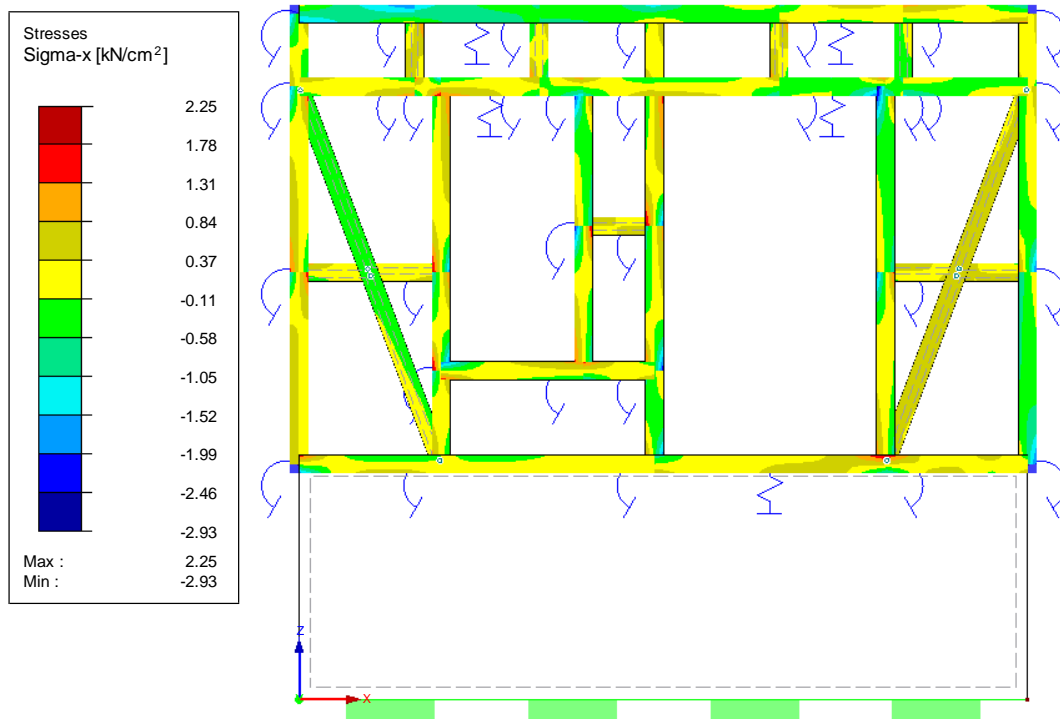
Max Sigma-x: 2.25, Min Sigma-x: -2.93 kN/cm²

Figure 6. 17: Normal stresses of timber in reinforced frame

CO 14: ULS (EQU) - Seismic
Members Stresses Tau-z
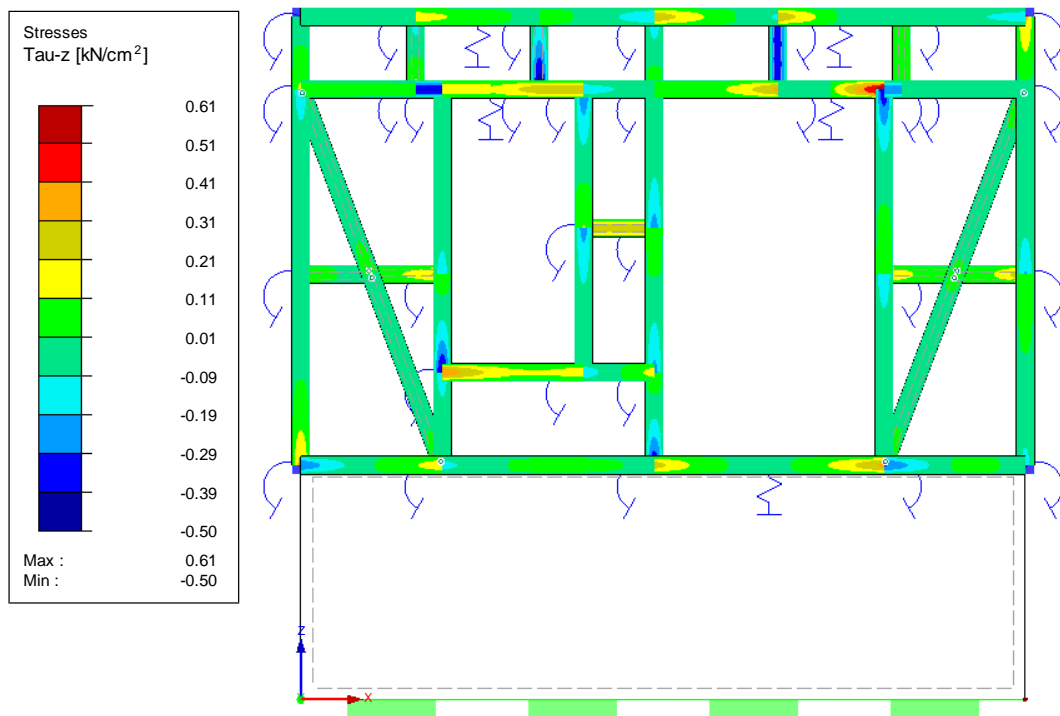
Max Tau-z: 0.61, Min Tau-z: -0.50 kN/cm²

Figure 6. 18: Shear stresses of timber in unreinforced frame

CO 14: ULS (EQU) - Seismic
Members Stresses Tau-z
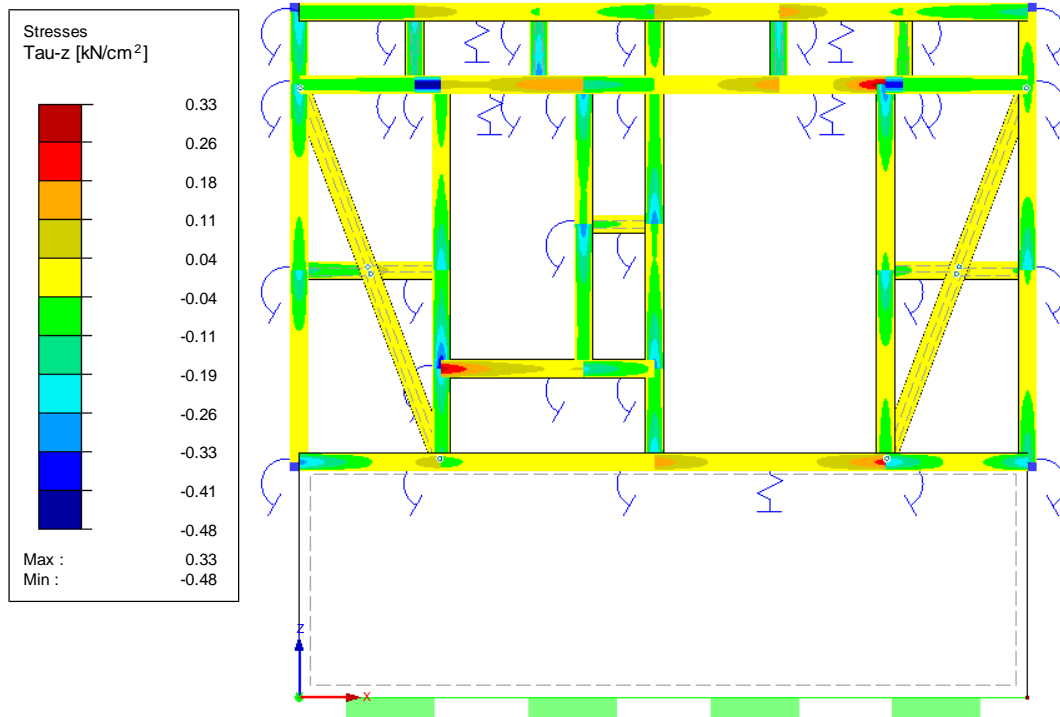
Max Tau-z: 0.33, Min Tau-z: -0.48 kN/cm²

Figure 6. 19: Shear stresses of timber in reinforced frame

CO 14: ULS (EQU) - Seismic
Surfaces Stresses Sigma-x,+
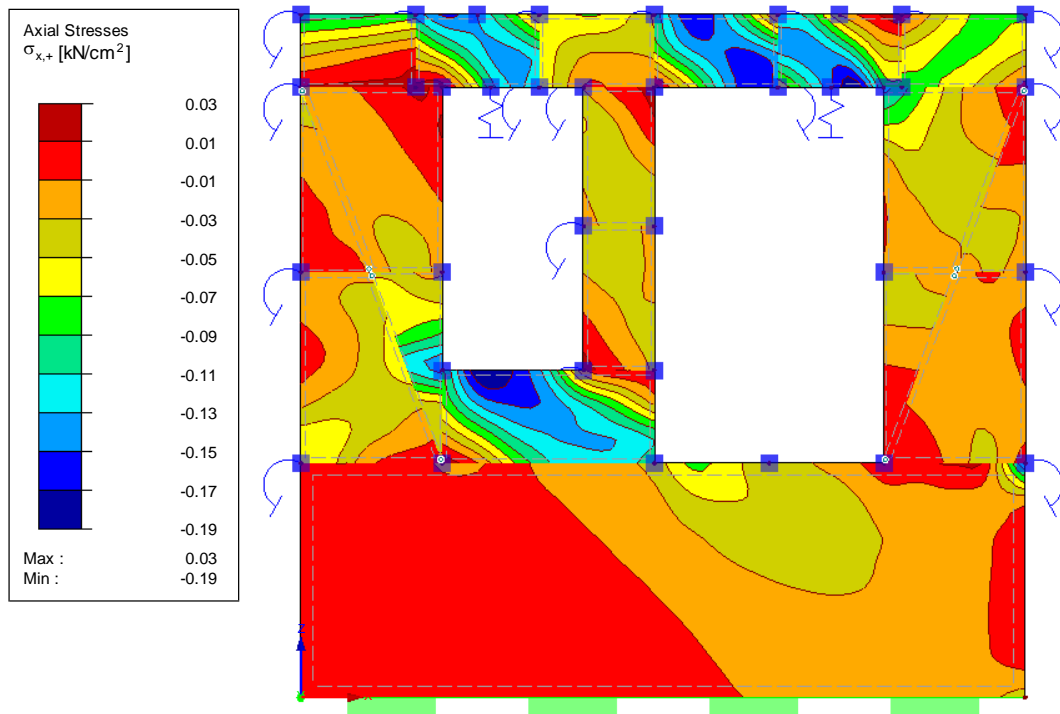
Max Sigma-x,+: 0.03, Min Sigma-x,+: -0.19 kN/cm²

Figure 6. 20: Normal stresses at masonry surfaces in unreinforced frame (sigma-x)

CO 14: ULS (EQU) - Seismic
Surfaces Stresses Sigma-x,+
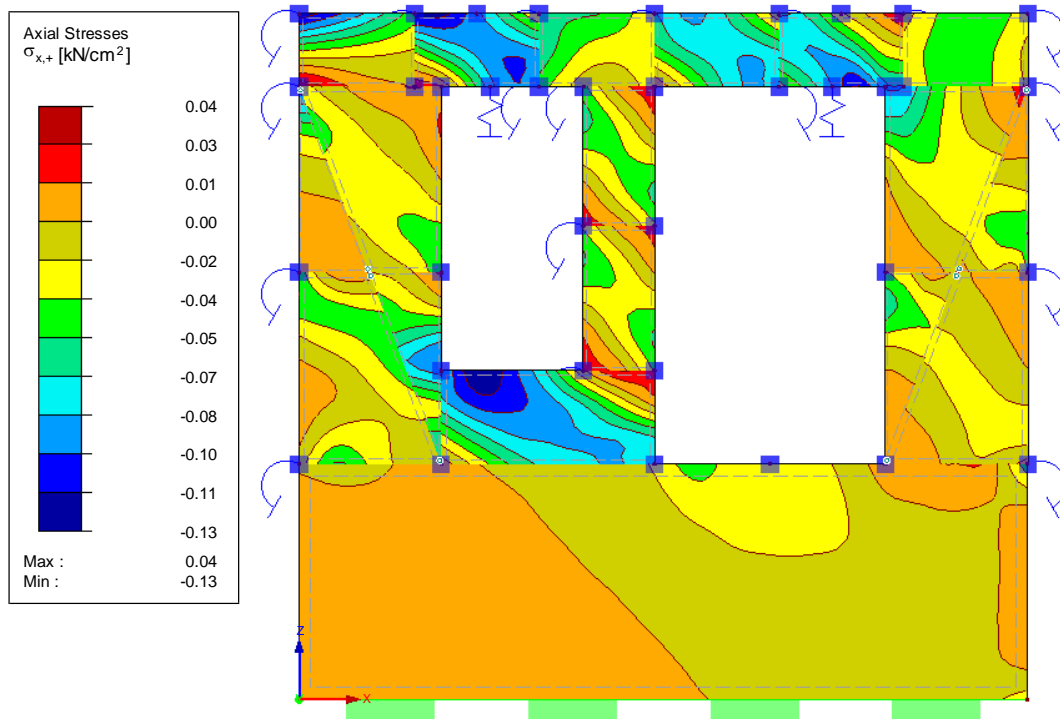
Max Sigma-x,+: 0.04, Min Sigma-x,+: -0.13 kN/cm²

Figure 6. 21: Normal stresses at masonry surfaces in reinforced frame (sigma-x)

CO 14: ULS (EQU) - Seismic
Surfaces Strains Eps-x,+
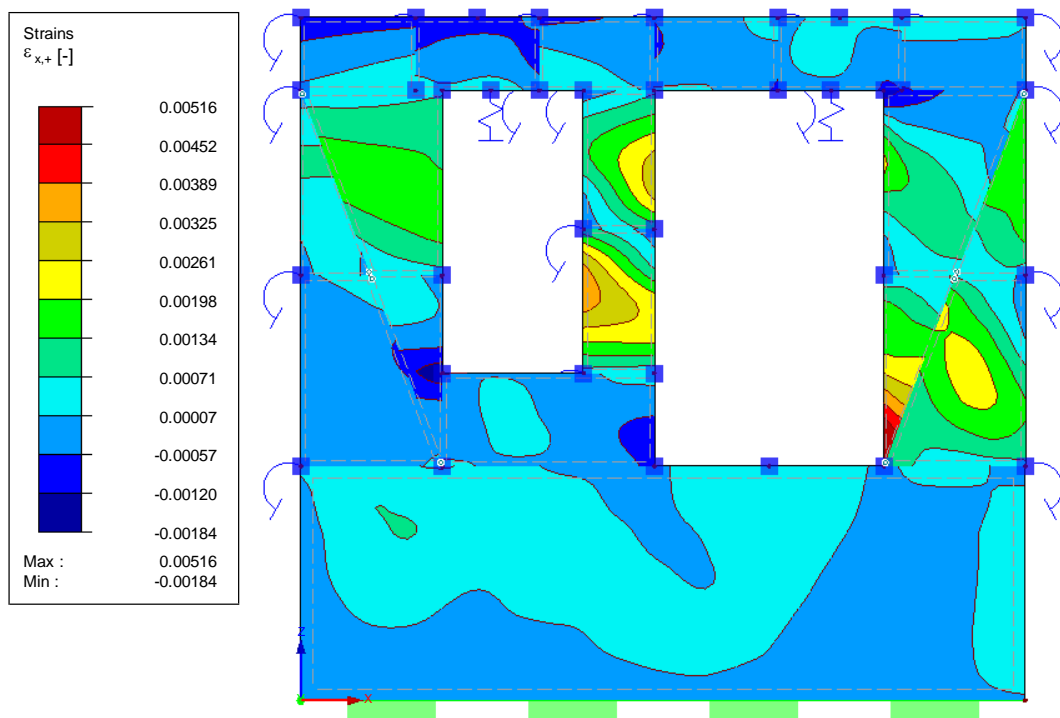
Max Eps-x,+: 0.00516, Min Eps-x,+: -0.00184 -

Figure 6. 22: Elastic strains at masonry surfaces in unreinforced frame (eps-x)

CO 14: ULS (EQU) - Seismic
Surfaces Strains Eps-x,+

Strains
$\varepsilon_{x,+}$ [-]

	0.00424
	0.00373
	0.00321
	0.00269
	0.00217
	0.00166
	0.00114
	0.00062
	0.00010
	-0.00041
	-0.00093
	-0.00145
Max :	0.00424
Min :	-0.00145
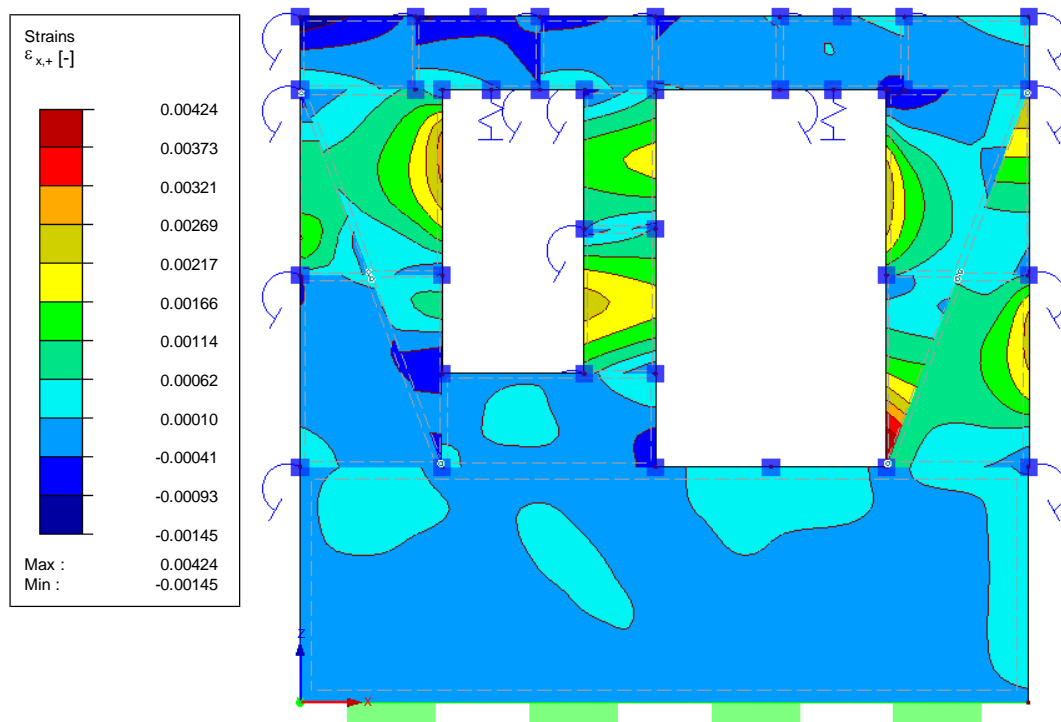
Max Eps-x,+: 0.00424, Min Eps-x,+: -0.00145 -

Figure 6. 23: Elastic strains at masonry surfaces in reinforced frame (eps-x)

The frame system has been subjected to uniform distributed and equivalent seismic forces. The results regarding normal stresses and shear stresses of timber, normal stresses in sigma-x on masonry surfaces for the unreinforced and reinforced frames have been given in Figure 6.16-6.21. Compression stresses of timber members are mostly seen in the edge of the window. Maximum compression stress of timber members in sigma-x is 33 MPa in unreinforced frame, while 22 MPa in reinforced frame, in other words, a %34 of reduction has been (Figure 6.16-6.17). Left diagonal brace suffer pure tension (17.5 MPa) which leading to physical separation of elements. After the reinforcement of joints, the tensile stress decreased to 10 MPa. Besides, shear stresses of timber members are significantly detected in base timber plate. Maximum shear stress of timber members is 6 MPa in unreinforced frame, while 3 MPa in reinforced frame, in other words, a %50 reduction was obtained (Figure 6.18-6.19).

Furthermore, in masonry surfaces normal stresses (sigma-x) for unreinforced and reinforced frames (Figure 6.20-6.21) have been analyzed. Normal stresses at masonry surfaces (sigma-x) in both unreinforced and reinforced frames are similar, compression stresses are 0.3 MPa for both conditions. This is mostly seen at the masonry infill next to the window. Maximum stresses of compression of masonry surfaces in sigma-y are 0.6 MPa in unreinforced frame and 0.3 MPa

in reinforced frame; in other words, %50 decreasement is obtained. Shear stresses in masonry surfaces of unreinforced frame are 1.2 MPa and 0.6 MPa in reinforced frame; this corresponds to a %50 decreasement.

The maximum moment, (5.26 kN.m) has seen just on the window opening, where the lap joint was located and thus, it exposed the bending. Thereafter, the whole structure deforms significantly.

With reinforcement, bending moment reached 3.9 kN.m, thereby a %26 decreasement is seen. Moreover, the distributed elastic strains in sigma x on masonry surfaces in unreinforced and reinforced structures are given in Figure 6.22-6.23.

Elastic strains of masonry surfaces are substantially seen at the left side of base timber plate in unreinforced and reinforced frames. Elastic strain in the unreinforced frame is 0.005 $\mu\varepsilon$ and 0.004 $\mu\varepsilon$ for the reinforced frame; this is a %20 decreasement. Plastic strains at masonry surfaces are also substantially seen at the left side of base timber plate in unreinforced and reinforced frames. Plastic strain of unreinforced frame reached 0.016 $\mu\varepsilon$, while it was 0.009 $\mu\varepsilon$ for reinforced frame. A %44 decreasement is detected. Elastic strain values at masonry surfaces are higher than plastic strains at masonry surfaces in both of unreinforced and reinforced frames.

The permanent plastic deflections of masonry surfaces occurred in edge of window opening at the negative side of the strain axis when the stress passed to compression. Besides, plastic deformations of masonry surfaces observed in upper surface of base timber plate at the positive side of the strain axis when the stress turns into tension.

Most vulnerable point of the timber structure is the lap joint between beams on the upper of window, where nonlinear hinges progressively reach the status of failure. There is a notable reduction in the stiffness due to absence of masonry infill of opening. The increase of opening areas has disadvantageous results at the global response. When more windows and doors exist, the frame system is more vulnerable in terms of lateral load capacity.

Corresponding to applied progressive loads, the results of displacements of the frame are obtained (Table 6.4). Then, the comparison of lateral forces-displacements diagrams are given in Figure 6.24. The results show that reinforcement of the joints with CFRP, significantly enhances the stiffness of joints and flexural strength of structure. Also, analysis indicates that reinforced frame with CFRP lead to improve nonlinear behavior of timber joints under high stresses and reduces deformation in an approximately %35 at same level of load. Besides, the unreinforced frame endures until the load of 108 kN, while the reinforced frame bears until 144 kN (Figure 6.24).

The values of stresses, strains and displacements are considerable low due to the geometrical parameters of system. If the weight and the height or storey of structure is increased, overall vulnerability can be increased.

Table 6. 4: Applied loads and displacements

	Maximum Lateral Displacement			
	Unreinforced		Reinforced	
	Disp (mm)	Force (kN)	Disp (mm)	Force (kN)
C01	0	0	0	0
C02	0.83	9	0.708	9
C03	1.675	18	1.411	18
C04	2.797	27	2.219	27
C05	4.224	36	3.201	36
C06	5.822	45	4.299	45
C07	7.558	54	5.484	54
C08	9.423	63	6.721	63
C09	10.611	68.4	7.491	68.4
C10	11.436	72	8.012	72
C11	13.659	81	9.359	81
C12	16.043	90	10.759	90
C13	20.33	108	13.721	108
C14			16.923	126
C15			20.33	144

Nonlinear axial and rotational hinges which have been assigned to the joints in reinforced frame, are stiffer than the hinges in unreinforced frame. This approach seems to have a direct impact at the stiffness and load capacity of the whole structure. Even though the global responses are different, the failure patterns are relatively same at both examined models.

The strengthening joints also concerns the behaviour of the friction-based connection in its own plane, and is intended to avoid the detachment of the connected members. Particularly, reinforcement can prevent loss of capacity and possible separation of friction surfaces due to the reduction of compression forces under lateral loading, the application of strengthening solution can maintain a stable structural behaviour.

In order to observe the effect of friction between timber members and masonry infill, without infill material, the frame has been reloaded again. Only, the ground floor continued to exist as masonry in the configuration of analysis (Figure 6.25). The deformations corresponding to the each applied loads are given in Table 6.5. In this way, the comparison of the reinforced and unreinforced frames without infill materials was seen clearly (Figure 6.26). The unreinforced frame without infill materials endures until the load of 81 kN, while the reinforced frame

without infill materials bears until 126 kN. Besides, the deformation of system decreased after reinforcement at the same level of load (Figure 6.27-6.28).
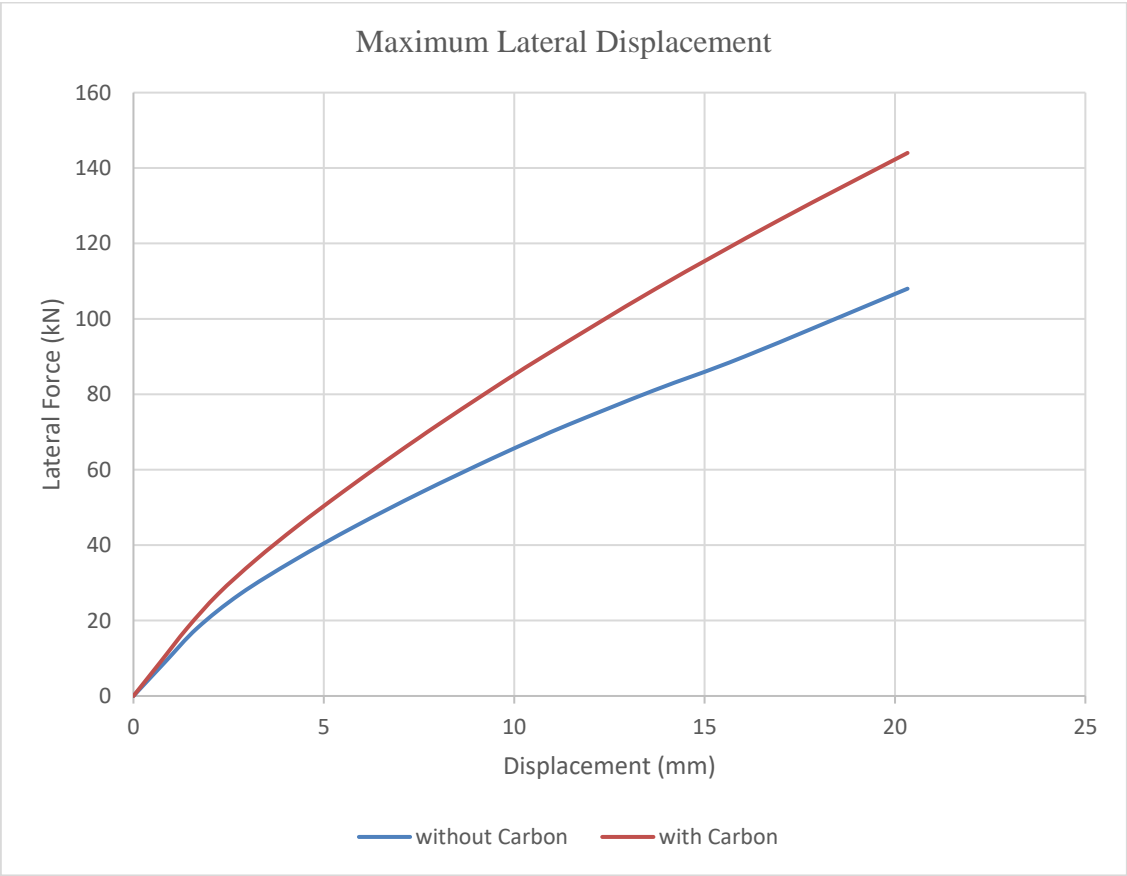
Figure 6. 24: The comprasion of global analysis results between unreinforced and reinforced frames
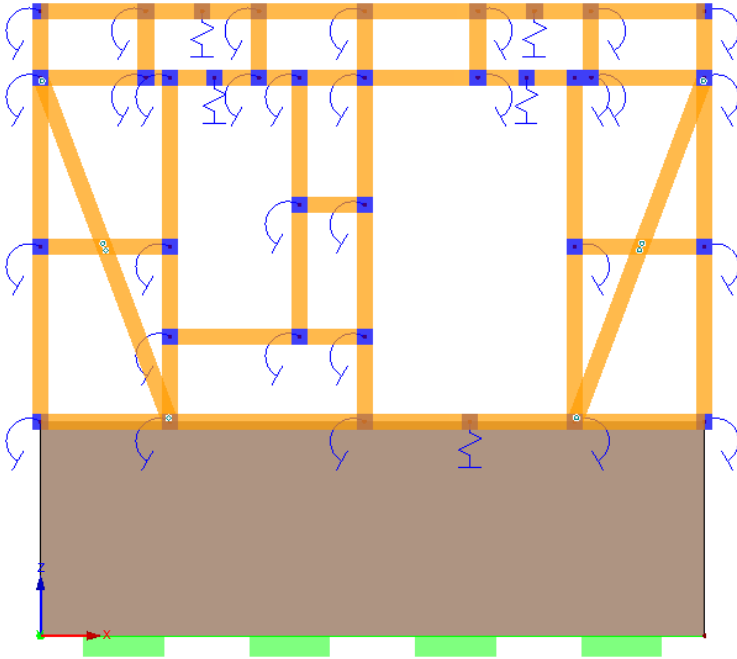
Figure 6. 25: The frame configuration without infill materials for analysis

Figure 6. 26: The comprasion of global analysis results between unreinforced and reinforced frames without infill material

Table 6. 5: Applied loads and displacements of frames without infill material

	Maximum Lateral Displacement			
	Unreinforced (No infill)		Reinforced (No infill)	
	Disp (mm)	Force (kN)	Disp (mm)	Force (kN)
C01	0	0	0	0
C02	2.49	9	1.8	9
C03	5.63	18	3.7	18
C04	9.03	27	5.7	27
C05	12.83	36	7.8	36
C06	16.95	45	10.06	45
C07	21.36	54	12.35	54
C08	25.91	63	14.73	63
C09	28.78	68.4	16.18	68.4
C10	30.69	72	17.16	72
C11	35.51	81	19.65	81
C12			22.18	90
C13			27.3	108
C14			35.51	126
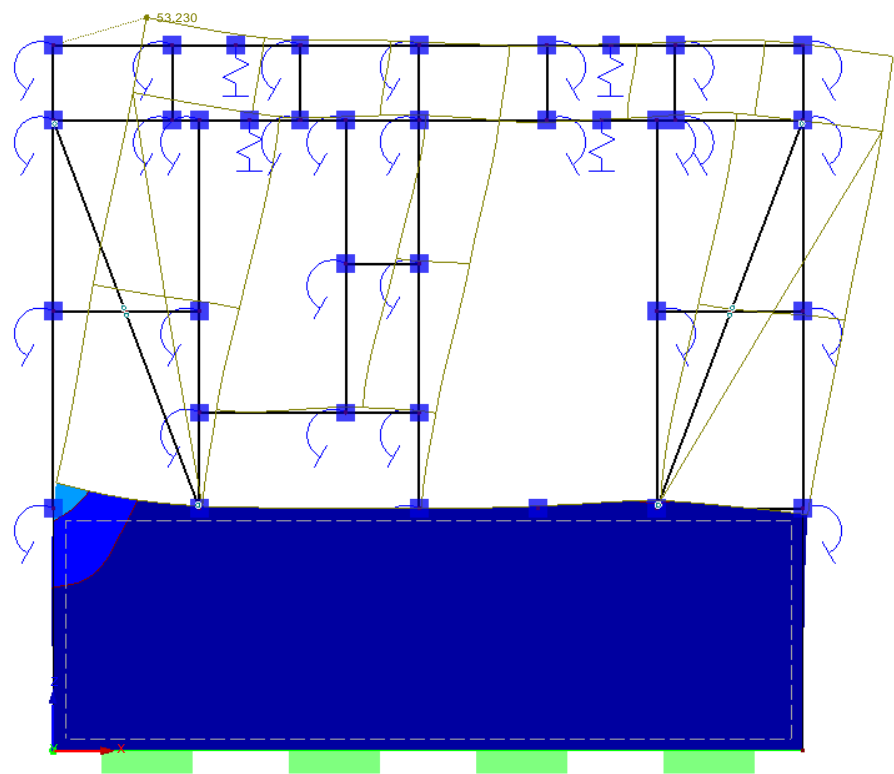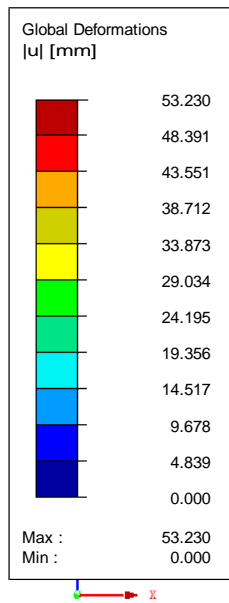
Figure 6. 27: Global deformation of unreinforced frame without infill material
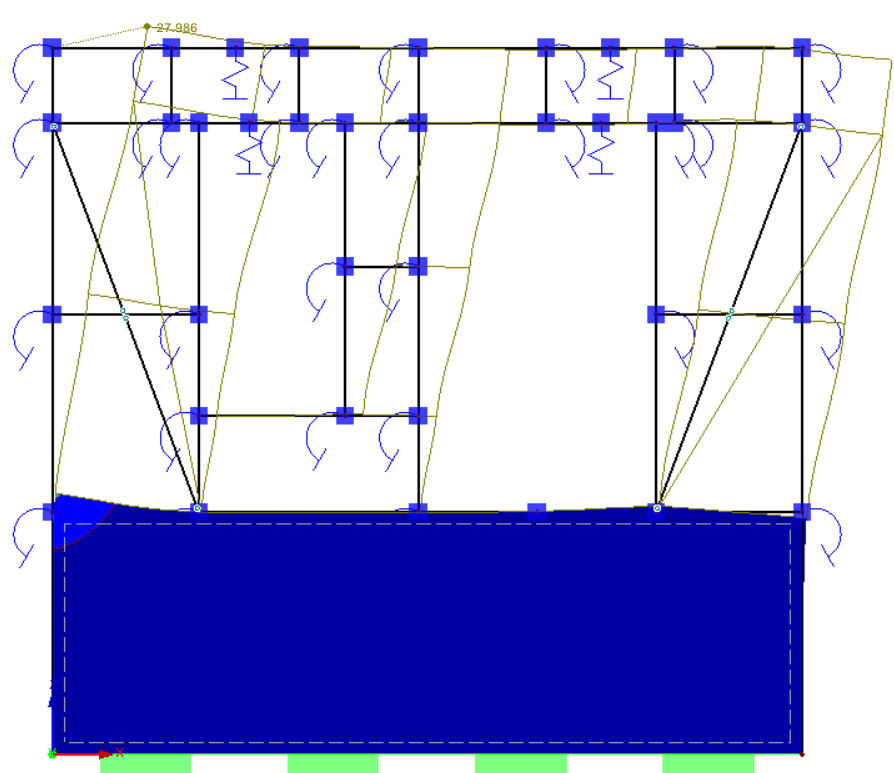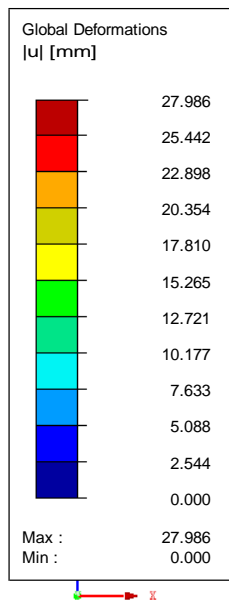
Figure 6. 28: Global deformation of reinforced frame without infill material

146

CO 13: ULS (EQU) - Seismic
Members Internal Forces N
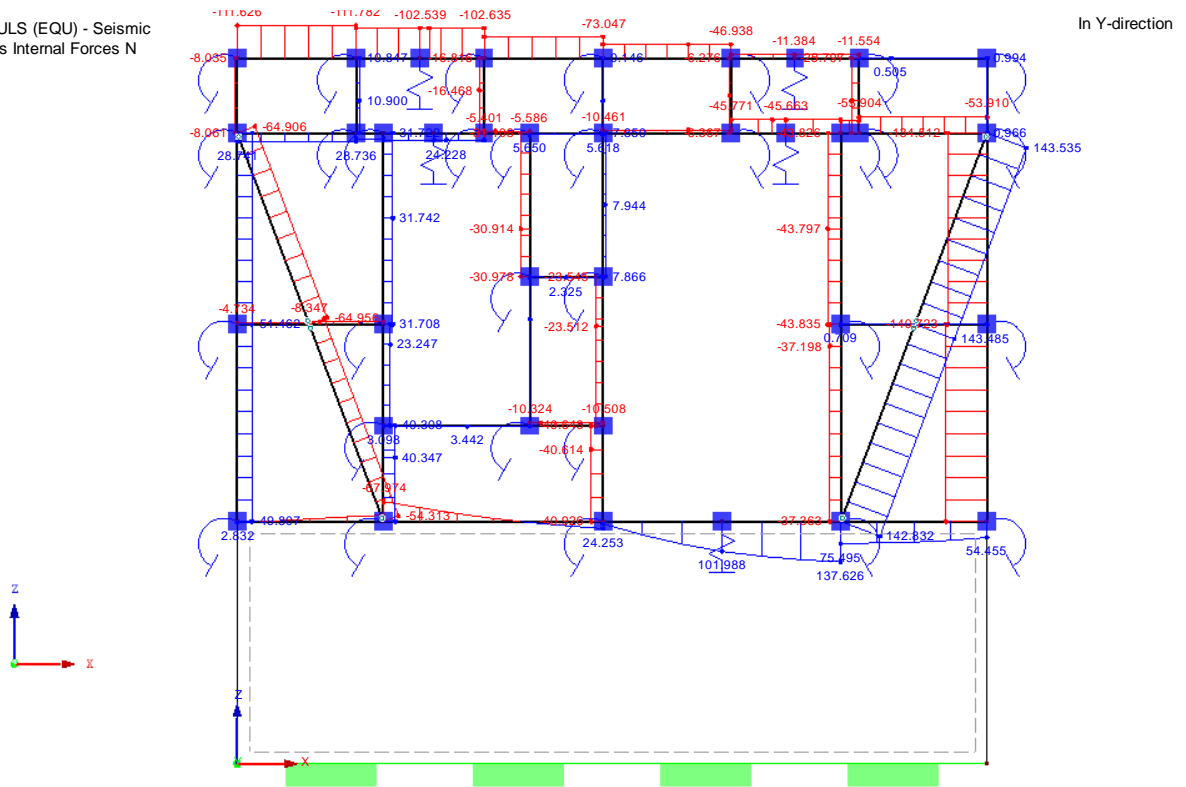
Max N: 143.535, Min N: -140.802 kN

Figure 6. 29: Normal forces of unreinforced frame without infill material

CO 13: ULS (EQU) - Seismic
Members Internal Forces N
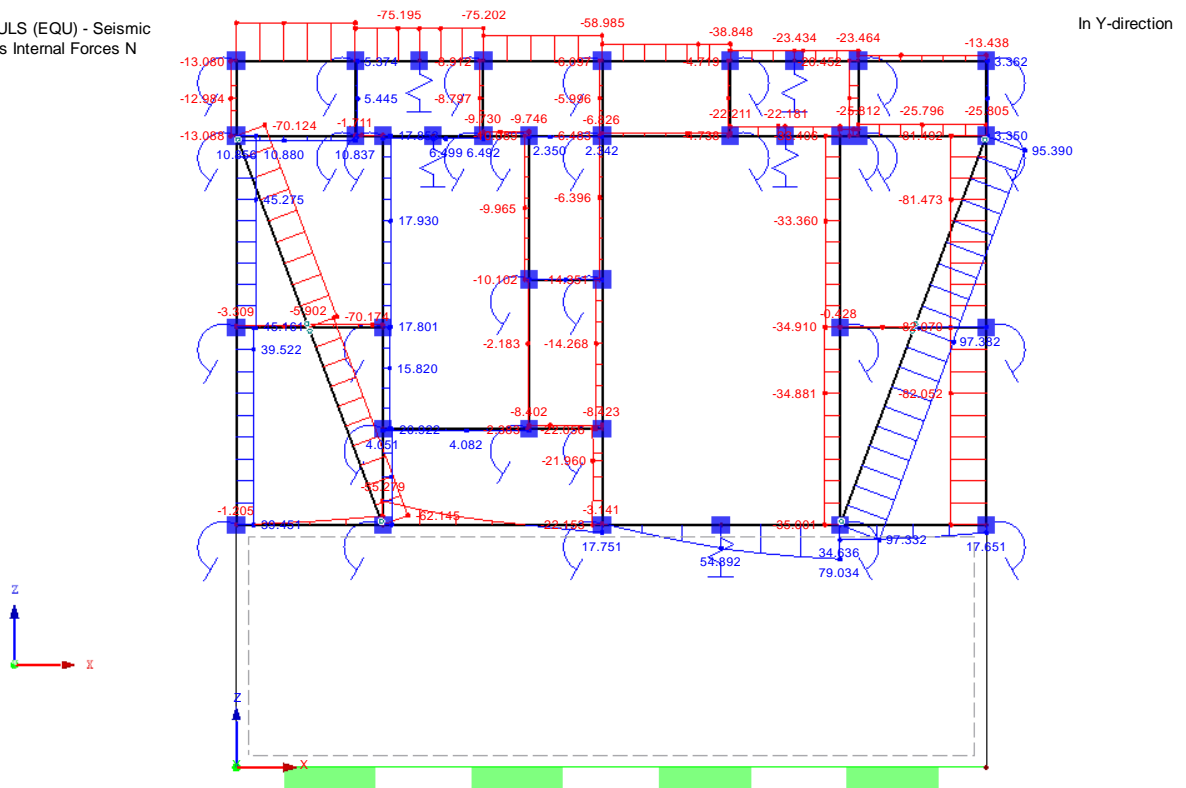
In Y-direction

Max N: 97.382, Min N: -87.740 kN

Figure 6. 30: Normal forces of reinforced frame without infill material

147
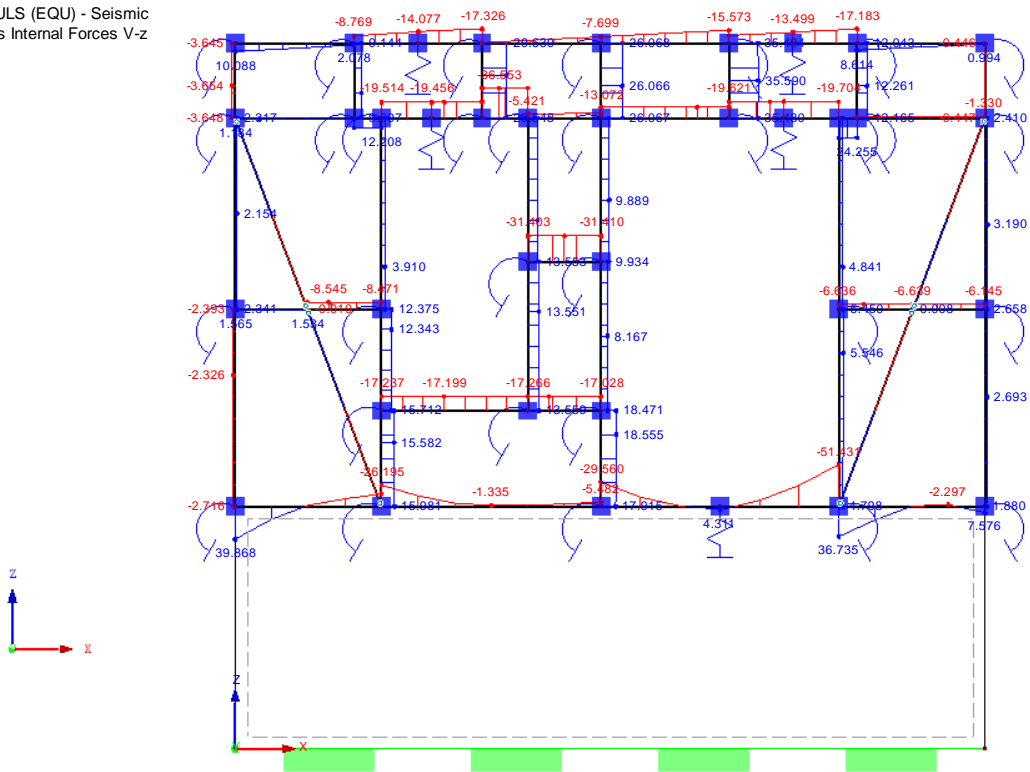
Figure 6. 31: Shear forces of unreinforced frame without infill material
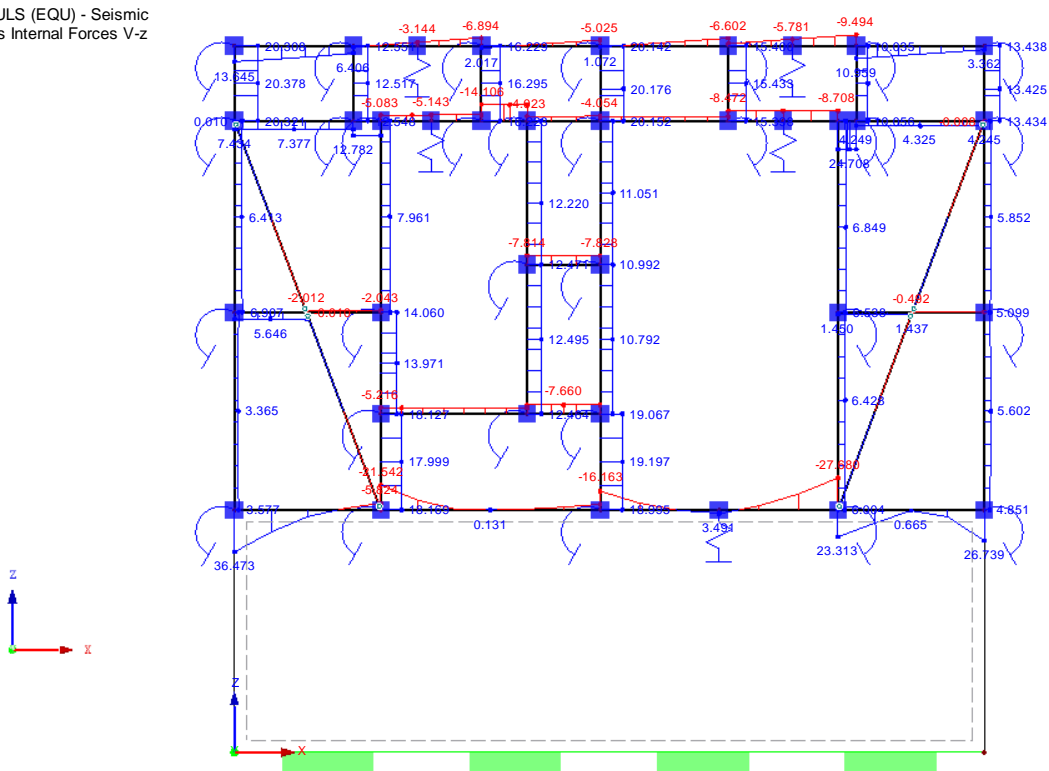
Figure 6. 32: Shear forces of reinforced frame without infill material

148
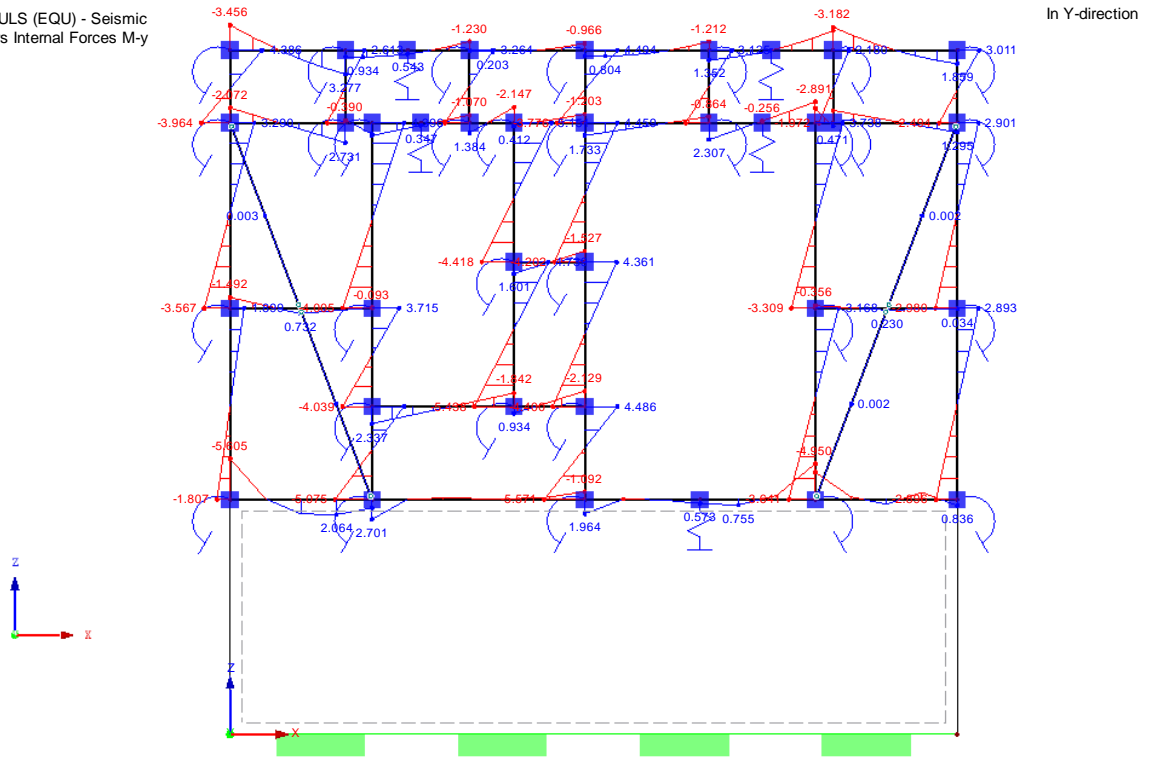
Figure 6. 33: Bending moment of unreinforced frame without infill material
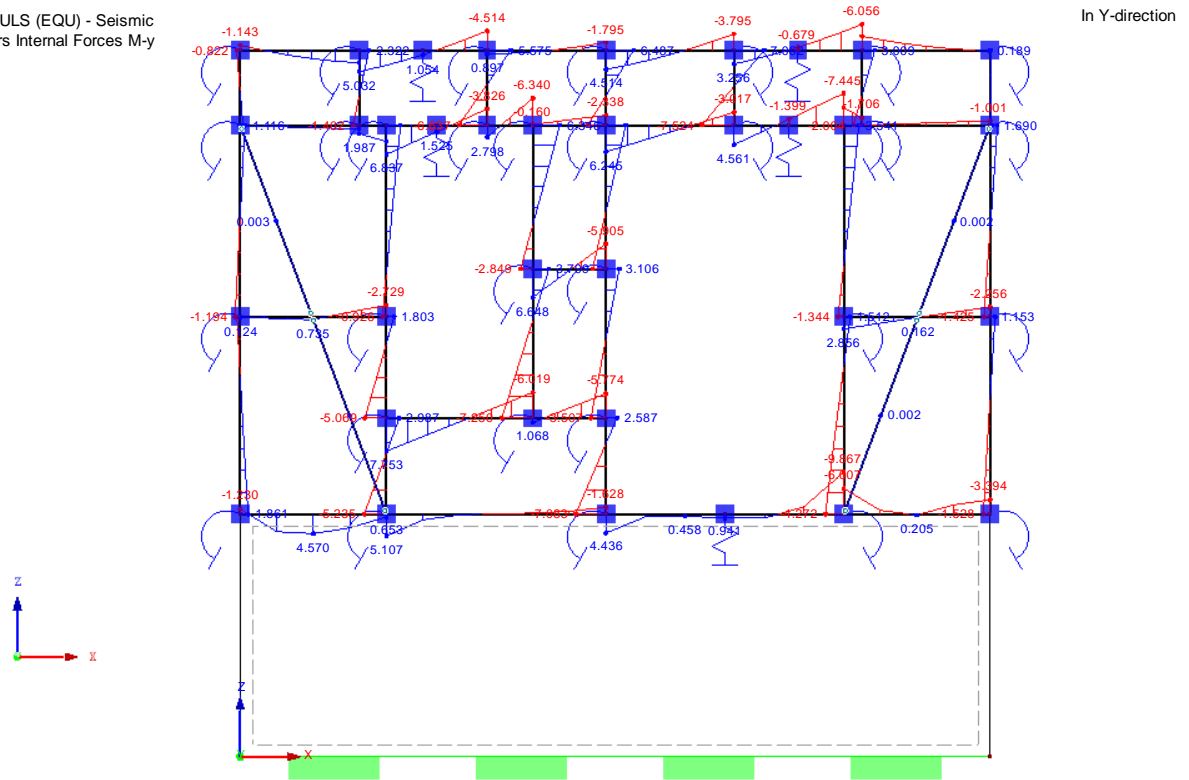
Figure 6. 34: Bending moment of reinforced frame without infill material

CO 13: ULS (EQU) - Seismic
Members Stresses Sigma-x

Stresses
Sigma-x [kN/cm^2]

	8.90
	7.26
	5.62
	3.98
	2.33
	0.69
	-0.95
	-2.59
	-4.23
	-5.87
	-7.51
	-9.16
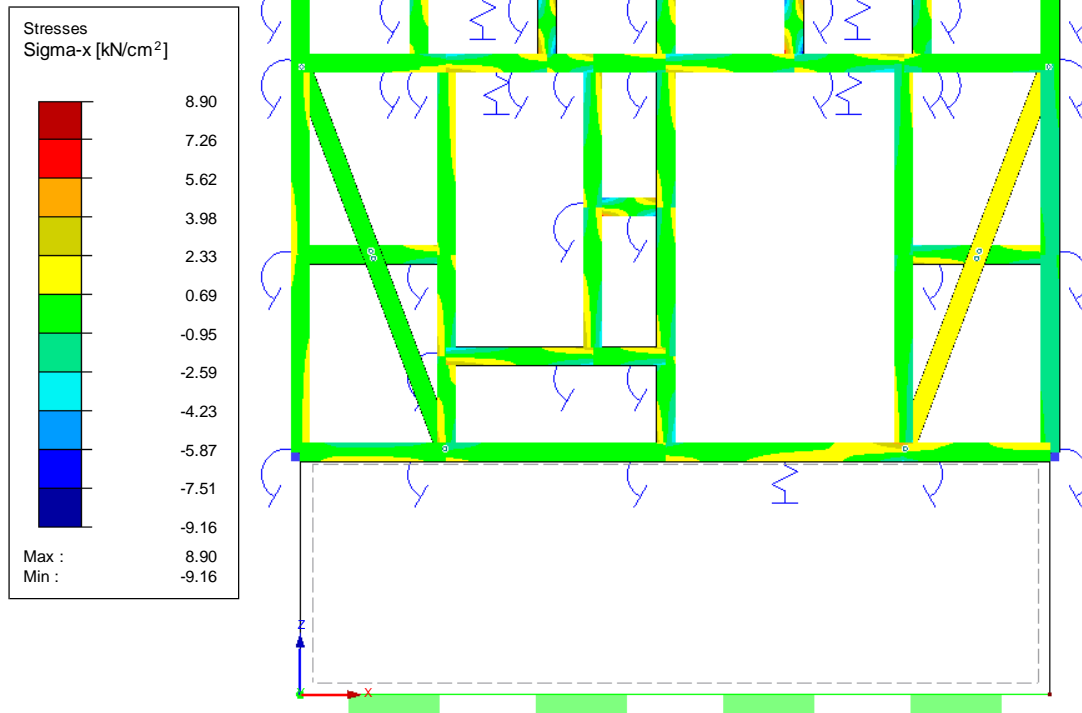
Max : 8.90
Min : -9.16

Max Sigma-x: 8.90, Min Sigma-x: -9.16 kN/cm^2

Figure 6. 35: Normal stresses of timber in unreinforced frame without infill material

CO 13: ULS (EQU) - Seismic
Members Stresses Sigma-x

Stresses
Sigma-x [kN/cm^2]

	3.92
	3.17
	2.43
	1.68
	0.94
	0.19
	-0.55
	-1.30
	-2.04
	-2.78
	-3.53
	-4.27
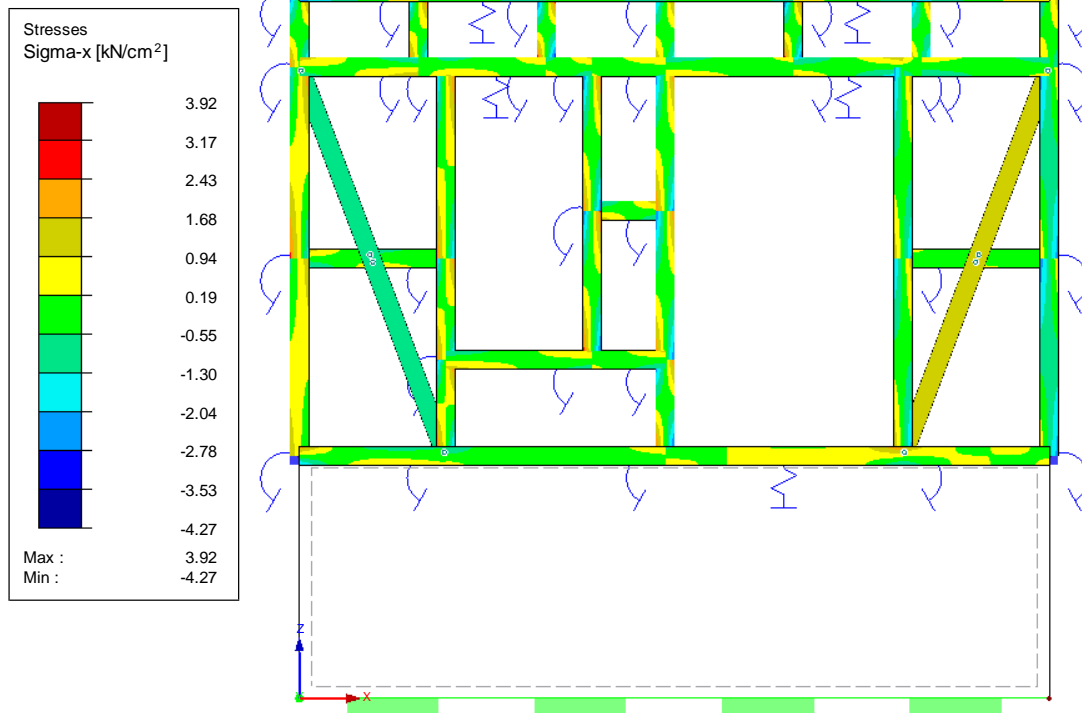
Max : 3.92
Min : -4.27

Max Sigma-x: 3.92, Min Sigma-x: -4.27 kN/cm^2

Figure 6. 36: Normal stresses of timber in reinforced frame without infill material

150
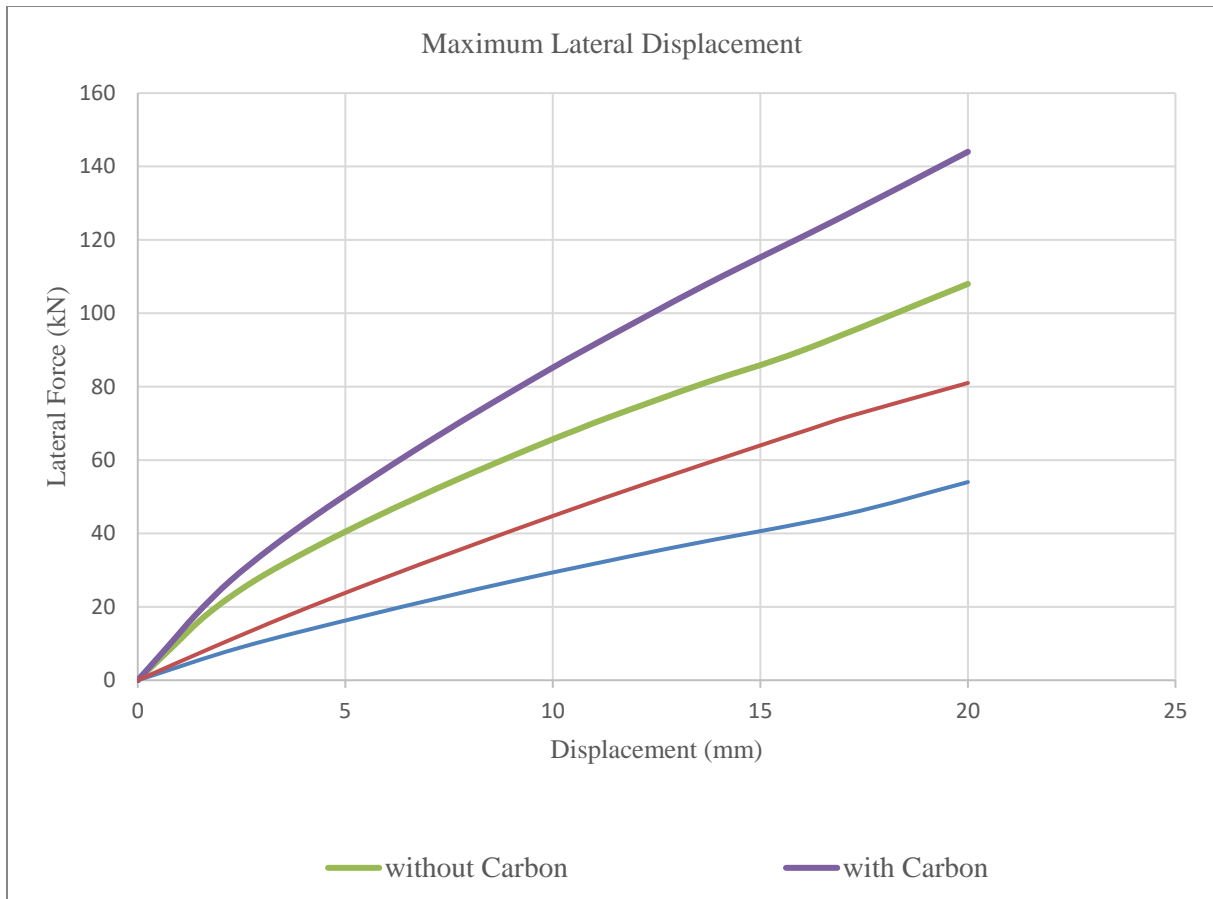
Figure 6. 37: The comprasion of all global analysis results

When there is no interaction of infill with the timber frame, timber members are much more flexible than frame with infill. In other words, infill materials increase the stiffness and lateral load strength of frame. Under lateral loads, the existence of infill change the structural mechanism of transferring the induced lateral forces from a frame action mechanism into truss action mechanism. Such change in load transfer mechanism leads to reduction in the induced straining actions in terms of bending moments and shearing forces and axial forces.

Moreover, the unreinforced frame without infill finally reached its capacity at larger deformation than that of carbon fiber reinforced frame with infill but approximately at the same lateral load (Figure 6.37). Minimum displacement and stresses are obtained in the cases where the frame is made up of reinforced with CFRP. After reinforcement, the deformation of system decreased as %35 in frame with infill while %43 decreasement was seen in frame without infill. In either case, CFRP increases the strength properties of timber elements subjected to lateral loads. Besides, strain was detected along the CFRP reinforced joints, it was seen that carbon fibers were subjected to high stress. This showed the high performance of CFRP in terms of bonding during stress-transfer process.

The degradation of stiffness due to the increment of lateral loads is highest in unreinforced frame without infill. Besides, the lateral drift is calculated as the ratio between the lateral top displacement and the height at which the lateral load is applied. It is seen that the cyclic lateral drift is highest in unreinforced frame without infill, due to the absence of infill caused the frame to loosen.

Furthermore, the ductility of the structure is considered, which is is an important factor for the evaluation of the seismic behaviour of structures in seismic regions. It is related to the ability of the structure to deform nonlinearly without significant loss of strength. Displacement ductility is defined here as the area at the below of each curves corresponding to the same displacement value. For instance, if the frame system reached to 20 mm, the area under the curves is widest in reinforced frame with infill materials. It is seen that timber frame walls without infill presented lower values of ductility for both load cases when compared to infill timber frame. This means that the filling of the timber frame leads to improvement of the ductility as it result from the change on the resisting mechanism from shear to flexure.

Besides, it should be noticed that the lower values of ductility for timber frame is associated to considerable higher levels of damage. It appears that the presence of infill and more importantly reinforcement with CFRP improves the seismic behaviour of the frame as improve ductility with a lower level of damage.

In addition to these, reinforcement significantly increases the energy dissipation capacity of connections. Because of the brittle failure mode in unreinforced joints, little energy gets dissipated after failure of joints.

7. CONCLUSIONS

This thesis aims to assess the influence of the joint stiffness in the monotonic and cyclic behaviour of Turkish traditional timber system (Hımış) identifying and evaluating new strengthening technique with carbon fiber reinforced polymers (CFRP). The study is based on three methodologies: the literature review, experimental analysis, numerical analysis (small scale about timber joints and global analysis of frame).

Firstly, an extensive literature review has been made about general traditional timber frame system and particularly focused on timber joints in Turkish timber structure. Among many types of traditional joints, mostly the mortise-tenon, which is preferable for beam-column connections is used in Turkish traditional timber house. Another common typology of joint, the lap or half-lap joints, which is preferable for beam-beam connections, was selected within the scope of thesis in order to analyze their role in the whole system.

Secondly, in order to evaluate the internal forces of timber members and determine the critical places in himis timber structure, a numerical analysis has been performed on the an accurate geometric frame configuration, in which the choice of location timber joints is arbitrary. As a finite element program, RSTAB has been used in order to calculate the internal forces, deformations and support reactions of frame. The frame has been analysed by performing dynamic non-linear implicit analysis. The numerical analysis of frame results highlight the efficiency of the joints, to assess the global behaviour of traditional timber system, identify the critical areas (particularly joints specifically which were detected weakest parts of the timber frame under bending load), to plan the upgrade intervention and to quantify the effect of reinforcement. Depending on the result of analysis, maximum bending moments are seen upper of window and door openings, where the lap joints are located and also, at the below part of frame, where the column and beam are connected with mortise-tenon joint. These joints are exposed the high bending, thereafter the whole structure deforms significantly. Because, the internal forces of the members transfer the loads by each of connections.

Subsequently, some characterization tests on the selected type of timber, which used in experiments related to timber joints, are carried out. In Turkish traditional timber house, as a type of timber mostly pine is used. These tests were compression in both directions and bending test of timber. The compressive strength in parallel to fiber and perpendicular to fibers, bending strength, global modulus of elasticity are calculated with the formula according the standard. Then, two different types of timber joints (lap joint and mortise-tenon joints) are analyzed under monotonic and cyclic bending loadings. Subsequently, the joints locally strengthened with carbon fiber textile have been tested in order to increase the flexural strength and load-bearing capacity of joint have been tested. The comparative result between reinforced and un-reinforced specimens show that the rotational stiffness of reinforced mortise tenon joint specimens and translational stiffness of reinforced lap joint specimens have been higher than the unreinforced specimens which led to more brittle behaviour. The rotational behavior of the degraded mortise tenon joints and the translational behavior of lap joints are semi-rigid. After the reinforcement, specimens reached to higher load. It can be observed that CFRP has provided the reduction of

deformation as 23% and the increasement of load bearing capacity 325% under cyclic bending loading. Experiments gave an insight of the behaviour of two joints under bending load and they have proved that the reinforced specimens showed more ductile behaviour.

Furthermore, the numerical analysis have been performed for calibrate the experimental results from monotonic and cyclic tests of timber joints, using finite element program, ANSYS. Timber and CFRP composites have been modelled as an elastic orthotropic constitutive model until failure. The geometry of finite element model, loading, boundry conditions and material axes were defined using same parameters from experiments. A significant fitting between experimental and numerical results is observed both in terms of stiffness and lateral resistance. For numerical analysis of lap joint, the CFRP shows an increase of the ultimate load by about 800% and a change of failure mode is observed with greater ductility. Also, for numerical analysis of mortise-tenon joint, the CFRP provides an increase of the ultimate load by about 313% and has a ductile compression failure mode. Both of the results from experimental tests and ones achieved by the numerical models show that the rotational and translational stiffness assumed for the connections have particular importance in terms of deformation of timber frame under seismic loading conditions.

In the case of reinforcement of existing timber traditional structures against to earthquake, a realistic interpretation of the global structural behaviour has to be carried out. In typical configuration of timber structure, the commonly used hinge models are inadequate; because in real structures, where all joints have moment resisting capability. The semi-rigid modelling of timber connections, using nonlinear moment-rotation and force-displacement laws and hysteretic rules, intend to represent the behaviour of timber structures with all the structural components. In last chapter, the original and strenghened traditional timber connections were modelled, using a nonlinear spring element available in a structural frame analysis software, RSTAB in order to analyze the normal, shear and moment forces, deformations of frame and stresses of timber members and masonry infill in terms of global scale. Besides, in order to observe the effect of friction between timber members and masonry infill, the frame was loaded without infill material as well. Under lateral load, the load path is primarily characterized by the timber frame and braces (diagonal) system, nonlinear hysteretic response is governed by the opening and closing actions of connections. The analysis indicates that reinforcement of the joints with CFRP, significantly enhances the stiffness of joints and flexural strength of structure. Also, after reinforcement, the deformation of system has decreased as %35 in frame with infill while %43 decreasement has seen in frame without infill material. When the results are evaluated, the values of stresses, strains and displacements of frame are considerable low due

to the geometrical parameters of system. Normally, Hımış traditional timber frame systems have a great variability in terms of geometry, namely height to length ratio of the wall, height to length ratio of a single cell, sectional dimensions of timber elements, positioning of diagonals. If the weight and the height or storey of structure is increased, overall vulnerability can be increased.

Besides, in order to represent the behaviour of semi-rigid joints, spring models have been derived from the results of experiments. The average of force-displacement curves of lap joint specimens under monotonic bending loads was used for obtain the translational spring. Also, the average of moment-rotation curves of mortise-tenon joint specimens has been defined for rotational spring. Following, non-linearity effects concentrated hinges have been applied to the joints in global analysis. The rotational and shear stiffness have not obtained for lap joints within the experiments. For this reason, the study has to be evaluated in defined limited extend. For a wide range of research, all nonlinear axial, rotational and shear hinges for each of joints in the frame have to be defined.

Consequently, according to the analyses and literature researches of earthquake damages of himis structure, it has been seen that these types of structures are less deformed after reinforced the joints of frame. Briefly, it is possible to conclude that:

- The results of analysis have shown that the seismic response of traditional timber frame varies greatly with the type of infill, the type of connection and diagonal geometry. The great influence on the behaviour of the frame is given by the quality of the joints as well as the connectivity between timber and masonry, behaviour that is in accordance with experimental results.

- The opening ratios have disadvantageous results at the global response of frame. When more windows and doors exist, the frame is more vulnerable in terms of lateral load capacity.

- The multi-storey configuration or increase in height also influences negatively the global response of timber frame. As distance between the ground and the centre of mass and weight is increased, the structure becomes more vulnerable under lateral loading.

- Masonry infill not only affects the lateral stiffness, load and strength of frame, but also contributes significantly to energy dissipation.

- Timber connections in traditional Turkish structures are always complemented with nails to provide resistance against tensile or shear forces. Furthermore, nails contribute the ductility and the ability of dissipating energy in the structure.

155

- Most vulnerable points of the structure are the lap joints (beam-beam connections) and mortise tenon joints (beam-column connections), where nonlinear hinges are noted at early stage of the analysis and also progressively reach the status of failure. Besides, the diagonals concentrate high tension and compression stresses and as a result, hinges near the failure level are obvious.

- The failure mode of the specimens indicated that the joints are weak, but the timber members are strong. In any case, the timber beam bending capacity is dependent on the bearing capacity of connection, this controls the stability of lateral force-deformation response of system under lateral loads.

- When the specimens are subjected to lateral loading, the semi-rigid joint connections are experienced bending moments, which create tension perpendicular to the wood grain and a longitudinal shear stress, it causes the premature splitting at the joints, thus connections are easily damaged under lateral loading. Reinforcement with CFRP prevents the seperation of joint and specimen is able to resist the high lateral loads.

- The strengthening joints concerns the behaviour of the friction-based connection in its own plane, and is intended to avoid the detachment of the connected members. Particularly, reinforcement can prevent loss of capacity and possible separation of friction surfaces due to the reduction of compression forces under lateral loading, the application of strengthening solution can maintain a stable structural behaviour.

The global strength and ductility that are the two most important parameters for structure in seismic area and it should be aware of the seismic behaviour of traditional structure. In case of the structure was not constructed properly to resist earthquakes, it requires the rehabilitation for better performance. Innovative techniques can play an important role in the rehabilitation of the traditional structures. Whilst respecting the original structure concept and, therefore, their authenticity, CFRP strengthening technique is capable of improving the global strength, ductility and energy dissipation capacity of the structures. In particular, ease of handling and application, their light weight are some factors that are advantageous in the strengthening of timber joints.

REFERENCES

Aksoy, D., Ahunbay, Z. (2005). Geleneksel ahşap iskeletli Türk konutu'nun deprem davranışları. İtü Dergisi, Istanbul, Mart.

Aktas, Y. D. (2017). Seismic resistance of traditional timber frame hımış structures in Turkey: a brief overview, International Wood Products Journal, 20 January.

Aktas, Y. D., Turer, A. (2016). Seismic performance evaluation of traditional timber Hımış frames: Capacity spectrum method based assessment, Bulletin of Earthquake Engineering, November.

American Wood Council (1993). Wood structural design data. 1986 edition with 1992 revisions, American Forest & Paper Association, Washington.

Andor, K., Lengyel A., Polgar, R., Fodor T., and Karacsonyi Z. (2015). Flexural stiffness and strength enhancement of horizontally glued laminated wood beams with GFRP and CFRP composite sheets. Construction and Building Materials 99, p. 200-207.

Arıoğlu, E., Anadol K. (1978). Response of rural dwellings to recent destructive earthquakes in Turkey (1967-1977) and design criteria of earthquake resistant rural dwellings. Housing Science 2.3, p. 237-258.

ASME BPV Code. (1998). Structural steel fatigue data at zero mean stress. Section 8, Div 2, Table 5-110.1.

Bayülke, N. (2001). Ahşap yapılar ve deprem, Türkiye Mühendislik Haberleri, 414, 2001/4.

Blass, H.J., Krams, J. and Romani, M. (2002). Verstärkung von BS-Holz-Trägern mit horizontal und vertikal angeordneten CFK-Lamellen; Bautechnik, 79(10), p.684-690.

Borri A., Corradi M. and Grazini A. (2005). A method for flexural reinforcement of old wood beams with CFRP materials; Composites: Part B, 36(2), p.143-153.

Buell T.W. and Saadatmanesh H. (2005). Strengthening Timber Bridge Beams Using Carbon Fibre; Journal of Structural Engineering, 131(1), p.173-187.

De la Rosa Garcia, P., Escamilla A.C., and Garcia M.N.G (2013). Bending reinforcement of timber beams with composite carbon fiber and basalt fiber materials. Compos Part B, 2013: 55, p: 528-536.

Dinehart, D. W., Shenton III, H. W. (1998). Comparison of static and dynamic response of timber shear walls. Journal of Structural Engineering, 124:6, 1104-1113.

Dogangun, A., Tuluk, I., and Livaoglu, R. (2015). Traditional wooden buildings and their damages during earthquakes in Turkey. Karadeniz Technical University, December 2015.

Eldem, S. H. (1984). Türk evi: Osmanlı dönemi/Turkish houses: Ottoman period. Istanbul: Türkiye Anıt, Çevre, Turizm Değerlerini Koruma Vakfı.

Erman, E. (2011). A survey structural timber joint classifications and a proposal taxonomy. Architectural Science Review, 42:3, 169-180, October 2011.

Gezer, A., Aydemir, B. (2010). The effect of the wrapped carbon fiber reinforced polymer material on fir and pine woods. Material and Design 31, 3564-3567, 2010.

Gibson, L.J., Ashby, M.F. (1997). Cellular solids. Structures and properties, Second edition. Cambridge University Press.

Glos, P. (1981). Zur Modellierung des Festigkeitsverhaltens von Bauholz bei Druck-, Zug- und Biegebeanspruchung. Berichte zur Zuverlässigkeitstheorie der Bauwerke, SFB 96, Munich, Germany.

Graham, F.D., Emery T.J. (1951). Audel´s carpenters and builders guide Theo Audel and Co., New York.

Greenland, A., Crews, K. and Bakoss S. (1999). Application of advanced fibre composite reinforcements to structural timber. In: Proceedings of Pacific Timber Engineering Conference, vol.1, p. 93.

Hassan, R., Ibrahim, A. and Ahmad, Z. (2008). Bending behavior of dowelled mortise and tenon joints in Kempas. Scientific Research Journal, Vol.5 No.1, p. 1-11.

Holmberg, S., Persson, K. and Petersson, H. (1999). Nonlinear mechanical behavior and analysis of wood and fibre materials. Computers and Structures, 72, p. 459-480.

Issa Camille A, Kmeid Ziad. (2005). Advanced wood engineering: glulam beams. Constr. Build Mater 2005, 19(2), p. 99–106.

JCSS. (2006). Probabilistic model code, part 3: resistance models.

Johnston, A. R., Dean, P. K. and Shenton III, H. W. (2006). Effects of vertical load and hold-down anchors on the cyclic response of wood framed shear walls. Journal of Structural Engineering, 132:9, p. 1426-1434.

Korkmaz, H.H., Korkmaz, S.Z., and Donduren, M.S. (2010). Earthquake hazard and damage on traditional rural structures in Turkey. Nat. Hazards Earth Syst. Sci. 10, p 605-622.

Larsson, G. (2017). High capacity timber joints, proposal of the shear plate dowel joint. Lund University, Sweden, Licentiate Thesis, January 2017.

Lam, F., Prion, H. G. L., and He, M. (1997). Lateral resistance of wood shear walls with large sheathing panels. Journal of Structural Engineering, 123:14, p. 1666-1673.

Lukic, R., Poletti, E., Rodrigues, H. and Vasconcelos, G. (2018). Numerical modelling of the cyclic behaviour of the timber-framed structures. Engineering Structure, 165, p. 210-221, 14 March 2018.

Matsushita, S. (2004). Comparative study of the structure of traditional timber housing in Turkey and Japan, Middle East Technical University, MSc Thesis, March 2004.

Nadir, Y., Nagarajan, P., Ameen M., Mohammed A. and Muhammed A. M. (2016). Flexural stiffness and strength enhancement of horizontally glued laminated wood beams with GFRP and CFRP composite sheets. Construction and Building Materials 112, p. 547-555.

Nie, X. (2015). Failure mechanism of rolling shear failure in cross-laminated timber. The University of British Colombia, MSc. Thesis, November 2015.

Nunes, R.D. (2017). Constructive characterization of Pombaline buildings and simplified pushover analysis of frontal walls. Universidade Nove de Lisboa, PhD Thesis March 2017.

Oztank, N. (2008). Traditional timber Turkish houses and structural details. Dokuz Eylul University, Izmir.

Palma, P., Garcia, H. and Ferreira, J. (2012). Behaviour and repair of carpentry connections-rotational behaviour of the rafter and tie beam connection in timber roof structures. Journal of Cultural Heritage.

Pang, W., Rosowsky, D., Pei, S. and Lindt, J. (2007). Evolutionary parameter hysteretic Model for wood shear walls, Journal of Structural Engineering, 133:8.

Poletti, E., Vasconcelos, G. (2014). Seismic behavior of traditional timber frame walls: experimental results on unreinforced walls, Bull Earthquake Eng 2015:13, p. 885-916.

Radford, D.W., Van Goethem D., Gutkowski R.M. and Peterson M.L. (2002). Composite repair of timber structures, Construction and Building Materials, 16.

Schober, K.U. and Rautenstrauch, K. (2006). Post-strengthening of timber structures with CFRP's; Materials and Structures, 40(1), p.27-35.

Schober, K.U, Harte, A.M., Kliger, R., Jockwer, R. and Chen, J.F. (2015). FRP reinforcement of timber structures, Construction and Building Materials 97, p. 106-118.

Sumiyoshi T., Matsui G. (1990). Wood Joints In Classical Japanese Architecture.

Silva, P., Cachim, P. and Juvandes, L. (2004). Técnicas avançadas de reforço de estruturas de Madeira com compósitos reforçados com fibras (FRP), In: Proceeding 1st Iberic Congress Cimad'04-Wood in Construction, Guimaraes, p. 613–622.

Trung, V. A. N., Le Roy R., and Caron J. F. (2015). Multi-reinforcement of timber beams with composite materials: experiments and fracture modeling. Compos. Struct. 123: 233–245.

Şahin, G.N. (2017). Observations on earthquake resistance of traditional timber framed houses in Turkey, Build Environ 42, p. 840-851, 2017.

Vasconcelos, G., Poletti, E. (2015). Traditional timber frame walls: mechanical behavior analysis and retrofitting. Handbook of research on seismic assessment and rehabilitation of historic structures, p. 30-59.

Wan, J. Smith, S. and Qiao, P. (2010). FRP-to-softwood joints: experimental investigation, In: Proceedings of Fifth International Conference on FRP Composites in Civil Engineering, CICE 2010, Beijing, China, p. 951–954.

Winandy, J.E. (1994). Wood properties. USDA-Forest Service, Forest Products Laboratory, Arntzen, Charles J. ed. Encyclopedia of Agricultural Science. Orlando, Vol. 4, p. 549-561.

Yang, Y.L., Liu, J.W., Xiong, G.J. (2013). Flexural behavior of wood beams strengthened with HFRP, Construction and Building Materials, 43, p. 118-124.

Url-1 *<http://www.ahsap.org/bilgi/yapi-sistemleri>,* Turkish Timber Association, March.2018.

STANDARDS

EN 408:2010. Timber structures-Structural timber and glued laminated timber-Determination of some physical and mechanical properties. Brussels, 16 July 2012.

EN 1996-1-1:Eurocode 6. Design of masonry structures-Part 1-1: General rules for reinforced and unreinforced masonry structures. November 2005.

BS EN 26891:1991. Timber structures –Joints made with mechanical fasteners- General principles for the determination of strength and deformation characteristics. Brussels, 31 July 1991.

BS EN 338:2009. Structural timber - Strength classes. Brussels.